Soil Moisture-driven Drought Evaluation under Present and Future Conditions

Hyunwoo Kang

Dissertation submitted to the faculty of the Virginia Polytechnic Institute and State University in partial fulfillment of the requirements for the degree of

Doctor of Philosophy
in
Biological Systems Engineering

Venkataramana Sridhar

W. Cully Hession

Jactone Arogo Ogejo

Bradford F Mills Jr

August 6, 2018
Blacksburg, VA

Keywords: Drought, soil moisture, climate change, drought forecasting, economic impacts

Soil Moisture-driven Drought Evaluation under Present and Future Conditions

Hyunwoo Kang

Abstract

Drought is one of the most severe natural disasters and detrimentally impacts water resources, agricultural production, the environment, and the economy. Climate change is expected to influence the frequency and severity of extreme droughts. This dissertation evaluates drought conditions using a variety of hydrologic modeling approaches include short-term drought forecasting, long-term drought projection, and a coupled surface-groundwater dynamic drought assessment. The economic impacts of drought are also explored through a linked economic impact model. Study results highlight the need for various drought assessment approaches and provide insights into the array of tools and techniques that can be employed to generate decision-support tools for drought mitigation plans and water resource allocation. For short-term drought forecasting, the Soil and Water Assessment Tool (SWAT) and Variable Infiltration Capacity (VIC) models are used with a meteorological forecasting dataset. Results indicate that eight weeks of lead-time drought forecasting show good drought predictability for the Contiguous United States (CONUS). For the drought projection at a finer scale, both SWAT and VIC models are applied with Coupled Model Intercomparison Project Phase 5 (CMIP5) climate model outputs to derive multiple drought indices for the Chesapeake Bay watershed and five river basins in Virginia. The results indicate that current climate change projections will lead to increased drought in the entire Chesapeake Bay watershed and Virginia river basins because of increases in the sum of evapotranspiration, and surface and groundwater discharge. The impacts of climate change on future agricultural droughts and associated economy-wide implications are then evaluated using the VIC and IMPLAN (IMpact analysis for PLANning) model for the several congressional districts in Virginia. The result indicated that increases in agricultural drought in the future would lead to decreases in agricultural productions and job losses. Finally, a coupled framework using the VIC and MODFLOW models is implemented for the Chesapeake Bay and the Northern Atlantic Coastal Plain aquifer system, and the results of a drought index that incorporates groundwater conditions performs better for some drought periods. Hydrologic modeling framework with multiple hydrologic models and various scales can provide a better understanding of drought assessments because the comparisons and contrasts of diverse methods are available.

Soil Moisture-driven Drought Evaluation under Present and Future Conditions

Hyunwoo Kang

General Audience Abstract

Drought is one of the most severe natural hazards and negatively impacts the water resources, agricultural production, the environment, and the economy. Climate change influences the frequency and severity of extreme droughts. This dissertation assesses drought conditions using various hydrologic-modeling methods, which are drought forecasting, climate change impacts on drought, economic influences of droughts, and a coupled model approach. Study results highlight the need for various drought evaluation techniques that can generate decision-support tools for drought mitigation plans and water resource management. For short-term drought forecasting, two hydrologic models are used with a meteorological forecasting dataset. Results indicate that eight weeks of lead-time drought forecasting show good drought predictability for the Contiguous United States (CONUS). For the drought projection at a finer scale, two models are also used with multiple climate models for the Chesapeake Bay (CB) watershed and five river basins in Virginia. The results indicate that current climate change projections will lead to increased drought in the entire CB watershed and Virginia river basins. The impacts of climate change on future agricultural droughts and associated economy-wide implications are then evaluated using the hydrologic and economic models for the several congressional districts in Virginia. The results indicate that increases in agricultural drought in the future would lead to decreases in agricultural productions and job losses. Finally, a coupled model is implemented for the CB and the Northern Atlantic Coastal Plain (NACP) aquifer system, and the results of a drought index that incorporate groundwater conditions performs better for some drought periods. Hydrologic modeling framework with multiple hydrologic models and various scales can provide a better understanding of drought assessments because the comparisons and contrasts of diverse methods are available.

Dedication

For my parents, brother, and grandmother, you have supported me throughout my entire academic career. Thank you.

Acknowledgements

I am very grateful to the Institute for Critical Technology and Applied Science (ICTAS) doctoral scholarship program that funded all my doctoral works. I would like to thank my advisor, Dr. Sridhar for his sincere support. I am sure that my doctoral works would not be finished without his guidance. Special thanks to my committee members; Dr. Hession and Dr. Ogejo advised the overall direction of the dissertation, and Dr. Mills supplied the specific advice of Chapter 4.
Thanks to the College of Agriculture and Life Sciences, College of Engineering, and Department of Biological Systems Engineering at Virginia Tech for giving me a great chance to study and work in Blacksburg.

Finally, I would like to thank the members of Hydro systems labs; Dr. Sridhar, Prasanth Valayamkunnath, MadusankaThilakarathne, Vinit Sehgal, Syed Ali, and Parthkumar Modi for their endless assistance.

Table of contents

List of Figures

Chapter 2

Chapter 3

Chapter 4

Chapter 5

List of Tables

Chapter 2

Chapter 3

Chapter 4

Chapter 5

Chapter 1. Introduction

Drought is one of the most common natural disasters, and it negatively affects the environment, water resources, agriculture, and the economy (Sternberg, 2011; Vasiliades and Loukas, 2009; Esfahanian et al., 2017). Droughts are prevalent in many parts of the globe, and their impacts are being aggravated by the intensification of agriculture, population growth, and increased water use. The negative impacts of droughts include reduced surface and groundwater resources, diminished hydropower generation, and deteriorated water quality in streams, rivers, and aquifers. In recent decades, the global surface temperature has increased significantly, and these increases are expected to result in more extreme climatic conditions. Climate changes are also affecting the hydrologic cycle as well as the frequency and severity of extreme climatic events, which raises concerns about potential impacts on the occurrence of extreme droughts.

Droughts are characterized by multiple climatological and hydrological parameters, such as precipitation, evapotranspiration, temperature, soil moisture, streamflow, and groundwater. Therefore, a comprehensive understanding of the relationships between hydrometeorological parameters is necessary to develop measures for early warning and impact management. In addition, drought assessment is essential for freshwater planning and management. However, the evaluation of droughts is very complicated. First, it is difficult to determine the initiation and the termination of drought events, because droughts develop slowly and often go unrecognized until they have begun to cause serious problems. Second, there is no universal definition of droughts. Finally, droughts are non-structural hazards and spread over large geographical areas.

Drought monitoring and forecasting methods are commonly used for drought evaluations. The accuracy of drought monitoring and forecasting is influenced by the selection of a drought indicator, which can provide a synthetic and objective description of drought conditions. Many drought indicators have been developed and used for quantifying, monitoring, and determining the onset of, or recovery from, droughts, for declaring drought severity, and for forecasting droughts. Indicators are based on different methods, including the use of statistical techniques, simple water and energy balance models, hydrologic models, and/or a blend of these methods. Furthermore, meteorological, agricultural, hydrological, and socio-economic perspectives of droughts can be quantified by drought indicators (Sridhar et al., 2008; Tsakiris et al., 2007; Niemeyer, 2008).

The most common drought indicator is the US Drought Monitor (USDM), which was established by the US Department of Agriculture (USDA), National Drought Mitigation Center

(NDMC), and National Oceanic and Atmospheric Administration (NOAA). The USDM is a composite index that includes indicators, climate indices, and local reports from more than 350 expert observers across the entire US. In addition, the USDM provides a weekly map of drought with five drought categories based on a percentile classification in the US. Furthermore, the USDM can identify both short- and long-term drought conditions.

Meteorological drought is associated with a lack of precipitation for a specific time, hydrological drought is a lack of surface and subsurface water resources from a management system, agricultural drought is related with declining soil moisture and resulting crop failure, and socio-economic drought is an inadequate supply of water systems to support demand for an economic good such as crops. The response to drought depends on the type of drought that has occurred in a given area, and drought characterization is crucial for drought management operations. Thus, it is important to use multiple drought indices for identifying the diverse aspects of drought conditions, because multiple types of droughts existed (e.g., meteorological, agricultural, hydrological, and socio-economic droughts).

The Standardized Precipitation Index (SPI; McKee et al., 1993) is one of the most common indices for evaluating meteorological drought, and it is based on long-term precipitation observations. With the same framework of computation of the SPI, the Standardized Soil Moisture Index (SSI; Hao and AghaKouchak, 2013) is utilized to quantify agricultural drought based on soil moisture. With all of these ongoing efforts, the challenge for evaluating drought has been identifying a single meteorological or hydrologic variable that is an appropriate indicator over both space and time. This has hindered the advancement of drought prediction capabilities, generation of solid drought management plans, and risk assessment (Hao and AghaKouchak, 2013). In response, the Multivariate Standardized Drought Index (MSDI), based on multiple hydro-climatic variables, was developed and applied to identify historic droughts in the US (Hao and AghaKouchak, 2013; Hao and AghaKouchak, 2014).

The monthly and seasonal drought outlook provided by the Climate Prediction Center (CPC) of the NOAA is an operational drought forecasting method, and it is based on official CPC precipitation and temperature outlooks, various short- and medium-range forecasting tools and models (e.g., North American Ensemble Forecast System (NAEFS) precipitation outlooks (Toth et al., 2005), dynamical models (Coupled Forecast System model version 2 (CFSv2) (Saha et al.,

2014), the 384-hour total precipitation forecasts from several runs of the Global Forecast System (GFS; Mitchell et al., 2005), and El Nino and La Nina conditions.

Even though these drought indicators are useful and they can reflect the multiple perspectives (meteorological, agricultural, hydrological, and socio-economic) of droughts, a comprehensive understanding of the processes of droughts including hydrologic modeling and economic effects is still necessary. These approaches enable water resource managers and policymakers to better prepare for and respond to droughts. In addition, drought forecasting and projection methods are practically applied for the management of water resources, risk assessment, and drought mitigation.

The overall goal of this dissertation is to understand, quantify, and map drought-impacted areas in several regions of the US. The maintained objective of this study is to demonstrate that the evaluation of drought using soil moisture-based drought indices is essential for the improved prediction of current and future climatic conditions.

1) The first objective of this dissertation is to develop a methodology for short-term drought forecasting using the hydrologic models, meteorological forecasting dataset, and drought indices. The Soil and Water Assessment Tool (SWAT) and Variable Infiltration Capacity (VIC) models were utilized to estimate hydrologic variables and drought indices for the Contiguous U.S. (CONUS), and the Coupled Forecast System model versions 2 (CFSv2) provided the near-real-time meteorological forecasting dataset. The first objective is described in Chapter 2, and the status of this work is as follows:

Kang, H., Sridhar, V.

Citation: Kang, H. and Sridhar, V., 2018. Improved Drought Prediction Using Near Real-Time Climate Forecasts and Simulated Hydrologic Conditions. Sustainability 10(6): 1799.

2) The second objective is to evaluate climate change impacts on droughts conditions for the Chesapeake Bay watershed Both SWAT and VIC models were applied over the Chesapeake Bay watershed and five river basins in Virginia with the Coupled Model Intercomparison Project Phase 5 (CMIP5) climate model ensembles and derived drought indices. This objective is described in Chapter 3, and the status of this work is as follows:

Kang, H., Sridhar, V.

Citation: Kang, H. and Sridhar, V., 2017. Combined statistical and spatially distributed hydrological model for evaluating future drought indices in Virginia. Journal of Hydrology: Regional Studies, 12, pp.253-272.

Kang, H., Sridhar, V.

Citation: Kang, H. and Sridhar, V., 2018. Assessment of Future Drought Conditions in the Chesapeake Bay Watershed. JAWRA Journal of the American Water Resources Association, 54(1), pp.160-183.

3) The third objective is to assess economy-wide impacts of drought using soil moisture estimations from the VIC model, CMIP5 climate model outputs, and the IMPLAN model (IMPLAN: IMpact analysis for PLANning) for three congressional districts in Virginia that have different hydrologic and economic characteristics. This objective is described in Chapter 4, and the status of this work is as follows:

Kang, H., Sridhar, V., Mills, B.

Status: Manuscript in preparation

4) The last objective is to evaluate droughts using the surface and groundwater coupled modelover the Northern Atlantic Coastal Plain (NACP) aquifer system in the Chesapeake Bay watershed. A coupled framework of VICMF (VIC-MODFLOW) model was utilized for the NACP region, and multiple drought indices were used for the drought assessment. This objective is described in Chapter 5, and the status of this work is as follows:

Kang, H., Sridhar, V.

Status: Manuscript in preparation

1.1. Reference

AghaKouchak, A., 2014. A baseline probabilistic drought forecasting framework using standardized soil moisture index: application to the 2012 United States drought. Hydrology and Earth System Sciences, 18(7), pp.2485-2492.

Ahn, S.R., Jeong, J.H. and Kim, S.J., 2016. Assessing drought threats to agricultural water supplies under climate change by combining the SWAT and MODSIM models for the Geum River basin, South Korea. Hydrological Sciences Journal, 61(15), pp.2740-2753.

Arnold, J.G., Srinivasan, R., Muttiah, R.S. and Williams, J.R., 1998. Large area hydrologic modeling and assessment part I: model development. JAWRA Journal of the American Water Resources Association, 34(1), pp.73-89.

Bailey, R.T., Wible, T.C., Arabi, M., Records, R.M. and Ditty, J., 2016. Assessing regional-scale spatio-temporal patterns of groundwater–surface water interactions using a coupled SWAT-MODFLOW model. Hydrological Processes, 30(23), pp.4420-4433.

Benestad, R.E. and Haugen, J.E., 2007. On complex extremes: flood hazards and combined high spring-time precipitation and temperature in Norway. Climatic Change, 85(3-4), pp.381-406.

Cook, B.I., Ault, T.R. and Smerdon, J.E., 2015. Unprecedented 21st century drought risk in the American Southwest and Central Plains. Science Advances, 1(1), p.e1400082.

Diffenbaugh, N.S., Swain, D.L. and Touma, D., 2015. Anthropogenic warming has increased drought risk in California. Proceedings of the National Academy of Sciences, 112(13), pp.3931-3936.

Ding, Y., Hayes, M.J. and Widhalm, M., 2011. Measuring economic impacts of drought: a review and discussion. Disaster Prevention and Management: An International Journal, 20(4), pp.434-446.

Esfahanian, E., Nejadhashemi, A.P., Abouali, M., Adhikari, U., Zhang, Z., Daneshvar, F. and Herman, M.R., 2017. Development and evaluation of a comprehensive drought index. Journal of environmental management, 185, pp.31-43.

Gringorten, I.I., 1963. A plotting rule for extreme probability paper. Journal of Geophysical Research, 68(3), pp.813-814.

Gutzler, D.S. and Robbins, T.O., 2011. Climate variability and projected change in the western United States: regional downscaling and drought statistics. Climate Dynamics, 37(5-6), pp.835-849.

Hao, Z. and AghaKouchak, A., 2013. Multivariate standardized drought index: a parametric multi-index model. Advances in Water Resources, 57, pp.12-18.

Hao, Z. and AghaKouchak, A., 2014. A nonparametric multivariate multi-index drought monitoring framework. Journal of Hydrometeorology, 15(1), pp.89-101.

Halmstad, A., Najafi, M.R. and Moradkhani, H., 2013. Analysis of precipitation extremes with the assessment of regional climate models over the Willamette River Basin, USA. Hydrological Processes, 27(18), pp.2579-2590.

Hayes, M., Svoboda, M., Le Comte, D., Redmond, K.T. and Pasteris, P., 2005. Drought monitoring: New tools for the 21st century (pp. 53-69). Taylor and Francis.

Jha, M., Pan, Z., Takle, E.S. and Gu, R., 2004. Impacts of climate change on streamflow in the Upper Mississippi River Basin: A regional climate model perspective. Journal of Geophysical Research: Atmospheres, 109(D9).

Karl, T.R., Gleason, B.E., Menne, M.J., McMahon, J.R., Heim, R.R., Brewer, M.J., Kunkel, K.E., Arndt, D.S., Privette, J.L., Bates, J.J. and Groisman, P.Y., 2012. US temperature and drought: Recent anomalies and trends. Eos, Transactions American Geophysical Union, 93(47), pp.473-474.

Liang, X., Lettenmaier, D.P., Wood, E.F. and Burges, S.J., 1994. A simple hydrologically based model of land surface water and energy fluxes for general circulation models. Journal of Geophysical Research: Atmospheres, 99(D7), pp.14415-14428

Liang, X., Xie, Z. and Huang, M., 2003. A new parameterization for surface and groundwater interactions and its impact on water budgets with the variable infiltration capacity (VIC) land surface model. Journal of Geophysical Research: Atmospheres, 108(D16).

Luo, L. and Wood, E.F., 2007. Monitoring and predicting the 2007 US drought. Geophysical Research Letters, 34(22).

Masterson, J.P., Pope, J.P., Fienen, M.N., Monti, Jack Jr., Nardi, M.R., and Finkelstein, J.S., 2016, Documentation of a groundwater flow model developed to assess groundwater availability in the Northern Atlantic Coastal Plain aquifer system from Long Island, New York, to North Carolina (ver. 1.1, December 2016): U.S. Geological Survey Scientific Investigations Report 2016–5076, 70 p., http://dx.doi.org/10.3133/sir20165076.

Mao, Y., Nijssen, B. and Lettenmaier, D.P., 2015. Is climate change implicated in the 2013–2014 California drought? A hydrologic perspective. Geophysical Research Letters, 42(8), pp.2805-2813.

McKee, T.B., N.J. Doesken, and J. Kleist, 1993. Drought Monitoring with Multiple Time Series. 8th Conference on Applied Climatology, Boston, American Meteorological Society.

Mishra, A.K. and Singh, V.P., 2010. A review of drought concepts. Journal of hydrology, 391(1), pp.202-216.

Mishra, V., Cherkauer, K.A. and Shukla, S., 2010. Assessment of drought due to historic climate variability and projected future climate change in the midwestern United States. Journal of Hydrometeorology, 11(1), pp.46-68.

Mitchell, K., Wei, H., Lu, S., Gayno, G., Meng, J. and Center, N.E.M., 2005. NCEP implements major upgrade to its medium-range global forecast system, including land-surface component. GEWEX News, 15(4), pp.8-9.

Mo, K.C., 2008. Model-based drought indices over the United States. Journal of Hydrometeorology, 9(6), pp.1212-1230.

Narasimhan, B. and Srinivasan, R., 2005. Development and evaluation of Soil Moisture Deficit Index (SMDI) and Evapotranspiration Deficit Index (ETDI) for agricultural drought monitoring. Agricultural and Forest Meteorology, 133(1), pp.69-88.

Niu, G.Y., Yang, Z.L., Dickinson, R.E., Gulden, L.E. and Su, H., 2007. Development of a simple groundwater model for use in climate models and evaluation with Gravity Recovery and Climate Experiment data. Journal of Geophysical Research: Atmospheres, 112(D7).

Oki, T. and Kanae, S., 2006. Global hydrological cycles and world water resources. science, 313(5790), pp.1068-1072.

Shukla, S. and Lettenmaier, D.P., 2011. Seasonal hydrologic prediction in the United States: understanding the role of initial hydrologic conditions and seasonal climate forecast skill. Hydrology and Earth System Sciences, 15(11), pp.3529-3538.

Saha, S., Moorthi, S., Wu, X., Wang, J., Nadiga, S., Tripp, P., Behringer, D., Hou, Y.T., Chuang, H.Y., Iredell, M. and Ek, M., 2014. The NCEP climate forecast system version 2. Journal of Climate, 27(6), pp.2185-2208.

Sridhar, V. R., Billah, M. M. and Hildreth, J. 2017. Development of a coupled surface and groundwater hydrological model (VIC-MODFLOW) and evaluation in the Snake River Basin under a changing climate. Groundwater. In review.

Swain, D.L., Tsiang, M., Haugen, M., Singh, D., Charland, A., Rajaratnam, B. and Diffenbaugh, N.S., 2014. The extraordinary California drought of 2013/2014: Character, context, and the role of climate change. Bulletin of the American Meteorological Society, 95(9), p.S3.

Sternberg, T., 2011. Regional drought has a global impact. Nature, 472(7342), pp.169-169.

Tallaksen, L.M. and Van Lanen, H.A. eds., 2004. Hydrological drought: processes and estimation methods for streamflow and groundwater (Vol. 48). Elsevier.

Taylor, K.E., Stouffer, R.J. and Meehl, G.A., 2012. An overview of CMIP5 and the experiment design. Bulletin of the American Meteorological Society, 93(4), pp.485-498.

Toth, Z., Desmarais, J.G., Brunet, G., Zhu, Y., Verret, R., Wobus, R., Hogue, R. and Cui, B., 2005. The North American Ensemble Forecast System (NAEFS). In Geophysical Research Abstracts (Vol. 7, p. 02501).

Vasiliades, L. and Loukas, A., 2009. Hydrological response to meteorological drought using the Palmer drought indices in Thessaly, Greece. Desalination, 237(1-3), pp.3-21.

Virginia Department of Emergency (VDEM), 2013. Commonwealth of Virginia hazard mitigation plan. Chapter 3: Hazard identification and risk assessment.

Wang, D., Hejazi, M., Cai, X. and Valocchi, A.J., 2011. Climate change impact on meteorological, agricultural, and hydrological drought in central Illinois. Water Resources Research, 47(9).

Wuebbles, D., Meehl, G., Hayhoe, K., Karl, T.R., Kunkel, K., Santer, B., Wehner, M., Colle, B., Fischer, E.M., Fu, R. and Goodman, A., 2014. CMIP5 climate model analyses: climate extremes in the United States. Bulletin of the American Meteorological Society, 95(4), pp.571-583.

Chapter 2. Evaluation of drought forecasting method using identification of drought processes and near real time forecasting approach

2.1. Abstract

Short-term drought forecasting is helpful for establishing drought mitigation plans and for managing risks that often ensue in water resource systems. Additionally, hydrologic modeling using high-resolution spatial and temporal data is used to simulate the land surface water and energy fluxes, including runoff, baseflow, and soil moisture, which are useful for drought forecasting. In this study, the Soil and Water Assessment Tool (SWAT) and Variable Infiltration Capacity (VIC) models are used for short-term drought forecasting in the contiguous United States (CONUS), as many areas in this region are frequently affected by varying drought intensities. Weekly-to-seasonal meteorological inputs are provided by the Climate Prediction Center (CPC) for the retrospective period (January 2012 to July 2017) and Climate Forecasting System version 2 (CFS v2) for the forecasting period (August 2017 to April 2018), and these inputs are used to estimate agricultural and groundwater drought conditions. For drought assessment, three drought indices, namely, the Standardized Soil Moisture index (SSI), the Multivariate Standardized Drought Index (MSDI), and the Standardized Baseflow index (SBI), were analyzed. The accuracy of the forecasting results was verified using several a performance measure (Drought area agreement (%); DA). Generally, eight weeks of lead time forecasting showed good drought predictability from both the SWAT and VIC models for the MSDI simulations (62% for SWAT and 64% for VIC for all drought categories). However, the DA values for eight weeks lead time forecasting for SSI were 23% (SWAT) and 10% (VIC) and 7% (SWAT) and 7% (VIC) for the SBI, respectively. In addition, the accuracies of drought predictions remarkably decreased after eight weeks, and the average DA values were 36% for SWAT and 38% for VIC due to an increase in the uncertainties associated with meteorological variables in CFS v2 products. For example, there are increases in the total number of grids where the absolute values of monthly differences between CFSv2 and CPC observations exceed 20 mm and 1 °C during the forecasting period. Additionally, drought forecasting using only one variable (i.e., SSI and SBI) showed low prediction performances even for the first eight weeks. The results of this study provide insights

into drought forecasting methods and provide a better understanding to plan for timely water resource management decisions.

2.2. Introduction

Droughts have negatively affected water resource management, agriculture, the environment and the economy around the globe (Sternberg, 2011; Sheffield and Wood, 2012). During the last few decades, the severity and frequency of droughts in the United States (U.S.) have been exceptionally high in the West, the Great Lakes States and the Southeastern U.S. (Changnon et al., 2000; Karl et al., 2012; Clark et al., 2016). The severity and frequency of recent droughts in the U.S. coincide with high temperatures and evaporative demand (McEvoy, 2015), affecting many areas in the Contiguous U.S. (CONUS) (Clark et al., 2016).

An early drought warning framework with short-term drought forecasting (e.g., monthly or seasonal) would provide information regarding the initiation, propagation, and termination of droughts, which are essential for stakeholders and decision-makers (AghaKouchak, 2014). Additionally, seasonal drought forecasting plays a significant role in establishing proper policies to plan for available water resources as well as drought preparedness, mitigation, and risk management. Accurate drought forecast systems would enable optimal operation of irrigation systems by mitigating the detrimental effects of droughts (Hayes et al., 2005). In recent decades, several drought forecasting systems have evolved to perform the evaluation of hydrologic/drought conditions across the CONUS, such as the Climate Prediction Center's (CPC) Seasonal Drought Outlook (Steinemann, 2006), the National Integrated Drought Information System's (NIDIS's) Drought Early Warning Systems (DEWS), Princeton University's drought forecast system (Luo and Wood, 2007), and a probabilistic drought forecasting framework (Yan et al., 2017). Although these studies have proposed some advanced drought forecasting methods such as probabilistic drought forecasting (Yan et al., 2017), the model-based Drought Monitoring and Prediction System (DMAPS; Luo and Wood, 2007), and the dynamical or statistical-dynamical seasonal forecasting (Ribeiro and Pires 2016),the effects of climate change on droughts across various regions of the globe suggests the need for more reliable methods in predicting extreme events (Mishra and Singh 2010; Halmstad et al. 2013).

Drought indices are used for evaluating drought levels, drought impacts (Niemeyer, 2008), long-term drought projections, and seasonal drought forecasting (Kang and Sridhar, 2017; Sehgal and Sridhar, 2018; Thilakarathne and Sridhar, 2017; Kang and Sridhar, 2018). Several drought indices have been developed and applied to evaluate multiple categories of drought (e.g., meteorological, agricultural, hydrological, and socio-economic droughts). The Standardized Precipitation Index (SPI) (McKee et al., 1993) is one of the most widespread indices that is used to evaluate meteorological droughts (Mishra and Singh, 2009; Zargar et al., 2011; Paulo et al., 2016) and is used for drought forecasting (Belayneh et al., 2014). In the same framework as SPI, the Standardized Soil Moisture Index (SSI; Hao and AghaKouchak, 2013; Hao and AghaKouchak, 2014) is used to quantify agricultural drought conditions. Additionally, the Multivariate Standardized Drought Index (MSDI), which is computed using multiple hydrometeorological variables, is used to identify historic droughts in the U.S. (Hao and AghaKouchak, 2013; Hao and Aghakouchak, 2014). The diverse applications with multiple drought indices allow the consideration of various aspects of drought conditions. In this study, the SSI, MSDI, and Standardized Baseflow Index (SBI) were used, as they represent multiple aspects of drought conditions including agricultural, multivariate, and hydrological droughts in the CONUS.

Drought prediction is commonly based on drought indices, which are estimated using deterministic or statistical model simulations of hydrometeorological variables such as evapotranspiration, runoff, and soil moisture (Madadgar and Moradkhani, 2013, Sehgal and Sridhar, 2018). The SPI was widely used for short-term drought forecasting (Cancelliere et al., 2007; Morid et al., 2007; Belayneh et al., 2014), and soil moisture-based drought indices were also applied (AghaKouchak, 2014; Zhang et al., 2017). Additionally, macro-scale hydrologic models have been employed for the calculation of hydrologic variables based on energy fluxes and water balance estimates, and have been effectively used to assess drought conditions (Sehgal and Sridhar, 2018). For example, the Variable Infiltration Capacity (VIC) (Liang et al., 1994) model is a useful tool for simulating hydrologic variables and drought indices (Mishra et al., 2010). Additionally, the Soil and Water Assessment Tool (SWAT) (Arnold et al., 1998) is an acceptable tool for computing and assessing drought conditions. Thus, hydrological models provide the basis for evaluating drought conditions with multiple drought indices, drought management, and suggesting mitigation strategies for stakeholders (Narasimhan and Srinivasan, 2005).

A myriad of studies have evaluated monthly to seasonal forecasting techniques; such investigations were limited to lead times of 1-3 months (Shukla and Lettenmaier, 2011), and a longer lead time drought prediction approach was not available (Hao et al., 2018). Hence, a drought forecasting approach with multiple hydrologic models, drought indices, and a longer lead time of meteorological input can facilitate drought preparation, drought mitigation strategies, and drought risk management for the near future. The objectives of this study were to integrate physically based water balance components from the VIC and SWAT models to derive drought indices with short-term meteorological forecasts of precipitation and temperature from the Coupled Forecast System Model version 2 (CFSv2) (Saha et al., 2014) for near-real-time drought forecasting with lead times up to 9 months for the CONUS. To achieve the objective, the SWAT and VIC models were used to estimate various hydrologic variables including soil moisture, baseflow, and evapotranspiration for both retrospective (January 2012 to July 2017) and forecasting (August 2017 to April 2018) periods. Additionally, multiple drought indices were derived at a weekly time step, and were used to develop weekly forecasts for the CONUS. Finally, an evaluation of drought forecasting with a lead time up to nine months and an assessment of spatial characteristics of droughts were performed by comparing the results to the U.S. Drought Monitor (USDM; Svoboda et al. 2002; Lorenz et al., 2017).

2.3. Methods

2.3.1. Study Area

The study area is the CONUS, where drought is an ongoing problem in multiple regions such as the South, West, Central High Plains, and the Southeastern regions in the CONUS. Figure 1(a) shows the entire CONUS and an example map of the USDM for February 22, 2018 that shows current drought conditions. Additionally, Figure 1(b) and (c) show the delineated sub-watersheds from the SWAT model (3,972 sub-watersheds) and the VIC model grids, respectively. Finally, Figure 1(d) shows the locations of soil moisture observation from the U.S. Climate Reference Network (USCRN) that were used for interpreting the simulation results.

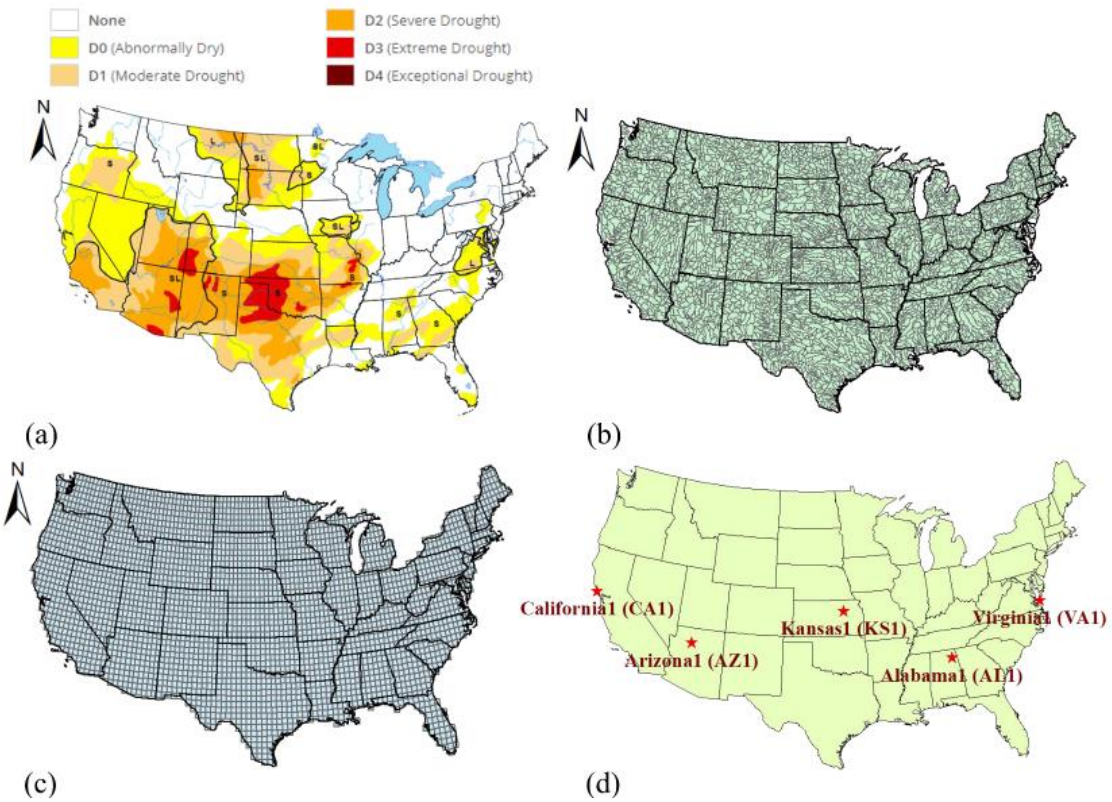

Figure 1. Map of the Contiguous United States (CONUS). (a) An example map of the United States Drought Monitor (USDM) on February 22, 2018 (Source: http://droughtmonitor.unl.edu/). (b) Entire sub-watersheds delineated by the Soil and Water Assessment Tool (SWAT) model (3,972 watersheds). (c) Entire grids for the Variable Infiltration Capacity (VIC) model (3,275 grids). (d) Locations of soil moisture observations from the United States Climate Reference Network (USCRN).

Droughts and heat waves have inflicted damages costing $210.1 billion from 1980-2011 in the U.S. (Smith and Katz, 2013). Additionally, the 2012-2013 drought caused $40 billion losses in agricultural areas, and two-thirds of the CONUS was affected (DHS, 2015). Furthermore, the 2012-2015 California drought was the most severe drought with a cumulative deficit of precipitation with a 1,000-year return period (Rippey, 2015; Robeson, 2015). Figure 2 shows drought maps and precipitation and temperature anomalies for the corresponding times for the retrospective period (2012 to 2017). From 2012 to 2015, there was significantly low precipitation or high temperature, which were the primary drivers of droughts. For example, Figure 2(a) shows the drought conditions of the USDM, the MSDI from SWAT and VIC, and precipitation and temperature anomalies on May 08, 2012. During this time, low precipitation in the West (Nevada, Utah, Arizona, and Colorado) and Southeast (Alabama, Georgia, and Florida), and high temperatures were recorded in Southwestern areas (California). Accordingly, moderate to severe

drought conditions appeared in the regions low precipitation or high temperature. In addition, less precipitation and higher temperatures occurred in the northern High Plains (Montana, North Dakota, Minnesota, South Dakota, and Nebraska) on July/18/2017, after which severe to exceptional drought conditions occurred (Figure 2(f)).

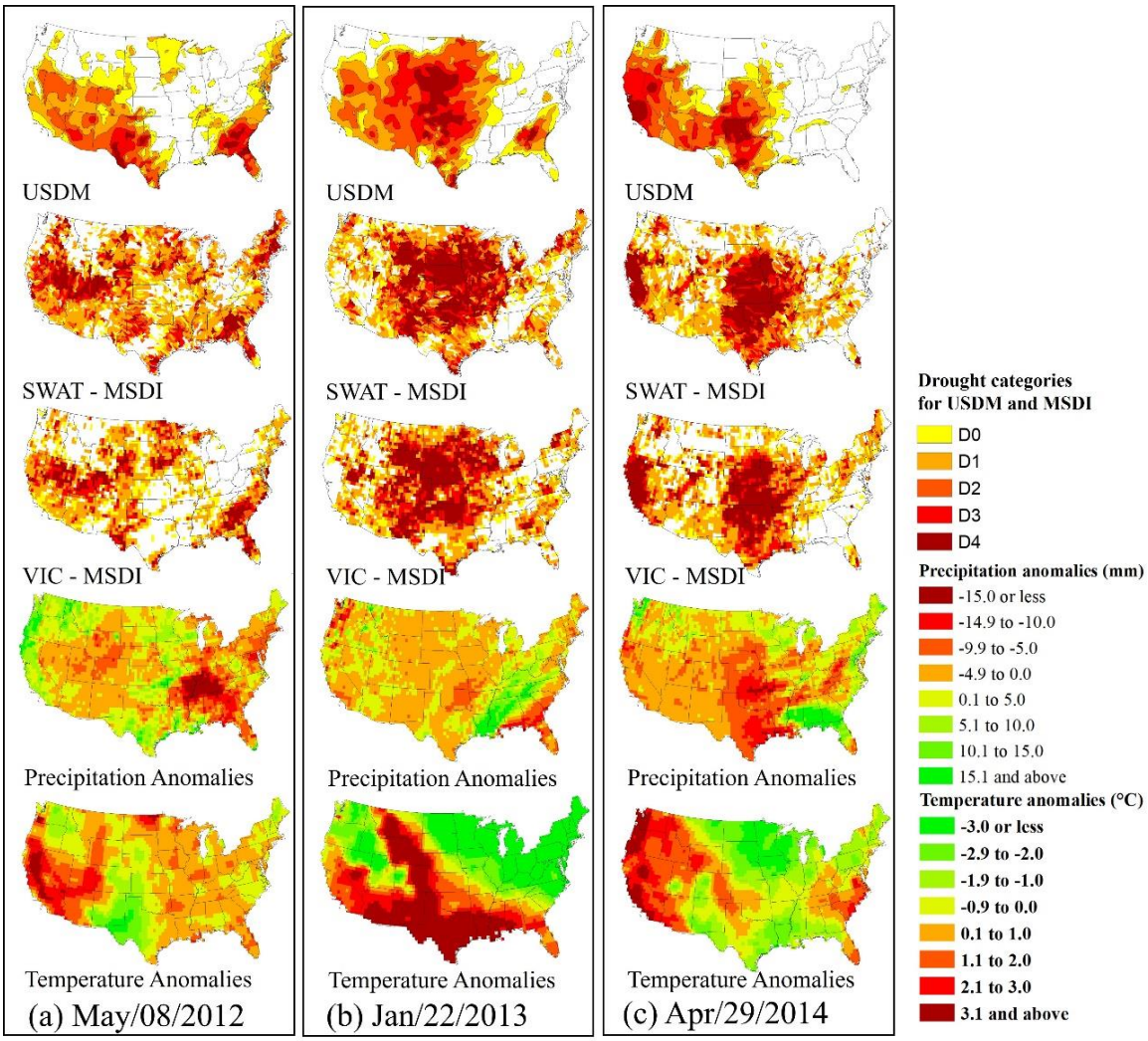

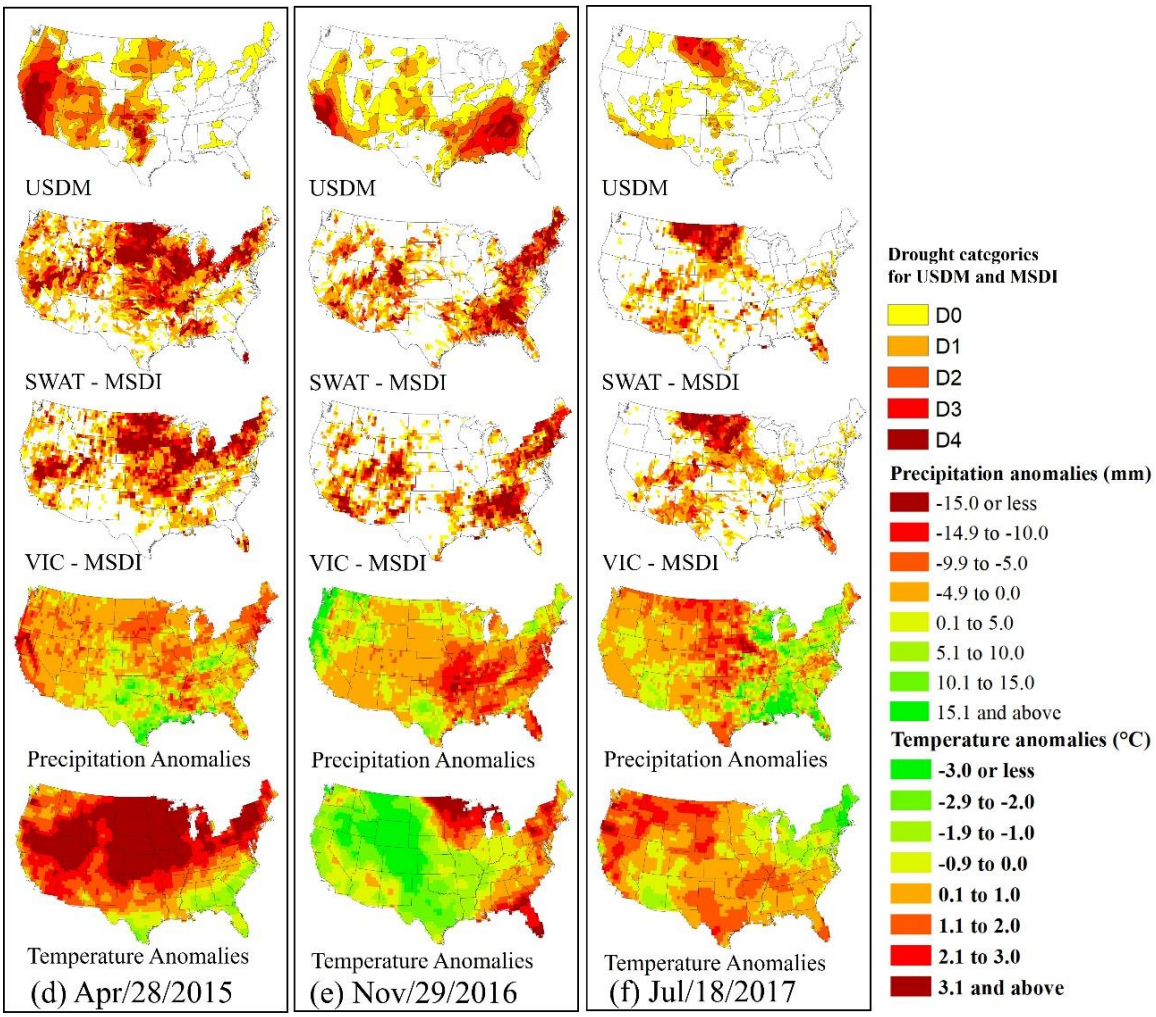

Figure 2. Spatial maps of drought conditions derived from the USDM, MSDI from SWAT and VIC, and precipitation and temperature anomalies for the retrospective period. For the USDM and MSDI maps, yellow to brown areas represent each category of drought conditions. For the maps of precipitation anomalies, orange or red areas indicate less precipitation than mean values, whereas yellowish green or green areas represent more precipitation than mean values. For the maps of temperature anomalies, yellowish green or green areas indicate lower temperatures than mean values, whereas orange or red areas represent higher temperatures than mean values. (a) Spatial maps of the USDM and MSDI, precipitation anomalies, and temperature anomalies for May/08/2012. (b) Spatial maps of the USDM and MSDI, precipitation anomalies, and temperature anomalies for Jan/22/2013. (c) Spatial maps of the USDM, precipitation anomalies, and temperature anomalies for Apr-29-2014. (d) Spatial maps of the USDM and MSDI, precipitation anomalies, and temperature anomalies for Apr-28-2015. (e) Spatial maps of the USDM and MSDI, precipitation anomalies, and temperature anomalies for Nov-29-2016. (f) Spatial maps of the USDM and MSDI, precipitation anomalies, and temperature anomalies for Nov-29-2016 (Jul-18-2017).

2.3.2. Hydrologic Models and Data

In this study, two hydrologic models were used to estimate several hydrologic variables and drought indices for both retrospective and nine-month lead forecasting of drought conditions. The VIC model (Liang et al., 1994) is a macro-scale hydrologic model, which has been extensively used to evaluate drought conditions over many river basins in the CONUS and elsewhere to assess retrospective droughts (Wang et al., 2009; Shukla et al., 2015), to evaluate drought under a future climate (Mishra et al., 2010; Mao et al., 2015) and to forecast over short-term periods (Wood et al., 2012; Luo and Wood, 2007; Sheffield et al., 2014).

The hydrologic estimation of the VIC model depends on the interaction between soil and vegetation layers in each grid cell and forcing variables such as precipitation and temperature. In this study, the VIC model was applied at 0.5-degree resolution with atmospheric forcing from the Climate Prediction Center's (CPC) global daily precipitation and temperature data (Chen et al., 2008; Xie et al., 2010). CPC precipitation and temperature data were available from 1979 to present (July 2017; 39 years), which was sufficient for simulating long-term hydrologic variables and computing drought indices (Guttman, 1999). Additionally, other model parameters were derived from Nijssen et al. (2001a and 2001b). For the CONUS, the VIC model was represented with 3,275 grids (Figure 1(c)).

The SWAT model (Arnold et al., 1998; Neitsch et al., 2011; Arnold et al., 2012) is a river basin-scale, semi-distributed, and continuous-time model that simulates hydrologic processes in large river basins with mixed land uses and soil types. SWAT is widely used to evaluate drought conditions in many river basins in the U.S. to assess the impacts of climate change on droughts (Wang et al., 2011; Ashraf Vaghefi et al., 2014; Ahn et al., 2016; Kang and Sridhar, 2017), and drought forecasting (Sehgal and Sridhar, 2018). Additionally, SWAT showed higher potential and suitability for drought forecasting at the continental scale (Trambauer et al., 2013). The SWAT model is primarily based on hydrologic response units, which are a specific combination of land use, soil, and slope. Additionally, the model classifies three storage volumes in hydrologic response units (HRUs), which are the unsaturated soil profile layer (0-2 m), the shallow aquifer (2-20 m), and the deep aquifer (>20 m). The SWAT model simulates infiltration, surface runoff, lateral flow, shallow and deep aquifers baseflow, and evapotranspiration. The SWAT model requires a digital elevation model (DEM), soil, and meteorological input such as precipitation and

temperature. In this study, a 30 arc-second DEM from the U.S. Geological Survey (Jones et al., 1997) was used, a soil map with a 1: 250,000 scale was obtained from State Soil Geographic data (STATSGO) (USDA, 1991), and a land use map was obtained from National Land Cover Data (NLCD) (Homer et al., 2004). In this study, 3,973 sub-watersheds were delineated using the SWAT model to consider all of the climate grids in the CONUS.

The retrospective simulation periods for both the VIC and SWAT models were 1979 to July 2017 with input data for 30 years (Guttman, 1999). Additionally, the period from January 2012 to July 2017 was selected for the evaluation of drought areas because continuous and diverse severities of drought conditions occurred over the CONUS during this period (Griffin and Anchukaitis, 2014; Livneh and Hoerling, 2016).

For the historic simulation, 0.5 degree resolution data of daily precipitation and temperature were obtained from the CPC Global Unified precipitation and temperature database (https://www.esrl.noaa.gov/; Chen et al., 2008; Xie et al., 2010). The CPC provides 0.5 degree resolution precipitation rate (unit: kg/m2/s) and temperature (unit: K) data at the global scale in a NetCDF format. These variables were transformed into daily precipitation (unit: mm) and temperature (unit: °C) data that were then used as inputs for both the SWAT and VIC models. For the forecasting simulation analysis, forecast variables up to nine months into the future were also transformed and used for future simulation including CFSv2 precipitation rate (unit: kg/m2/s) and temperature (unit: K) data (https://nomads.ncdc.noaa.gov/modeldata/cfsv2_forecast_ts_9mon/).

2.3.3. CFSv2

The Coupled Forecast System Model version 2 (CFSv2; Saha et al., 2014) uses real-time data to compute atmospheric variables with a lead time up to nine months, including four-time initializations a day. Additionally, CFSv2 consists of a spectral atmospheric model (Global Forecast System; GFS) at a T126 (approximately 0.937°) resolution with 64 hybrid vertical levels and the advanced version of the ocean model (Griffies et al., 2004). Precipitation and temperature data were obtained from the CFSv2 data for the period between August 2017 and April 2018. Since the spatial resolution of CFSv2 is T126 (approximately 0.937°), it should be downscaled to 0.5 degree for the SWAT and VIC models. Thus, kriging, a spatial interpolation method, was applied to the downscaling process for each day of forecasting (August 2017 to April 2018). Also, mean

values of precipitation and temperature data from the four initialization (00, 06, 12, and 18 hours) at August-01-2017 were used. To remove the bias from the forecast data, a bias correction was performed by adding or subtracting the difference in weekly accumulated CFSv2 precipitation for each climate grid with reference to the CPC dataset (1979 to 2017). Figure 3(a) shows the time series of weekly raw and bias-corrected precipitation for the entire CONUS, and there is an overall overestimation of precipitation from the CFSv2 raw data. Additionally, Figure 3(b) shows the spatial map of precipitation differences between raw and bias-corrected data, and the overestimated precipitation from CFSv2 raw data was evident for the entire domain, specifically the eastern and west coast regions. Figure 3(c) and Figure 3(d) show the time series and spatial map of temperature differences between the raw and bias-corrected data, and there is an overestimation in the western areas of the CONUS, as well as an underestimation in the northern High Plains.

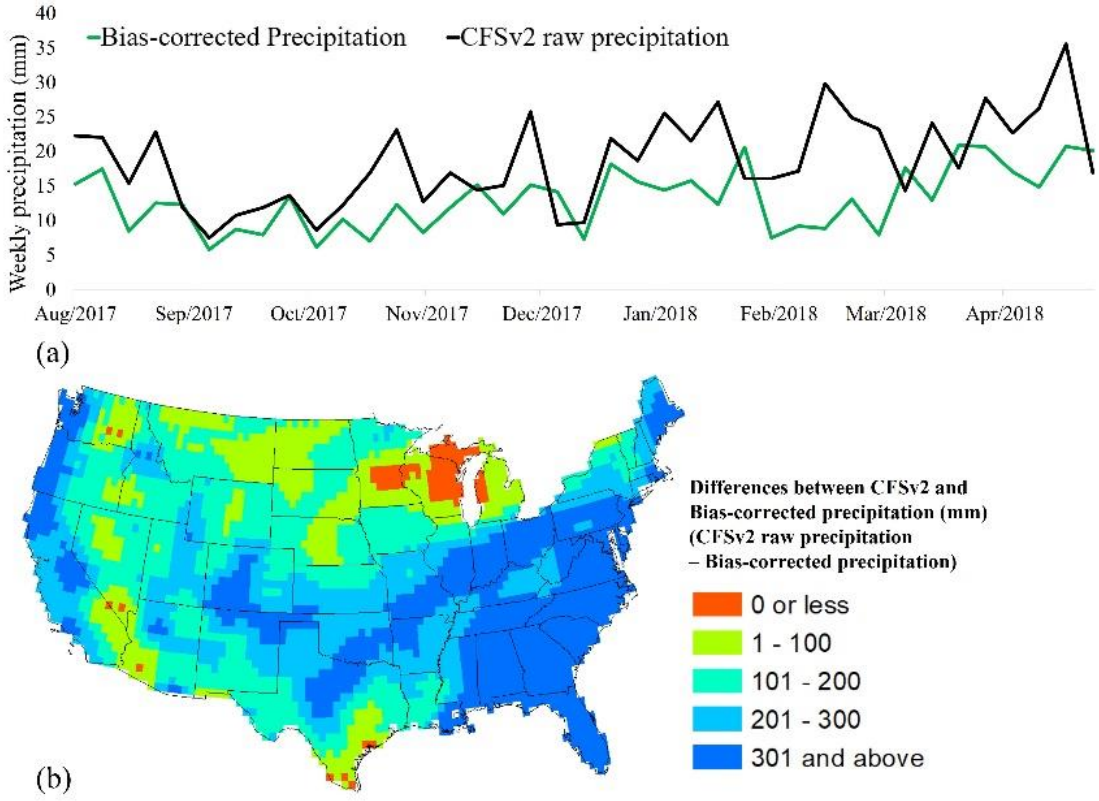

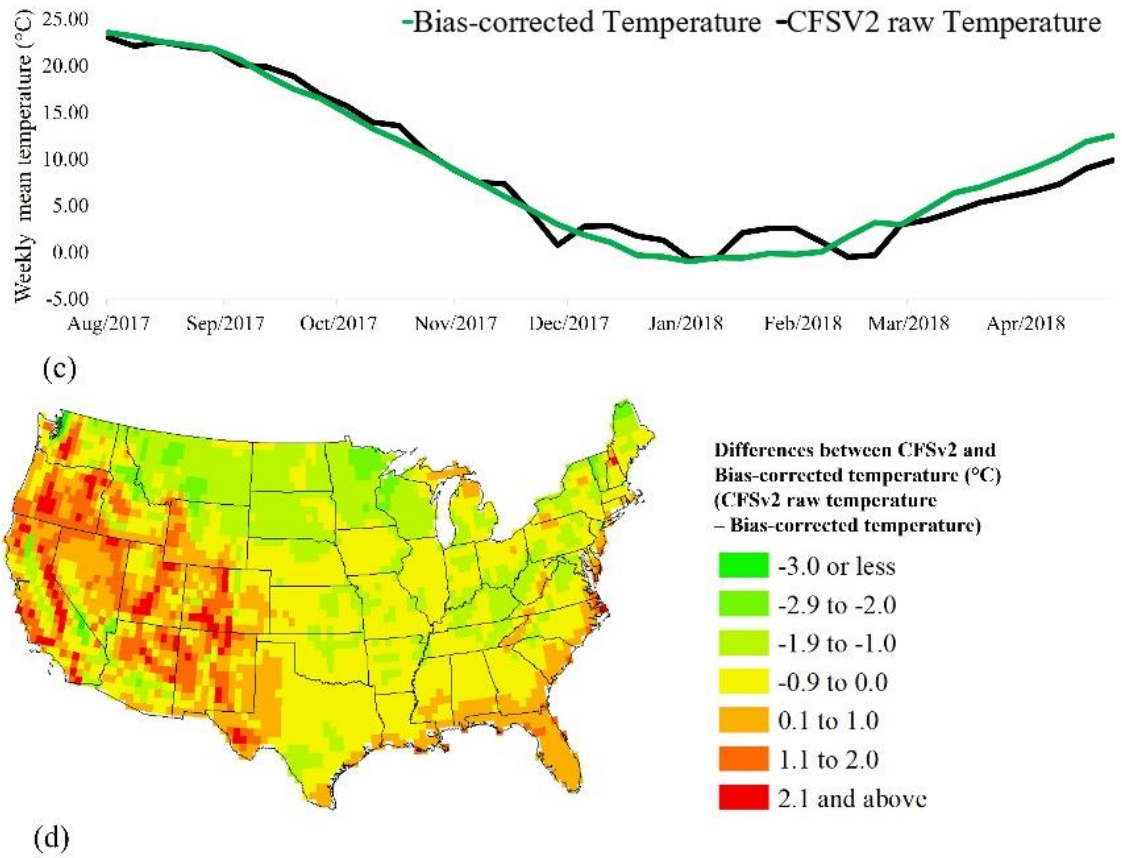

Figure 3. Comparisons of raw and bias-corrected precipitation and temperature from the CFSv2 dataset. (a) Time series for weekly precipitation from raw (black line) and bias-corrected (green) data for the CONUS. The X-axis represents the forecasting period, and the Y-axis shows weekly precipitation. (b) Spatial map of differences between raw and bias-corrected precipitation during the forecasting period (August 2017 to April 2018). Positive values indicate that higher precipitation was estimated by CFSv2 compared to the mean values of historic observations (1979 to July 2017), and they are symbolized as light blue to blue. Negative values indicate that less precipitation was estimated by CFSv2, and they are symbolized as red. (c) Time-series for weekly mean temperature from raw (black line) and bias-corrected (green) data for the CONUS. The X-axis represents the forecasting period, and the Y-axis shows weekly mean temperature. (d) Spatial map of differences between raw and bias-corrected temperature during the forecasting period (August 2017 to April 2018). Positive values indicate that a higher temperature was estimated by CFSv2 compared to the mean values of historic observations (1979 to July 2017), and they are symbolized as orange to red. Negative values indicate that a lower temperature was estimated by CFSv2, and they are symbolized as yellowish green to green.

2.3.3. USDM and drought categories

The USDM is the most representative drought indicator in the U.S. and this indicator produces a weekly map of drought conditions in collaboration with the U.S. Department of Agriculture (USDA), the National Drought Mitigation Center (NDMC), and the National Oceanic and Atmospheric Administration (NOAA) (Svoboda et al. 2002). The USDM is a composite index

that includes many indicators (e.g., Palmer Drought Severity Index, SPI, Keetch-Byram Drought Index, modeled soil moisture, 7-day average streamflow, precipitation anomalies, and satellite vegetation health), climate indices, and local reports from more than 350 expert observers across the entire U.S. Additionally, the USDM provides a weekly map of drought with five drought categories, and is classified based on a percentile approach (Table 1). Furthermore, the USDM can identify both short and long-term drought conditions, and it provides consistent drought conditions in the U.S.

Table 1. Descriptions of drought categories associated with the USDM and drought indices derived from the two models used in this study.

USDM Category	**Description**	**Range of Drought Indices**
D0	Abnormally dry	−0.50 to −0.79
D1	Moderate drought	−0.80 to −1.29
D2	Severe drought	−1.30 to −1.59
D3	Extreme drought	−1.60 to −1.99
D4	Exceptional drought	−2.0 or less

2.3.4. Drought indices

In this study, the VIC and SWAT models were used to compute the input variables of several drought indices such as the Standardized Soil Moisture Index (SSI), the Standardized Baseflow Index (SBI), and the Multivariate Standardized Drought Index (MSDI) to assess the historic and forecasted drought conditions in the CONUS. For example, model-estimated baseflow was used to compute SBI, and soil moisture was used to calculate the SSI and MSDI.

The computation of multivariate drought indices included using joint probability and distribution models (Hao and Aghakouchak, 2013; Aghakouchak, 2015; Kang and Sridhar, 2017), and the MSDI was computed using the joint probability of long-term precipitation and soil moisture records (Hao and Aghakouchak, 2013; Aghakouchak, 2015). The joint distribution of two variables is described as:

$$P(X \leq x, Y \leq y) = p \tag{1}$$

where p is the joint probability of the precipitation and soil moisture. Additionally, the MSDI can be computed as follows (Hao and Aghakouchak, 2013):

$$\text{MSDI} = \emptyset^{-1}(p) \tag{2}$$

where $\emptyset$ is the standard normal distribution function.

In this study, the Gringorten plotting position formula, which is an alternative calculation that can be used to compute empirical joint probability, was used (Gringorten 1963; Yue et al. 1999; Benestad and Haugen 2007) and is defined as follows:

$$P(x_k, y_k) = \frac{m_k - 0.44}{n + 0.12} \tag{3}$$

where m_k is the number of occurrences of the pair (x_i, y_i) for $x_i \leq x_k$ and $y_i \leq y_k$, and n is the number of the observations. To compute SSI and SBI, the univariate form of the Gringorten plotting formula (Equation 4) (Gringorten, 1963) was used and is defined as follows:

$$P(x_i) = \frac{i - 0.44}{n + 0.12} \tag{4}$$

where n is the number of observations and i is the rank of the observed values from the smallest to the largest. The weekly scales of SSI, SBI, and MSDI (25-week scale) were computed using the input and output variables from the VIC and SWAT models, and were subsequently used to evaluate historic and forecasted drought conditions in the CONUS.

2.4. Results and Discussion

2.4.1. Validation of Retrospective Drought Conditions with USDM

2.4.1.1. Comparisons to USDM Drought Maps of Drought Areas

The drought severity maps from the drought indices and the two models were compared with the respective USDM drought severity maps to evaluate the accuracy of the drought indices. Figure 4 provides comparisons of the drought indices from two models and the USDM severity

areas for the retrospective period, which is from January 2012 to July 2017. Since the USDM drought areas were estimated based on a weekly time step, the three drought indices (MSDI, SSI, SBI) were calculated at the same temporal scale for the corresponding dates with USDM. Overall, the total drought area for the CONUS region decreased in the retrospective period, and the overall trend of drought areas was captured by the drought indices from the two models.

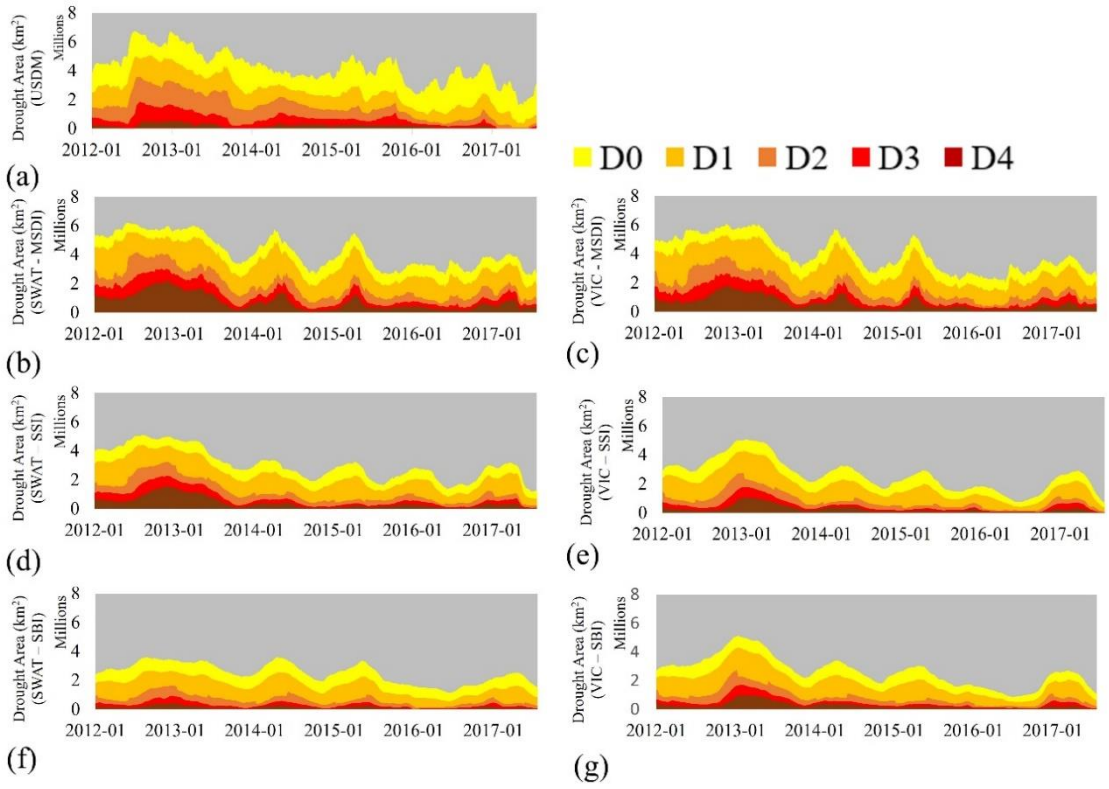

Figure 4. Weekly Comparisons of drought areas of the United States Drought Monitor (USDM) and drought indices computed from the Variable Infiltration Capacity (VIC) and Soil and Water Assessment Tool (SWAT) models for the period between 2012 and 2017. (a) Weekly drought categories from the USDM. (b) Weekly drought categories from the results of the SWAT model and MSDI. (c) Weekly drought categories from the results of the VIC model and MSDI. (d) Weekly drought categories from the results of the SWAT model and SSI. (e) Weekly drought categories from the results of the VIC model and SSI. (f) Weekly drought categories from the results of the SWAT model and SBI. (g) Weekly drought categories from the results of the VIC model and SBI.

For the results of MSDI, mean values of total drought area (D0 to D4 categories) were 4.22 million km^2 and 3.95 million km^2 for the SWAT and VIC models, respectively. Additionally, mean values of the total drought area were 3.06 million km^2 and 2.61 million km^2 for the SSI simulation and 2.51 million km^2 and 2.65 million km^2 for the SBI simulation. Overall, the MSDI simulations estimated more drought areas than other drought indices, and the SWAT model simulated larger

drought areas except for the results of SBI. Figure 5 shows the mean values of MSDI, SSI, SPI, and QQ, which is the sum of surface runoff and baseflow for the entire CONUS during the retrospective period, and Figure 5a,b show the results of the SWAT and VIC models, respectively. QQ was calculated as the sum of the surface runoff and baseflow, and SPI was computed using precipitation and Equation (4). The same approach was employed with SSI and SBI. As shown in Figure 5, the mean values of MSDI, SSI, SBI, and SPI were −0.70, −0.37, −0.27, and −0.06 for the SWAT model and were −0.49, −0.08, −0.08, and −0.06 for the VIC model. The results of SPI were similar because it used the same precipitation input (CPC precipitation data). However, the mean values of MSDI and SSI from the SWAT model were lower than those from the VIC model, which indicated higher drought severities and larger drought areas from the SWAT model. These results occurred because of the differences in the estimation of runoff between these two models. For instance, the SWAT model used the Soil Conservation Service (SCS) curve number (CN) (USDA Soil Conservation Service, 1972) and the VIC model used the variable infiltration curve method (Wood et al., 1992). For example, SPI values continuously increased during January 2016, and there was a sudden increase in QQ values from the SWAT model (red circled zone). Due to the impact of the peak QQ, the SSI values (orange line) did not follow the SPI values since a higher QQ resulted in lower soil moisture. However, the QQ values from the VIC model at the same time were relatively low, and SSI values followed the SPI. Thus, these results imply that different runoff estimation methods led to differences in simulated soil moisture, and they ultimately impact the results of drought indices and drought assessments. Specifically, the higher sensitivity of the SCS CN method in the SWAT model appeared to cause these discrepancies (Boughton, 1989).

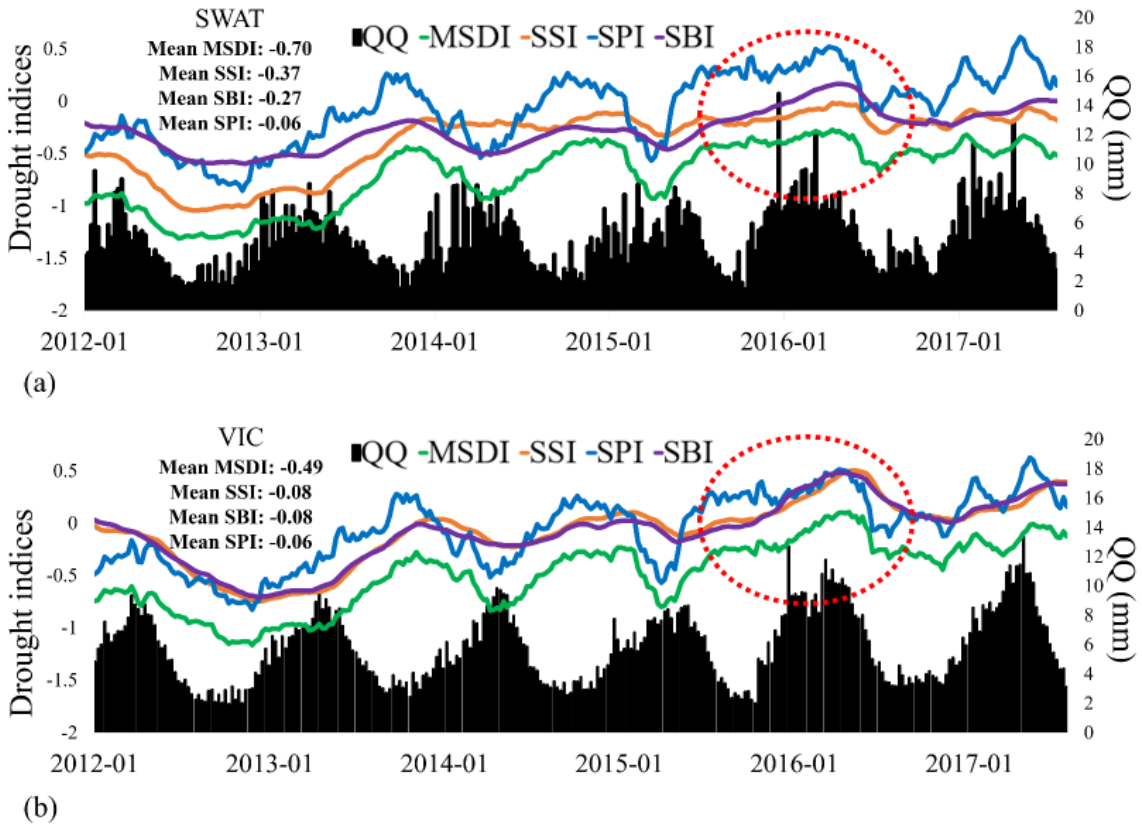

Figure 5. Time-series of mean values of MSDI, SSI, SBI, SPI, and QQ for the CONUS during the retrospective period. Each line indicates the drought index (Green: MSDI, Orange: SSI, Violet: SBI, Blue: SSI), and they are represented by the primary Y-axis (Left). Black bars show the QQ values, and they are represented by the secondary Y-axis (Right). (a) Results of the SWAT model. (b) Results of the VIC model.

Figure 6 shows the values of the drought agreement (DA) area for each drought index. DA was calculated as a rate of intersected areas where drought severities were correctly captured per total area of the USDM. Additionally, Table 2 provides the mean values of DA for the drought indices during the retrospective period. Overall, the performances of the VIC model were slightly higher than those of the SWAT model from all the three drought indices, and it was also affected by the different methods water budget estimation associated with the SWAT and VIC models. Additionally, the retrospective period (2012 to 2017) was the time that the second lowest precipitation (six-year mean) was recorded in the last 30 years in the CONUS (Table 3). The SWAT model responded more sensitively than the VIC model, which was represented by the lower mean values of the drought indices (e.g., MSDI and SSI) (Figure 5).

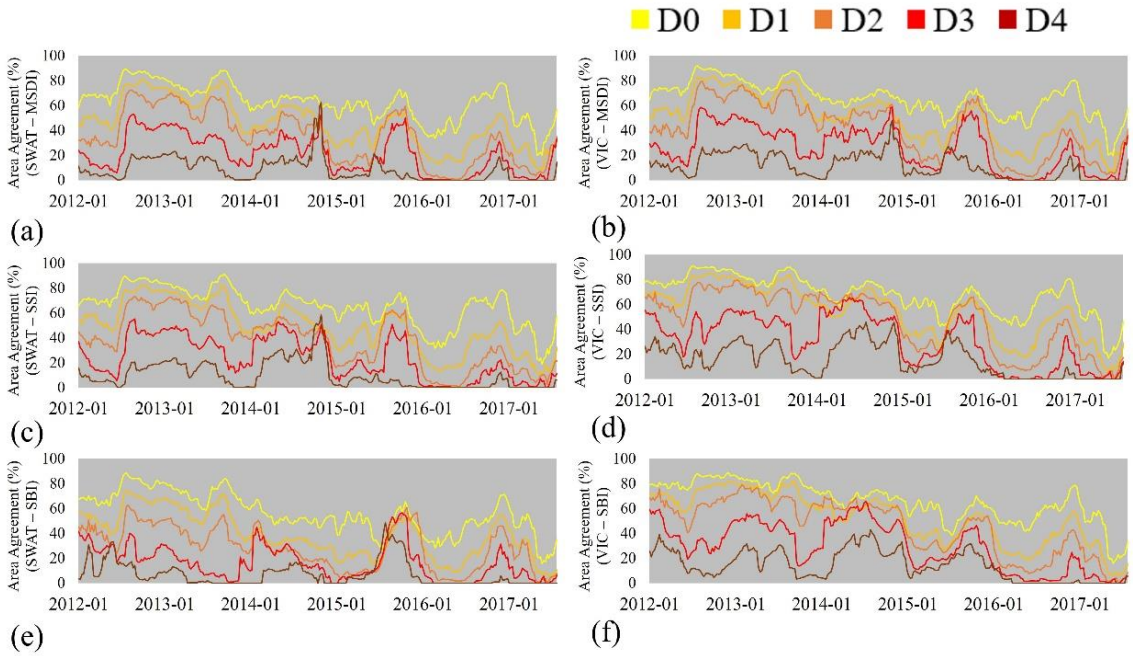

Figure 6. Weekly time-series of Drought Agreement (DA) values for each drought category from the two models. The DA was calculated as the ratio of the intersected area to the total area of the USDM (Intersected area/USDM area). (a) DA values of MSDI from the SWAT model. (b) DA values of MSDI from the VIC model. (c) DA values of SSI from the SWAT model. (d) DA values of SSI from the VIC model. (e) DA values of SBI from the SWAT model. (f) DA values of SBI from the VIC model.

Table 2. Mean drought agreement (DA) values for three drought indices from the SWAT and VIC models during the retrospective period (January 2012 to July 2017) (unit: %).

Model	Drought Indices	D0	D1	D2	D3	D4
SWAT-DA	MSDI	63	45	35	21	9
	SSI	65	48	37	23	9
	SBI	55	38	28	16	7
VIC-DA	MSDI	66	49	41	26	12
	SSI	67	54	47	30	15
	SBI	65	51	44	28	14

Table 3. Annual precipitation and six years' mean precipitation for the CONUS during last 36 years (unit: mm).

Years	Annual Precipitation	Six Years Mean (1982–1983)	Years	Annual Precipitation	Six Years Mean (1988–1993)	Years	Annual Precipitation	Six Years Mean (1994–1999)
1982	848	795	1988	653	770	1994	771	800
1983	869		1989	730		1995	826	
1984	784		1990	812		1996	858	
1985	750		1991	816		1997	798	
1986	793		1992	792		1998	847	
1987	729		1993	819		1999	699	
Years	Annual Precipitation	Six years mean (2000–2005)	Years	Annual Precipitation	Six years mean (2006–2011)	Years	Annual Precipitation	Six years mean (1982–1983)
2000	686	726	2006	727	765	2012	671	754
2001	699		2007	734		2013	746	
2002	699		2008	789		2014	750	
2003	735		2009	808		2015	825	
2004	810		2010	789		2016	771	
2005	730		2011	741		2017	759	

The DA values of MSDI, SSI, and SBI from the VIC model (66%, 67%, and 65%) and MSDI and SSI from the SWAT model (63% and 65%) were similar, but the accuracy of SBI from the SWAT model was different (55%). In the case of the VIC model, the trends of drought areas (Figure 4) and the time series (Figure 5) of SSI and SBI were analogous, which indicated that soil moisture and baseflow responded comparably under the same hydro-climatologic conditions (e.g., precipitation and temperature). However, the performances of SSI and SBI from the SWAT model were not comparable due to the fluctuation in runoff estimations. In the case of extreme or exceptional drought conditions (D3 or D4), drought areas were partially captured by drought indices, which indicated that drought indices overstated the drought severity. This was mainly because the period of climatology for the drought indices (39 years) was shorter than that of the USDM, which contained a much longer record of ground-based observations (Svoboda et al., 2002; Hao and AghaKouchak, 2014). Additionally, the drought indices were based solely on precipitation, soil moisture, and baseflow conditions, whereas the USDM combined various input variables, even including subjective inputs from local climatologists (Svoboda et al., 2002).

The dataset for the VIC model (Nijssen et al., 2001b) was calibrated by the previous study (Nijssen et al., 2001a). Additionally, the SWAT model was not calibrated, but there were no significant differences between the calibrated VIC and uncalibrated SWAT model for the drought estimation during the retrospective period. The main intent was to evaluate how each of these two models was able to perform in capturing the drought and, interestingly, it was found that the results of uncalibrated model are valid for the CONUS region.

2.4.1.2. Discussions of Drought Categories and USCRN Observation Sites

Figure 7 shows comparisons of soil moisture percentiles from the U.S. Climate Reference Network (USCRN), weekly precipitation and temperature, and USDM drought categories at several sites in the California (CA1), Arizona (AZ1), Kansas (KS1), Alabama (AL1), and Virginia (VA1). Extreme to exceptional drought events (D3 to D4 category) from the results of soil moisture percentile are highlighted by blue boxes, and weekly precipitation and temperature and USDM categories at the corresponding times are highlighted by red boxes. Additionally, Table 4 shows some properties of the USCRN sites. These five sites were selected because various drought severities occurred during the retrospective period, and long-term soil moisture observations were available for these locations. As shown in Figure 7, extreme to exceptional drought events normally occurred under conditions of lower precipitation and higher temperature. However, even though the weekly soil moisture percentile was less than 2% (standard of D4; Table 1), it was not commonly judged as D4 by the USDM for these five sites. However, in the case of other drought categories and total drought events, more drought events occurred at the three sites (AZ1, KS1, and AL1 sites) (Figure 8). Thus, it can be inferred that the USDM maps were usually conservative in designating the exceptional drought conditions (D4), which was the reason that DA values for extreme drought conditions were lower than the abnormal or moderate drought.

Table 4. Some properties of United States Climate Reference Network (USCRN) sites.

Site Name	USCRN Code	Longitude	Latitude	Observation Period
CA1	CA_Fallbrook_5_NE	−123.07	38.32	September 2011—Current
AZ1	AZ_Yuma_27_ENE	−112.34	35.76	August 2009—Current
KS1	KS_Manhattan_6_SSW	−96.61	39.1	August 2009—Current
AL1	AL_Selma_13_WNW	−85.96	34.29	June 2009—Current
VA1	VA_Cape_Charles_5_ENE	−75.93	37.29	June 2011—Current

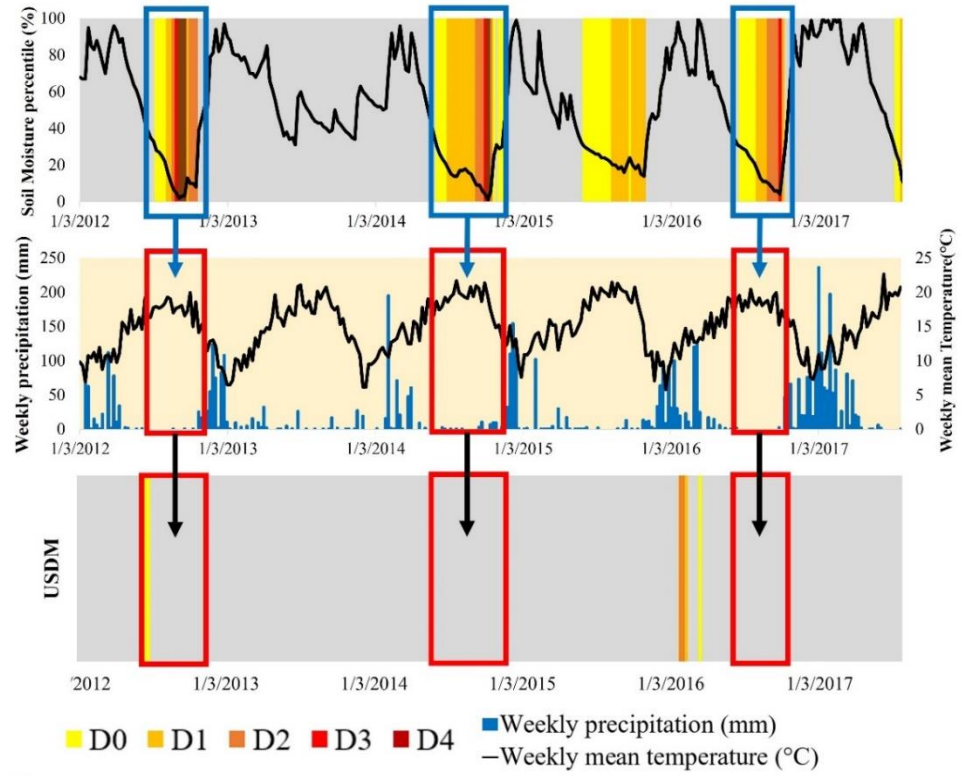
Soil Moisture percentile (%)
Weekly precipitation (mm)
Weekly mean Temperature(°C)
USDM
1/3/2012
1/3/2013
1/3/2014
1/3/2015
1/3/2016
1/3/2017
D0 D1 D2 D3 D4
Weekly precipitation (mm)
Weekly mean temperature (°C)

(a)

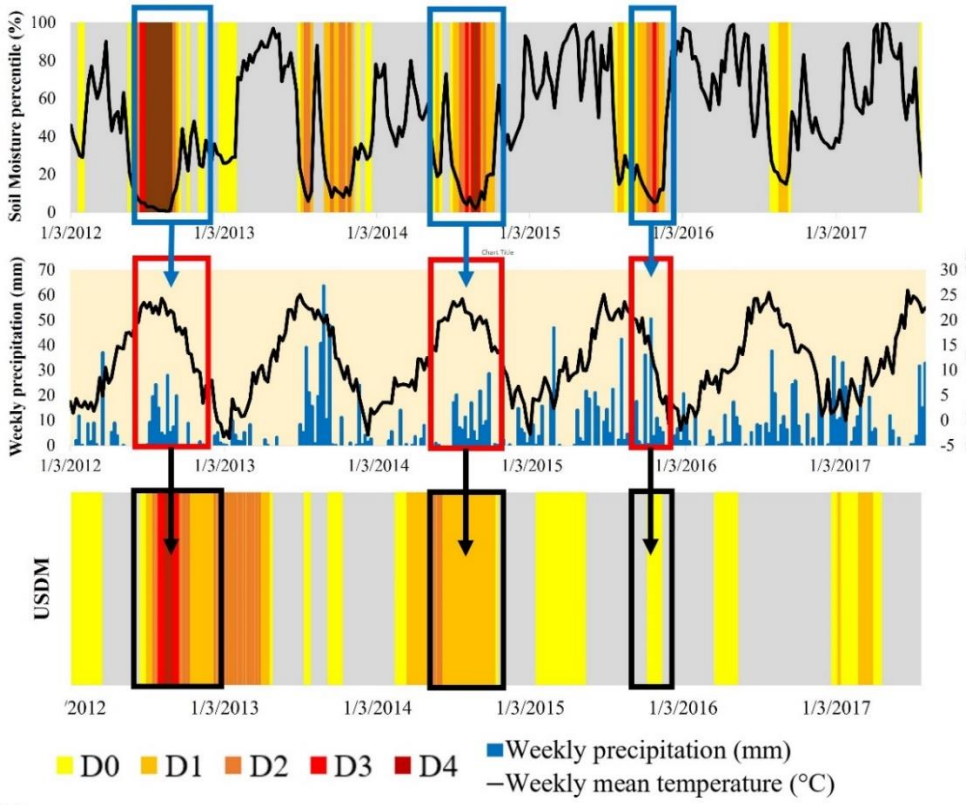
Soil Moisture percentile (%)
Weekly precipitation (mm)
USDM
1/3/2012
1/3/2013
1/3/2014
1/3/2015
1/3/2016
1/3/2017
D0 D1 D2 D3 D4
Weekly precipitation (mm)
Weekly mean temperature (°C)

(b)

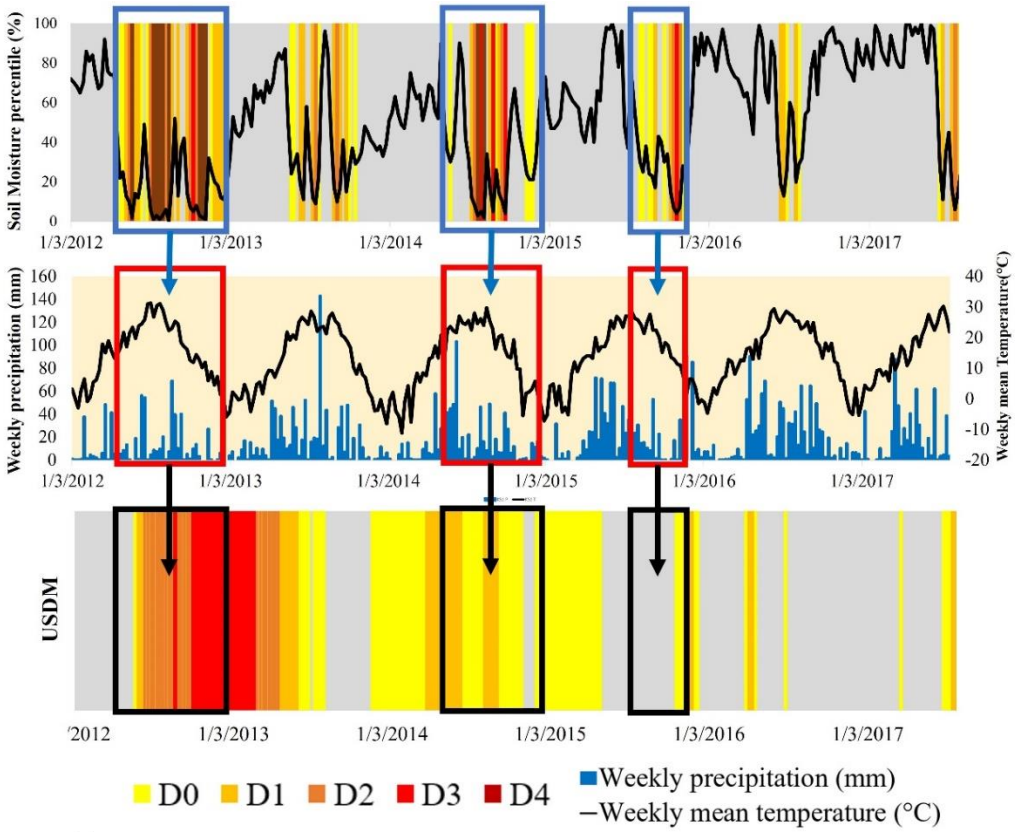
Soil Moisture percentile (%)
Weekly precipitation (mm)
Weekly mean Temperature(°C)
USDM
1/3/2012
1/3/2013
1/3/2014
1/3/2015
1/3/2016
1/3/2017
D0 D1 D2 D3 D4
Weekly precipitation (mm)
Weekly mean temperature (°C)

(c)

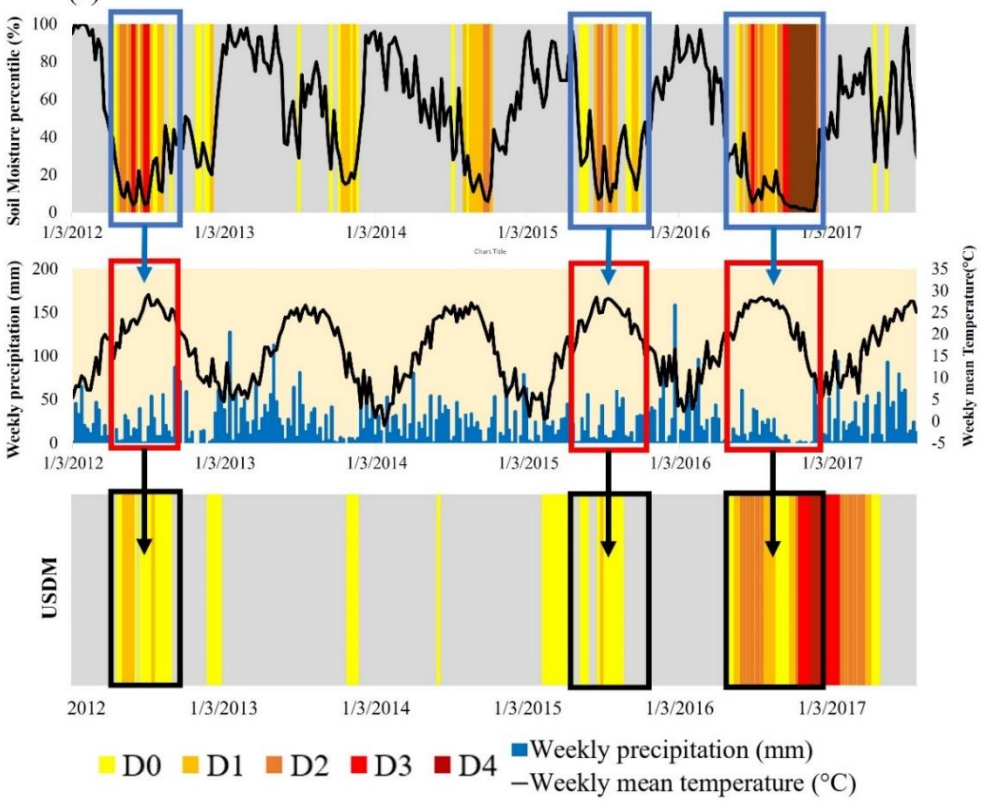
Soil Moisture percentile (%)
Weekly precipitation (mm)
Weekly mean Temperature(°C)
USDM
2012
1/3/2013
1/3/2014
1/3/2015
1/3/2016
1/3/2017
D0 D1 D2 D3 D4
Weekly precipitation (mm)
Weekly mean temperature (°C)

(d)

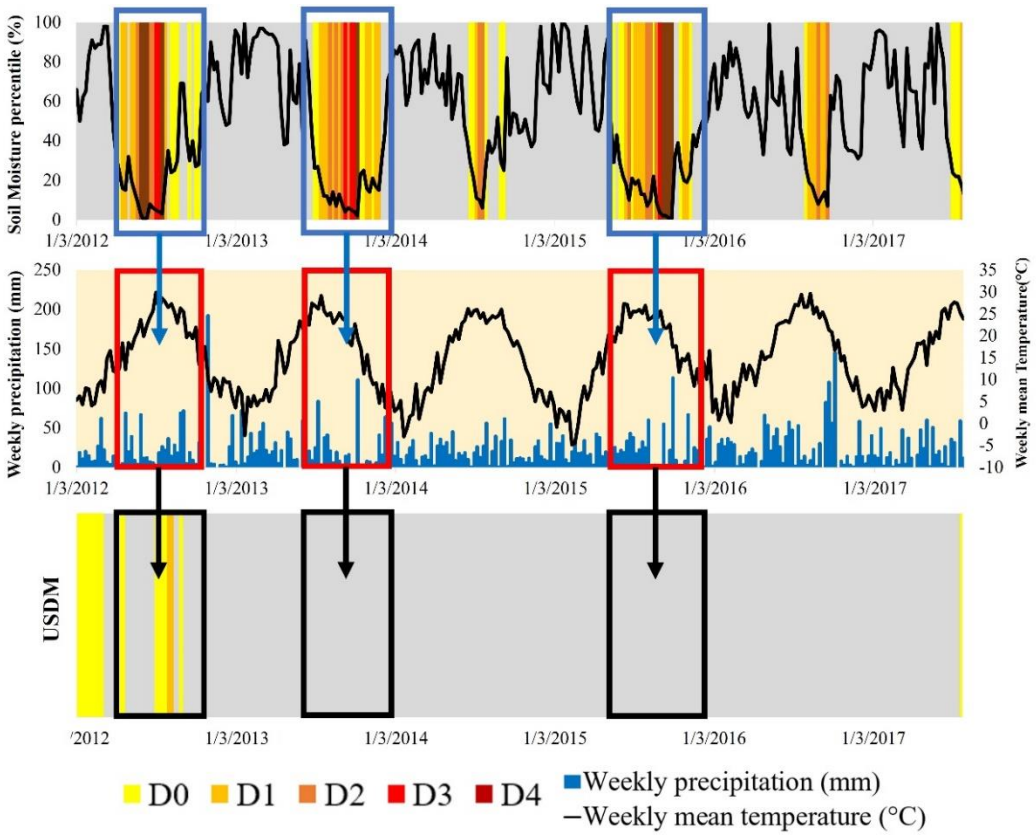

(e)

Figure 7. Time series and color maps of soil moisture percentile (first figure), time series of weekly precipitation and temperature (second map), and color map of the USDM (third figure) at the USCRN observation sites for the retrospective period. For the first map, the black line indicates the time-series of soil moisture percentile, and yellow to brown bars represent drought categories. For the second figure, the black line represents the time-series of weekly mean temperature (°C), and the blue bars indicate the weekly precipitation (mm). For the third figure, the yellow to brown bars represent the drought categories. All boxes represent a period of drought events that includes the D3 or D4 drought category based on soil moisture percentiles (red or brown). (a) Results from the CA1 site. (b) Results from the AZ1 site. (c) Results from the KS1 site. (d) Results from the AL1 site. (e) Results from the VA1 site.

2.4.1.3. Comparisons with USDM Drought Maps (Drought Occurrence-Based)

In this study, model-estimated drought occurrences were evaluated by comparisons with weekly USDM maps for the retrospective period (January 2012 to July 2017), and two performance matrices were used. The matrices are:

(a) Index of agreement (IA, Unit: %): Percent of drought occurrences that correctly captured a drought severity of USDM for the total weeks in the watershed.
(b) Index of disagreement (ID, Unit: %): Percent of drought occurrences that failed to capture a drought severity of USDM for the total weeks in the watershed.

Figure 9 shows a classification of Hydrologic Unit Code 6 (HUC6) watersheds for which IA and ID were estimated. All of the HUC6 watersheds in the CONUS were divided into twelve groups, and each group was assigned a number from one to twelve. Each sub-watershed from the VIC and SWAT models was aggregated to HUC6 resolution, and the X-axis of Figure 9 represents the code numbers of HUC6. As shown in Figure 9, high numbers represent southwestern regions, whereas low numbers indicate northeastern regions in the CONUS. Additionally, Figures 10 and 11 show the IA and ID assessments of MSDI from the two models for five drought severities including abnormal (D0 and drought indices < -0.5), moderate (D1 and drought indices < -0.8), severe (D2 and drought indices < -1.3), extreme (D4 and drought indices < -1.6), and exceptional drought conditions (D4 and drought indices < -2.0). The categorization of drought severities provides a relative accuracy of the drought indices in capturing the USDM of a given severity.

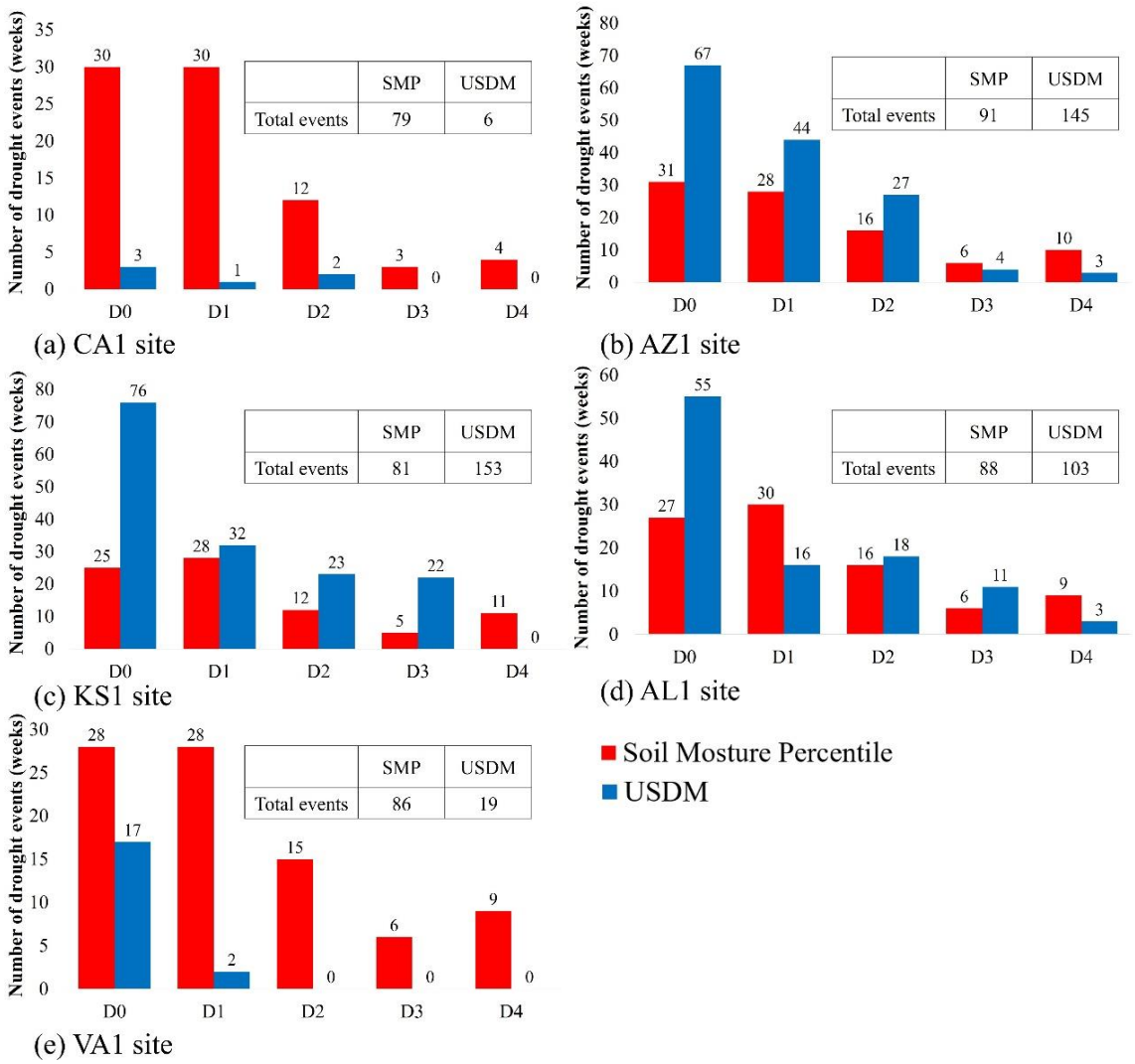

Figure 8. Bar charts and attached tables for drought events (all drought categories) based on soil moisture percentile (SMP) and USDM at USCRN observation sites. The Y-axis represents the number of drought events (weeks) and the X-axis indicates each drought category. The red bars represent drought events based on the soil moisture percentile, whereas blue bars indicate drought events based on the USDM. The attached tables shows the total number of drought events. (a) The CA1 site. (b) The AZ1 site. (c) The KS1 site. (d) The AL1 site. (e) The VA1 site.

The results of IA and ID from MSDI and SSI estimation from two models indicate that the mean values of IA were found to be approximately 70% for D0 category (Table 5) for both the SWAT and VIC models, and the results of the two models were similar. Overall, the IA values in the central to southwestern regions were normally higher than in the northeastern areas. Figure 12a,b show the total drought occurrences suggested by the USDM and annual precipitation during the retrospective period (January 2012 to July 2017, 291 weeks). The amount of precipitation was understandably low in areas where a higher number of droughts occurred, and certain areas were

affected by droughts for the entire period (e.g., California). Additionally, it was found that the ID values were higher in areas with high precipitation, and there was a linear relationship between annual precipitation and ID values. The correlation coefficient obtained from Pearson's correlation test was 0.54 (p-value < 0.05), and the R2 value was 0.29 (p-value < 0.05) with a 95% of confidence interval (Figure 12c).

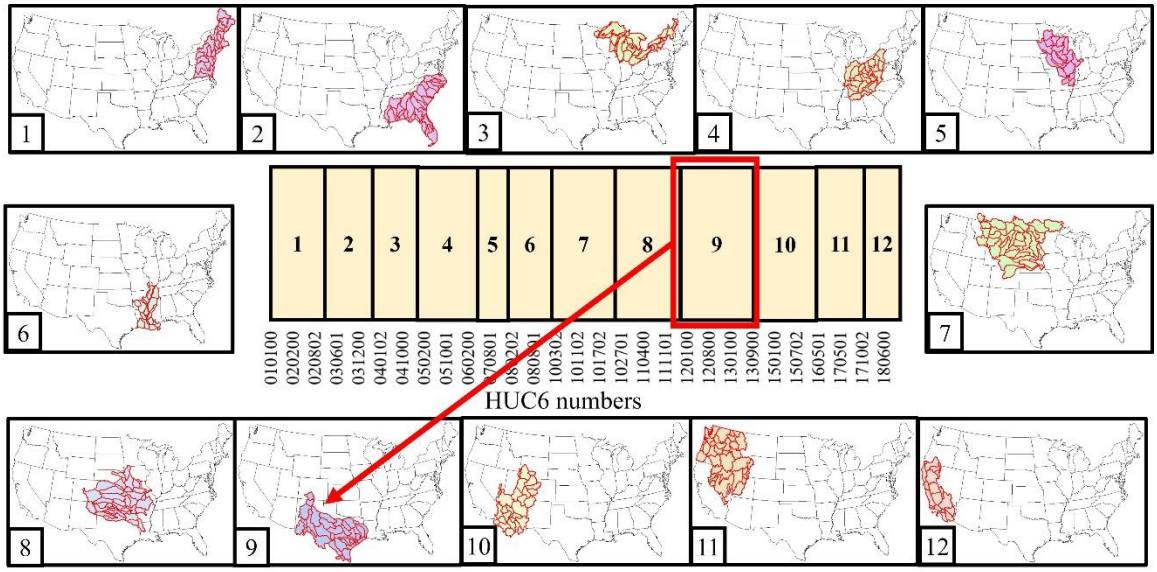

Figure 9. Classification of Hydrologic Unit Code 6 (HUC6) watersheds. The X-axis represents the code numbers of HUC6. All of the HUC6 watersheds in the CONUS were classified into twelve groups, and each group was assigned a number from one to twelve. For example, HUC6 watersheds starting with the numbers "12" and "13" were assigned to group number "9", which is highlighted with the red box and arrow.

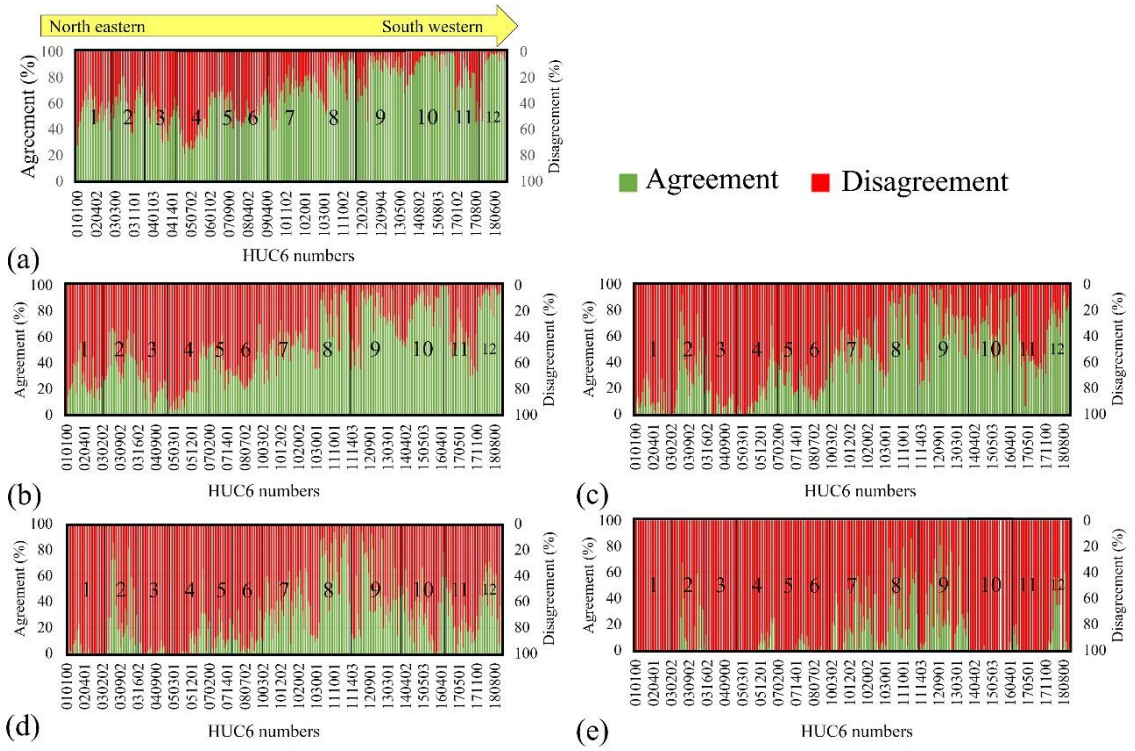

Figure 10. Results of drought occurrence evaluations for all HUC 6 watersheds for the CONUS (317 sub-watersheds): Index of Agreement (IA) and Index of Disagreement (ID) between the USDM and MSDI from the SWAT model for five drought categories during the retrospective period (January 2012 through July 2017). The Y-axis on the left (primary axis) represents the values of agreement, whereas the Y-axis on the right (secondary axis) indicates the values of disagreement. The X-axis shows the HUC6 numbers, which were classified into twelve groups (Figure 8). (a) Results of D0. (b) Results of D1. (c) Results of D02 (d) Results of D3. (e) Results of D4.

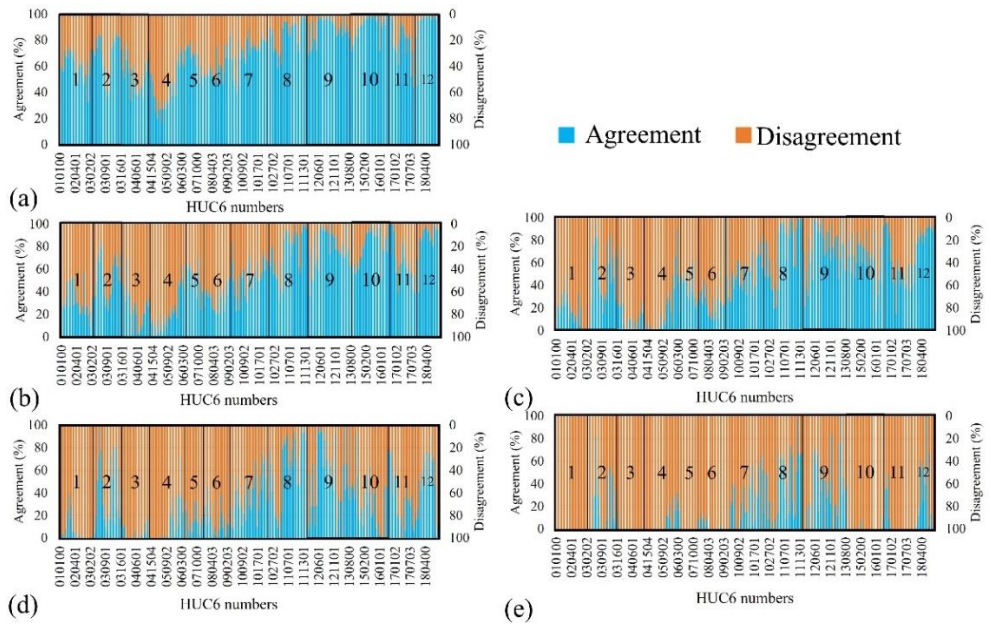

Figure 11. Results of drought occurrence evaluations for all HUC 6 watersheds for the CONUS (317 sub-watersheds): Index of Agreement (IA) and Index of Disagreement (ID) between the USDM and MSDI from the VIC model for five drought categories during the retrospective period (January 2012 through July 2017). The Y-axis on the left (primary axis) represents the values of agreement, whereas the Y-axis on the right (secondary axis) indicates the values of disagreement. The X-axis shows the HUC6 numbers, which were classified into twelve groups (Figure 8). (a) Results of D0. (b) Results of D1. (c) Results of D02 (d) Results of D3. (e) Results of D4.

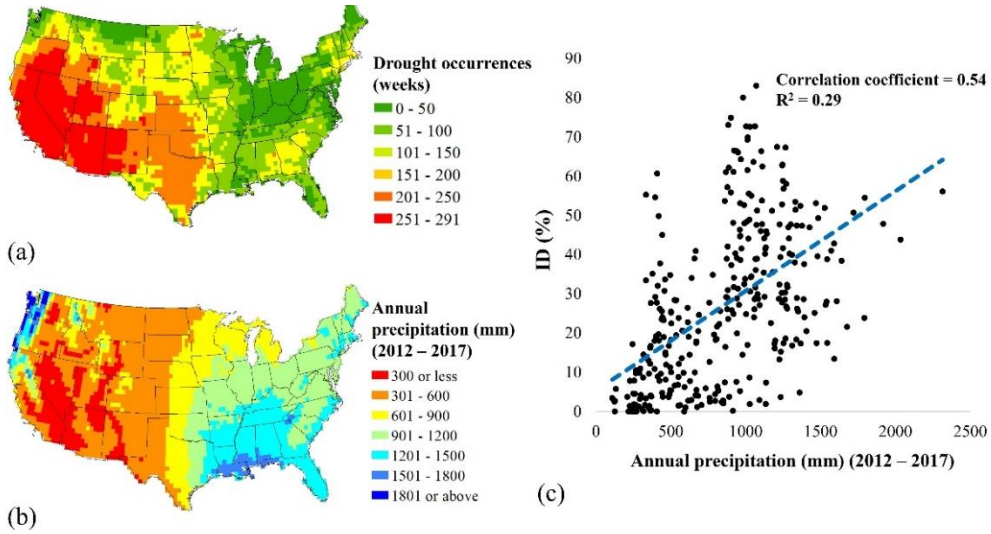

Figure 13. Spatial maps of drought occurrences (unit: weeks) and annual precipitation (unit: mm) using the retrospective period (291 weeks), as well as a scatter plot that shows a relationship between annual precipitation and the Index of Disagreement (ID). (a) Spatial map of drought occurrences. Red areas indicate locations where more droughts occurred, whereas green areas represent regions with fewer droughts. (b) Spatial map of annual precipitation. Red areas indicate locations with lower precipitation, whereas blue areas represent regions with higher precipitation. (c) Scatter plot. The Y-axis represents the ID (%) and the X-axis shows the annual precipitation (mm).

Table 5. Mean values of index of agreement (IA) values for drought indices from the SWAT and VIC models (unit: %).

Model	Drought Indices	D0	D1	D2	D3	D4
SWAT	MSDI	70	53	43	28	12
	SSI	71	56	46	29	12
	SBI	64	48	37	21	7
VIC	MSDI	72	56	48	32	13
	SSI	74	60	52	35	17
	SBI	71	56	47	28	12

In addition, the results indicated that the performances of MSDI were the worst in Region 4 (Ohio River Valley), Region 1 (New England), Region 3 (Great Lakes), and Region 2 (Southeastern U.S.) where drought occurrences were low and annual precipitation was high. This was because the drought indices used in this study were based on the empirical probabilistic method, and they were calculated from a relative comparison of a specific week in each year (Hao and AghaKouchak, 2014). Thus, even if the actual precipitation was higher than in other regions (e.g., Region 4), it would be declared as a drought-hit area when the precipitation at a certain time was lower than the mean precipitation.

2.4.2. Evaluation of Drought Forecasting with Weekly Maps of USDM

In this study, seasonal drought forecasts leading up to nine months into the future using two hydrologic models and the CFSv2 meteorological dataset were developed and analyzed, and forecasted drought areas from drought indices were evaluated with USDM maps. The forecasting period was August 2017 to April 2018, but the drought area evaluation with USDM maps was performed during August 2017 to January 2018, which was expected to serve as a hindcast validation. After July 2017, an increase in drought areas was reported by the USDM (Figure 13a) over a period of six months, and results of all drought indices showed an increase in total drought areas. Compared to the last week of July 2017, there was a 2% increase in the first week of October, a 48% increase in the third week of December, and a 59% increase in the second week of January 2018 from the USDM results.

Table 6 shows the mean DA values for all drought indices and categories from the two models, and Figure 14 shows the time series of DA values for two models and drought indices. Overall, the results of MSDI were the highest among the drought indices, and the abnormal drought

category (D0) was the highest. The DA values of MSDI from the SWAT model were 64, 60, 47, 34, and 25% for all drought categories, and 62, 61, 48, 35, and 25% for the VIC model. Thus, the results of the MSDI implied that the MSDI was better than the other drought indices for forecasting purposes, and the performances of the two models were similar since the mean value of differences for all drought categories was less than 2%. Additionally, DA values for SSI were 42, 35, 16, 2, and 1% for the SWAT model and were 35, 27, 9, 2, and 0% for the VIC model. Finally, DA values for SBI were 25, 13, 6, 2, and 0% for the SWAT model and were 29, 22, 9, 2, and 0% for the VIC model. Thus, results of drought forecasting imply that the predictability of drought forecasting using only one variable (i.e., soil moisture and baseflow) was more uncertain than multiple variables.

The mean DA values of MSDI were the highest in the two models, and DA values decreased as the drought severity increased. These results imply that a drought index considered by one hydro-meteorological variable is more uncertain in forecasting drought conditions. Additionally, the disagreement rates of simulated drought conditions increase with increasing lead-time of the forecast (Figure 14), which would be closely associated with increasing meteorological uncertainty from CFSv2 with increasing lead time. Hao and AghaKouchak (2014) described the properties of the MSDI, and the MSDI was able to capture the drought onset comparable to the precipitation pattern and was able to capture drought persistence similar to the soil moisture, which implied the improved performance of drought monitoring compared to the SPI or SSI. Additionally, the MSDI showed advanced achievements in certain areas where the SPI or SSI did not properly represent the drought conditions. Thus, it can be said that these properties of the MSDI also lead to better performances of drought forecasting with mitigating uncertainties.

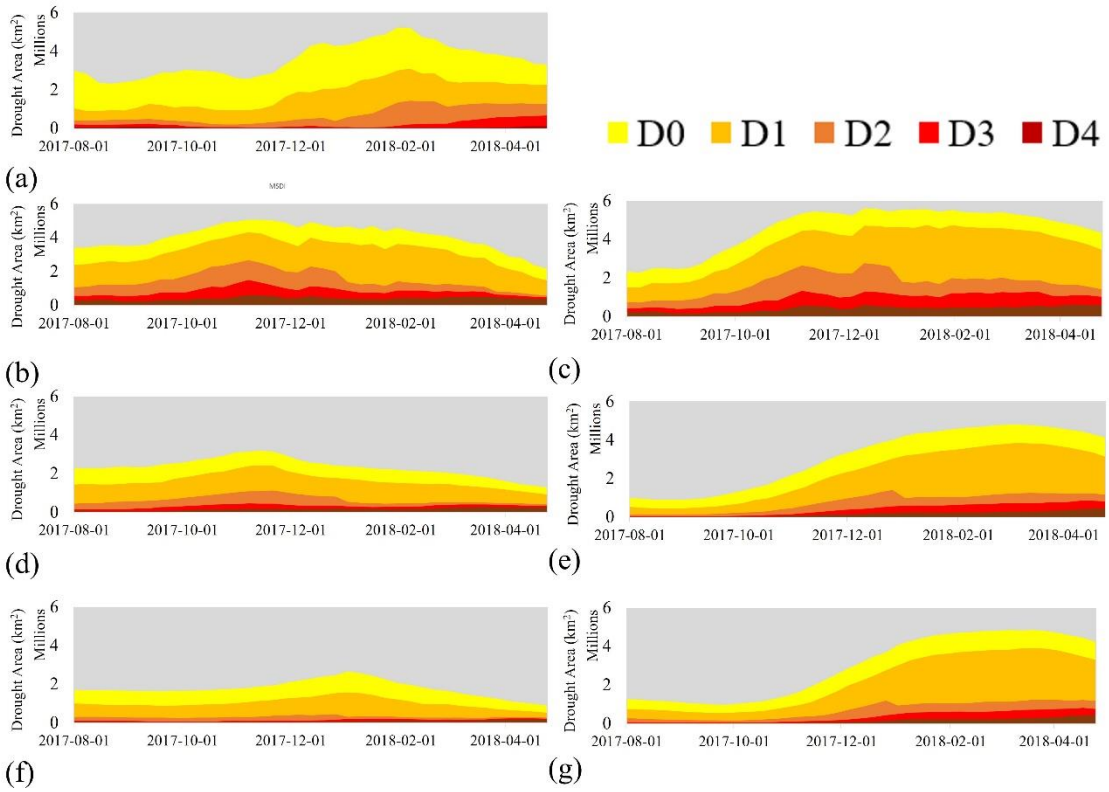

Figure 13. Weekly Comparisons of drought areas of the USDM and drought indices computed from the VIC and SWAT models for the period between 2012 and 2017. (a) Weekly drought categories from the USDM. (b) Weekly drought categories from the results of MSDI from the SWAT model. (c) Weekly drought categories from the results of MSDI from the VIC model. (d) Weekly drought categories from the results of SSI from the SWAT model. (e) Weekly drought categories from the results of SSI from the VIC model. (f) Weekly drought categories from the results of SBI from the SWAT model. (g) Weekly drought categories from the results of SBI from the VIC model.

Table 6. Mean DA values for drought indices and categories from the two models for the forecasting period between August 2017 and January 2018 (unit: %). Higher values indicate that the drought indices captured drought conditions better compared to USDM categories.

Model	Drought Indices	D0	D1	D2	D3	D4
SWAT	MSDI	64	60	47	34	25
	SSI	42	35	16	2	1
	SBI	25	13	6	2	0
VIC	MSDI	62	61	48	35	25
	SSI	35	27	9	2	0
	SBI	29	22	9	2	0

Figures 15 shows spatial maps and bar charts that indicate increases in precipitation and temperature uncertainty with increasing lead time. Figure 15a shows the spatial maps for grids where the absolute values of differences between monthly CPC observations and CFSv2 exceed 20 mm for the forecasting period (August 2017 to January 2018). If a value obtained by subtracting the CPC observation from CFSv2 is less than −20 mm, it is symbolized as red, and represents an underestimation of precipitation by CFSv2. However, if a value is more than 20 mm, it is displayed in green, and indicates an overestimation by CFSv2. Additionally, Figure 15b shows the total number of grids that exceed −20 or 20 mm for each month of the forecasting period. Figures 15c,d show the results of monthly temperature with the same approach, but the exceedance level is 1 °C. As shown in Figures 16b and 15d, the total number of grids increased with lead time for both precipitation and temperature, which indicated increasing meteorological uncertainty from CFSv2. In addition, another possible uncertainty was the resolution of the CFSv2 dataset (0.937°) and the kriging interpolation because it downscaled 926 grids (0.937°) to 3275 grids (0.5°).

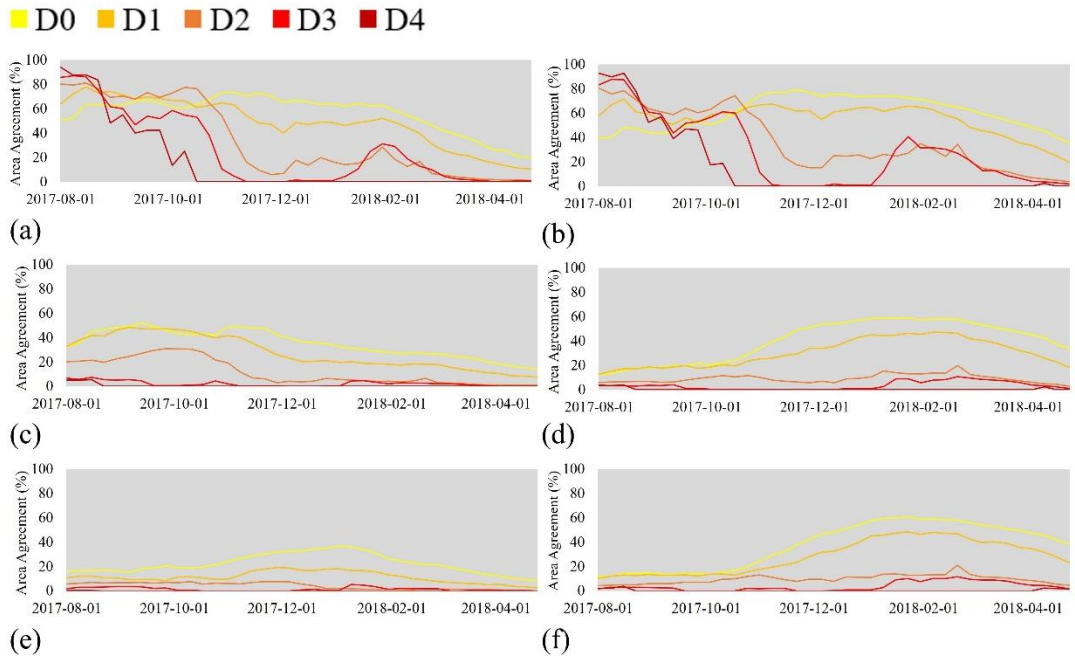

Figure 14. Weekly time series of Drought agreement (DA) values of drought indices from the two models for the forecasting period (August 2017 to April 2018). The DA was calculated as a ratio of the intersected area to the total area of USDM (Intersected area between USDM and drought indices/USDM). (a) Weekly time-series of DA from the results of MSDI from the SWAT model. (b) Weekly time-series of DA from the results of MSDI from the VIC model. (c) Weekly time-series of DA from the results of SSI from the SWAT model. (d) Weekly time-series of DA from the results of SSI from the VIC model. (e) Weekly time-series of DA from the results of SBI from the SWAT model. (f) Weekly time-series of DA from the results of SBI from the VIC model.

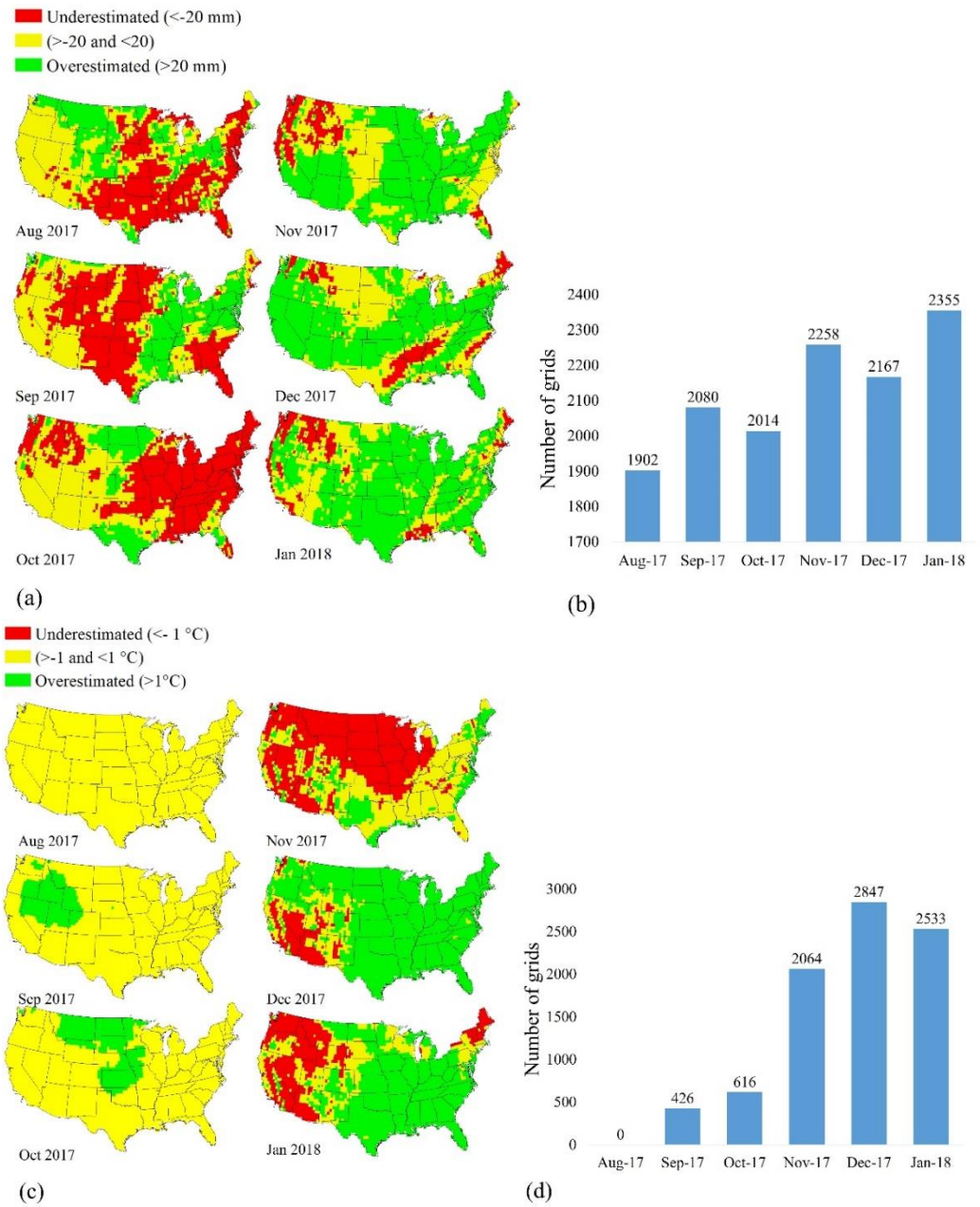

Figure 15. Spatial maps and bar charts for a number of grids where the absolute value of differences between monthly precipitation from CPC observations and CFSv2 exceed 20 mm, and monthly mean temperature exceed 1 °C. (a) Spatial maps for a number of grids where the absolute values of differences between monthly precipitation from CPC observation and CFSv2 exceed 20 mm. If a value obtained by subtracting the CPC observation from CFSv2 is less than −20 mm, it is symbolized as red and represents an underestimation compared to CFSv2. However, if the value is more than 20 mm, it is displayed in green and indicates an overestimation compared to CFSv2. Finally, if the value is between −20 and 20 mm, it is symbolized as yellow. (b) Total number of grids where the absolute values of monthly differences exceed 20 mm (c) Spatial maps for a number of grids where the absolute values of differences exceed 1 °C. If a value obtained by subtracting the CPC observation from CFSv2 is less than − 1 °C, it is symbolized as red and represents an underestimation compared to CFSv2. However, if the value is more than 1 °C, it is displayed in green and indicates an overestimation compared to CFSv2. Finally, if the value is between −1 °C and 1 °C, it is symbolized as yellow. (d) Total number of grids where the absolute values of monthly differences exceed 1 °C for the forecasting period

Figure 16 shows drought severity maps for the CONUS that indicate forecasted drought conditions from the drought indices from August 2017 to January 2018. During the first two months (August and September 2017) with the MSDI estimation, the mean values of DA for all drought categories were 68% and 63% for the SWAT and VIC models, respectively. Thus, it can be said that drought areas and all severities were relatively comparable with the USDM for the first two months. However, during the next two months (October and November 2017), the mean DA values were 42% and 43% for the SWAT and VIC models. Additionally, the mean DA values were 26% and 33% for the last two months (December 2017 to January 2018). More specifically, from November 2017 through January 2018, there were overestimations of predicted droughts (e.g., California, Oregon, and Washington) by the two models, and some of the actual drought conditions from the USDM were not captured by the two models (e.g., Arizona). These results also imply that simulating drought conditions with increasing lead-time of the forecast is dependent on the accuracy of temperature and precipitation forecasts derived from the climate models.

Additionally, an analysis of drought occurrence probabilities for the forecasting period was carried out. Figure 17 the comparisons of drought probability from the USDM, VIC-MSDI, and SWAT-MSDI. Due to the meteorological uncertainties from the CFSv2 (Figure 15), some drought areas were not captured by the MSDI estimations, and some drought areas were overestimated by the MSDI.

Finally, we carried out an analysis of the box and whisker charts for each category of the drought areas for the forecasting period (August 2017 to April 2018). As shown in Figure 18a–e, blues boxes indicate the results of the USDM drought categories, and other boxes indicate the results of drought indices from the SWAT and VIC models. The range of boxes from the MSDI closely overlapped with USDM for the D0 category, which showed the highest DA values during the forecasting period.

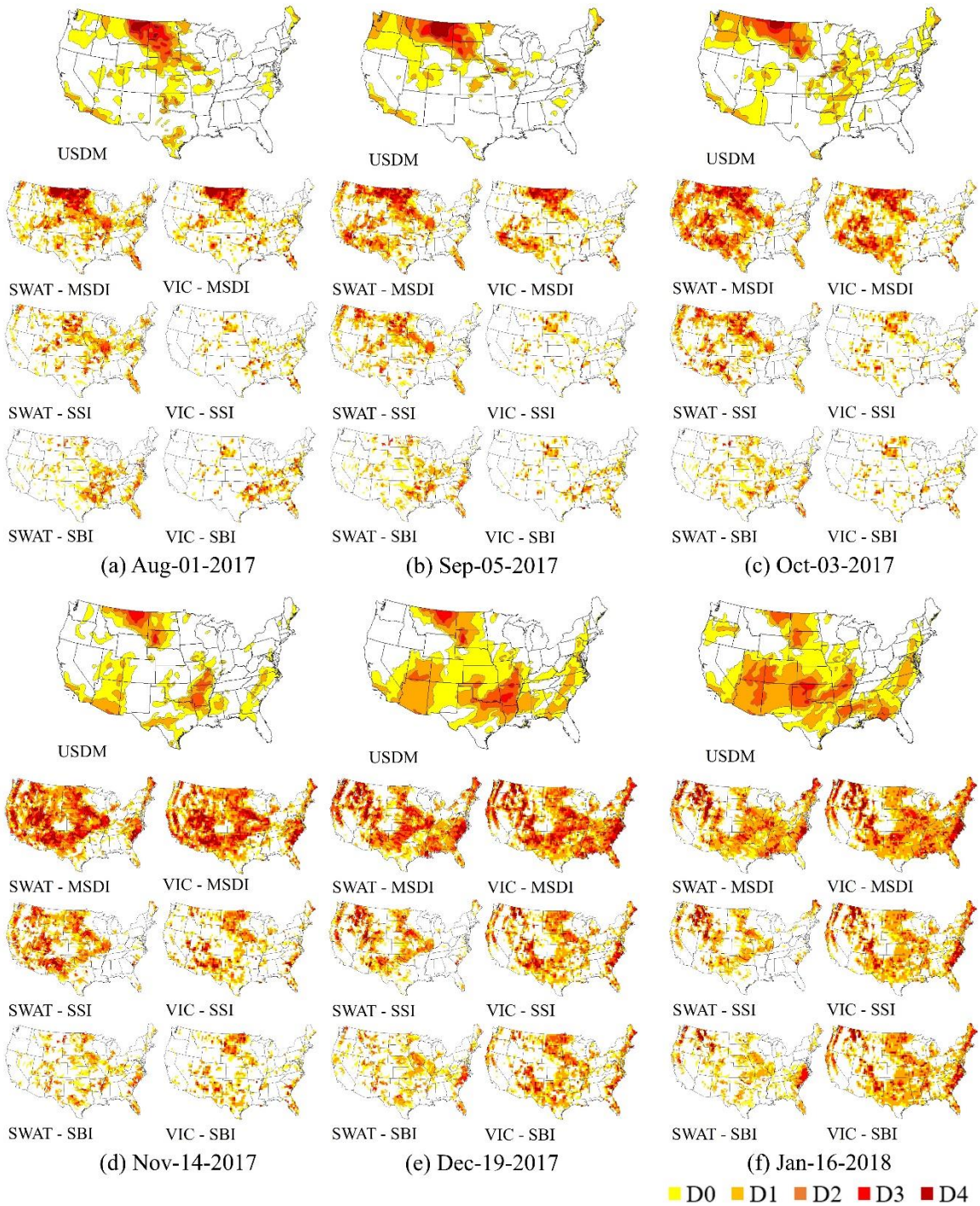

Figure 16. Spatial maps of drought conditions from the USDM and drought indices from the SWAT and VIC models for the forecasting period (August 2017 to April 2018). For the USDM, MSDI, SSI, and SBI maps, yellow to brown areas represent the five categories of drought conditions. (a) USDM and MSDIs for 1 August 2017. (b) USDM and MSDIs for 5 September 2017. (c) USDM and MSDIs for 3 October 2017. (d) USDM and MSDIs for 14 November 2017. (e) USDM and MSDIs for 19 December 2017. (f) USDM and MSDIs for 16 January 2018.

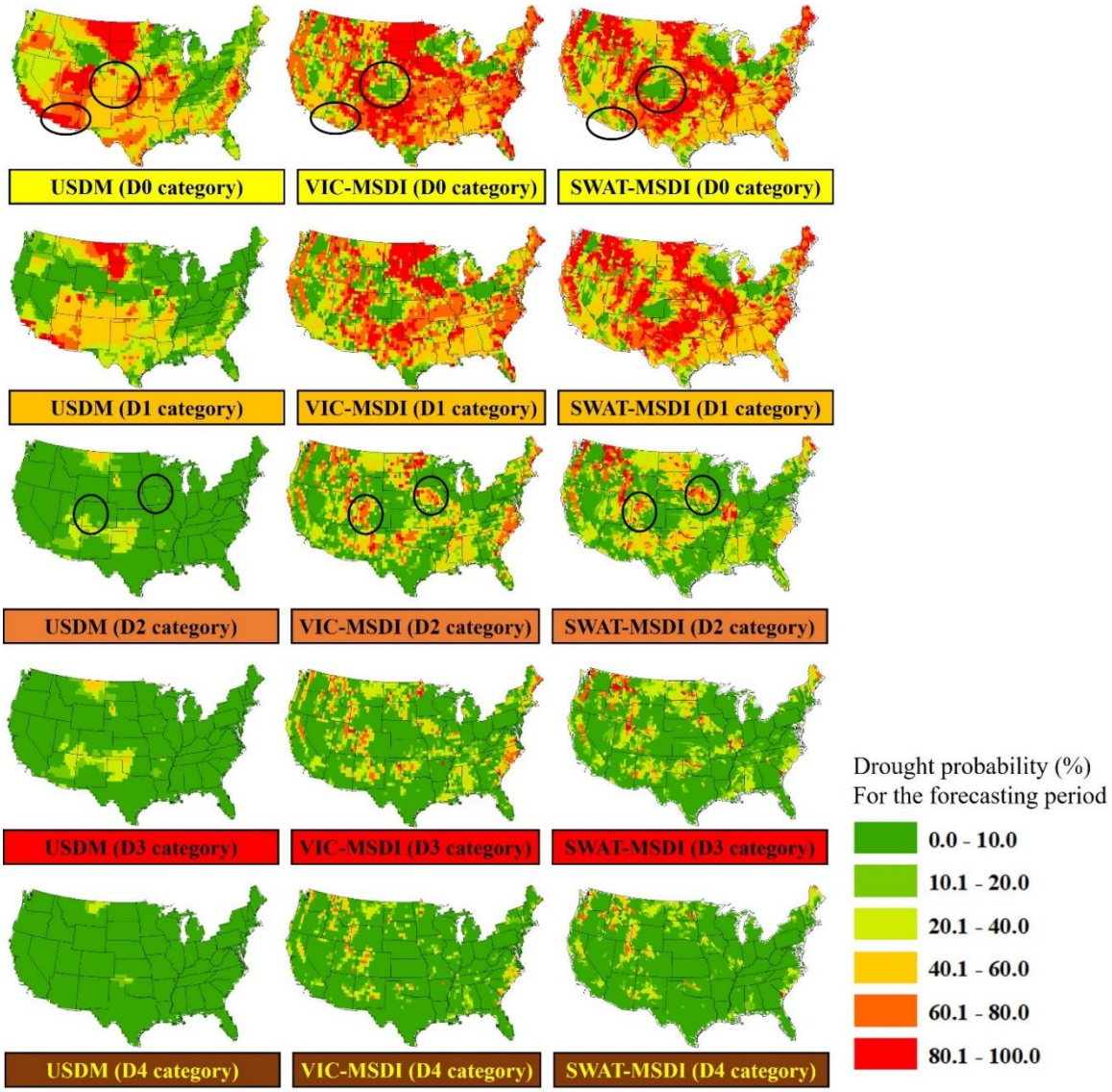

Figure 17. Spatial maps of drought probability for the USDM, VIC-MSDI, and SWAT-MSDI during the forecasting period (August 2017 – April 2018). Yellow, orange, and red areas represent the higher drought probability, while green areas represent lower drought probability.

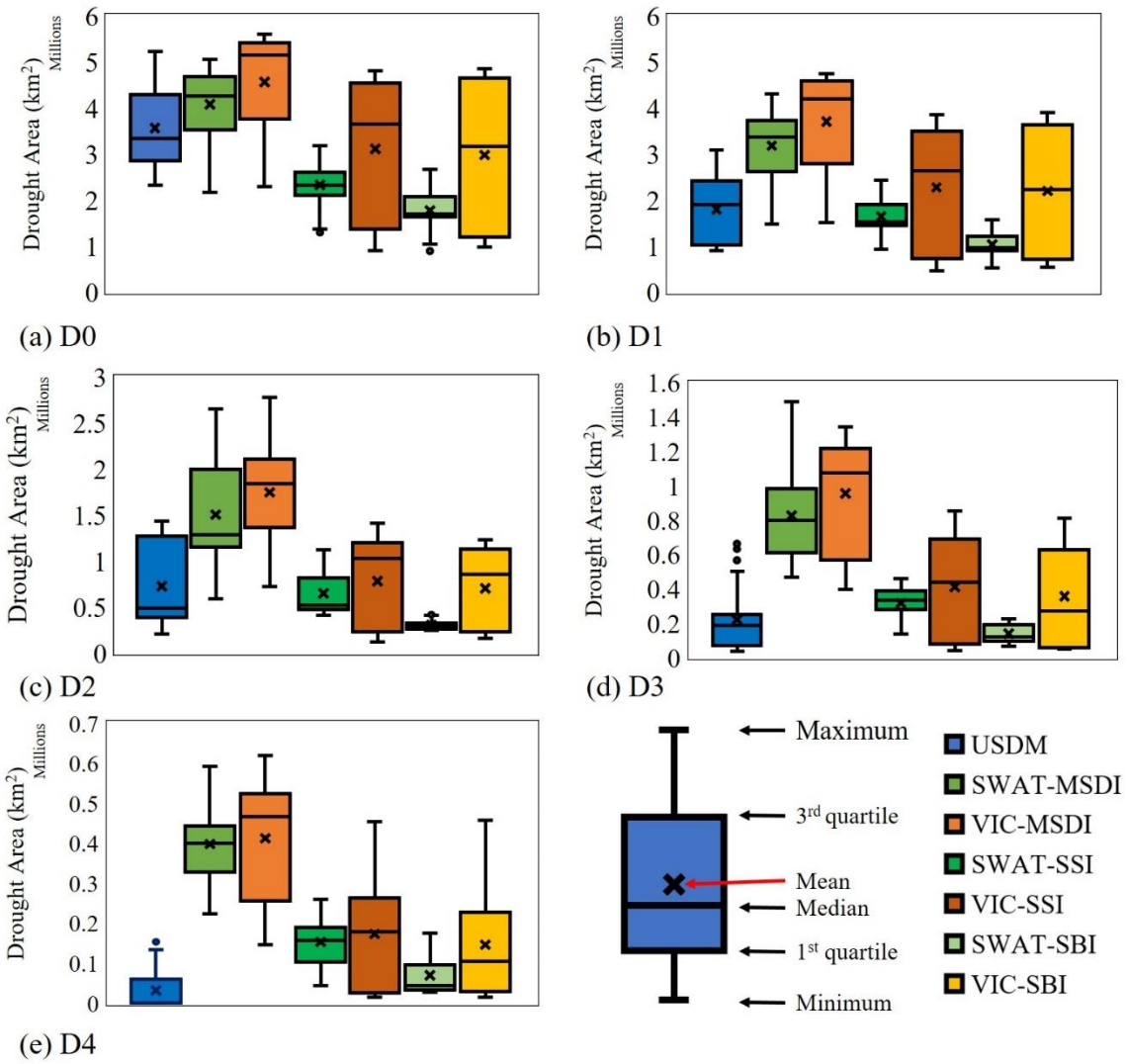

Figure 18. Box and whisker charts for each category of the drought areas. Each color of boxes represents the results of USDM and drought indices for the forecasting period (August 2017 to April 2018). The blue box shows the results of USDM, the green box represents SWAT-MSDI, orange boxes represent VIC-MSDI, the blue-green box represents SWAT-SSI, the brown box represents VIC-SSI, light green represents SWAT-SBI, and yellow box represents VIC-SBI. The upper and lower whiskers represent maximum and minimum values, first quartile represents 25%, median represents 50%, and third quartile represents 75% of the values.

2.5. Conclusion

A reliable drought monitoring and forecasting framework is essential for water resource management and drought mitigation strategies. This study investigated a retrospective drought simulation and near-real-time drought forecasting method using simulated hydrometeorological variables using the SWAT and VIC models with CFSv2 for the CONUS. The retrospective analysis was performed for January 2012 to July 2017, and drought forecasting was performed for August 2017 through April 2018 with a weekly time step of drought indices. The accuracies of the retrospective and forecasting methods is evaluated by comparisons of the weekly USDM maps and simulated drought maps of drought indices for the CONUS region. The important findings of this study are as follows:

(1) For the retrospective period, the mean DA values were 63% and 66% for the MSDI simulation from the SWAT and VIC models and were 65% and 66% for SSI simulation (D0 category). In addition, the mean IA values were 70% and 72% for the MSDI simulation and were 71% and 72% for the SSI simulation (D0 category). The results imply that drought simulations with two models and multiple drought indices are useful in monitoring overall drought conditions for the CONUS.

(2) For the forecasting period, the mean DA values were 65% and 62% for the MSDI simulation for the SWAT and VIC models, which indicates that a forecast using the MSDI estimation in the SWAT and VIC models with CFSv2 is capable of reliable real-time drought forecasting. However, the mean DA values were 42% and 35% for the SSI estimation and were 25% and 29% for the SBI simulation from the SWAT and VIC models. Thus, an evaluation of drought forecasting using multiple hydrometeorological components (e.g., precipitation and soil moisture) from multiple hydrologic models would provide an advanced understanding of the characteristics of drought and would reduce uncertainties that arise from using only one model and variable.

(3) Drought forecasting by the MSDI estimation for two months of lead time was relatively reliable (68% and 63% for the SWAT and VIC models). However, drought forecasting with increasing lead-times would be associated with increasing meteorological uncertainty.

Additionally, drought forecasting using only one variable (i.e., SSI and SBI) was not predictable even in the first two months (23% and 10% for SSI; 7% and 7% for SBI).

(4) The USDM is commonly conservative in judging an exceptional drought condition (D4), even though percentiles of soil moisture observation were less than 2% (D4 category). However, in the case of other drought categories (D0 to D3), some drought events predicted by the USDM commonly exceeded the results of soil moisture percentiles. Thus, these results would imply an underestimation of exceptional drought area monitoring from the USDM.

(5) For the results of retrospective and forecasting periods, the sources of uncertainties can be manifold; (a) USDM uses a more complicated method than the drought indices; (b) USDM may use other meteorological inputs, not just precipitation and temperature from CPC or CFSv2; (c) there are increasing meteorological uncertainties from CFSv2 with increasing lead time; and (d) the spatial resolutions of CFSv2 and CPC are different.

(6) The proposed method provides weekly drought maps, which is better than the current approach which only provides an overall, seasonal outlook on drought trends (e.g., CPC drought outlook). Additionally, weekly forecasting maps for the entire CONUS can contribute to water resource management, crop planning, drought risk management, and adopting drought mitigation strategies in advance.

Since the proposed approach has some uncertainties associated with estimating drought forecasting, combination with a remote sensing dataset (e.g., NDVI) and multiple climate indices (e.g., North Atlantic Oscillation) would provide a better assessment of drought forecasting in the future (Marj and Meijerink, 2011).

2.6. Reference

AghaKouchak, A., 2014. A baseline probabilistic drought forecasting framework using standardized soil moisture index: application to the 2012 United States drought. Hydrology and Earth System Sciences, 18(7), pp.2485-2492.

AghaKouchak, A., 2015. A multivariate approach for persistence-based drought prediction: Application to the 2010–2011 East Africa drought. Journal of Hydrology, 526, pp.127-135.

Ahn, S.R., Jeong, J.H. and Kim, S.J., 2016. Assessing drought threats to agricultural water supplies under climate change by combining the SWAT and MODSIM models for the Geum River basin, South Korea. Hydrological Sciences Journal, 61(15), pp.2740-2753.

Arnold, J.G., Srinivasan, R., Muttiah, R.S. and Williams, J.R., 1998. Large area hydrologic modeling and assessment part I: model development. JAWRA Journal of the American Water Resources Association, 34(1), pp.73-89.

Arnold, J.G., Moriasi, D.N., Gassman, P.W., Abbaspour, K.C., White, M.J., Srinivasan, R., Santhi, C., Harmel, R.D., Van Griensven, A., Van Liew, M.W. and Kannan, N., 2012. SWAT: Model use, calibration, and validation. Transactions of the ASABE, 55(4), pp.1491-1508.

Ashraf Vaghefi, S., Mousavi, S.J., Abbaspour, K.C., Srinivasan, R. and Yang, H., 2014. Analyses of the impact of climate change on water resources components, drought and wheat yield in semiarid regions: Karkheh River Basin in Iran. hydrological processes, 28(4), pp.2018-2032.

Belayneh, A., Adamowski, J., Khalil, B. and Ozga-Zielinski, B., 2014. Long-term SPI drought forecasting in the Awash River Basin in Ethiopia using wavelet neural network and wavelet support vector regression models. Journal of Hydrology, 508, pp.418-429.

Boughton, W.C., 1989. A review of the USDA SCS curve number method. Soil Research, 27(3), pp.511-523.

Cancelliere, A., Di Mauro, G., Bonaccorso, B. and Rossi, G., 2007. Drought forecasting using the standardized precipitation index. Water resources management, 21(5), pp.801-819.

Changnon, S.A., Pielke Jr, R.A., Changnon, D., Sylves, R.T. and Pulwarty, R., 2000. Human factors explain the increased losses from weather and climate extremes. Bulletin of the American Meteorological Society, 81(3), pp.437-442.

Chen, M., Shi, W., Xie, P., Silva, V., Kousky, V.E., Wayne Higgins, R. and Janowiak, J.E., 2008. Assessing objective techniques for gauge-based analyses of global daily precipitation. Journal of Geophysical Research: Atmospheres, 113(D4).

Clark, J.S., Iverson, L., Woodall, C.W., Allen, C.D., Bell, D.M., Bragg, D.C., D'amato, A.W., Davis, F.W., Hersh, M.H., Ibanez, I. and Jackson, S.T., 2016. The impacts of increasing drought on forest dynamics, structure, and biodiversity in the United States. Global Change Biology, 22(7), pp.2329-2352.

DHS, 2015. National preparedness report, U.S. Dept. of Homeland Security, 1-87.

Griffies, S.M., Harrison, M.J., Pacanowski, R.C. and Rosati, A., 2004. A technical guide to MOM4. GFDL Ocean Group Tech. Rep, 5, p.371.

Griffin, D. and Anchukaitis, K.J., 2014. How unusual is the 2012–2014 California drought?. Geophysical Research Letters, 41(24), pp.9017-9023.

Gringorten, I.I., 1963. A plotting rule for extreme probability paper. Journal of Geophysical Research, 68(3), pp.813-814.

Guttman, N.B., 1999. Accepting the standardized precipitation index: a calculation algorithm. JAWRA Journal of the American Water Resources Association, 35(2), pp.311-322.

Halmstad, A., Najafi, M.R. and Moradkhani, H., 2013. Analysis of precipitation extremes with the assessment of regional climate models over the Willamette River Basin, USA. Hydrological Processes, 27(18), pp.2579-2590.

Hao, Z. and AghaKouchak, A., 2013. Multivariate standardized drought index: a parametric multi-index model. Advances in Water Resources, 57, pp.12-18.

Hao, Z. and AghaKouchak, A., 2014. A nonparametric multivariate multi-index drought monitoring framework. Journal of Hydrometeorology, 15(1), pp.89-101.

Hao, Z., Singh, V.P. and Xia, Y., 2018. Seasonal drought prediction: advances, challenges, and future prospects. Reviews of Geophysics.

Hayes, M., Svoboda, M., Le Comte, D., Redmond, K.T. and Pasteris, P., 2005. Drought monitoring: New tools for the 21st century (pp. 53-69). Taylor and Francis.

Homer, C., Huang, C., Yang, L., Wylie, B. and Coan, M., 2004. Development of a 2001 national land-cover database for the United States. Photogrammetric Engineering & Remote Sensing, 70(7), pp.829-840.

Jones, C.B., 1997 Geographical Information Systems and Computer Cartography. Harlow,Addison Wesley Longman.

Kang, H. and Sridhar, V., 2017. Combined statistical and spatially distributed hydrological model for evaluating future drought indices in Virginia. Journal of Hydrology: Regional Studies, 12, pp.253-272.

Kang, H. and Sridhar, V., 2018. Assessment of Future Drought Conditions in the Chesapeake Bay Watershed. JAWRA Journal of the American Water Resources Association, 54(1), pp.160-183.

Karl, T.R., Gleason, B.E., Menne, M.J., McMahon, J.R., Heim, R.R., Brewer, M.J., Kunkel, K.E., Arndt, D.S., Privette, J.L., Bates, J.J. and Groisman, P.Y., 2012. US temperature and drought: Recent anomalies and trends. Eos, Transactions American Geophysical Union, 93(47), pp.473-474.

Liang, X., Lettenmaier, D.P., Wood, E.F. and Burges, S.J., 1994. A simple hydrologically based model of land surface water and energy fluxes for general circulation models. Journal of Geophysical Research: Atmospheres, 99(D7), pp.14415-14428.

Livneh, B. and Hoerling, M.P., 2016. The physics of drought in the US Central Great Plains. Journal of Climate, 29(18), pp.6783-6804.

Lorenz, D.J., Otkin, J.A., Svoboda, M., Hain, C.R., Anderson, M.C. and Zhong, Y., 2017. Predicting US Drought Monitor states using precipitation, soil moisture, and evapotranspiration anomalies. Part I: Development of a nondiscrete USDM index. Journal of Hydrometeorology, 18(7), pp.1943-1962.

Luo, L. and Wood, E.F., 2007. Monitoring and predicting the 2007 US drought. Geophysical Research Letters, 34(22).

Madadgar, S. and Moradkhani, H., 2013. A Bayesian framework for probabilistic seasonal drought forecasting. Journal of Hydrometeorology, 14(6), pp.1685-1705.

Mao, Y., Nijssen, B. and Lettenmaier, D.P., 2015. Is climate change implicated in the 2013–2014 California drought? A hydrologic perspective. Geophysical Research Letters, 42(8), pp.2805-2813.

Marj, A.F. and Meijerink, A.M., 2011. Agricultural drought forecasting using satellite images, climate indices and artificial neural network. International journal of remote sensing, 32(24), pp.9707-9719.

McEvoy, D.J., 2015. Physically based evaporative demand as a drought metric: Historical analysis and seasonal prediction. University of Nevada, Reno.

McKee, T.B., N.J. Doesken, and J. Kleist, 1993. Drought Monitoring with Multiple Time Series. 8th Conference on Applied Climatology, Boston, American Meteorological Society.

Mishra, A.K. and Singh, V.P., 2009. Analysis of drought severity-area-frequency curves using a general circulation model and scenario uncertainty. Journal of Geophysical Research: Atmospheres, 114(D6).

Mishra, A.K. and Singh, V.P., 2010. A review of drought concepts. Journal of hydrology, 391(1-2), pp.202-216.

Mishra, V., Cherkauer, K.A. and Shukla, S., 2010. Assessment of drought due to historic climate variability and projected future climate change in the midwestern United States. Journal of Hydrometeorology, 11(1), pp.46-68.

Mishra, A.K. and Singh, V.P., 2010. A review of drought concepts. Journal of hydrology, 391(1-2), pp.202-216.

Morid, S., Smakhtin, V. and Bagherzadeh, K., 2007. Drought forecasting using artificial neural networks and time series of drought indices. International Journal of Climatology, 27(15), pp.2103-2111.

Narasimhan, B. and Srinivasan, R., 2005. Development and evaluation of Soil Moisture Deficit Index (SMDI) and Evapotranspiration Deficit Index (ETDI) for agricultural drought monitoring. Agricultural and Forest Meteorology, 133(1-4), pp.69-88.

Neitsch, S.L., Arnold, J.G., Kiniry, J.R. and Williams, J.R., 2011. Soil and water assessment tool theoretical documentation version 2009. Texas Water Resources Institute.

Niemeyer, S., 2008. New Drought Indices. Water Management, 80:267-274,

Nijssen, B., O'donnell, G.M., Hamlet, A.F. and Lettenmaier, D.P., 2001a. Hydrologic sensitivity of global rivers to climate change. Climatic change, 50(1-2), pp.143-175.

Nijssen, B., O'Donnell, G.M., Lettenmaier, D.P., Lohmann, D. and Wood, E.F., 2001b. Predicting the discharge of global rivers. Journal of Climate, 14(15), pp.3307-3323.

Paulo, A., Martins, D. and Pereira, L.S., 2016. Influence of precipitation changes on the SPI and related drought severity. An analysis using long-term data series. Water Resources Management, 30(15), pp.5737-5757.

Rippey, B.R., 2015. The US drought of 2012. Weather and Climate Extremes, 10, pp.57-64.

Robeson, S.M., 2015. Revisiting the recent California drought as an extreme value. Geophysical Research Letters, 42(16), pp.6771-6779.

Saha, S., Moorthi, S., Wu, X., Wang, J., Nadiga, S., Tripp, P., Behringer, D., Hou, Y.T., Chuang, H.Y., Iredell, M. and Ek, M., 2014. The NCEP climate forecast system version 2. Journal of Climate, 27(6), pp.2185-2208.

Sehgal, V. and Sridhar, V., 2018. Effect of hydroclimatological teleconnections on the watershed-scale drought predictability in the southeastern United States. International Journal of Climatology. doi:10.1002/joc.5439.

Sheffield, J. and Wood, E.F., 2012. Drought: past problems and future scenarios. Routledge.

Sheffield, J., Wood, E.F., Chaney, N., Guan, K., Sadri, S., Yuan, X., Olang, L., Amani, A., Ali, A., Demuth, S. and Ogallo, L., 2014. A drought monitoring and forecasting system for sub-Sahara African water resources and food security. Bulletin of the American Meteorological Society, 95(6), pp.861-882.

Shukla, S. and Lettenmaier, D.P., 2011. Seasonal hydrologic prediction in the United States: understanding the role of initial hydrologic conditions and seasonal climate forecast skill. Hydrology and Earth System Sciences, 15(11), pp.3529-3538.

Shukla, S., Safeeq, M., AghaKouchak, A., Guan, K. and Funk, C., 2015. Temperature impacts on the water year 2014 drought in California. Geophysical Research Letters, 42(11), pp.4384-4393.

Smith, A.B. and Katz, R.W., 2013. US billion-dollar weather and climate disasters: data sources, trends, accuracy and biases. Natural hazards, 67(2), pp.387-410.

Steinemann, A.C., 2006. Using climate forecasts for drought management. Journal of Applied Meteorology and Climatology, 45(10), pp.1353-1361.

Sternberg, T., 2011. Regional drought has a global impact. Nature, 472(7342), p.169.

Svoboda, M., LeComte, D., Hayes, M., Heim, R., Gleason, K., Angel, J., Rippey, B., Tinker, R., Palecki, M., Stooksbury, D. and Miskus, D., 2002. The drought monitor. Bulletin of the American Meteorological Society, 83(8), pp.1181-1190.

Thilakarathne, M. and Sridhar, V., 2017. Characterization of future drought conditions in the Lower Mekong River Basin. Weather and Climate Extremes, 17, pp.47-58.

Trambauer, P., Maskey, S., Winsemius, H., Werner, M. and Uhlenbrook, S., 2013. A review of continental scale hydrological models and their suitability for drought forecasting in (sub-Saharan) Africa. Physics and Chemistry of the Earth, Parts A/B/C, 66, pp.16-26.

USDA (U.S. Department of Agriculture) Soil Conservation Service, 1972. National Engineering Handbook, Hydrology (Section 4, Chapters 4–10). GPO, Washington, D.C.

Wang, A., Bohn, T.J., Mahanama, S.P., Koster, R.D. and Lettenmaier, D.P., 2009. Multimodel ensemble reconstruction of drought over the continental United States. Journal of Climate, 22(10), pp.2694-2712.

Wang, D., Hejazi, M., Cai, X. and Valocchi, A.J., 2011. Climate change impact on meteorological, agricultural, and hydrological drought in central Illinois. Water Resources Research, 47(9).

Wood, E.F., Lettenmaier, D.P. and Zartarian, V.G., 1992. A land-surface hydrology parameterization with subgrid variability for general circulation models. Journal of Geophysical Research: Atmospheres, 97(D3), pp.2717-2728.

Wood, E.F., Chaney, N., Sheffield, J. and Yuan, X., 2012, December. Development of an Experimental African Drought Monitoring and Seasonal Forecasting System: A First Step Towards a Global Drought Information System. In AGU Fall Meeting Abstracts.

Xie, P., Chen, M. and Shi, W., 2010, January. CPC unified gauge-based analysis of global daily precipitation. In Preprints, 24th Conf. on Hydrology, Atlanta, GA, Amer. Meteor. Soc (Vol. 2).

Yan, H., Moradkhani, H. and Zarekarizi, M., 2017. A probabilistic drought forecasting framework: a combined dynamical and statistical approach. Journal of Hydrology, 548, pp.291-304.

Zargar, A., Sadiq, R., Naser, B. and Khan, F.I., 2011. A review of drought indices. Environmental Reviews, 19(NA), pp.333-349.

Zhang, X., Tang, Q., Liu, X., Leng, G. and Li, Z., 2017. Soil moisture drought monitoring and forecasting using satellite and climate model data over Southwestern China. Journal of Hydrometeorology, 18(1), pp.5-23.

Chapter 3. Evaluation of climate change impacts on droughts conditions using ensembles of climate change models

3.1. Abstract

Impacts of climate change on the severity and intensity of future droughts can be evaluated based on precipitation and temperature projections, multiple hydrological models, simulated hydrometeorological variables, and various drought indices. The objective of this chapter is to assess climate change impacts on future drought conditions and water resources in the Chesapeake Bay (CB) watershed and five river basins in Virginia. In this study, the Soil and Water Assessment Tool (SWAT) and the Variable Infiltration Capacity model were used to simulate a Modified Palmer Drought Severity Index (MPDSI), a Standardized Soil Moisture index (SSI), a Multivariate Standardized Drought Index (MSDI), along with Coupled Model Intercomparison Project Phase 5 (CMIP5) climate models for both historical and future periods (f1: 2020-2049, f2: 2050-2079). The results of the SSI suggested that there was a general increase in agricultural droughts in the entire CB watershed and Virginia river basin due to increases in surface and groundwater flow and evapotranspiration. However, MPDSI and MSDI showed an overall decrease in projected drought occurrences due to the increases in precipitation in the future. The results of this study suggest that it is crucial to use multiple modeling approaches with specific drought indices that combine the effects of both precipitation and temperature changes.

3.2. Introduction

Droughts are known to be pervasive in nature, and their detrimental impacts on the environment, agriculture, the economy, and water resources require a greater understanding of their onset, duration, and severity (Vasiliades and Loukas, 2009; Sheffield and Wood, 2012; Sternberg, 2011). In the recent decades, droughts have been occurring more often in many regions around the world, and these are aggravated by climate change (Dai, 2011). Specifically, global temperature is expected to increase quite consistently because of the increase in greenhouse gas (GHG) emissions (IPCC, 2007; Pachauri et al., 2014; Qin et al., 2014), and a warming climate also

results in increased frequency of catastrophic droughts and floods worldwide (Mishra and Singh, 2011; Leonard et al., 2014). Thus, assessment of future droughts is essential for water resource planning and management (Mishra and Singh, 2010). The severities and frequencies of drought events in the United States (U.S.) have increased dramatically recently (Changnon et al., 2000; Karl et al., 2012). Approximately 10% of the land area in the U.S. has experienced drought conditions at least once during the 20th Century (NCDC, 2002) and 17% of weather-associated disasters that occurred in the U.S. between 1980 and 2003 (Ross and Lott, 2003) were related to drought. The western parts of the U.S. have recently experienced extreme droughts, which began in 2012 (Diffenbaugh et al., 2015; Mao et al., 2015). Low winter precipitation and decreased mountain snowpack, which are the telltale signs of global warming (AghaKouchak et al., 2014; Swain et al., 2014), aggravated the severity of this drought (Mao et al., 2015). In addition, various global climate models (GCMs) projected that drying tendencies in soil moisture, streamflow, and precipitation would occur in many parts of low- and mid-latitude countries due to increases in GHG and global warming (Wang, 2005; Burke et al., 2006; Sheffield and Wood, 2008; Dai, 2011, 2013; Kumar et al., 2014; Mishra et al., 2014; Chen et al., 2015; Rajsekhar et al., 2015; Thilakarathne and Sridhar, 2017). Furthermore, there is a significant trend that dry areas become drier and wet areas become wetter with a poleward enlargement of the subtropical dry zones (Tallaksen and Van Lanen, 2004).

Spatio-temporal measurements of hydrologic variables are required to analyze and characterize regional droughts (Mo, 2008; Sridhar et al., 2013). However, due to the lack of high-resolution and long-term observations, large-scale hydrologic models have been applied to an estimation of the energy fluxes and land surface water as well as hydrologic variables such as evapotranspiration (ET), runoff, and soil moisture that are used to evaluate climate change impacts on future droughts (Mishra et al., 2010; Wang et al., 2011; Kang and Sridhar, 2017; Sehgal et al., 2017; Seong et al., 2018).

For instance, the Soil and Water Assessment Tool (SWAT) (Arnold et al., 1998) is a powerful tool to estimate and evaluate the impact of climate change on the hydrological cycle and drought conditions (Jha et al., 2004; Wu and Johnston, 2007; Xu et al., 2009). Additionally, the Variable Infiltration Capacity (VIC) (Liang et al., 1994) model is an alternative tool which has been effectively applied to simulate the impacts of climate change, especially for assessing drought conditions (Mishra et al., 2010). Therefore, hydrological models can serve as the foundation for

evaluating drought conditions regarding various drought indices, management, and mitigation strategies (Narasimhan and Srinivasan, 2005; Hoekema and Sridhar, 2013).

Drought indices are effectively used for assessing the onset and recovery (Tsakiris et al., 2007; Sridhar et al., 2008), detecting drought, evaluating drought impacts (Niemeyer, 2008), declaring drought levels such as intensity or severity, short-term drought forecasting, and long-term future drought projection. Droughts are commonly classified into several categories, which include meteorological drought, hydrological drought, agricultural drought, and socioeconomic drought (American Meteorological Society, 2004). Meteorological drought is associated with a lack of precipitation for a specific time, hydrological drought is defined as a lack of surface and subsurface water resources from a management system, agricultural drought is related with declining soil moisture and following crop failure, and socio-economic drought is an inadequate supply of water systems and demand for an economic good such as crop yields. The response to drought depends on identifying which type of drought has occurred in a given area, and drought characterization is crucial for drought management operations. Thus, it is important to use multiple drought indices for identifying diverse aspects of drought conditions.

The Standardized Precipitation Index (SPI) (McKee et al., 1993) is one of the most prevalent indices for evaluating meteorological drought (Mishra and Singh, 2009; Zargar et al., 2011; Thilakarathne and Sridhar, 2017), and it is based on long-term precipitation observations. These observations are used to derive a specific probability distribution, which is then transformed into a standard normal distribution and an SPI mean value of zero (McKee et al., 1993; Edwards and McKee, 1997). With the same framework of SPI computation, the Standardized Soil Moisture Index (SSI) (Hao and AghaKouchak, 2013) is applied to quantify agricultural drought using soil moisture as an input. Oftentimes the mean value of the precipitation is set to zero, and values above zero indicate wet conditions, while values below zero indicate dry conditions (Table 1). The Palmer Drought Severity Index (PDSI) (Palmer, 1965) is widely used but has several issues that have been largely reported (Alley, 1984), and hence there is a constant review of other available indices for their ability to portray droughts more efficiently (Kang and Sridhar, 2017; Sehgal et al., 2017). PDSI assumes that all precipitation is rain; thus, PDSI values at high elevation areas and during winter seasons are often problematic (Alley, 1984). Hence, the Surface Water Supply Index (SWSI) (Shafer and Dezman, 1982; Hoekema and Sridhar, 2011) is frequently used as a supplement to PDSI in mountainous areas because SWSI considers snowpack and other unique

conditions (Hayes et al., 2007) in addition to using Modified PDSI (MPDSI) for assessment of drought. Therefore, multiple drought indices should be applied for a more comprehensive understanding of drought conditions. Despite all of these ongoing research efforts, the challenge in evaluating drought still remains for establishing a single meteorological or hydrologic variable because of the present difficulty in finding an appropriate indicator that covers both space and time. This hinders the advancement of drought prediction capabilities, reliable drought management plans and risk assessment (Hao and AghaKouchak, 2013). As a result, a Multivariate Standardized Drought Index (MSDI), which is based on multiple hydro-climatic variables, was developed and applied to identify historical droughts in the U.S. (Hao and AghaKouchak, 2013, 2014). In this study, SSI, MSDI, and MPDSI were used, and each of them represented agricultural, multivariate, and meteorological aspects of drought conditions in the Chesapeake Bay (CB) watershed. The diversity of drought indices for different drought types enables evaluation of more aspects and applications of droughts.

A myriad of studies that used hydrological models and drought indices have offered insights into future drought projections and the climate change impacts in the southwestern and central U.S. (Hoerling and Eischeid, 2007; Loukas et al., 2008; Seager et al., 2007; Strzepek et al., 2010; Gutzler and Robbins, 2011). However, only a few studies provide future drought projections using physically based hydrological models and correlation analysis of multiple drought indices, despite the recurring droughts that affected the southeastern and mid-Atlantic areas in the U.S. (Wilhite and Hayes, 1998; Changnon et al., 2000; VDEM, 2013). For example, some regions in the mid-Atlantic region experienced severe or extreme droughts in 2002, 2007 and 2012, but these drought events were not entirely examined due to the lack of data and the complexity of assessing the return periods of these droughts (VDEM, 2013). Therefore, the objectives of this study were to assess the occurrence of droughts in the CB watershed and five river basins in Virginia, and to characterize spatio-temporal changes during future droughts using physically based hydrological models, multiple drought indices, and high-resolution datasets. To achieve these objectives, the VIC and SWAT models were employed for the CB watershed to estimate multiple drought indices for both historical and future periods using meteorological inputs (precipitation and temperature) from a suite of GCMs derived from the Coupled Model Intercomparison Project Phase 5 (CMIP5) products. In addition, the SWAT model was applied for the five river basins in Virginia. The simulated hydrological variables were physically interpreted and used in calculating the drought

indices to draw conclusions on the relative changes in both historical and future droughts. The following sections illustrate the methods, results and discussions related to future drought conditions, which can provide a better understanding of the spatial heterogeneity of droughts across the CB watershed and five river basins in Virginia.

3.3. Methods

Figure 1 shows a flow diagram of the overall methodologies and approaches that were used in this study. First, input data required for SWAT and VIC models were prepared. Second, historical simulations were performed at daily time steps. Third, simulated streamflows were calibrated using the observed data from multiple gauging stations, and the historical simulations were validated for the accuracy of the model estimations. It was assumed that other estimated water budget variables, including ET and soil moisture, were appropriate for estimating the drought indices once the streamflow estimations were verified to be reasonably accurate. Following this, three drought indices were calculated through the historical and future periods, and using seasonal comparisons and time series, the spatial occurrences of future droughts were evaluated.

Table1. Classification of Standardized Precipitation Index (SPI), Standardized Soil Moisture Index, and Multivariate Standardized Drought Index Values (McKee et al., 1993).

SPI values	**Drought category**
2.0 and above	Extremely wet
1.5 to 1.99	Very wet
1.0 to 1.49	Moderately wet
-0.99 to 0.99	Near normal
-1.0 to -1.49	Moderate drought
-1.50 to -1.99	Severe drought
-2.0 or more	Extreme drought

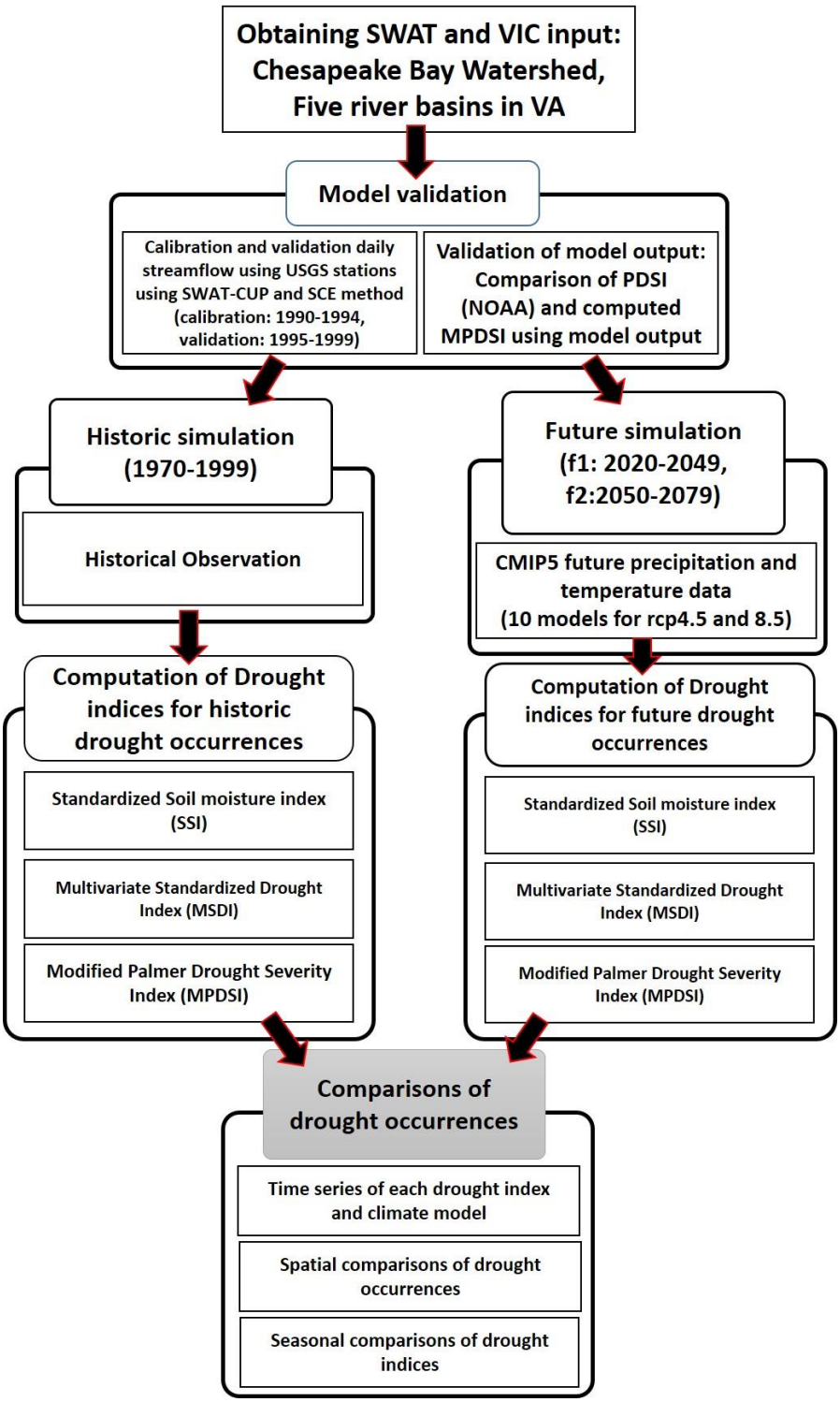

Figure 1. Flow diagram of the overall processes of hydrological modeling and drought projection. SWAT, Soil and Water Assessment Tool; SWAT-CUP, SWAT-Calibration and Uncertainty Programs; VIC, Variable Infiltration Capacity; SCE, Shuffled Complex Evolution; CMIP5, Coupled Model Intercomparison Project 5; NOAA, National Oceanic and Atmospheric Administration.

3.3.1. Study Area

Our study area is the CB watershed, which contains parts of Delaware (DE), Maryland (MD), New York (NY), Pennsylvania (PA), Virginia (VA), West Virginia (WV), and the entire District of Columbia (DC). In addition, the CB watershed contains the Susquehanna, Potomac, Patuxent, Rappahannock, York, and James River basins. The total drainage area of the CB watershed is 165,800 km2. Figure 2 shows the topography and location of the CB watershed and the location of U.S. Geological Survey (USGS) stream gauge stations. Surface elevations range from 5 m at the eastern areas to 1,481 m in the western areas. The mean annual precipitation for the CB watershed is 1,073 mm, and the mean annual temperature is 10.75°C. Over half of the five basins consist of forest (54.5%), while the remainder is covered by pasture/hay (14.9%), developed areas (10.8%), cultivated crops (9.5%), and woody wetlands (4.4%).

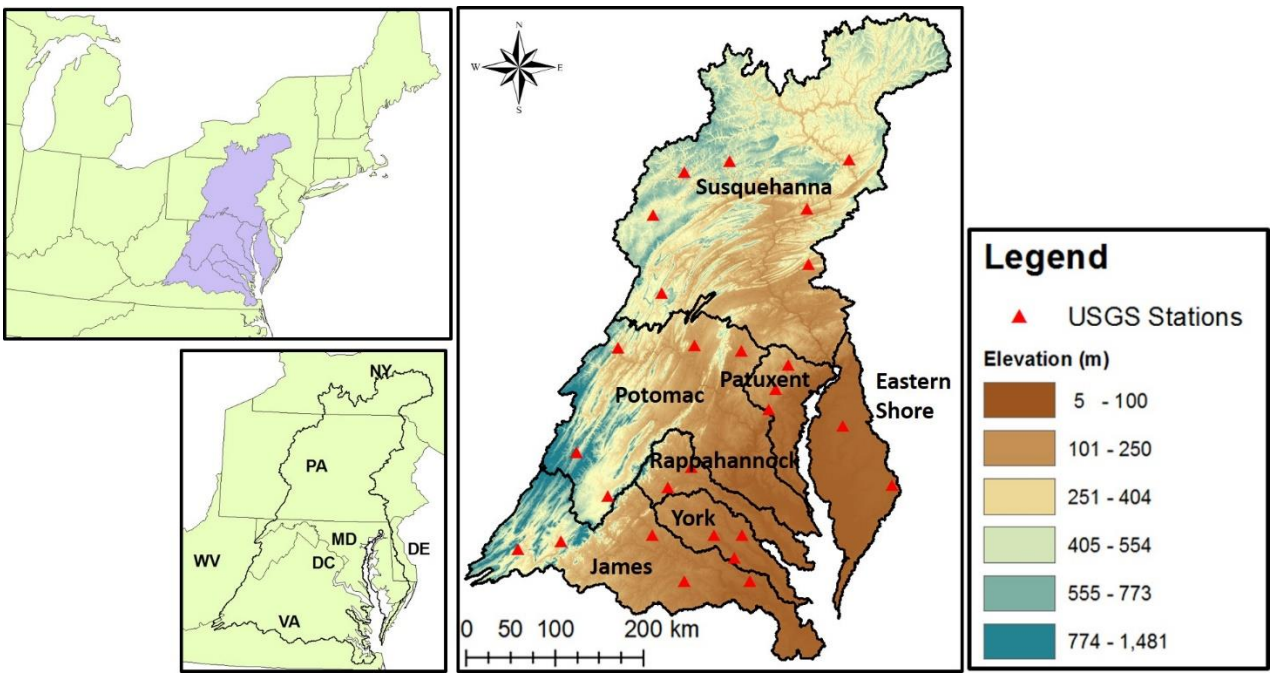

Figure 2. Location Map of the Chesapeake Bay (CB) Watershed. Red triangles indicate U.S. Geological Survey (USGS) stream gauge stations. DC, District of Columbia; DE, Delaware; MD, Maryland; NY, New York; PA, Pennsylvania; VA, Virginia; WV, West Virginia.

In addition, Figure 3 shows the locations of James, Roanoke, New, Rappahannock, and York river basins in Virginia. These basins were selected because they cover 62% of the Commonwealth of Virginia and reflect hydrological and political boundaries that reflect the

overall hydrological conditions in Virginia. Furthermore, these basins have experienced several severe droughts recently. The James, Rappahannock, and York river basins are the sub-basins of the Chesapeake Bay watershed, and the New River is part of the Ohio River basin. The total drainage area of the five river basins is 74,298 km2 (James: 26,773 km2, Roanoke: 24,117 km2, New: 10,016 km2, Rappahannock: 6544 km2, and York: 6848 km2). Figure 3(a) shows the location and topography of the five river basins, and the location of stream gauge stations. Land-surface elevations range from 5 m at the eastern coastline to the western mountainous areas (1738 m). The mean annual precipitation for the James, Roanoke, New, Rappahannock, and York river basins are 1118 mm to 1172 mm. Furthermore, the mean annual temperature for the five river basins range from 13.15 °C to 13.90 °C. In addition, about sixty percent of the five basins consist of forest (58.85%), whereas the other forty percent is covered by pasture/hay (16.59%), developed areas (8.52%), cultivated crops (3.29%), and woody wetlands (3.85%). Figure 4(a) provides a time series of the mean values of PDSI from the National Oceanic and Atmospheric Administration (NOAA) (ftp://ftp.ncdc.noaa.gov/) and monthly precipitation data from 1970 to 2015 in the CB watershed and Virginia; Figure 4(b) represents the time series of PDSI values for each climate division. In the early and mid-1980s, late 1990s, and early and late 2000s, severe and extreme droughts struck these regions.

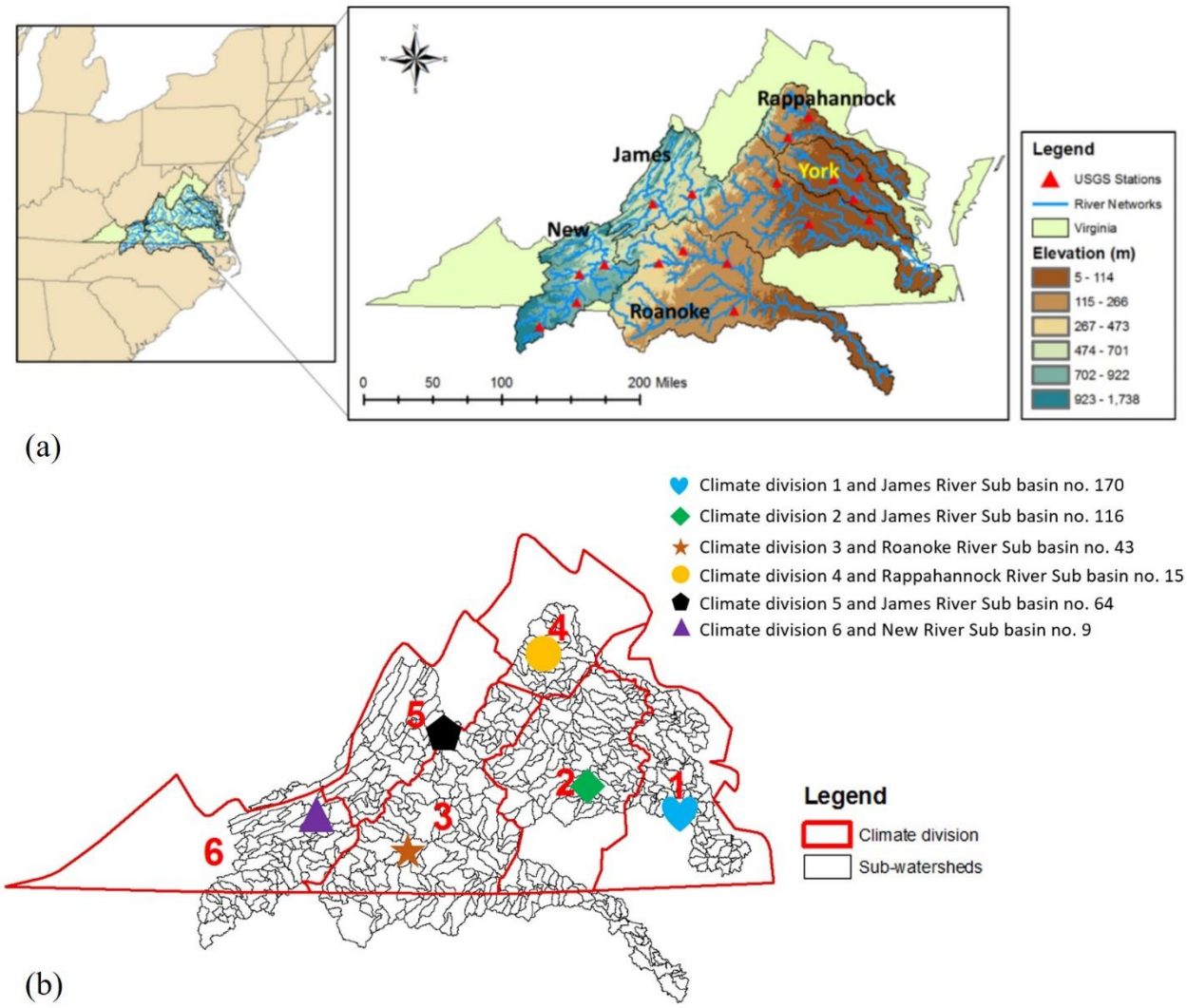

Figure 3. Location map of the five river basins and climate divisions in Virginia. (a) Red triangles indicate USGS stream gauge stations, and blue lines represent the river networks. (b) Red lines indicate the climate divisions in Virginia, and black lines represent the sub-watersheds in the five river basins.

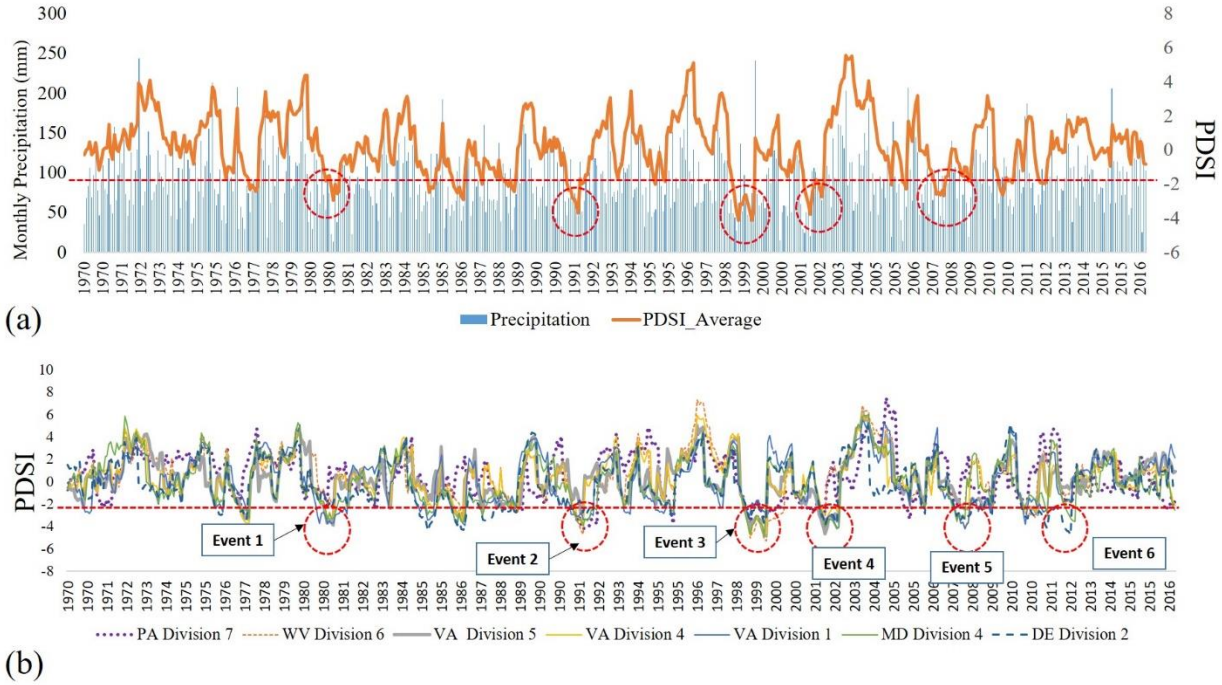

Figure 4. Comparisons of Monthly Precipitation and Palmer Drought Severity Index (PDSI) in the study areas. The red and dashed line represents the moderate to extreme drought condition (-2 or less), and the red and dashed circles outline the drought events. (a) Comparisons of monthly precipitation and PDSI in the CB watershed (climate division average). (b) Comparisons of PDSI (each climate division) for historic periods and drought events in the study areas.

3.3.2. Hydrologic Simulation Models

The SWAT (Arnold et al., 1998) is a hydrological model that is widely used to estimate large river basins with mixed land uses. SWAT simulates hydrologic and water quality variables, as well as climate change impacts (Wang et al., 2011; Ashraf Vaghefi et al., 2014; Ahn et al., 2016). The foundation for SWAT is hydrological response units (HRUs) that are a particular combination of soil, land cover, and slope. The SWAT model simulates the water budget based on a simple water balance equation (Equation 1).

$$SW_t = SW_0 + \sum_{i=1}^{t} P_{day} - Q_{surf} - E_a - W_{seep} - Q_{gw} \quad (1)$$

where, SW_0 is the initial soil water content on day i (mm), SW_t is the final soil water content (mm) on day i, t is the time (days), P_{day} is the amount of precipitation on day i (mm), Q_{surf} is the surface runoff on day i (mm), E_a is the evapotranspiration on day i (mm), W_{seep} is the water entering to the vadose zone from the soil profile on day i (mm), and Q_{gw} is the return flow on day i (mm).

SW_t was used to calculate the Standardized Soil Moisture Index (SSI), Multivariate Standardized Drought Index (MSDI), and Modified Palmer Drought Severity Index (MPDSI). However, to calculate the MPDSI, additional variables such as Q_{surf}, Q_{gw}, and E_a were used.

In addition, the model compartmentalizes three storage volumes in HRU, that is, the unsaturated soil profile layer (0-2 m), the shallow aquifer (2-20 m), and the deep aquifer (>20 m). Soil water and hydrological processes simulate shallow and deep aquifer baseflows, lateral flow, surface runoff, infiltration, evaporation, and plant water uptake. For the simulation of ET and potential ET (PET), the Penman-Monteith (Monteith, 1965) method was considered in this study. Surface runoff was simulated based on the modified SCS (Soil Conservation Service) curve number (CN) method (USDA Soil Conservation Service, 1972) using daily precipitation data. The SWAT model needs a digital elevation model (DEM), land use, soil, and daily values of meteorological input. In this study, a 100 m 9 100 m DEM was used from the National Elevation Dataset (NED) (Gesch, 2007), a soil map was generated from State Soil Geographic data (STATSGO) (USDA, 1991) at a scale of 1:250,000, and a land use map was obtained from the National Land Cover Data (NLCD) (Homer et al., 2004).

The VIC model (Liang et al., 1994) is a macro scale hydrologic model, and it has been widely used to simulate the drought conditions of many river basins in the U.S. (Wang et al., 2011; Shukla et al., 2011; Mao et al., 2015). The variability in land cover in the VIC model is classified based on the types of vegetation or bare soil, and the soil is divided into three layers. Additionally, the hydrologic computation depends on the interaction between soil and vegetation in a single grid cell and weather variables. In this study, the VIC model was implemented at 1/8th-degree resolution (0.125°) of atmospheric forcing (daily precipitation, maximum and minimum temperatures, and wind speed). Model parameters such as soil and vegetation information were obtained from the Land Data Assimilation Systems (LDAS) (http://ldas.gsfc.nasa.gov/).

The SWAT model was calibrated using daily streamflow and the SWAT calibration and uncertainty assessment tool (SWAT-CUP) (Abbaspour, 2011). The VIC model was calibrated using the Shuffled Complex Evolution method and daily streamflow (Duan et al., 1993; Thyer et al., 1999; Vrugt et al., 2003). For the SWAT model, we identified 11 parameters for calibration and validation (calibration: 1990-1994, validation: 1995-1999) (Table 2), while 8 parameters were used for the VIC model (Table 3).

Table 2. Description of the Soil and Water Assessment Tool Input Parameters Selected for the Streamflow Calibration.

Parameter	**Description**	Min	Max
r_CN2.mgt	Curve number for moisture condition II	-0.2	0.2
v_ALPHA_BF.gw	Base flow alpha factor	0	1
v_GW_DELAY.gw	Ground water delay time	0	450
v_GWQMN.gw	Threshold water Depth in shallow aquifer for back discharge	0	2000
v_EPCO.hru	Plant uptake compensation factor	0.01	1
v_ESCO.hru	Soil evaporation compensation factor	0.01	1
v_SLSUBBSN.hru	Average slop length	10	150
v_OV_N.hru	Manning's *n* value for overland flow	0	0.8
v_CH_N2.rte	Manning's *n* value for main channel	0	0.3
v_CH_K2.rte	Main channel conductivity	0	150
v_SURLAG.bsn	Surface runoff lag coefficient	1	24

v_: denotes the default parameter is replaced by a given value, and r _: means the existing parameter value is multiplied by (1+ a given value).

Table 3. Description of the Variable Infiltration Capacity Input Parameters Selected for the Streamflow Calibration.

Parameter	**Description**	Max	Min
b	Variable infiltration curve parameter	0.4	0.001
Dsmax	Maximum baseflow velocity	30	0.1
Ds	Fraction of Dsmax where nonlinear base flow occurs	1.0	0.01
Ws	Fraction of maximum soil moisture above which nonlinear base flow occurs	1.0	0
D1	Top soil layer depth	1.0	0.1
D2	Mid soil layer depth	0.4	0.1
D3	Deep soil layer depth	0.8	0.1
Infilt	Variable infiltration curve parameter	Max	Min

For the SWAT model calibration, there are some limitations of using the curve number for an application of future drought projections. In this study, the SCS CN was one of the calibration parameters, and the calibration processes were performed based on the current land use in the CB watershed. Thus, the fitted CN values could not consider the land use shifts in future periods. In addition, a major limitation of the CN2 is that it fails to consider the effects of specific rainfall intensity and duration (Simanton et al., 1996; King et al., 1999) (e.g., runoff generated by high-intensity and short duration precipitation). However, high-intensity precipitation events and floods would be expected to increase in the future due to the impacts of climate change.

Using the daily streamflow data from USGS stream gauge stations (Table 4, Figure 2, and Figure 3) for calibration and validation, the model evaluation was performed based on the Nash-Sutcliffe coefficient (NSE) (Nash and Sutcliffe, 1970) (Equation 2). To avoid the effects that reservoirs and dams may have on streamflows, gauge stations located in the upstream areas were selected.

$$\mathrm{NSE} = \left(\frac{\sum_{i=1}^{n} Q_s - Q_{obs}}{\sum_{i=1}^{n} Q_{obs} - \overline{Q_o}}\right) \quad (2)$$

where Q_s is the simulated river discharge at time i, Q_{obs} is the observed river discharge at time i, and $\overline{Q_o}$ is the mean value of the observed flow in the calibration processes. NSE values range from 1 (perfect match) to -∞, and they show how well the plots of the observed and the simulated values fits with the 1:1 line.

Table 4. Description of the USGS Stream Gauge Stations.

Parameter	Description	Latitude	longitude	River name
USGS02034000	RIVANNA RIVER AT PALMYRA	37°51'28"	78°15'58"	James
USGS02024000	MAURY RIVER NEAR BUENA VISTA	37°45'45"	79°23'30"	James
USGS02018000	CRAIG CREEK AT PARR	37°39'57"	79°54'42"	James
USGS02042500	CHICKAHOMINY RIVER NEAR PROVIDENCE FORGE	37°26'10"	77°03'40"	James
USGS02040000	APPOMATTOX RIVER AT MATTOAX	37°25'17"	77°51'33"	James
USGS01664000	RAPPAHANNOCK RIVER AT REMINGTON	38°31'50"	77°48'50"	Rappahannock
USGS01666500	ROBINSON RIVER NEAR LOCUST DALE	38°19'30"	78°05'45"	Rappahannock
USGS01674500	MATTAPONI RIVER NEAR BEULAHVILLE	37°53'02"	77°09'55"	York
USGS01671100	LITTLE RIVER NEAR DOSWELL	37°52'21"	77°30'48"	York
USGS01673550	TOTOPOTOMOY CREEK NEAR STUDLEY	37°39'45"	77°15'29"	York
USGS01500000	OULEOUT CREEK AT EAST SIDNEY	42°20'00"	75°14'06"	Susquehanna
USGS01534000	Tunkhannock Creek near Tunkhannock	41°33'30"	75°53'42"	Susquehanna
USGS01539000	Fishing Creek near Bloomsburg	41°04'41"	76°25'53"	Susquehanna
USGS01541500	Clearfield Creek at Dimeling	40°58'18"	78°24'22"	Susquehanna
USGS01544000	First Fork Sinnemahoning Cr near Sinnemahoning	41°24'06"	78°01'28"	Susquehanna
USGS01548500	Pine Creek at Cedar Run	41°31'18"	77°26'52"	Susquehanna
USGS01576500	Conestoga River at Lancaster	40°03'00"	76°16'39"	Susquehanna
USGS01601500	WILLS CREEK NEAR CUMBERLAND	39°40'11"	78°47'17"	Potomac
USGS01607500	SO FK SO BR POTOMAC R AT BRANDYWINE	38°37' 53"	-79°14' 37"	Potomac
USGS01614500	CONOCOCHEAGUE CREEK AT FAIRVIEW	39°42'59"	77°49'29"	Potomac
USGS01627500	SOUTH RIVER AT HARRISTON	38°13' 07"	-78° 50' 12"	Potomac
USGS01639000	MONOCACY RIVER AT BRIDGEPORT	39°40'45"	77°14'04"	Potomac
USGS01582500	GUNPOWDER FALLS AT GLENCOE	39°32'59"	76°38'10"	Patuxent
USGS01594000	LITTLE PATUXENT RIVER AT SAVAGE	39°08'04"	76°48'58"	Patuxent River
USGS01485000	POCOMOKE RIVER NEAR WILLARDS	38°23'20"	75°19'28"	Eastern Shore
USGS01491000	CHOPTANK RIVER NEAR GREENSBORO	38°59'50"	75°47'09"	Eastern Shore
USGS03170000	LITTLE RIVER AT GRAYSONTOWN	37°02'15"	80°33'25"	New
USGS03167000	REED CREEK AT GRAHAMS FORGE	36°56'20"	80°53'15"	New
USGS03165000	CHESTNUT CREEK AT GALAX	36°38'45"	80°55'10"	New
USGS03161000	SOUTH FORK NEW RIVER NEAR JEFFERSON	36°23'36"	81°24'25"	New
USGS02059500	GOOSE CREEK NEAR HUDDLESTON	37°10'23"	79°31'14"	Roanoke
USGS02062500	ROANOKE (STAUNTON) RIVER AT BROOKNEAL	37°02'22.0"	78°56'44.6"	Roanoke
USGS02056900	BLACKWATER RIVER NEAR ROCKY MOUNT	37°02'42"	79°50'40"	Roanoke
USGS02077670	MAYO CR NR BETHEL HILL	36°32'27"	78°52'19"	Roanoke

3.3.3. Drought Indices

In this study, both SWAT and VIC were used to calculate the input variables of various drought indices as the Modified Palmer Drought Severity Index (MPDSI) (Mo and Chelliah., 2006), Standardized Soil Moisture Index (SSI), and Multivariate Standardized Drought Index (MSDI) to evaluate future droughts. For instance, SWAT-estimated SW_t was used for calculating MPDSI, SSI, and MSDI. Simulated ET, PET, surface runoff, and baseflow were also used to calculate the MPDSI.

In some studies, multivariate drought indicators have examined using joint distribution and probability (Hao and Aghakouchak, 2013; Aghakouchak, 2015). In order to adopt this approach, the MSDI was derived and applied using the joint probability of long-term precipitation and soil moisture observations (Hao and Aghakouchak, 2013; Aghakouchak, 2015). The joint distribution of two variables are described as:

$$P(X \leq x, Y \leq y) = p \tag{3}$$

where, p is joint probability of the precipitation and soil moisture. The MSDI can be defined as follows (Hao and Aghakouchak, 2013):

$$\text{MSDI} = \emptyset^{-1}(p) \tag{4}$$

where $\emptyset$ is the standard normal distribution function.

In this study, Grigorten plotting position formula, an alternative method to derive empirical joint probability was used to alleviate the computational concern to fit the parametric distributions (Gringorten 1963; Yue et al. 1999; Benestad and Haugen 2007), and it can be expressed as follows:

$$P(x_k, y_k) = \frac{m_k - 0.44}{n + 0.12} \tag{5}$$

where m_k is the number of occurrences of the pair (x_i, y_i) for $x_i \leq x_k$ and $y_i \leq y_k$, and n is the number of the observations. After the joint probability was achieved from Equation 5, it was used to Equation 4 to estimate the MSDI. To compute SSI and SPI, the univariate form of the Gringorten plotting formula (Equation 6) (Gringorten, 1963) was used.

$$P(x_i) = \frac{i-0.44}{n+0.12} \quad (6)$$

where n is the number of observations, and i is the rank of the observed values from the smallest.

Historic and future MPDSI values were calculated using the input and output from SWAT and VIC, and they were as follows: precipitation, ET, PET, soil moisture, and runoff. MPDSI uses water budget framework and the alteration between the climatological and actual calculation known as "Climatically appropriate for existing conditions (CAFEC)" which is expressed as follows:

$$d = P - CAFEC, \text{ where} \quad (7)$$

$$\mathrm{CAFEC} = \alpha\mathrm{PE} + \beta\mathrm{PR} + \gamma\mathrm{PRO} + \delta\mathrm{PL} \quad (8)$$

where PE is the potential evapotranspiration, PR is the potential recharge, PRO is the potential runoff, and PL is the potential soil moisture loss, the coefficient $\alpha, \beta, \gamma,$ and δ are the ratio of the mean variables. More comprehensive explanations of MPDSI are available from Mo and Chelliah (2006). In this study, the weekly scale of SSI, MSDI (25-week scale), and MPDSI were calculated by using the input and output variables from SWAT and VIC models, and they were used to evaluate future drought conditions in the CB watershed.

3.3.4. Climate Projections

The effectiveness of a climate model to simulate present climate and historical tendencies results provides higher confidence in the projected future climate scenarios (Reifen and Toumi, 2009; Wuebbles et al., 2014). The Climate Modeling Intercomparison Project Phase 5 (CMIP5) provides multi-model simulations of historic and future climates that correspond to diverse greenhouse-gas (GHC) emissions scenarios (Taylor et al., 2012). Several studies have assessed the CMIP5 outputs at both global and regional scales (Jin and Sridhar, 2012; Feng et al., 2014; Hao et al., 2013; Schubert and Lim, 2013; Sheffield et al., 2013; Sillmann et al., 2013; Sridhar et al., 2013), and reported that the multi-model ensemble mean of CMIP5 outputs show reasonable

spatial trends of hydro-climatic variables. Especially, Nasrollahi et al. (2014) investigated spatio-temporal robustness of CMIP5 climate models across the globe, and their results suggest that most CMIP5 models agreed with observed global trends in projecting the extent and severity of future drought conditions.

3.3.5. Model Analysis Description for Historic and Future Drought Projection

The VIC and SWAT models were run at a daily time step for the historic (1970-1999) and future periods (f1: 2020-2049, f2:2050-2079) with Representative Concentration Pathways (RCP) 4.5 and 8.5 scenarios. There were 1,248 climate grid points in the CB watershed and 480 grid points in the five river basins from the CMIP5 climate models at $1/8^{th}$ degree resolution.

For the historic simulation, calibration and validation was performed using daily streamflows from thirty-four USGS stations to derive a proper parameter set. Also, other outputs from these models such as ET, PET, soil moisture, and runoff were indirectly validated with comparisons of PDSI from NOAA and with computed MPDSI from the output of VIC and SWAT models. Based on the results of the calibration and validation, both historic and future simulations were carried out to compute drought indices (SSI, MSDI, and MPDSI). Lastly, the historic and future drought indices were compared based on weekly and seasonal time series plots, as well as spatial analysis of drought occurrences.

Historic and future drought occurrences were determined as a noticeable drought event when the SSI and MSDI values were less than -1 (moderate to extreme drought), the MPDSI values were less than -2 (moderate to extreme drought). Afterwards, the differences between the historic and future drought occurrences were computed at a sub-basin (SWAT) or $1/8^{th}$ grid (VIC) level in order to quantify the relative change in droughts. The historic simulation period was from 1970 to 1999, and future simulation periods were performed during two time windows, 2020-2049 (f1) and, 2050-2079 (f2).

3.4. Results and Discussion

3.4.1. Past and Future Climate

Table 5 shows the changes in precipitation and temperature for each CMIP5 model between the historical and future periods, averaged over the entire CB watershed. Overall, the magnitudes of change in precipitation and temperature during the f2 period were higher than during the f1 period for both RCP 4.5 and RCP 8.5. For the CB watershed, the maximum precipitation increase for RCP 4.5 was 14.1% in the S7 model during the f2 period, while there was a 3.7% decrease in precipitation in the S9 model during the f1 period. Additionally, the maximum precipitation increase for RCP 8.5 was 9.3% in the S4 model during the f2 period, whereas there was a decrease in precipitation by 2.3% in the S9 model during the f1 period. In addition, the maximum temperature increase for RCP 4.5 was 3.6°C in the S2 model during the f2 period, while the minimum temperature increase was 0.9°C in the S9 model during the f1 period. Finally, the maximum temperature increase for RCP 8.5 was 4.4°C in the S1 model during the f2 period, whereas there was an increase of 1.0°C in temperature in the S9 model during the f1 period.

Table 6 shows the changes in precipitation and temperature for the five river basins, the maximum precipitation increase for RCP 4.5 was 17% in the S7 model during the f2 period, whereas there was a 3.4% decrease in precipitation in the S9 model during the f1 period. Furthermore, the maximum temperature increase for RCP 4.5 was 3.0 °C in the S1 model during the f2 period, whereas the minimum temperature increase was 0.9 °C in the S9 model during the f1 period. Furthermore, the maximum precipitation increase for RCP 8.5 was 20.7% in the S3 model during the f2 period, whereas there was a decrease in precipitation by 1.6% in the S9 model during the f2 period. Furthermore, the maximum temperature increase for RCP 8.5 was 4.3 °C in the S8 model during the f2 period, whereas there was an increase of 0.9 °C in temperature in the S9 model during the f1 period.

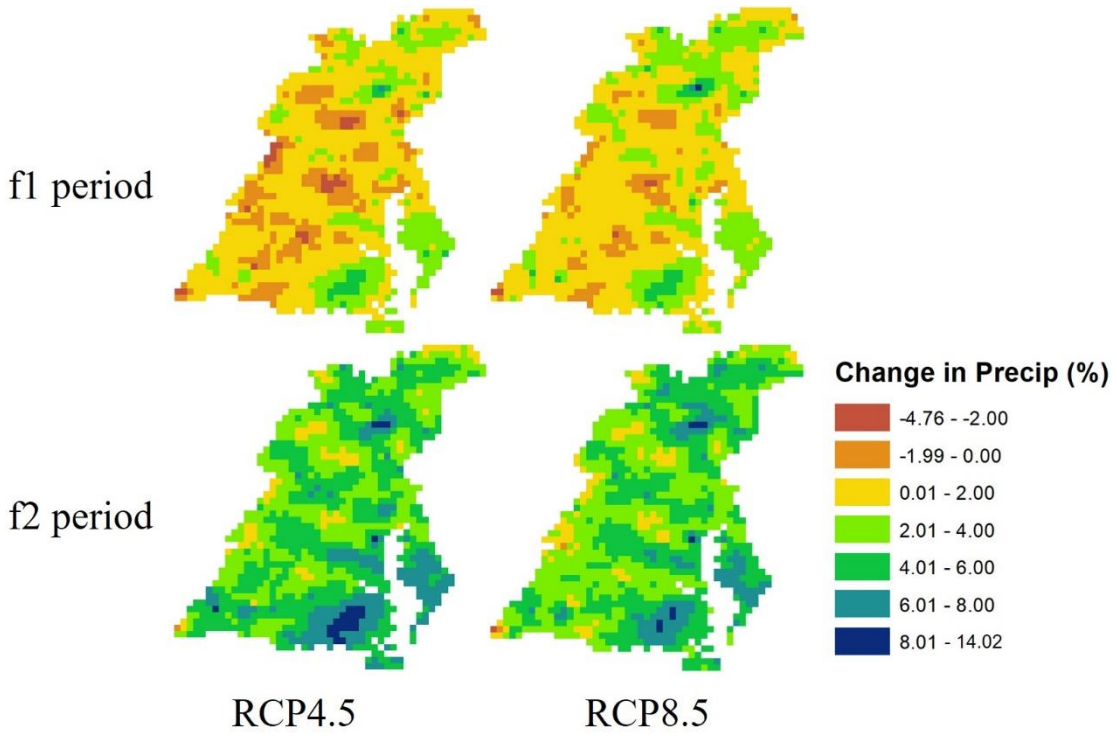

Figure 5. Spatial maps of change in precipitation for each RCP and period. Negative values are represented in brown, and they indicate a decrease in precipitation. Positive values are represented in yellow, green, and navy, and they indicate an increase in precipitation in the future.

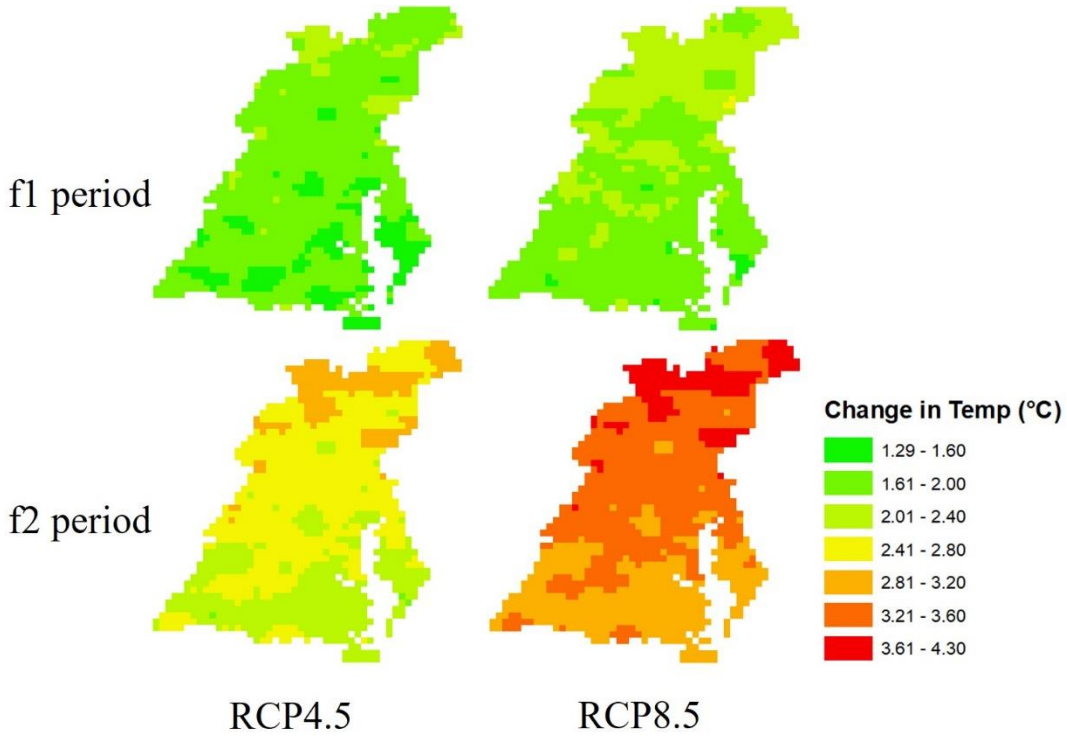

Figure 6. Spatial maps of change in temperature for each RCP and period. Low increases in temperature are represented in green, whereas high increases in temperature are represented in orange and red.

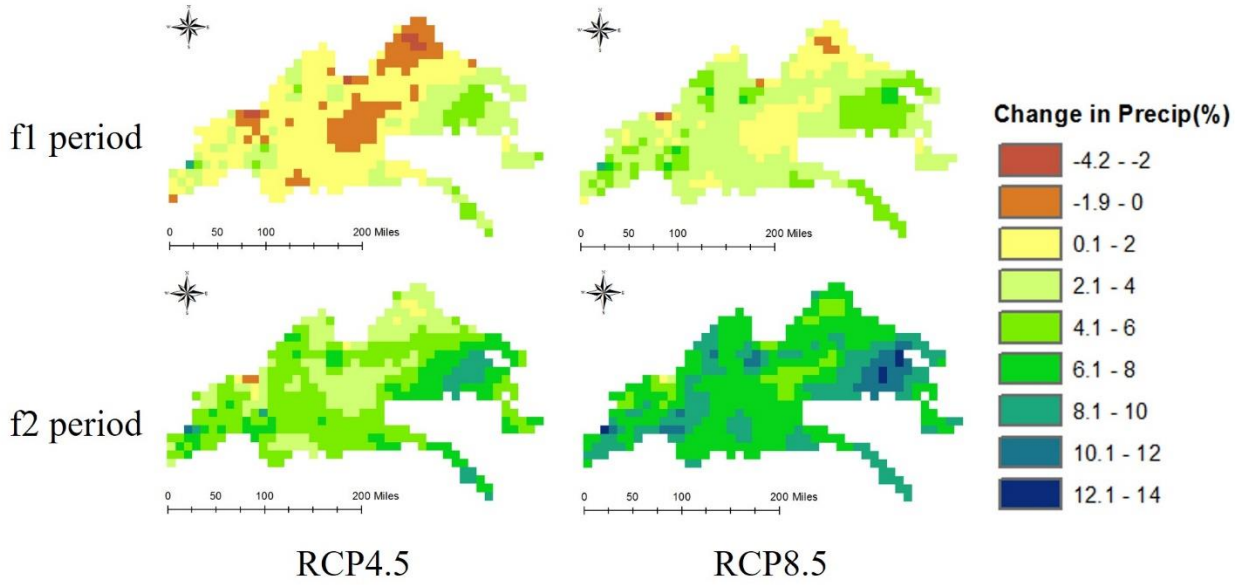

Figure 7. Spatial maps of precipitation change for each RCP and period. Negative values are represented in brown and indicate a decrease in precipitation. Positive values are represented in yellow, green, and navy, and they indicate an increase in precipitation in the future.

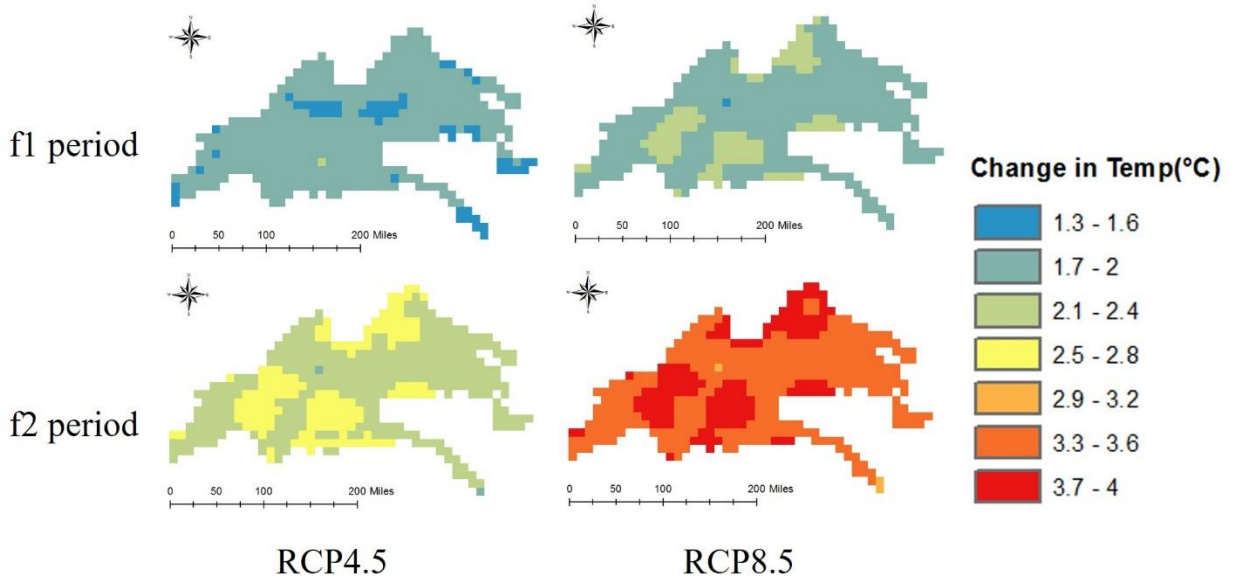

Figure 8. Spatial maps of temperature change in each RCP and period. Low increases in temperature are represented in blue, whereas high increases in temperature are represented in orange and red.

Table 5. List of the CMIP5 general circulation model (GCMs) and changes in precipitation and temperature for the CB watershed.

CMIP5 model Abbreviation	RCP4.5				RCP8.5			
	Change in Precipitation (%)		Change in Temperature (°C)		Change in Precipitation (%)		Change in Temperature (°C)	
	f1	f2	f1	f2	f1	f2	f1	f2
S1: access1-0	-0.44	1.20	2.03	3.16	0.42	2.20	2.32	4.42
S2: bcc-csm1-1.1	-1.02	-3.16	2.12	3.61	-0.24	4.19	1.68	2.63
S3: canesm2	-1.07	2.24	2.36	3.21	-0.21	5.46	2.46	4.42
S4: ccsm4	2.46	7.94	1.98	2.67	5.36	9.27	2.14	3.77
S5: cesm1-bgc.1	2.69	11.39	1.77	2.62	5.70	6.69	1.98	3.53
S6: cnrm-cm5.1	4.54	4.64	1.49	2.37	0.13	4.82	1.84	3.40
S7: csiro-mk3-6-0	3.31	14.10	1.83	2.73	3.41	5.09	1.71	3.73
S8: gfdl-esm2g.1	1.37	5.68	1.58	2.00	3.11	1.82	1.69	3.26
S9: inmcm4	-3.66	-1.50	0.90	1.25	-2.30	-1.73	1.04	2.25
S10: ipsl-cm5a-mr	-0.06	1.91	1.99	2.77	-1.98	3.11	2.09	4.18

Table 6. List of the CMIP5 general circulation model (GCMs) and changes in precipitation and temperature for the five river basins.

CMIP5 model Abbreviation	RCP4.5				RCP8.5			
	Change in Precipitation (%)		Change in Temperature (°C)		Change in Precipitation (%)		Change in Temperature (°C)	
	f1	f2	f1	f2	f1	f2	f1	f2
S1: access1-0	2.0	4.1	1.9	3.0	2.1	4.3	2.2	4.1
S2: bcc-csm1-1.1	0.5	-2.0	1.6	2.4	-0.3	4.7	1.9	3.3
S3: canesm2	2.8	10.1	2.2	2.9	4.3	20.7	2.5	4.0
S4: ccsm4	9.5	8.5	1.7	2.5	10.9	17.1	1.8	3.6
S5: cesm1-bgc.1	5.3	16.9	1.7	2.5	10.7	10.4	1.9	3.3
S6: cnrm-cm5.1	8.6	6.1	1.4	2.2	3.2	6.4	1.7	3.1
S7: csiro-mk3-6-0	6.3	17.0	1.7	2.3	9.9	11.4	1.8	3.5
S8: gfdl-esm2g.1	4.9	10.7	1.6	1.9	11.3	19.8	2.2	4.3
S9: inmcm4	-3.4	0.2	0.9	1.1	0.9	-1.6	0.9	2.2
S10: ipsl-cm5a-mr	2.9	5.1	1.9	2.6	3.4	12.3	2.2	4.2

Figures 5 and 6 show the spatial maps of the ensemble mean for precipitation and temperature changes over the CB watershed. As shown in Figure 4, the downstream areas of the James and York River basins showed the highest precipitation increase in both RCP 4.5 and RCP 8.5, while the upstream or western areas of the James and Potomac River basins and the mid-sections of the Potomac and Susquehanna River basins showed the lowest precipitation increase or decrease in precipitation. In addition, the temperature increase was highest in the northern areas of the CB watershed, as shown in red and orange colors. In contrast, the lowest temperature increase was in the southern areas of the CB watershed represented in green color. Figure 7 and

Figure 8 shows the precipitation and temperature change for each CMIP5 model and five river basins. In the case of the RCP 4.5 scenarios in the f1 period, the maximum precipitation increase was 7.71% in the S4 model for the New River basin, and the maximum temperature increase was 2.28 °C in the S3 model for the Rappahannock River basin. However, there was 7.12% decrease in precipitation in the S9 model for the Roanoke River basin, and the minimum temperature increase was 0.80 °C in the S9 model in the York River basin. For the RCP 4.5 and f2 period, the maximum precipitation increase was 15.83% in the S5 model for the York River basin, and the maximum temperature increase was 3.09 °C in the S3 model for the Rappahannock River basin. However, there was a 4.82% decrease in precipitation in the S2 model for the Roanoke River basin, and the minimum temperature increase was 1.11 °C in the S9 model for the York River basin (Table 7).

Table 7. Ensemble means of precipitation and temperature change in the five River basins.

River basins	RCP4.5				RCP8.5			
	Change in Precipitation (%)		Change in Temperature (°C)		Change in Precipitation (%)		Change in Temperature (°C)	
	f1	f2	f1	f2	f1	f2	f1	f2
James	1.46	5.08	1.62	2.32	3.09	7.84	1.89	3.53
New	1.62	4.89	1.67	2.33	3.44	7.74	1.92	3.53
Rappahannock	0.26	3.87	1.68	2.40	1.85	7.12	1.96	3.64
Roanoke	1.12	4.93	1.71	2.38	2.88	7.66	1.96	3.56
York	2.25	5.92	1.62	2.33	3.48	8.68	1.90	3.56

3.4.2. Model Evaluation

In this study, daily streamflow generated from two hydrologic models were calibrated and validated using SWAT-CUP and the Shuffled Complex Evolution method for SWAT and VIC, respectively. The calibration period was from 1990 to 1994, and the validation period was from 1995 to 1999. Table 8 (CB watershed) and Table 9 (Five basins in VA) present the results of the calibration and validation for gauging stations, and for roughly all locations, the Nash and Sutcliffe Efficiency (NSE) (Nash and Sutcliffe, 1970) values were higher than or close to 0.5, which was assumed to be satisfactory for daily simulation (Moriasi et al., 2007). Historical drought occurrences were also assessed based on the comparisons of historical PDSI derived for each climate division from NOAA (ftp://ftp.ncdc.noaa.gov/) and the MPDSI values calculated by the output variables from the SWAT and VIC simulations.

For each climate division, historical drought events between 1970 and 1999 were evaluated to determine whether the MPDSI values from VIC and SWAT models precisely captured the drought conditions, which were defined by PDSI values of -2 or less. During this period, each climate division experienced a few drought events, and Figures 9 and 10 show a comparison of PDSI and MPDSI values for the CB watershed. Notably, the MPDSI values based on SWAT results captured 55-87% of the drought events in this period, and the MPDSI values computed by VIC model results captured 61-78% of the drought events. Figure 11 provides a comparison of PDSI and MPDSI values for the five river basins. Clearly, MPDSI values based on the model results captured 62–84% of the drought conditions in this 20-year period. The highest agreement was shown in a comparison of climate division 4 and the Rappahannock River basin (84%), and the lowest agreement was shown in a comparison of climate division 5 and the James River basin (62%). Several factors were attributed to the low levels of agreements. First, the climate divisions were larger than the sub-watersheds and grids. Second, several input variables of MPDSI were not explicitly included in the calibration. Finally, the PET estimation methods were different for the PDSI (Thornthwaite) and MPDSI (Penman and Monteith) methods. The Thornthwaite approach is based on a simple function of average surface temperature and latitude (Thornthwaite, 1948), whereas the Penman and Monteith method needs supplementary variables such as solar radiation, water vapor content, and wind speed.

Table 8. Results of calibration and validation for 26 stream gauge locations in the CB watershed.

Station name	Type	SWAT	VIC	Station name	SWAT	VIC
USGS02034000 (James River)	Calibration	0.59	0.58	USGS01541500 (Susquehanna River)	0.48	0.66
	Validation	0.50	0.54		0.55	0.57
USGS02024000 (James River)	Calibration	0.56	0.58	USGS01544000 (Susquehanna River)	0.50	0.63
	Validation	0.61	0.60		0.54	0.47
USGS02018000 (James River)	Calibration	0.48	0.60	USGS01548500 (Susquehanna River)	0.47	0.51
	Validation	0.56	0.61		0.48	0.51
USGS02042500 (James River)	Calibration	0.66	0.52	USGS01576500 (Susquehanna River)	0.50	0.67
	Validation	0.72	0.54		0.32	0.57
USGS02040000 (James River)	Calibration	0.63	0.63	USGS01601500 (Potomac River)	0.48	0.56
	Validation	0.61	0.58		0.55	0.47
USGS01664000 (Rappahannock River)	Calibration	0.57	0.61	USGS01607500 (Potomac River)	0.53	0.36
	Validation	0.49	0.58		0.61	0.40
USGS01666500 (Rappahannock River)	Calibration	0.48	0.45	USGS01614500 (Potomac River)	0.58	0.62
	Validation	0.62	0.49		0.60	0.53
USGS01674500 (York River)	Calibration	0.65	0.50	USGS01627500 (Potomac River)	0.48	0.35
	Validation	0.64	0.47		0.60	0.46
USGS01671100 (York River)	Calibration	0.52	0.51	USGS01639000 (Potomac River)	0.55	0.47
	Validation	0.50	0.59		0.43	0.51
USGS01673550 (York River)	Calibration	0.60	0.54	USGS01582500 (Patuxent River)	0.65	0.32
	Validation	0.50	0.61		0.36	0.47
USGS01500000 (Susquehanna River)	Calibration	0.38	0.41	USGS01594000 (Patuxent River)	0.55	0.44
	Validation	0.39	0.44		0.61	0.42
USGS01534000 (Susquehanna River)	Calibration	0.39	0.53	USGS01485000 (Eastern Shore)	0.65	0.40
	Validation	0.64	0.47		0.62	0.53
USGS01539000 (Susquehanna River)	Calibration	0.50	0.58	USGS01491000 (Eastern Shore)	0.53	0.41
	Validation	0.60	0.45		0.57	0.30

Table 9. Results of calibration and validation for 18 stream gauge locations in the fiver river basins.

Station name	Type	NSE	R2	Station name	NSE	R^2
USGS02034000 (James River)	Calibration	0.59	0.58	USGS02059500 (Roanoke River)	0.60	0.62
	Validation	0.50	0.54		0.50	0.51
USGS02024000 (James River)	Calibration	0.56	0.58	USGS02062500 (Roanoke River)	0.54	0.54
	Validation	0.61	0.60		0.61	0.62
USGS02018000 (James River)	Calibration	0.48	0.60	USGS02056900 (Roanoke River)	0.46	0.50
	Validation	0.56	0.61		0.60	0.64
USGS02042500 (James River)	Calibration	0.66	0.52	USGS02077670 (Roanoke River)	0.59	0.60
	Validation	0.72	0.54		0.59	0.65
USGS02040000 (James River)	Calibration	0.63	0.63	USGS01674500 (York River)	0.65	0.50
	Validation	0.61	0.58		0.64	0.47
USGS01664000 (Rappahannock River)	Calibration	0.57	0.61	USGS01671100 (York River)	0.52	0.51
	Validation	0.49	0.58		0.50	0.59
USGS01666500 (Rappahannock River)	Calibration	0.48	0.45	USGS01673550 (York River)	0.60	0.54
	Validation	0.62	0.49		0.50	0.61
USGS03170000 (New River)	Calibration	0.41	0.55	USGS03165000 (New River)	0.62	0.63
	Validation	0.48	0.61		0.41	0.49
USGS03167000 (New River)	Calibration	0.64	0.65	USGS03161000 (New River)	0.62	0.66
	Validation	0.68	0.70		0.62	0.64

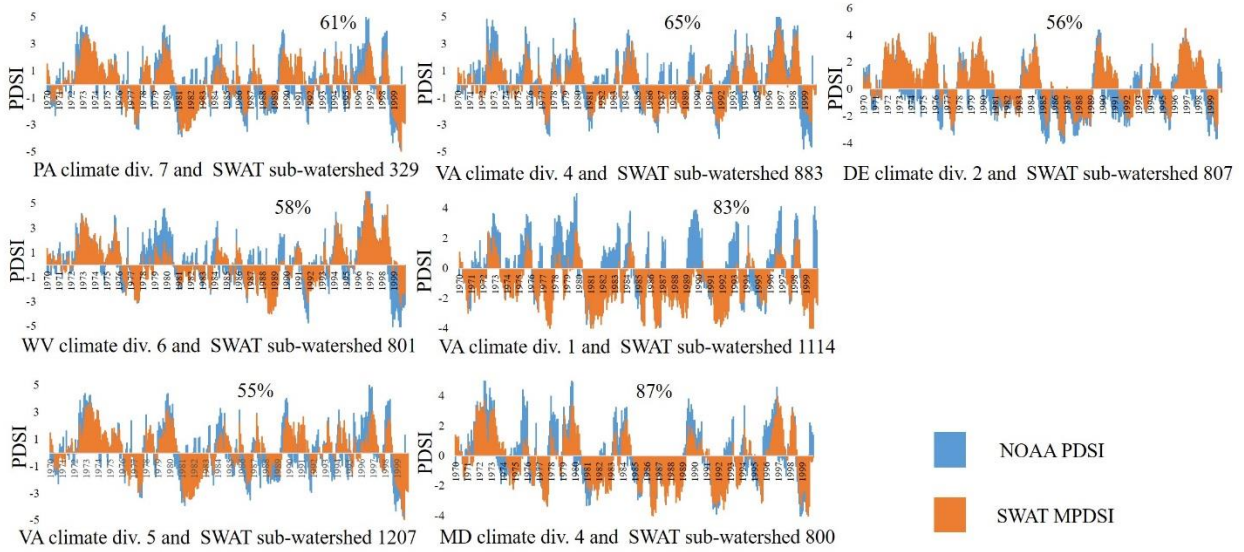

Figure 9. Comparison of PDSI from NOAA and Modified PDSI (MPDSI) from the SWAT model results for the CB watershed. The X-axis is the 30-year period, and the Y-axis represents the drought index. The blue bars represent the PDSI values from NOAA, and the red bars represent the MPDSI values from the SWAT model results.

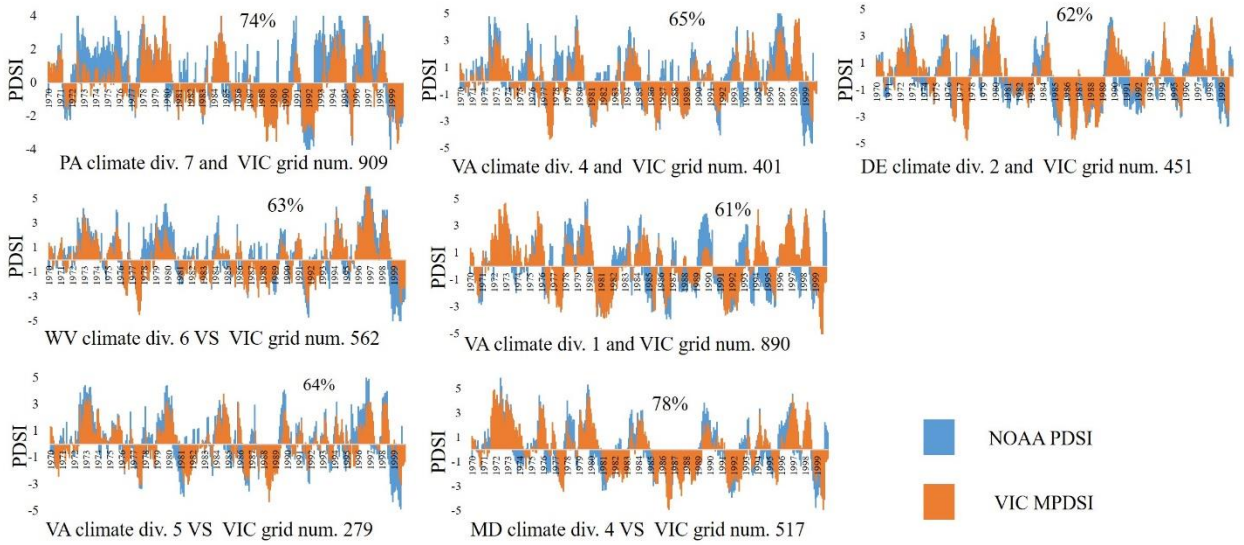

Figure 10. Comparison of PDSI from NOAA and Modified PDSI (MPDSI) from the VIC model results for the CB watershed. The X-axis is the 30-year period, and the Y-axis represents the drought index. The blue bars represent the PDSI values from NOAA, and the red bars represent the MPDSI values from the VIC model results.

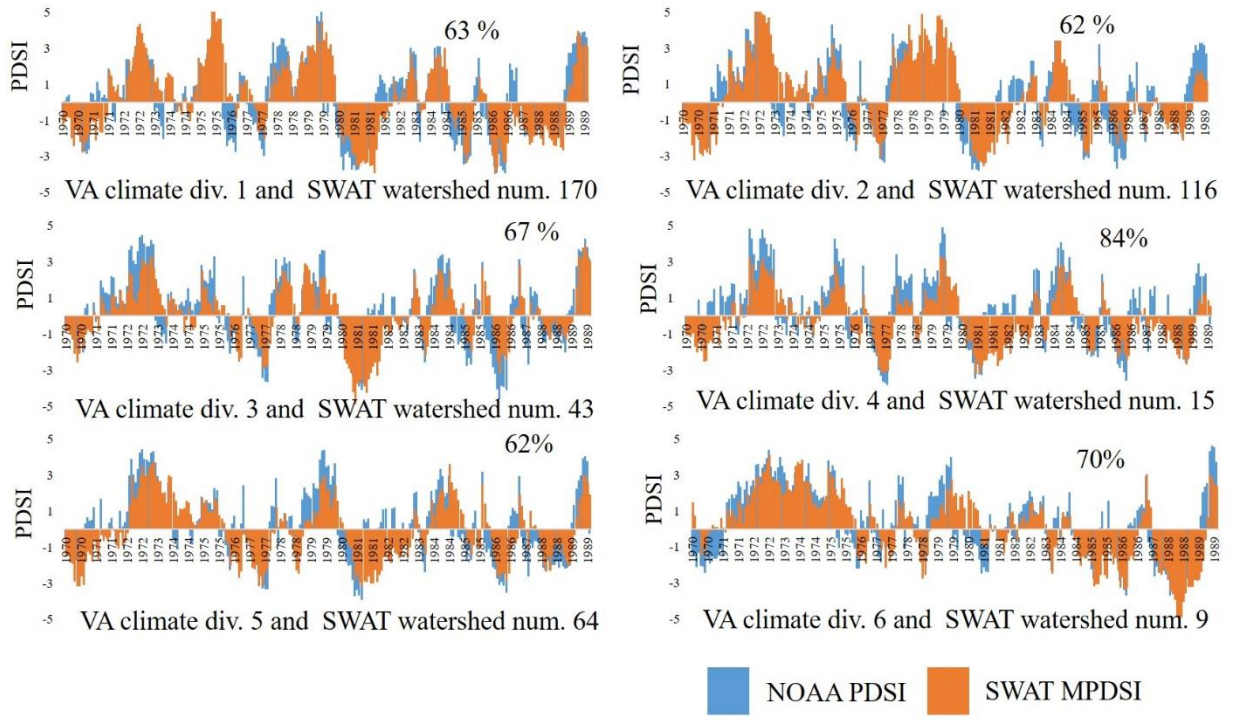

Figure 11. Comparison of PDSI from NOAA and MPDSI from the model results. The X-axis is the 20-year period, and the Y-axis represents the drought index. The X-axis is the 30-year period, and the Y-axis represents the drought index. The blue bars represent the PDSI values from NOAA, and the red bars represent the MPDSI values from the SWAT model results for the five river basins.

3.4.3. Time Series of Drought Indices

To illustrate the hydrometeorological relationships between precipitation and soil moisture, weekly evaluations of the SSI, MSDI, and MPDSI were carried out using water budget components from SWAT and VIC. Figure 12(a) and Figure 12(b) represent the weekly time series of SSI for the CB watershed. The mean values of SSI from VIC and SWAT for the historical period were 0.052 and 0.319 for RCP 4.5, and 0.114 and 0.381 for RCP 8.5, respectively. However, the mean values for the future periods, f1 and f2, were less than the historical means of SSI, indicating that future droughts based on SSI would be expected to increase based on the simulation results from both the models. Figure 13(a) shows the weekly time series of SSI for the average of the five river basins. The mean values of SSI for the historic period were 0.202 and 0.220 for RCP 4.5 and RCP 8.5. However, the mean values for the future periods were −0.117 and −0.108 for RCP 4.5, and −0.070 and −0.206 for RCP 8.5. Overall, since the results for future periods were lower than

the historic means of SSI, the future droughts computed based on SSI would be presumed to increase. More specifically, the biggest difference between historic and future mean values of SSI occurred in the New River basin, and they were 0.379 in the f1 period and 0.559 in the f2 period. However, the smallest difference was seen in the Roanoke River basin for the f1 period (0.262), and the James River basin during the f2 period (0.275).

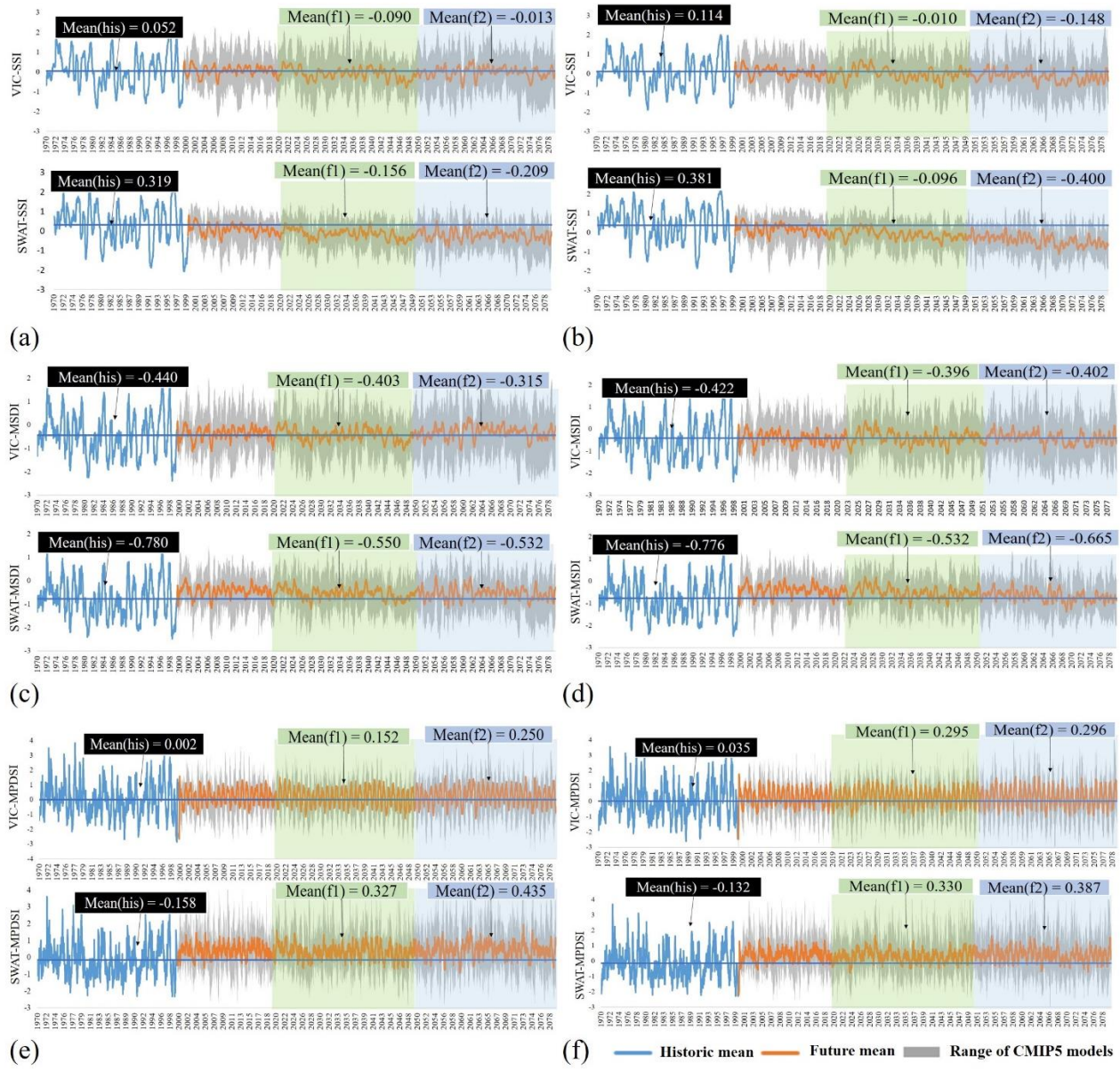

Figure 12. SWAT and VIC-Based Weekly Time Series of Drought Indices for the CB Watershed. The blue lines indicate the mean values for the historic period, and the orange lines are the mean values for the future period from 10 climate models. The transparent green and blue rectangles highlight the future periods. (a) SSI for RCP4.5. (b) SSI for RCP8.5. (c) MSDI for RCP4.5. (d) MSDI for RCP8.5. (e) MPDSI for RCP4.5. (f) MPDSI for RCP8.5.

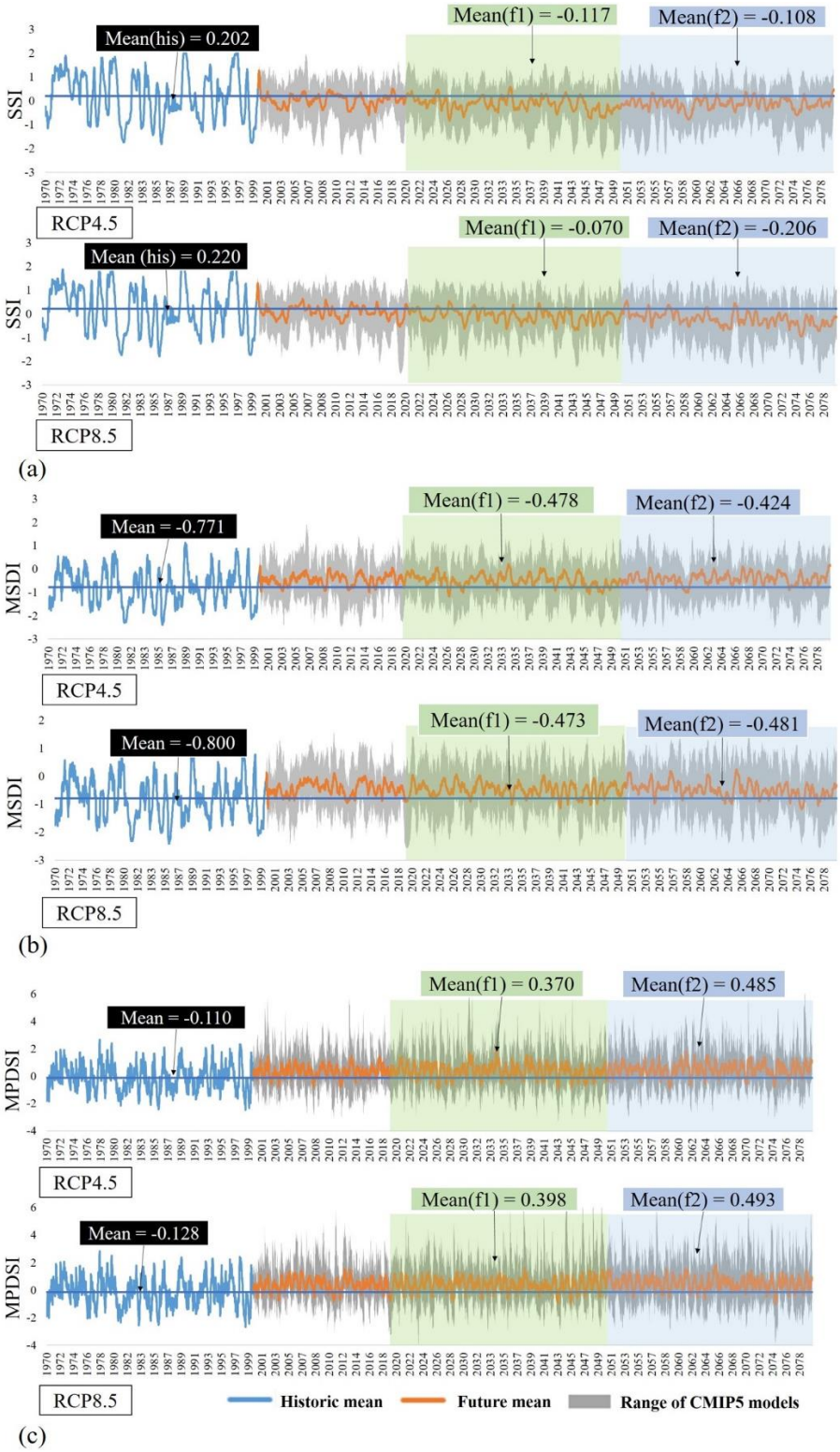

Figure 13. Weekly time series of (a) SSI, (b) MSDI, and (c) MPDSI for five river basins. The blue lines indicate the historic period, and the orange lines are the mean values for the future period from ten climate models. The transparent green and blue rectangles highlight the future periods.

Both SWAT and VIC are constructed based on the water balance approach, and the increase in drought occurrences based on the SSI were closely associated with the hydrologic variables such as precipitation, surface runoff, baseflow, and ET. Figures 9 and 10 show the comparisons of historical and future $EQ = E_a + Q_{surf} + Q_{gw}$ for both RCP 4.5 and RCP 8.5 for the CB watershed. EQ was calculated by the sum of the evapotranspiration (E_a), surface runoff (Q_{surf}), and amount of return flow (Q_{gw}). As shown in Figure 14 and 15, there were differences in EQ between historic and future periods. From the results of the SWAT model, the mean values of annual differences were 1.66 mm (f1) and 2.46 mm (f2) for RCP 4.5, and 1.77 mm (f1) and 2.56 mm (f2) for RCP 8.5. Also, the mean values of annual differences from VIC were 0.13 mm and 0.89 mm for RCP 4.5, and 0.24 mm and 0.84 mm for RCP 8.5. These results suggest that higher differences in EQ had a great impact on drought conditions, which were computed by SSI.

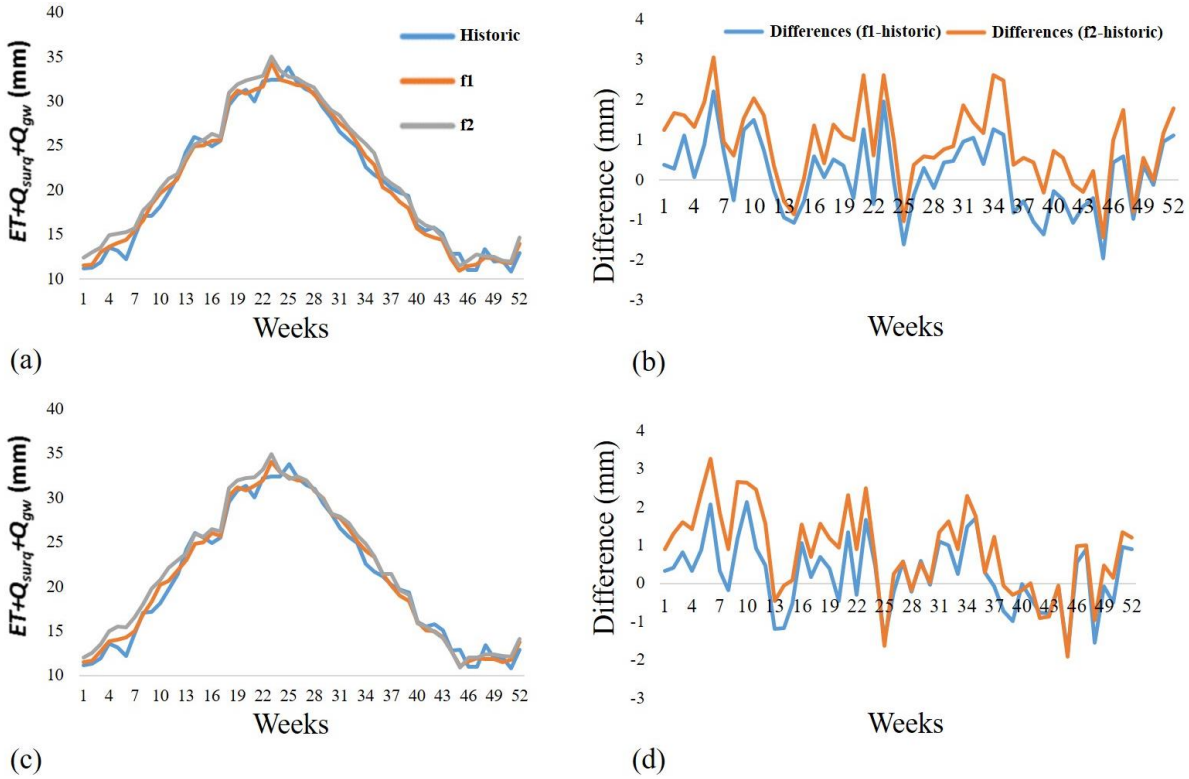

Figure 14. Seasonal Comparisons of the Mean Values of EQ in the CB Watershed from the VIC Model Results. (a, c) The blue lines are the weekly means of EQ for the historic period, whereas the orange and gray lines represent the future periods (Orange: f1, Gray: f2). (b, d) The blue and orange lines are the differences in EQ between historic and future periods. The blue lines indicate the differences between f1 and the historic values, whereas the orange lines represent the differences between f2 and the historic values. (a) Comparisons of mean values for RCP4.5. (b) Differences between historic and future periods (future - historic) for RCP4.5. (c) Comparisons of mean values for RCP8.5. (d) Differences between historic and future periods (future - historic) for RCP8.5.

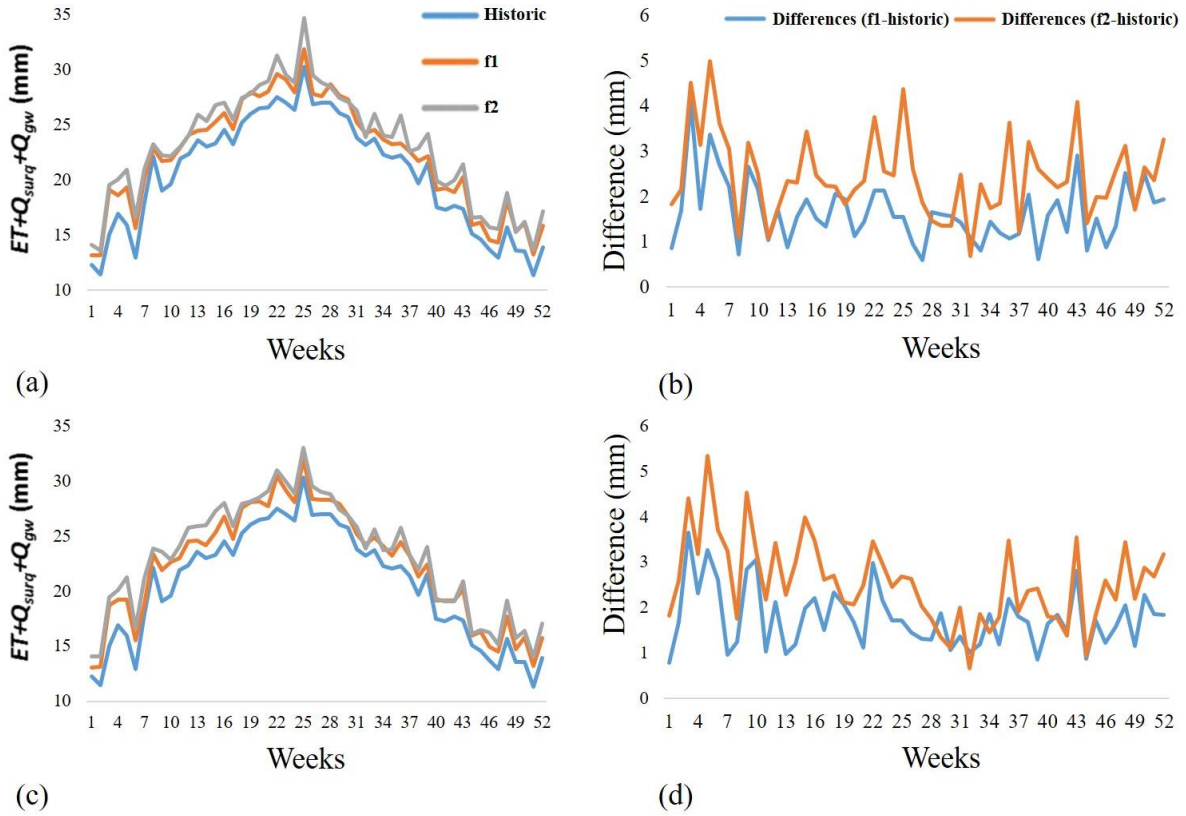

Figure 15. Seasonal Comparisons of the Mean Values of EQ in the CB Watershed from the SWAT Model Results. (a, c) The blue lines are the weekly means of EQ for the historic period, whereas the orange and gray lines represent the future periods (Orange: f1, Gray: f2). (b, d) The blue and orange lines are the differences in EQ between historic and future periods. The blue lines indicate the differences between f1 and the historic values, whereas the orange lines represent the differences between f2 and the historic values. (a) Comparisons of mean values for RCP4.5. (b) Differences between historic and future periods (future - historic) for RCP4.5. (c) Comparisons of mean values for RCP8.5. (d) Differences between historic and future periods (future - historic) for RCP8.5.

Figure 16 shows comparisons of EQ for the fiver river basins, and it implies that there was a projected overall increase in EQ for every week of the year in the future. Specifically, the greatest difference for RCP 8.5 and RCP 4.5 occurred during the crop-growing season. Thus, the comparisons of EQ implied that increases in the drought conditions based on SSI may have resulted in an increase in EQ and reductions in soil moisture, and, as a result, different patterns during the growing season were evident. For example, Figure A12 shows differences in soil moisture between historic and future periods (f1 and f2) for the New river basin in the S2 model, and it indicates that increased drought based on SSI could be directly related to a soil moisture deficit.

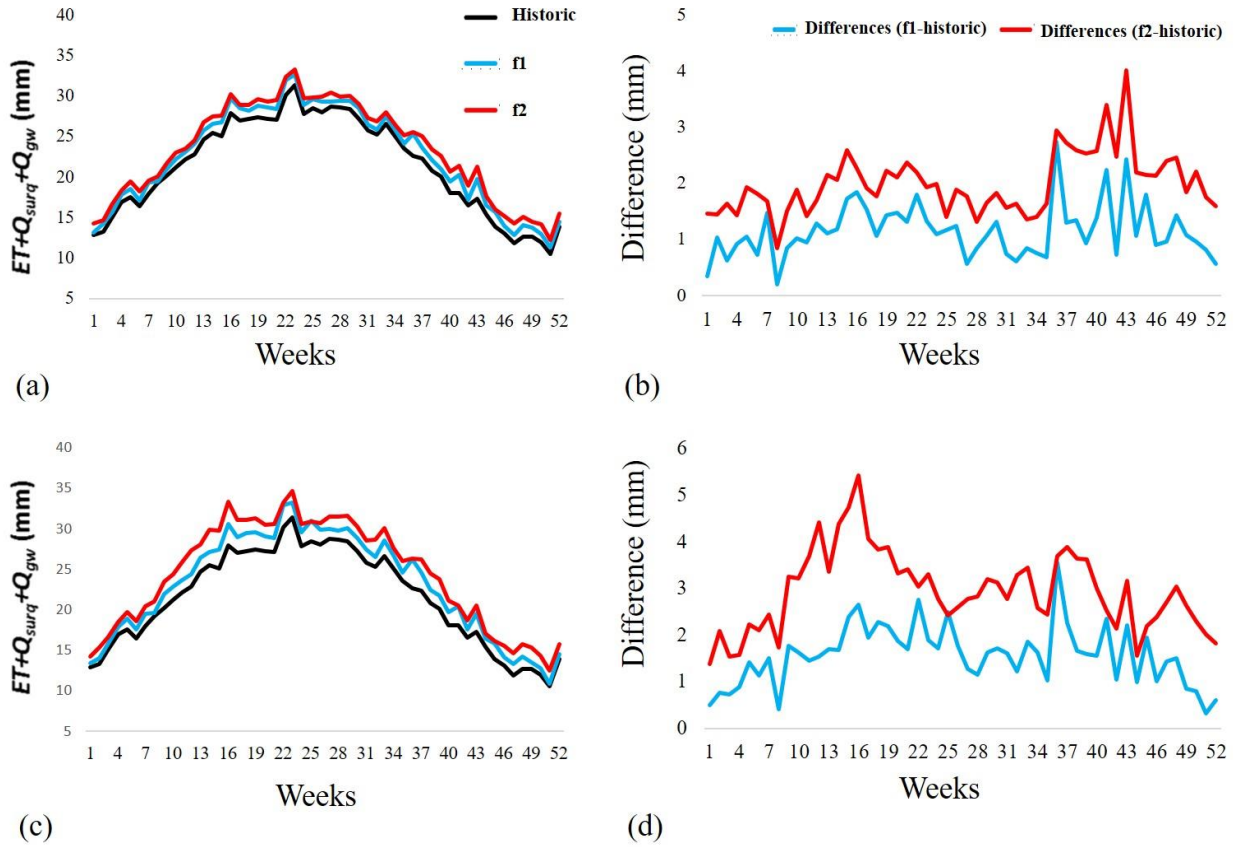

Figure 16. Seasonal comparisons of the mean values of EQ in the five river basins. (a)RCP4.5 (c) RCP8.5. The black lines are the weekly means of EQ for the historic period, whereas the blue and red lines represent the future periods (Blue: f1, Red: f2); (b) RCP4.5 (d) RCP8.5. Blue and red lines are the differences in EQ between historic and future periods. The blue lines indicate the differences between f1 and the historic values, whereas the red lines represent the differences between f2 and the historic values.

Soil moisture is a crucial variable of the climatic system since it plays a critical role in land-atmosphere feedbacks including plant transpiration, bare soil evaporation, and energy fluxes at the regional to global scales (Sridhar and Wedin, 2009; Seneviratne et al., 2010; Jaksa and Sridhar, 2015). In addition, accurate quantification of soil moisture and a statistically based soil moisture index would be significantly beneficial to reduce uncertainties in future climate projections, particularly for extreme events such as droughts as well as their agricultural impacts. Thus, the drought projection approaches based on the model-estimated soil moisture can contribute to drought projections since the soil moisture outputs from multiple models were used to diminish uncertainties.

Figures 12c and 12d represent the weekly time series of MSDI for the entire CB watershed. The mean values of MSDI from VIC and SWAT in the historical period were -0.440 and -0.780

for RCP 4.5, and -0.422 and -0.776 for RCP 8.5, respectively. By contrast, the mean values of MSDI for future periods were higher than the historical means. The largest difference between historical and future mean values of MSDI occurred during the f2 period for RCP 4.5 from SWAT (0.248), whereas the smallest difference occurred during the f2 period for RCP 8.5 from VIC (0.02). Unlike the computation of SSI, MSDI was estimated using the combination of precipitation and soil moisture. The MSDI-based drought evaluations were remarkably different from SSI because an increase in precipitation was expected in the future periods. For the five river basins, The mean values of MSDI in the historic period were −0.771 and −0.800 for RCP 4.5 and RCP 8.5. However, the mean values for the future periods were −0.478 and −0.424 for RCP 4.5, and −0.070 and −0.206 for RCP 8.5, respectively. In contrast, with the results of SSI, the mean values of MSDI for future periods were higher than the historic means of MSDI. The biggest difference between historic and future mean values of MSDI occurred in the Roanoke River basin during the f1 period (0.355) and the James River basin during the f2 period (0.382), whereas the smallest difference occurred in the Rappahannock River during the f1 period (0.233) and the New River basin during the f2 period (0.228), respectively. Unlike the computation of SSI, MSDI was calculated using precipitation and soil moisture. Since an increase in precipitation was expected in the future periods, the evaluations of drought conditions based on MDSI were remarkably different from SSI.

Determination of droughts based on a single hydro-climatic variable or index might be insufficient to obtain robust decision-making and risk assessment (Hao and AghaKouchak, 2013), and that is the reason why the MSDI was proposed. The MSDI is responsive to agricultural and meteorological drought conditions, and the onset of drought is influenced by precipitation and drought persistence, which in turn are dominated by soil moisture behavior (Hao and AghaKouchak, 2013). Therefore, the framework of MSDI can provide varied perspectives of droughts by combining multiple variables probabilistically.

Finally, Figures 12e and 12f show the weekly time series of MPDSI for the entire CB watershed. The mean values of MSDI from VIC and SWAT for the historical period were 0.002 and -0.158 for RCP 4.5, and 0.035 and -0.132 for RCP 8.5, respectively. Similar to the implications of MSDI, the future mean values of MPDSI were higher than the historical means from both VIC and SWAT. Therefore, the results imply that there will be a decrease in meteorological droughts in the future. In particular, the biggest difference between mean values of MPDSI occurred during

the f2 period for RCP 4.5 from SWAT (0.593), whereas the smallest difference occurred during the f1 period for RCP 4.5 from VIC (0.150). For the five river basins, The mean values of MPDSI for the historic period were −0.110 and −0.128 for RCP 4.5 and RCP 8.5. Additionally, the mean values for future periods were 0.370 and 0.485 for RCP 4.5, and 0.398 and 0.493 for RCP 8.5, respectively. Similar to the results of MSDI, the mean values of MPDSI for future periods were larger than the historic means of MPDSI. Thus, the results imply that there was a decrease in meteorological droughts projected for the future. More specifically, the biggest difference between the historic and future mean values of MPDSI occurred in the York River basin during the f1 period (0.547), and in the Roanoke River basin during the f2 period (0.643). Whereas the smallest difference occurred in the Rappahannock River during the f1 period (0.444), and in the New River basin during the f2 period (0.57), respectively. Since MPDSI is a meteorological drought index, their values are highly influenced by increases in precipitation. Thus, the mean values of MPDSI for future periods were higher than the historic values. Additionally, the overall differences between historic and future periods of MPDSI were higher than MSDI, which can reflect both agricultural and meteorological perspectives of drought conditions.

3.4.4. Seasonal Comparisons of Drought Indices

Seasonal comparisons of the historical and future drought conditions are beneficial to understand what seasons are susceptible to droughts. Therefore, seasonal drought management and mitigation plans would be based on these comparisons. Especially, evaluation of droughts during the crop-growing season might be critical to crop production. Additionally, droughts in the winter seasons are significant due to groundwater recharge during the winter months (November to February) as it controls baseflow to stream during March-May.

Figure 17 represents the seasonal comparisons of historical and future drought indices in the CB watershed. In case of SWAT, the results of SSI demonstrate that there was an overall decrease in SSI for all of the years in the future periods for both RCP 4.5 and RCP 8.5. More specifically, greater differences were observed in the periods between April and September (approximately 13-40 weeks per year), which implies an overall increase in agricultural drought severities in the future, particularly during the crop-growing seasons. However, the results of SSI from VIC showed that there was a decrease in SSI for specific periods of the year for both RCP

4.5 and RCP 8.5. Particularly, historical SSI values were lower than the future periods between the spring and summer months (approximately 13-28 weeks per year) but were higher for other months. These results imply an increase in agricultural droughts from late summer to spring months (approximately July to April).

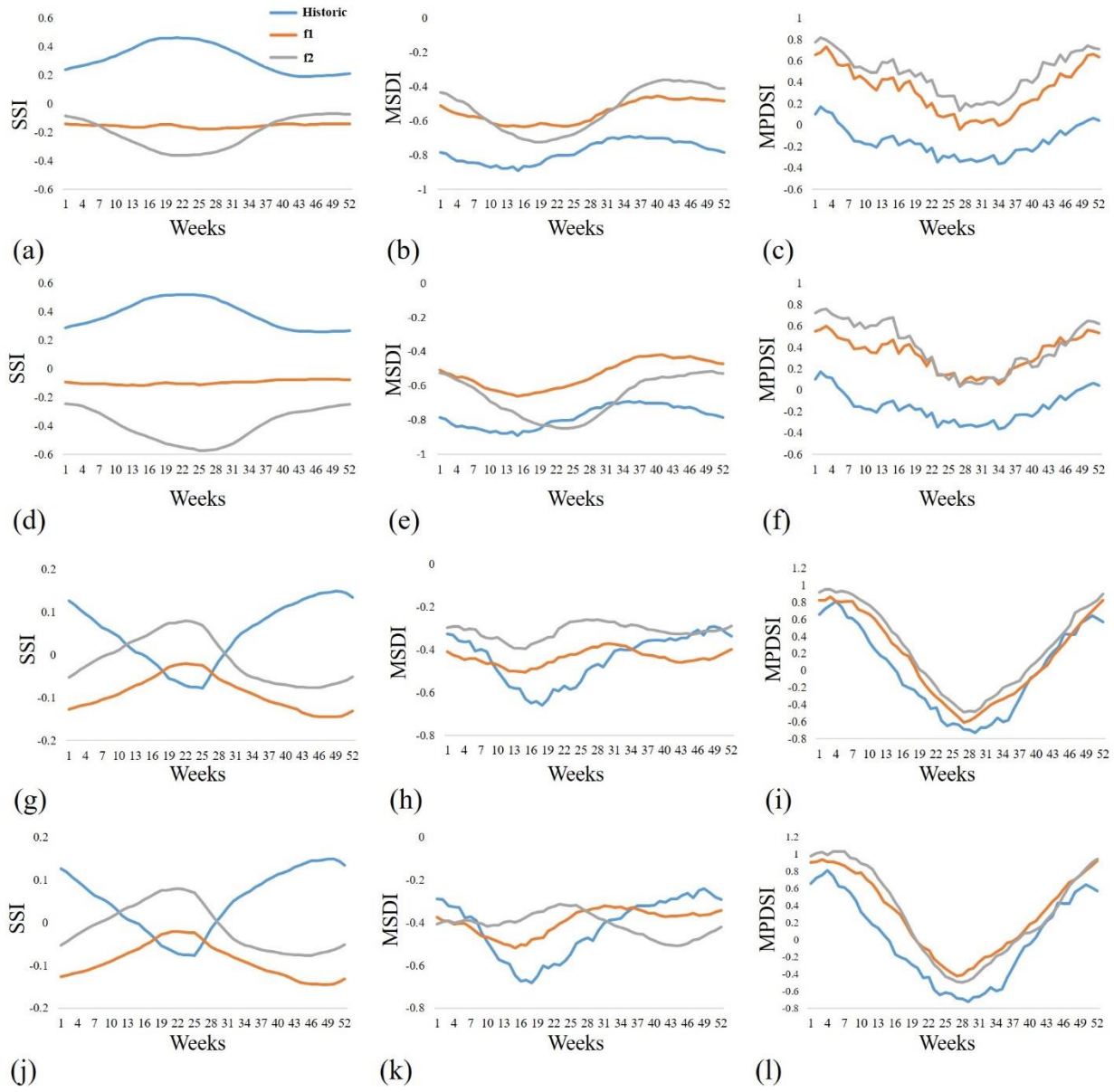

Figure 17. Seasonal Comparisons of the Mean Values of Drought Indices in the CB Watershed. The blue lines are the weekly means of the drought indices for the historic period, whereas the orange and gray lines represent the future periods (Orange: f1, Gray: f2). (a) SSI for RCP4.5 from SWAT, (b) MSDI for RCP4.5 from SWAT, (c) MPDSI for RCP4.5 from SWAT. (d) SSI for RCP8.5 from SWAT. (e) MSDI for RCP8.5 from SWAT, (f) MPDSI for RCP8.5 from SWAT, (g) SSI for RCP4.5 from VIC, (h) MSDI for RCP4.5 from VIC, (i) MPDSI for RCP4.5 from VIC, (j) SSI for RCP8.5 from VIC, (k) MSDI for RCP8.5 from VIC, (l) MPDSI for RCP8.5 from VIC.

In contrast, the results of MSDI from SWAT indicate that the ensemble means in the future would be higher than the historical periods, and they suggest a decrease in drought severities from multivariate perspectives of droughts in all seasons. However, the results of MSDI from VIC indicate that the mean values of future periods for specific months (August to February) would be lower than the historical periods, which implied an increase in drought severities for these particular months. Similar to the time series analyses, an increase in precipitation hugely influenced the calculation of MSDI, which counterbalanced the decline of soil moisture in the future. Similar to the results of MSDI, the ensemble means of the future periods for MPDSI were higher than the historical means for both SWAT and VIC, which suggested that there was an overall decrease in meteorological drought severities when considering variables that are sensitive to understanding droughts such as soil moisture, precipitation, and ET.

Figure 18 shows the seasonal comparisons of drought indices between historic and future periods in the five river basins. The results of SSI indicate that there was an overall decrease in SSI values for all weeks of the year in the future for both RCP 4.5 and RCP 8.5. Specifically, greater differences between historic and future mean values of SSI were found in the periods between April and September (approximately 13–30 weeks of year) for both the f1 and f2 periods. The results of seasonal comparisons of SSI implied that overall agricultural drought severities increased in the future, specifically during the crop growing seasons (April–September) in the five river basins. However, the results of MSDI show that the ensemble means of future periods were higher than the historic periods, and it implied that there was an overall decrease in drought severities from multivariate perspectives of droughts in all seasons. Similar to the time series analyses, an increase in precipitation greatly influenced the computation of MSDI, and it counterbalanced the decrease in soil moisture in the future. However, in the New River basin for the RCP 8.5 and the f2 period, higher drought severity was expected between 15–32 weeks per year. Similar to the results of MSDI, the ensemble means of the future periods for MPDSI were higher than that of the historic means, and this indicated that there was an overall decrease in drought severities when considering variables such as precipitation, soil moisture, and evapotranspiration, which are sensitive to predicting drought.

The climate change projections suggest an increase in precipitation and temperature in the CB watershed and five river basins, and therefore, future drought projections should be performed with reliable drought indices that can examine diverse hydrometeorological conditions in the

future. Thus, a drought index that can recognize various perspectives of drought conditions would be valuable to characterize seasonal future drought projections.

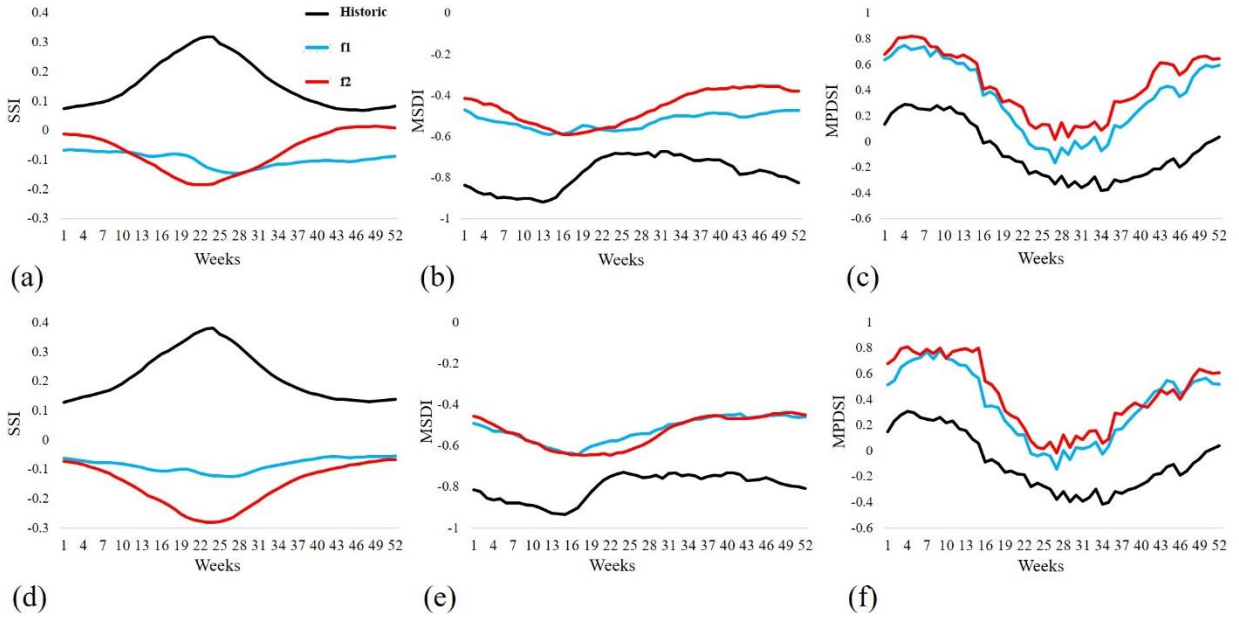

Figure 18. Seasonal comparisons of the mean values of the drought indices in the five river basins: (a) SSI for RCP4.5 (b) MSDI for RCP4.5 (c) MPDSI for RCP4.5 (d) SSI for RCP8.5 (e) MSDI for RCP8.5 (f) MPDSI for RCP8.5.The solid lines are the weekly means of the drought indices during the historic period, whereas the dashed lines represent the future periods.

3.4.5. Results of Drought Occurrences

Figures 19-21 show the spatial patterns of the drought occurrences based on SSI, MSDI, and MPDSI, and these were computed using the division of historical and future drought occurrences for each sub-watershed and grid (future/historical). For instance, a value equal to or >1 is shown in red or orange and indicates an increase in drought occurrences in the future. However, values <1 are represented in green or yellow-green and indicate a decrease in drought occurrences in the future.

As shown in Figure 19, there is an overall increase in agricultural drought occurrences in the future in some climate models such as S1, S2, S9, and S10 for both RCP 4.5 and RCP 8.5. In particular, the western areas of the James, Potomac, and Susquehanna River basins and the central areas of the Susquehanna River basin were vulnerable to agricultural droughts in the CB watershed

from both SWAT and VIC. In addition, the results of drought occurrences based on SSI showed that although there was an increase in precipitation during the future periods, agricultural droughts occurred more frequently in some regions. SWAT and VIC are based on the water balance approach, and the increase in drought occurrences was closely associated with the hydrologic variables such as surface runoff, baseflow, and ET. Figures 9 and 10 show the comparisons of historical and future differences in EQ from both the model outputs, and there was an overall increase in EQ in the future with a few exceptions in the VIC outputs. Therefore, the comparisons of EQ suggested that increase in agricultural droughts based on SSI were primarily due to decreases in soil moisture and increases in EQ.

Figure 20 shows spatial maps of drought occurrences based on the MSDI for the CB watershed. As shown in this figure, future drought occurrences varied among different regions and climate models. Overall, the spatial patterns of SWAT and VIC were comparable, and the western areas in the CB watershed were more vulnerable to droughts than the eastern and southern areas, but the ratios were less than the results of SSI. Drought evaluations based on MSDI used the multivariate variables (e.g., precipitation and soil moisture) and drought occurrences simulated by MSDI were different from SSI, which was influenced by the projected increase in precipitation in the future.

MPDSI-based spatial maps for the CB watershed are shown in Figure 21. There was distinct spatial heterogeneity for each climate model and future period. Since MPDSI is a meteorological drought index, it implies that drought occurrences based on MPDSI are influenced by increases in precipitation in the future. Similar to the results of MSDI, the western areas were more vulnerable to droughts than the eastern and southern areas where higher precipitation increases were expected. Furthermore, a decrease in precipitation or a slight increase are expected in the western areas of the James, Potomac, and Susquehanna River basins (Figure 4) and are associated with vulnerabilities of spatial drought occurrences by multiple drought indices.

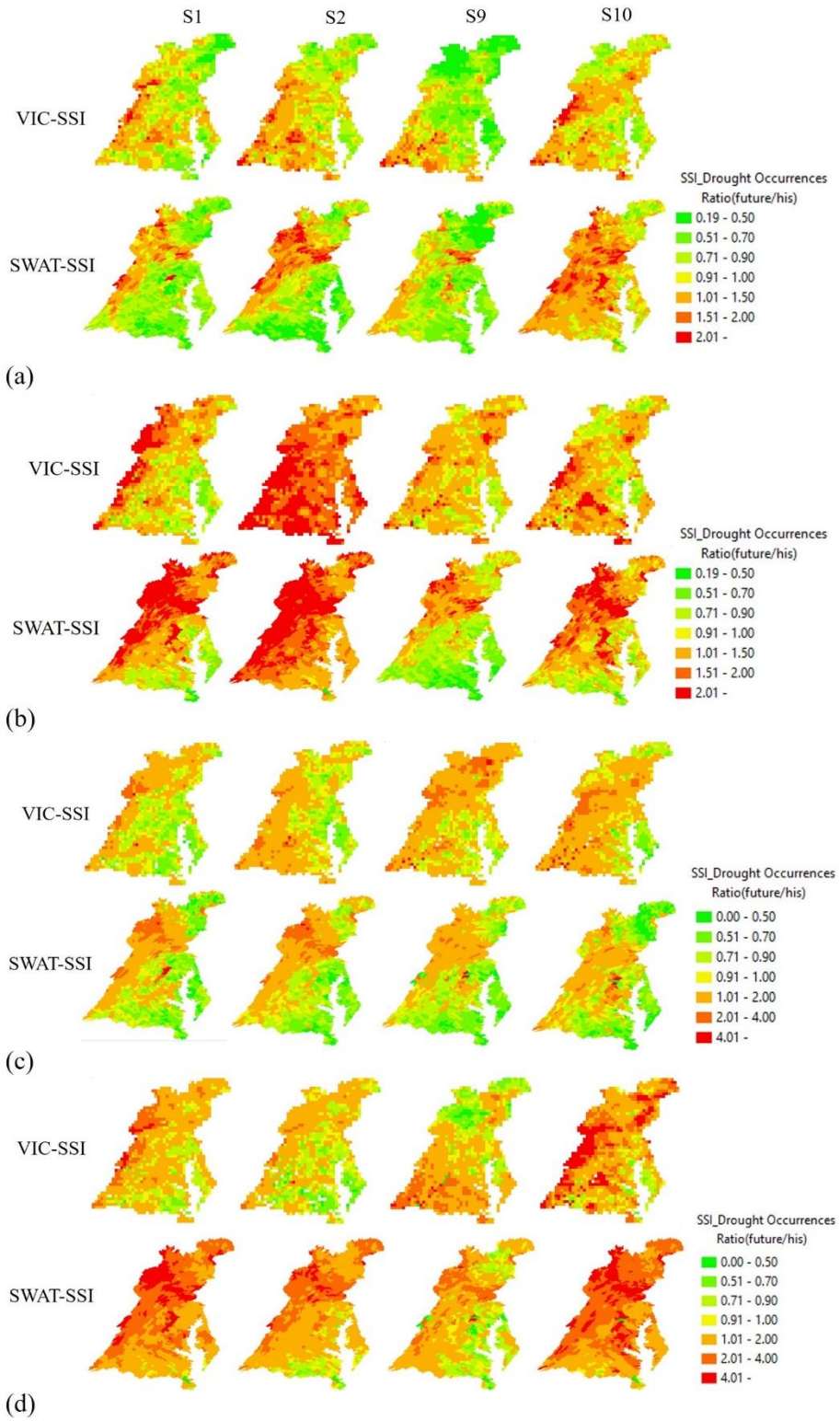

Figure 19. Spatial maps of the comparisons of drought occurrences based on the results of SSI between the historic and future periods (CB watershed). A value equal to or >1 is represented in red and indicates an increase in drought occurrences in the future. A value <1 is represented in green and indicates a decrease in drought occurrences in the future. (a) SSI for RCP4.5 and f1 period. (b) SSI for RCP4.5 and f2 period. (c) SSI for RCP8.5 and f1 period. (d) SSI for RCP8.5 and f2 period.

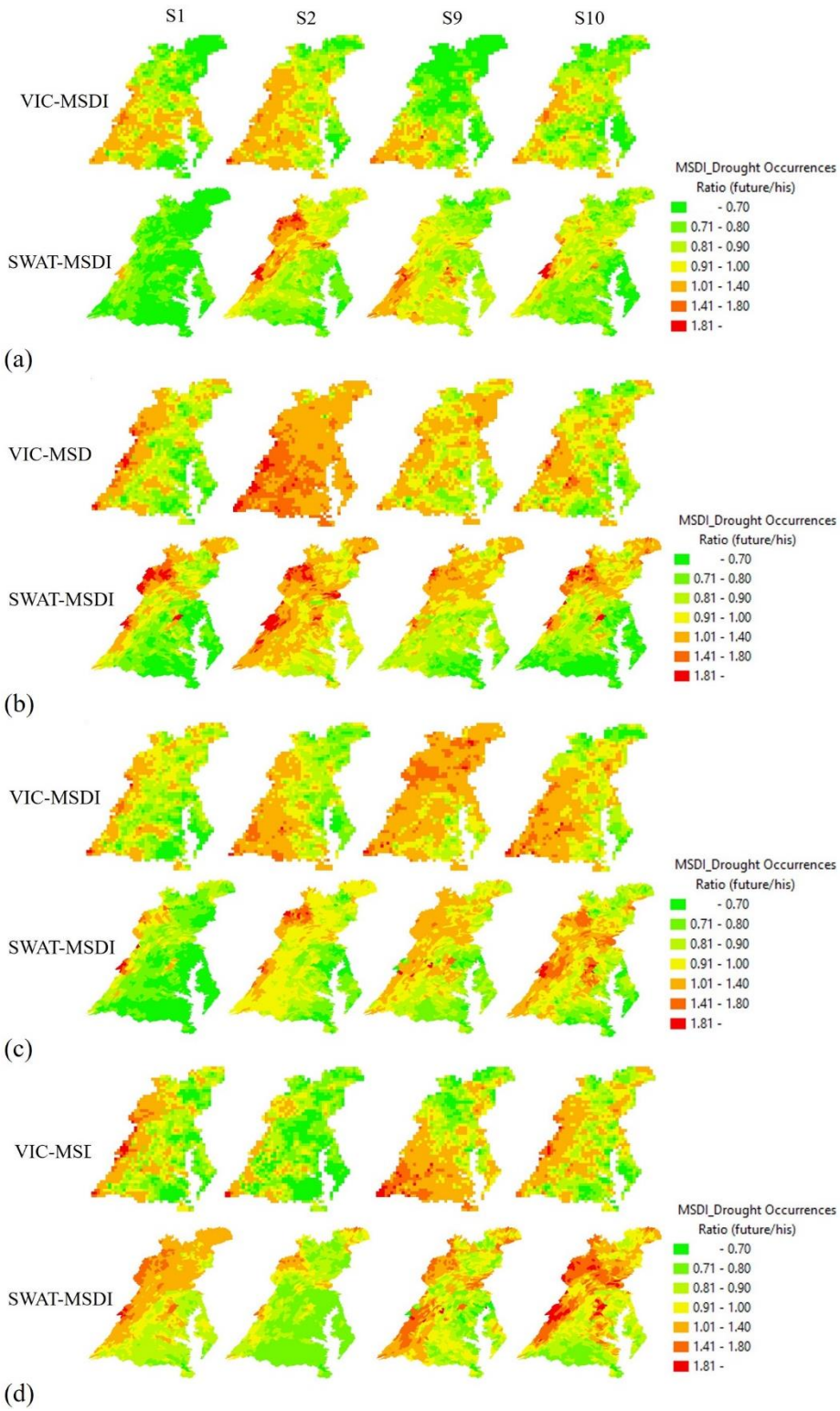

Figure 20. Spatial maps of the comparisons of drought occurrences based on the results of MSDI between the historic and future periods (CB watershed). A value equal to or >1 is represented in red and indicates an increase in drought occurrences in the future. A value <1 is represented in green and indicates a decrease in drought occurrences in the future. (a) SSI for RCP4.5 and f1 period. (b) SSI for RCP4.5 and f2 period. (c) SSI for RCP8.5 and f1 period. (d) SSI for RCP8.5 and f2 period.

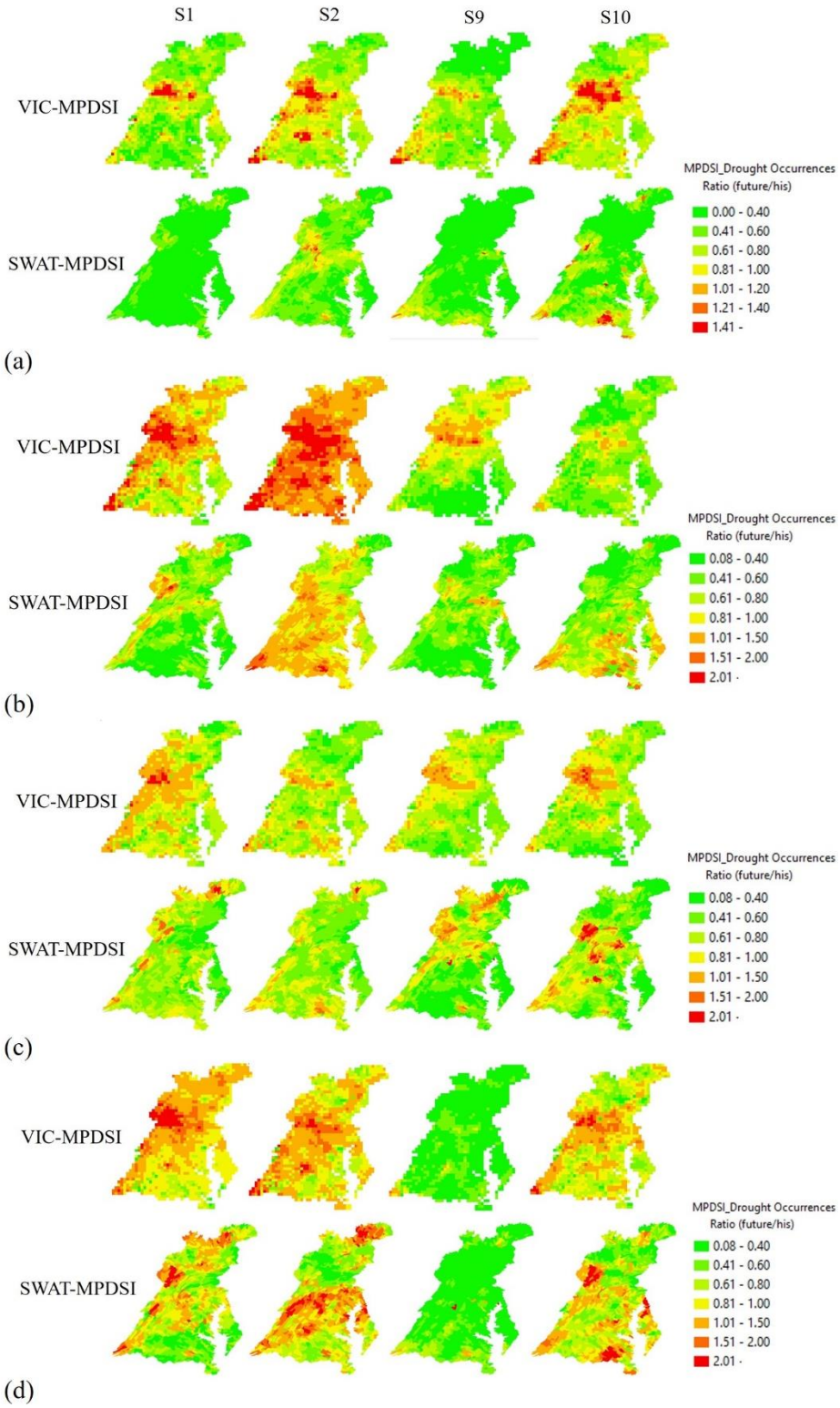

Figure 21. Spatial maps of the comparisons of drought occurrences based on the results of MPDSI between the historic and future periods (CB watershed). A value equal to or >1 is represented in red and indicates an increase in drought occurrences in the future. A value <1 is represented in green and indicates a decrease in drought occurrences in the future. (a) SSI for RCP4.5 and f1 period. (b) SSI for RCP4.5 and f2 period. (c) SSI for RCP8.5 and f1 period. (d) SSI for RCP8.5 and f2 period.

Table 10 is the ratio of drought occurrences in future periods based on the results of SSI. As shown in Table 10, there is an overall increase in drought occurrences in the future during both f1 and f2 periods in several climate models, such as S2 and S9, for both RCP 4.5 and RCP 8.5. The results of the ensemble mean indicate that there were 1.30 times more droughts in the New River basin for RCP 8.5 during the f2 period, and 1.13–1.81 times more droughts in the Rappahannock basin. From these results, it can be said that the New and Rappahannock river basins are vulnerable to agricultural droughts among the five river basins. Additionally, the results of SSI indicate that even though there was an increase in precipitation for the simulation periods, agricultural droughts occurred more frequently in some regions. As mentioned above, the SWAT model is based on the simple water balance approach, and the increase in drought conditions was related to the input variables, such as precipitation, Surface runoff, baseflow, and evapotranspiration.

For the results of MSDI, there was an overall decrease in drought occurrence for most of the climate models, while the areal extent also increased in S2 in the New River basin during the second future period (f2). MSDI was proposed to consider multivariate variables (precipitation and soil moisture) for drought evaluation, and it has been known that the onset and termination of droughts are influenced by both precipitation and soil moisture. Thus, drought occurrences derived by MSDI were different from SSI, which was influenced by increased precipitation in the future (Table 11). Table 12 is the ratio of drought occurrences for future periods based on the results of MPDSI. There was an overall decrease in drought occurrences in the future. Since MPDSI is a meteorological drought index, it can be said that drought occurrences estimated by MPDSI are influenced by the increases in precipitation in the future. Figure 18 shows the comparisons of historic and future change of EQ, and there was a projected overall increase in EQ for every week of the year in the future. Specifically, the greatest difference for RCP 8.5 and RCP 4.5 occurred during the crop-growing season. Thus, the comparisons of EQ implied that increases in the drought conditions based on SSI may have resulted in an increase in EQ and reductions in soil moisture, and, as a result, different patterns during the growing season were evident.

Table 10. Ratio of drought occurrences for historic and future periods in five river basins based on results of SSI

	James				New				Rappahannock				Roanoke				York			
	RCP4.5		RCP 8.5		RCP 4.5		RCP 8.5		RCP 4.5		RCP 8.5		RCP 4.5		RCP 8.5		RCP 4.5		RCP 8.5	
	f1	f2	f1	f2	f1	f2	f1	f2	f1	f2	f1	f2	f1	f2	f1	f2	f1	f2	f1	f2
S1	0.18	0.31	0.87	1.67	0.83	1.81	1.23	2.65	1.22	2.10	2.06	4.14	0.70	1.13	0.89	1.72	0.64	1.20	0.94	1.82
S2	0.61	1.62	0.80	1.17	0.76	2.26	1.03	1.89	1.40	3.13	1.54	2.50	0.63	1.65	0.79	1.33	0.67	1.50	0.75	1.12
S3	0.62	0.56	0.67	0.52	0.88	0.82	1.08	0.90	1.06	0.89	1.02	0.70	1.99	0.20	2.57	1.92	0.58	0.51	0.20	0.36
S4	0.35	0.46	0.32	0.49	0.38	0.66	0.38	0.73	0.47	0.93	0.45	0.74	0.10	0.21	0.65	1.13	0.33	0.65	0.37	0.51
S5	0.63	0.34	0.43	0.64	0.83	0.43	0.45	0.95	1.03	0.62	0.72	1.23	0.24	0.11	0.94	1.34	0.63	0.37	0.45	0.69
S6	0.39	0.52	0.66	0.81	0.51	0.73	0.89	0.95	0.54	0.85	1.26	1.35	0.39	0.58	0.63	0.80	0.35	0.57	0.66	0.82
S7	0.65	0.29	0.30	0.68	0.93	0.44	0.37	0.92	1.20	0.52	0.65	1.57	0.70	0.26	0.37	0.58	0.72	0.30	0.32	0.83
S8	0.65	0.45	0.39	0.25	0.81	0.48	0.32	0.35	1.02	0.83	0.65	0.51	0.76	0.40	0.38	0.22	0.71	0.52	0.51	0.33
S9	0.78	0.64	0.74	1.15	1.04	0.56	0.99	1.82	1.16	1.16	1.42	1.75	0.96	0.70	0.85	1.30	0.72	0.65	0.81	1.01
S10	1.04	0.90	0.82	1.47	1.28	1.24	0.88	1.86	2.20	2.34	1.92	3.63	1.10	0.87	0.94	1.42	1.08	1.13	0.89	1.67
Mean	0.59	0.61	0.60	0.89	0.83	0.94	0.76	1.30	1.13	1.34	1.17	1.81	0.76	0.61	0.90	1.18	0.64	0.74	0.59	0.92

*A value equal or greater than 1: increase in drought occurrences in the future periods

Table 11. Ratio of drought occurrences for historic and future periods in five river basins based on results of MSDI

	James				New				Rappahannock				Roanoke				York			
	RCP4.5		RCP 8.5		RCP 4.5		RCP 8.5		RCP 4.5		RCP 8.5		RCP 4.5		RCP 8.5		RCP 4.5		RCP 8.5	
	f1	f2	f1	f2	f1	f2	f1	f2	f1	f2	f1	f2	f1	f2	f1	f2	f1	f2	f1	f2
S1	0.51	0.54	0.66	0.85	0.68	1.04	0.86	1.12	0.69	0.82	0.74	1.01	0.68	0.79	0.72	0.89	0.57	0.72	0.62	0.81
S2	0.57	0.97	0.66	0.72	0.58	1.12	0.67	0.92	0.69	1.05	0.74	0.80	0.62	0.99	0.68	0.80	0.57	0.90	0.60	0.66
S3	0.57	0.45	0.58	0.45	0.73	0.56	0.72	0.58	0.80	0.58	0.78	0.54	0.80	0.51	0.72	0.52	0.52	0.42	0.31	0.36
S4	0.39	0.40	0.44	0.44	0.38	0.54	0.46	0.59	0.36	0.61	0.44	0.49	0.29	0.43	0.44	0.45	0.35	0.55	0.44	0.44
S5	0.60	0.34	0.41	0.56	0.70	0.42	0.43	0.72	0.67	0.39	0.48	0.68	0.46	0.26	0.44	0.54	0.57	0.34	0.42	0.54
S6	0.36	0.54	0.67	0.63	0.44	0.61	0.73	0.69	0.42	0.59	0.74	0.70	0.37	0.58	0.63	0.65	0.35	0.57	0.65	0.62
S7	0.58	0.27	0.35	0.60	0.68	0.43	0.46	0.76	0.68	0.31	0.43	0.70	0.59	0.27	0.38	0.57	0.58	0.28	0.34	0.60
S8	0.48	0.43	0.40	0.27	0.56	0.43	0.37	0.29	0.57	0.48	0.46	0.33	0.56	0.40	0.42	0.25	0.51	0.45	0.42	0.30
S9	0.71	0.60	0.71	0.83	0.94	0.65	0.79	1.12	0.70	0.66	0.79	0.84	0.87	0.69	0.80	0.92	0.65	0.57	0.71	0.77
S10	0.76	0.68	0.83	0.94	0.91	0.79	0.83	1.03	0.83	0.88	0.96	1.14	0.81	0.66	0.92	0.94	0.75	0.73	0.80	0.99
Mean	0.55	0.52	0.57	0.63	0.66	0.66	0.63	0.78	0.64	0.64	0.65	0.73	0.60	0.56	0.62	0.65	0.54	0.55	0.53	0.61

*A value equal or greater than 1: increase in drought occurrences in the future periods

Table 12. Ratio of drought occurrences for historic and future periods in five river basins based on results of MPDSI (%)

	James				New				Rappahannock				Roanoke				York			
	RCP4.5		RCP 8.5		RCP 4.5		RCP 8.5		RCP 4.5		RCP 8.5		RCP 4.5		RCP 8.5		RCP 4.5		RCP 8.5	
	f1	f2	f1	f2	f1	f2	f1	f2	f1	f2	f1	f2	f1	f2	f1	f2	f1	f2	f1	f2
S1	0.34	0.40	0.64	0.76	0.63	0.84	0.89	0.95	0.56	0.58	0.68	0.78	0.63	0.71	0.71	0.80	0.52	0.57	0.59	0.71
S2	1.28	0.69	0.58	0.56	0.54	1.21	0.62	0.73	0.59	1.06	0.70	0.63	0.60	1.13	0.67	0.69	0.49	0.90	0.55	0.54
S3	0.58	0.44	0.56	0.47	0.74	0.49	0.74	0.49	0.95	0.65	0.82	0.65	0.73	0.70	0.75	0.59	0.53	0.42	0.22	0.20
S4	0.32	0.28	0.30	0.30	0.28	0.48	0.32	0.34	0.30	0.56	0.33	0.33	0.36	0.51	0.44	0.45	0.31	0.46	0.32	0.32
S5	0.43	0.29	0.32	0.39	0.51	0.35	0.30	0.52	0.52	0.28	0.41	0.42	0.45	0.30	0.45	0.56	0.43	0.28	0.34	0.36
S6	0.24	0.36	0.55	0.56	0.30	0.37	0.60	0.51	0.31	0.39	0.58	0.62	0.29	0.41	0.53	0.62	0.23	0.38	0.50	0.54
S7	0.39	0.17	0.24	0.43	0.52	0.35	0.37	0.57	0.47	0.21	0.34	0.49	0.47	0.21	0.28	0.45	0.38	0.15	0.24	0.40
S8	0.40	0.37	0.40	0.37	0.48	0.40	0.22	0.20	0.47	0.41	0.33	0.23	0.51	0.36	0.31	0.23	0.37	0.34	0.28	0.22
S9	0.57	0.47	0.56	0.70	0.84	0.55	0.75	1.04	0.55	0.58	0.68	0.72	0.71	0.58	0.63	0.82	0.50	0.42	0.56	0.63
S10	0.81	0.74	0.81	0.74	0.87	0.78	0.83	0.79	0.84	0.83	0.85	0.79	0.85	0.76	0.87	0.76	0.70	0.74	0.81	0.81
Mean	0.54	0.42	0.50	0.53	0.57	0.58	0.56	0.61	0.56	0.55	0.57	0.57	0.56	0.57	0.56	0.60	0.45	0.47	0.44	0.47

*Negative values: increase in drought occurrences in the future periods

3.5. Conclusion

The warming of the global climate leads to increases in regional climatic variabilities and their impacts on drought conditions. Therefore, obtaining reliable drought projection and a monitoring framework are essential for drought mitigation plans and water resource management. In addition, robust interpretation of various perspectives of droughts would be advantageous to examine different drought characteristics (e.g., severities). This study examined future drought occurrences in the CB watershed and five river basins using high resolution of future climate model ensembles, two hydrological models (SWAT and VIC), and multiple drought indices. Both SWAT and VIC were calibrated and validated using the USGS streamflow stations and represent the potential applicability for the watershed. Additionally, historical MPDSI derived by two models was used to verify model performances for drought estimations.

The results of the SSI-based drought conditions suggested an overall increase in agricultural droughts in the entire study areas and that increases in drought conditions were associated with increases in ET and surface and groundwater discharge. However, the results of MSDI and MPDSI indicate overall decreases in drought occurrences, as both MSDI and MPDSI were influenced by increases in precipitation in the future, with distinct spatial differences. Thus, combined effects from both precipitation and temperature differences should be considered for the evaluation of future drought projections.

Assessment of future droughts using multiple water budget components from hydrological models and drought indices would provide an improved understanding of physical characteristics of drought, mitigation plans, and monitoring approaches because various factors related to the onset, persistence, recovery, and termination of droughts could be included. If future drought projections were based entirely on one hydrometeorological variable or one hydrologic model, they would present a less comprehensive outlook for the CB watershed and five river basins in Virginia. For instance, although there was an increase in precipitation in most areas of the CB watershed, agricultural drought occurrences in many regions were higher than in historical periods.

It is clear that an evaluation of future droughts is complex, but the utilization of multiple hydrologic models, climate models and drought indices at a relatively high resolution can offer better insights into the evolution of future drought predictions. Therefore, the drought projection

approaches described in this study can provide an array of techniques and tools relevant to drought assessment, drought risk mitigation strategies, and water resources management plans.

3.6. Reference

Abbaspour, K.C., 2011. User manual for SWAT-CUP4. SWAT calibration and uncertainty Programs, Swiss Federal Institute of Aquatic Science and Technology, Eawag, Duebendorf, Switzerland.

AghaKouchak, A., 2015. A multivariate approach for persistence-based drought prediction: Application to the 2010–2011 East Africa drought. Journal of Hydrology, 526, pp.127-135.

AghaKouchak, A., Cheng, L., Mazdiyasni, O. and Farahmand, A., 2014. Global warming and changes in risk of concurrent climate extremes: Insights from the 2014 California drought. Geophysical Research Letters, 41(24), pp.8847-8852.

Ahn, S.R., Jeong, J.H. and Kim, S.J., 2016. Assessing drought threats to agricultural water supplies under climate change by combining the SWAT and MODSIM models for the Geum River basin, South Korea. Hydrological Sciences Journal, 61(15), pp.2740-2753.

Alley, W.M., 1984. The Palmer drought severity index: limitations and assumptions. Journal of climate and applied meteorology, 23(7), pp.1100-1109.

Andreadis, K.M., Clark, E.A., Wood, A.W., Hamlet, A.F. and Lettenmaier, D.P., 2005. Twentieth-century drought in the conterminous United States. Journal of Hydrometeorology, 6(6), pp.985-1001.

Andreadis, K.M. and Lettenmaier, D.P., 2006. Trends in 20th century drought over the continental United States. Geophysical Research Letters, 33(10).

Arnold, J.G., Srinivasan, R., Muttiah, R.S. and Williams, J.R., 1998. Large area hydrologic modeling and assessment part I: model development 1. JAWRA Journal of the American Water Resources Association, 34(1), pp.73-89.

Ashraf Vaghefi, S., Mousavi, S.J., Abbaspour, K.C., Srinivasan, R. and Yang, H., 2014. Analyses of the impact of climate change on water resources components, drought and wheat yield in semiarid regions: Karkheh River Basin in Iran. hydrological processes, 28(4), pp.2018-2032.

Beersma, J.J. and Buishand, T.A., 2004. Joint probability of precipitation and discharge deficits in the Netherlands. Water resources research, 40(12).

Benestad, R.E. and Haugen, J.E., 2007. On complex extremes: flood hazards and combined high spring-time precipitation and temperature in Norway. Climatic Change, 85(3-4), pp.381-406.

Burke, E.J., Brown, S.J., Christidis, N., 2006. Modeling the recent evolution of global drought and projections for the twenty-first century with the Hadley Centre climate model. Journal of Hydrometeorology, 7(5), 1113-1125. http://dx.doi.org/10.1175/JHM544.1.

Cayan, D.R., Das, T., Pierce, D.W., Barnett, T.P., Tyree, M. and Gershunov, A., 2010. Future dryness in the southwest US and the hydrology of the early 21st century drought. Proceedings of the National Academy of Sciences, 107(50), pp.21271-21276.

Chang, T.J., 1991. Investigation of precipitation droughts by use of kriging method. Journal of Irrigation and Drainage Engineering, 117(6), pp.935-943.

Changnon, S.A., Pielke Jr, R.A., Changnon, D., Sylves, R.T. and Pulwarty, R., 2000. Human factors explain the increased losses from weather and climate extremes. Bulletin of the American Meteorological Society, 81(3), pp.437-442.

Clausen, B. and Pearson, C.P., 1995. Regional frequency analysis of annual maximum streamflow drought. Journal of Hydrology, 173(1-4), pp.111-130.

Dai, A., 2011. Drought under global warming: a review. Wiley Interdisciplinary Reviews: Climate Change, 2(1), pp.45-65.

Dai, A., 2013. Increasing drought under global warming in observations and models. Nature Climate Change, 3(1), p.52.

Duan, Q.Y., Gupta, V.K. and Sorooshian, S., 1993. Shuffled complex evolution approach for effective and efficient global minimization. Journal of optimization theory and applications, 76(3), pp.501-521.

Diffenbaugh, N.S., Swain, D.L. and Touma, D., 2015. Anthropogenic warming has increased drought risk in California. Proceedings of the National Academy of Sciences, p.201422385.

Edwards, D.C., 1997. Characteristics of 20th century drought in the United States at multiple time scales (No. AFIT-97-051). AIR FORCE INST OF TECH WRIGHT-PATTERSON AFB OH.

Estrela, M.J., Peñarrocha, D. and Millán, M., 2000. Multi-annual drought episodes in the Mediterranean (Valencia region) from 1950–1996. A spatio-temporal analysis. International Journal of Climatology: A Journal of the Royal Meteorological Society, 20(13), pp.1599-1618.

Feng, S., Hu, Q., Huang, W., Ho, C.H., Li, R. and Tang, Z., 2014. Projected climate regime shift under future global warming from multi-model, multi-scenario CMIP5 simulations. Global and Planetary Change, 112, pp.41-52.

Gesch, D.B., 2007. The National Elevation Dataset. In: Digital Elevation Model Technologies and Applications: The DEM User's Manual (Second Edition), D. Maune (Editor). American Society for Photogrammetry and Remote Sensing, Bethesda, Maryland, pp. 99-118.

Gringorten, I.I., 1963. A plotting rule for extreme probability paper. Journal of Geophysical Research, 68(3), pp.813-814.

Gutzler, D.S. and Robbins, T.O., 2011. Climate variability and projected change in the western United States: regional downscaling and drought statistics. Climate Dynamics, 37(5-6), pp.835-849.

Hao, Z. and AghaKouchak, A., 2013. Multivariate standardized drought index: a parametric multi-index model. Advances in Water Resources, 57, pp.12-18.

Hao, Z. and AghaKouchak, A., 2014. A nonparametric multivariate multi-index drought monitoring framework. Journal of Hydrometeorology, 15(1), pp.89-101.

Hao, Z., AghaKouchak, A. and Phillips, T.J., 2013. Changes in concurrent monthly precipitation and temperature extremes. Environmental Research Letters, 8(3), p.034014.

Hoekema, D.J. and Sridhar, V., 2011. Relating climatic attributes and water resources allocation: A study using surface water supply and soil moisture indices in the Snake River basin, Idaho. Water Resources Research, 47(7).

Hoekema, D.J. and Sridhar, V., 2013. A System Dynamics Model for Conjunctive Management of Water Resources in the S nake R iver B asin. JAWRA Journal of the American Water Resources Association, 49(6), pp.1327-1350.

Hoerling, M. and Eischeid, J., 2007. Past peak water in the Southwest. Southwest Hydrology, 6(1), pp.18-19.

Homer, C., Huang, C., Yang, L., Wylie, B. and Coan, M., 2004. Development of a 2001 national land-cover database for the United States. Photogrammetric Engineering & Remote Sensing, 70(7), pp.829-840.

IPCC, 2007. Climate Change 2007: The Physical Science Basis. In: Contribution of Working Group I to the Fourth Assessment Report of the Intergovernmental Panel on Climate Change, S. Solomon, D. Qin, M. Manning, Z. Chen, M. Marquis, K.B. Averyt, M. Tignor, and H.L. Miller (Editors). Cambridge University Press, Cambridge, United Kingdom and New York, New York, pp. 996.

Solomon, S., Qin, D., Manning, M., Averyt, K. and Marquis, M. eds., 2007. Climate change 2007-the physical science basis: Working group I contribution to the fourth assessment report of the IPCC (Vol. 4). Cambridge university press.

Jaksa, W.T. and Sridhar, V., 2015. Effect of irrigation in simulating long-term evapotranspiration climatology in a human-dominated river basin system. Agricultural and forest meteorology, 200, pp.109-118.

Jha, M., Pan, Z., Takle, E.S. and Gu, R., 2004. Impacts of climate change on streamflow in the Upper Mississippi River Basin: A regional climate model perspective. Journal of Geophysical Research: Atmospheres, 109(D9).

Jin, X. and Sridhar, V., 2012. Impacts of Climate Change on Hydrology and Water Resources in the Boise and Spokane River Basins 1. JAWRA Journal of the American Water Resources Association, 48(2), pp.197-220.

Kang, H. and Sridhar, V., 2017. Combined statistical and spatially distributed hydrological model for evaluating future drought indices in Virginia. Journal of Hydrology: Regional Studies, 12, pp.253-272.

Karl, T.R., Gleason, B.E., Menne, M.J., McMahon, J.R., Heim Jr, R.R., Brewer, M.J., Kunkel, K.E., Arndt, D.S., Privette, J.L., Bates, J.J. and Groisman, P.Y., 2012. US temperature and drought: Recent anomalies and trends. Eos, Transactions American Geophysical Union, 93(47), pp.473-474.

King, K.W., Arnold, J.G. and Bingner, R.L., 1999. Comparison of Green-Ampt and curve number methods on Goodwin Creek watershed using SWAT. Transactions of the ASAE, 42(4), p.919.

Kumar, S., Lawrence, D.M., Dirmeyer, P.A. and Sheffield, J., 2014. Less reliable water availability in the 21st century climate projections. Earth's Future, 2(3), pp.152-160.

Lakshmi, V., Piechota, T., Narayan, U. and Tang, C., 2004. Soil moisture as an indicator of weather extremes. Geophysical research letters, 31(11).

Leonard, M., Westra, S., Phatak, A., Lambert, M., van den Hurk, B., McInnes, K., Risbey, J., Schuster, S., Jakob, D. and Stafford-Smith, M., 2014. A compound event framework for understanding extreme impacts. Wiley Interdisciplinary Reviews: Climate Change, 5(1), pp.113-128.

Liang, X., Lettenmaier, D.P., Wood, E.F. and Burges, S.J., 1994. A simple hydrologically based model of land surface water and energy fluxes for general circulation models. Journal of Geophysical Research: Atmospheres, 99(D7), pp.14415-14428.

Liu, L., Hong, Y., Looper, J., Riley, R., Yong, B., Zhang, Z., Hocker, J. and Shafer, M., 2013. Climatological drought analyses and projection using SPI and PDSI: Case study of the Arkansas Red River Basin. Journal of Hydrologic Engineering, 18(7), pp.809-816.

Loukas, A., Vasiliades, L. and Tzabiras, J., 2008. Climate change effects on drought severity. Advances in Geosciences, 17, pp.23-29.

Mao, Y., Nijssen, B. and Lettenmaier, D.P., 2015. Is climate change implicated in the 2013–2014 California drought? A hydrologic perspective. Geophysical Research Letters, 42(8), pp.2805-2813.

McKee, T.B., Doesken, N.J. and Kleist, J., 1993, January. The relationship of drought frequency and duration to time scales. In Proceedings of the 8th Conference on Applied Climatology (Vol. 17, No. 22, pp. 179-183). Boston, MA: American Meteorological Society.

Mishra, A.K. and Singh, V.P., 2009. Analysis of drought severity-area-frequency curves using a general circulation model and scenario uncertainty. Journal of Geophysical Research: Atmospheres, 114(D6).

Mishra, A.K. and Singh, V.P., 2010. A review of drought concepts. Journal of hydrology, 391(1-2), pp.202-216.

Mishra, V., Cherkauer, K.A. and Shukla, S., 2010. Assessment of drought due to historic climate variability and projected future climate change in the midwestern United States. Journal of Hydrometeorology, 11(1), pp.46-68.

Mishra, A.K. and Singh, V.P., 2011. Drought modeling–A review. Journal of Hydrology, 403(1-2), pp.157-175.

Mishra, V., Shah, R. and Thrasher, B., 2014. Soil moisture droughts under the retrospective and projected climate in India. Journal of Hydrometeorology, 15(6), pp.2267-2292.

Mo, K.C. and Chelliah, M., 2006. The modified Palmer drought severity index based on the NCEP North American Regional Reanalysis. Journal of applied meteorology and climatology, 45(10), pp.1362-1375.

Mo, K.C., 2008. Model-based drought indices over the United States. Journal of Hydrometeorology, 9(6), pp.1212-1230.

Mohan, S. and Rangacharya, N.C.V., 1991. A modified method for drought identification. Hydrological Sciences Journal, 36(1), pp.11-21.

Monteith, J.L., 1965. Evaporation and environment. In: Proceedings of the State and Movement of Water in Living Organisms, 19th Symposia of the Society of Experimental Biology, Cambridge University Press, Swansea, UK/Cambridge, UK, 205–234.

Moriasi, D.N., Arnold, J.G., Van Liew, M.W., Bingner, R.L., Harmel, R.D. and Veith, T.L., 2007. Model evaluation guidelines for systematic quantification of accuracy in watershed simulations. Transactions of the ASABE, 50(3), pp.885-900.

Narasimhan, B. and Srinivasan, R., 2005. Development and evaluation of Soil Moisture Deficit Index (SMDI) and Evapotranspiration Deficit Index (ETDI) for agricultural drought monitoring. Agricultural and Forest Meteorology, 133(1-4), pp.69-88.

Nash, J.E. and Sutcliffe, J.V., 1970. River flow forecasting through conceptual models part I—A discussion of principles. Journal of hydrology, 10(3), pp.282-290.

Nasrollahi, N., AghaKouchak, A., Cheng, L., Damberg, L., Phillips, T.J., Miao, C., Hsu, K. and Sorooshian, S., 2015. How well do CMIP5 climate simulations replicate historical trends and patterns of meteorological droughts?. Water Resources Research, 51(4), pp.2847-2864.

National Climatic Data Center (NCDC), 2002. US National Percent Area Severely to Extremely Dry and Severely to Extremely Wet.

Nelsen, R.B., 2006. An Introduction to Copulas, 2nd. New York: SpringerScience Business Media. 269. Niemeyer, S., 2008. New Drought Indices. Water Management, 80, pp. 267–274, http://om.ciheam.org/article.php?IDPDF=800451.

Niemeyer, S., 2008. New Drought Indices. Water Management, 80, pp. 267-274, http://om.ciheam.org/article.php?IDPDF=800451.

Pachauri, R.K., Allen, M.R., Barros, V.R., Broome, J., Cramer, W., Christ, R., Church, J.A., Clarke, L., Dahe, Q., Dasgupta, P. and Dubash, N.K., 2014. Climate change 2014: synthesis report. Contribution of Working Groups I, II and III to the fifth assessment report of the Intergovernmental Panel on Climate Change (p. 151). IPCC.

Palmer, W.C., 1965. Meteorological drought. Weather Bureau Res. Paper 45, U.S. Dept. of Commerce. 58.

Qin, D., Plattner, G.K., Tignor, M., Allen, S.K., Boschung, J., Nauels, A., Xia, Y., Bex, V. and Midgley, P.M., 2014. Climate change 2013: The physical science basis. Contribution of Working Group I to the Fifth Assessment Report of the Intergovernmental Panel on Climate Change (eds TF Stocker et al.), pp.5-14.

Rajsekhar, D., Singh, V.P. and Mishra, A.K., 2015. Integrated drought causality, hazard, and vulnerability assessment for future socioeconomic scenarios: An information theory perspective. Journal of Geophysical Research: Atmospheres, 120(13), pp.6346-6378.

Reifen, C. and Toumi, R., 2009. Climate projections: Past performance no guarantee of future skill?. Geophysical Research Letters, 36(13).

Ross, T. and Lott, N., 2003. A climatology of 1980-2003 extreme weather and climate events (pp. 1-15). US Department of Commerece, National Ocanic and Atmospheric Administration, National Environmental Satellite Data and Information Service, National Climatic Data Center.

Saltelli, A., Ratto, M., Andres, T., Campolongo, F., Cariboni, J., Gatelli, D., Saisana, M. and Tarantola, S., 2008. Global sensitivity analysis: the primer. John Wiley & Sons.

Schubert, S.D. and Lim, Y.K., 2013. Climate variability and weather extremes: Model-simulated and historical data. In Extremes in a Changing Climate (pp. 239-285). Springer, Dordrecht.

Schuol, J., Abbaspour, K.C., Yang, H., Srinivasan, R. and Zehnder, A.J., 2008. Modeling blue and green water availability in Africa. Water Resources Research, 44(7).

Seager, R., Ting, M., Held, I., Kushnir, Y., Lu, J., Vecchi, G., Huang, H.P., Harnik, N., Leetmaa, A., Lau, N.C. and Li, C., 2007. Model projections of an imminent transition to a more arid climate in southwestern North America. Science, 316(5828), pp.1181-1184.

Sehgal, V., Sridhar, V. and Tyagi, A., 2017. Stratified drought analysis using a stochastic ensemble of simulated and in-situ soil moisture observations. Journal of hydrology, 545, pp.226-250.

Seneviratne, S.I., Corti, T., Davin, E.L., Hirschi, M., Jaeger, E.B., Lehner, I., Orlowsky, B. and Teuling, A.J., 2010. Investigating soil moisture–climate interactions in a changing climate: A review. Earth-Science Reviews, 99(3-4), pp.125-161.

Seong, C., Sridhar, V. and Billah, M.M., 2018. Implications of potential evapotranspiration methods for streamflow estimations under changing climatic conditions. International Journal of Climatology, 38(2), pp.896-914.

Shafer, B. and L. Dezman, 1982. Development of a Surface Water Supply Index (SWSI) to Assess the Severity of Drought Conditions in Snowpack Runoff Areas. Paper Presented at Proceedings of the Western Snow Conference.

Sheffield, J. and Wood, E.F., 2008. Projected changes in drought occurrence under future global warming from multi-model, multi-scenario, IPCC AR4 simulations. Climate dynamics, 31(1), pp.79-105.

Sheffield, J. and Wood, E.F., 2012. Drought: past problems and future scenarios. Routledge.

Sheffield, J., Barrett, A.P., Colle, B., Nelun Fernando, D., Fu, R., Geil, K.L., Hu, Q., Kinter, J., Kumar, S., Langenbrunner, B. and Lombardo, K., 2013. North American climate in CMIP5 experiments. Part I: Evaluation of historical simulations of continental and regional climatology. Journal of Climate, 26(23), pp.9209-9245.

Shukla, S. and Wood, A.W., 2008. Use of a standardized runoff index for characterizing hydrologic drought. Geophysical research letters, 35(2).

Sillmann, J., Kharin, V.V., Zhang, X., Zwiers, F.W. and Bronaugh, D., 2013. Climate extremes indices in the CMIP5 multimodel ensemble: Part 1. Model evaluation in the present climate. Journal of Geophysical Research: Atmospheres, 118(4), pp.1716-1733.

Simanton, J.R., Hawkins, R.H., Mohseni-Saravi, M. and Renard, K.G., 1996. Runoff curve number variation with drainage area, Walnut Gulch, Arizona. Transactions of the ASAE, 39(4), pp.1391-1394.

Sridhar, V. and Anderson, K.A., 2017. Human-induced modifications to land surface fluxes and their implications on water management under past and future climate change conditions. Agricultural and forest meteorology, 234, pp.66-79.

Sridhar, V., Hubbard, K.G., You, J. and Hunt, E.D., 2008. Development of the soil moisture index to quantify agricultural drought and its "user friendliness" in severity-area-duration assessment. Journal of Hydrometeorology, 9(4), pp.660-676.

Sridhar, V., Jaksa, W.T.A., Fang, B., Lakshmi, V., Hubbard, K.G. and Jin, X., 2013. Evaluating bias-corrected AMSR-E soil moisture using in situ observations and model estimates. Vadose Zone Journal, 12(3).

Sridhar, V. and Wedin, D.A., 2009. Hydrological behaviour of grasslands of the Sandhills of Nebraska: water and energy-balance assessment from measurements, treatments, and modelling. Ecohydrology: Ecosystems, Land and Water Process Interactions, Ecohydrogeomorphology, 2(2), pp.195-212.

Sternberg, T., 2011. Regional drought has a global impact. Nature, 472(7342), p.169.

Strzepek, K., Yohe, G., Neumann, J. and Boehlert, B., 2010. Characterizing changes in drought risk for the United States from climate change. Environmental Research Letters, 5(4), p.044012.

Stocker, T.F., Qin, D., Plattner, G.K., Tignor, M., Allen, S.K., Boschung, J., Nauels, A., Xia, Y., Bex, V. and Midgley, P.M., 2014. Intergovernmental Panel on Climate Change, Intergovernmental Panel on Climate Change, and Working Group I. Climate Change 2013: The Physical Science Basis: Working Group I Contribution to the Fifth Assessment Report of the Intergovernmental Panel on Climate Change, p.1535.

Swain, D.L., Tsiang, M., Haugen, M., Singh, D., Charland, A., Rajaratnam, B. and Diffenbaugh, N.S., 2014. The extraordinary California drought of 2013/2014: Character, context, and the role of climate change. Bull. Am. Meteorol. Soc, 95(9), pp.S3-S7.

Tallaksen, L.M. and Van Lanen, H.A. eds., 2004. Hydrological drought: processes and estimation methods for streamflow and groundwater (Vol. 48). Elsevier.

Taylor, K.E., Stouffer, R.J. and Meehl, G.A., 2012. An overview of CMIP5 and the experiment design. Bulletin of the American Meteorological Society, 93(4), pp.485-498.

Thornthwaite, C.W., 1948. An approach toward a rational classification of climate. Geographical review, 38(1), pp.55-94.

Thyer, M., Kuczera, G. and Bates, B.C., 1999. Probabilistic optimization for conceptual rainfall-runoff models: A comparison of the shuffled complex evolution and simulated annealing algorithms. Water Resources Research, 35(3), pp.767-773.

Tsakiris, G., Loukas, A., Pangalou, D., Vangelis, H., Tigkas, D., Rossi, G. and Cancelliere, A., 2007. Drought characterization. Drought management guidelines technical annex, pp.85-102.

U.S. Department of Agriculture (USDA), 1991. State Soil Geo-graphic (STATSGO) Database: Data Use Information. Miscella-neous Publication Number 1492, Washington, D.C.

USDA Soil Conservation Service, 1972. National Engineering Handbook, Hydrology, Section 4, Chapters 4–10. GPO, Washington, DC.

Vasiliades, L. and Loukas, A., 2009. Hydrological response to meteorological drought using the Palmer drought indices in Thessaly, Greece. Desalination, 237(1-3), pp.3-21.

Virginia Department of Emergency (VDEM), 2013. Commonwealth of Virginia hazard mitigation plan. Chapter 3: Hazard identification and risk assessment.

Vrugt, J.A., Gupta, H.V., Bouten, W. and Sorooshian, S., 2003. A Shuffled Complex Evolution Metropolis algorithm for optimization and uncertainty assessment of hydrologic model parameters. Water resources research, 39(8).

Wang, G., 2005. Agricultural drought in a future climate: results from 15 global climate models participating in the IPCC 4th assessment. Climate dynamics, 25(7-8), pp.739-753.

Wang, D., Hejazi, M., Cai, X. and Valocchi, A.J., 2011. Climate change impact on meteorological, agricultural, and hydrological drought in central Illinois. Water Resources Research, 47(9).

Wang, J., Kessner, A.L., Aegerter, C., Sharma, A., Judd, L., Wardlow, B., You, J., Shulski, M., Irmak, S., Kilic, A. and Zeng, J., 2016. A multi-sensor view of the 2012 central plains drought from space. Frontiers in Environmental Science, 4, p.45.

Wilhite, D.A. and Hayes, M.J., 1998. Drought planning in the United States: Status and future directions. In The arid frontier (pp. 33-54). Springer, Dordrecht.

Wu, K. and Johnston, C.A., 2007. Hydrologic response to climatic variability in a Great Lakes Watershed: A case study with the SWAT model. Journal of Hydrology, 337(1-2), pp.187-199.

Wuebbles, D.J., Kunkel, K., Wehner, M. and Zobel, Z., 2014. Severe weather in United States under a changing climate. Eos, Transactions American Geophysical Union, 95(18), pp.149-150.

Xu, Z.X., Pang, J.P., Liu, C.M. and Li, J.Y., 2009. Assessment of runoff and sediment yield in the Miyun Reservoir catchment by using SWAT model. Hydrological Processes: An International Journal, 23(25), pp.3619-3630.

Zargar, A., Sadiq, R., Naser, B. and Khan, F.I., 2011. A review of drought indices. Environmental Reviews, 19(NA), pp.333-349.

Chapter 4. Assessment of economic impacts of drought based on the hydrologic simulations and an analysis of economic-wide impacts

4.1. Abstract

The impacts of climate change on drought and affected economic activity can be simulated based on hydrologic models that predict reliable soil moisture, future climate projections, and historic relationships between drought indices and agricultural sector impacts. The objective of this study is to assess the potential impacts of climate change on future agricultural drought conditions and on the associated economic conditions in the high value agricultural sector of three congressional districts in Northern Virginia (VA). The Variable Infiltration Capacity (VIC) model is applied to estimate a SSI. Historic and future climate data is taken from Coupled Model Intercomparison Project Phase 5 (CMIP5) climate models and downscaled by the Multivariate Adaptive Constructed Analogs (MACA) method. Linear regression analysis is then carried out to determine the historic relationship between annual mean SSI values and the sector value of agricultural production for a seven-year period (2010–2016). The SSI results for future periods show an overall increase in agricultural droughts due to decreased crop growing season soil moisture that arises from decreased precipitation and increased evapotranspiration. Further, SSI changes are projected to result in decreases in agricultural production in future periods: 9.4% to 15.9% in the VA06 district and 0.5% to 4.1% in the VA11 district. However, in the VA08 district, increases of 65.0% to 78.1% are projected. The VA08 district is well developed where precipitation increases outweigh temperature increases and increases in soil moisture, leading to future agricultural production increases. Economy-wide impacts of these production changes are then evaluated with the IMpact analysis for PLANning (IMPLAN) model. Results indicate that the VA06 district loses 660 to 854 jobs due to the climate change impacts on droughts, while employment in the VA11 district remains virtually unchanged and the VA08 district gains jobs. Thus, projected economic impacts of climate change can vary considerably, even within geographically proximate areas.

4.2. Introduction

Drought is an unpredictable hydrometeorological event, which generates a notable decrease in water resources affecting a large area, often with considerable economic losses (CHJ, 2007; Ziolkowska, 2016). The agricultural sector frequently suffers the largest negative economic impact, in both irrigated and rain-fed areas (Ding et al., 2011). In many regions, climate change increases the frequency and severity of droughts (Dai, 2011) that generate economic losses. The severity of droughts in the US has increased significantly in the last several decades (Karl et al., 2012), and climate models suggest that changes in precipitation and temperature patterns will lead to an even higher frequency and longer duration of droughts in many areas of the US (Seager et al., 2007; Wuebbles et al., 2014; Kang and Sridhar, 2017; Kang and Sridhar, 2018). These changes in hydrometeorological conditions stand to considerably influence the US economy. Further, ample evidence exists indicating that drought has negative impacts on the agricultural sector economy. For example, the economic impact of the widespread 1988 drought in the Mid-Atlantic, Southeastern, Midwestern, and Northern Great Plains regions of the US was estimated at $40 billion (Riebsame et al., 1990). At the state level, economic losses of $7.62 billion were estimated in Texas's agricultural sector with the 2011 drought (Combs, 2011; Guerrero, 2012), and economic losses of $5.5 billion were estimated in the California agricultural sector from the 2014–2016 drought (Howitt et al., 2014; Howitt et al., 2015; Medellín-Azuara et al., 2016).

This chapter simulates the economic impacts of drought on the agricultural sector by establishing a direct relationship between drought and agricultural production and by using long-term observation of hydrometeorological variables to estimate a reliable drought indicator. Since high-resolution and long-term hydrometeorological observations are generally limited, physically based hydrologic models are employed as an alternative to simulate key hydrological variables, such as soil moisture, in the evaluation of agricultural drought in climate change projections (Nam et al., 2015; Cheng et al., 2016; Schlaepfer et al., 2017). The Variable Infiltration Capacity (VIC) (Liang et al., 1994) model is a useful tool that has been applied to estimate the impacts of climate change on the hydrologic cycle and drought conditions based on soil moisture simulation (Mishra et al., 2010; Leng et al., 2015).

Numerous studies have analyzed the impacts of droughts on agricultural production and the agricultural sector economy (Calatrava and Garrido, 2005; Peck and Adams, 2010; Howitt et

al., 2015; Ziolkowska, 2016). Bauman et al. (2013) evaluate the direct and indirect impacts of the 2011 drought on rural communities in Colorado using an Equilibrium Displacement Mathematical Programming (EDMP) model. Ziolkowska et al. (2016) analyze the economic implications of Texas's drought for the agricultural sector and broader economy with IMPLAN, a representative input–output (I–O) model. However, economic impacts to future drought projections based on a physically based hydrologic model and projections of drought indices are required for the Mid-Atlantic areas of the US. Soil moisture has been poorly observed over the historic period, and the VIC model has been a good alternative to generate realistic simulations of soil moisture and drought conditions for the historic and future periods with fine spatial resolution (Cayan et al., 2010).

The objectives of this study are to evaluate the economic impacts of droughts by first assessing drought frequency and severity under present and future conditions using the drought indices and soil moisture simulations and subsequently evaluating the broad economic impacts of drought on the agricultural sector and the wider economy with the IMPLAN model. Specifically, the VIC model is used to simulate soil moisture for historic (1977–2016) and future periods (f1: 2017–2056, f2:2057–2096). A soil moisture-based agricultural drought index (SSI) is then computed for the corresponding periods. Agricultural sector impacts of drought are established by estimating the relationship between historic agricultural production for the 2010–2016 period and the annual mean of the SSI with an Ordinary Least Square (OLS) regression model in three congressional districts of VA. Finally, future impacts of the climate change on economic production are simulated based on the future projections of the hydrology–drought and drought–agricultural sector relationships. The proposed approach can provide better information on the quantification of the costs of climate change, drought mitigation planning, risk assessment, and the proper design of sustainable and efficient water management strategies.

4.3. Methods

The overall approaches and methods applied in the study are shown in the flow diagram in Figure 1. First, the required input data to drive the VIC model are prepared at a 1/16-degree resolution (5–6 km) for Northern VA. Second, daily simulations for historical and future periods are performed. Third, a soil moisture-based drought index (SSI) is calculated at a weekly time step,

which provides a better indicator for evaluating and managing agricultural drought conditions than monthly or seasonal time steps. Fourth, regression analysis estimates the relationship between the mean annual SSI values and rain-fed agricultural product sector. The economy-wide impacts of agricultural production changes are simulated with the IMPLAN model during the retrospective period (2010–2016) for three congressional districts in Northern VA (VA06, VA08, and VA11). Finally, the economic impacts of climate change on the agricultural sector are evaluated using the IMPLAN model with agricultural sector production changes driven by SSI values under future climate change projections.

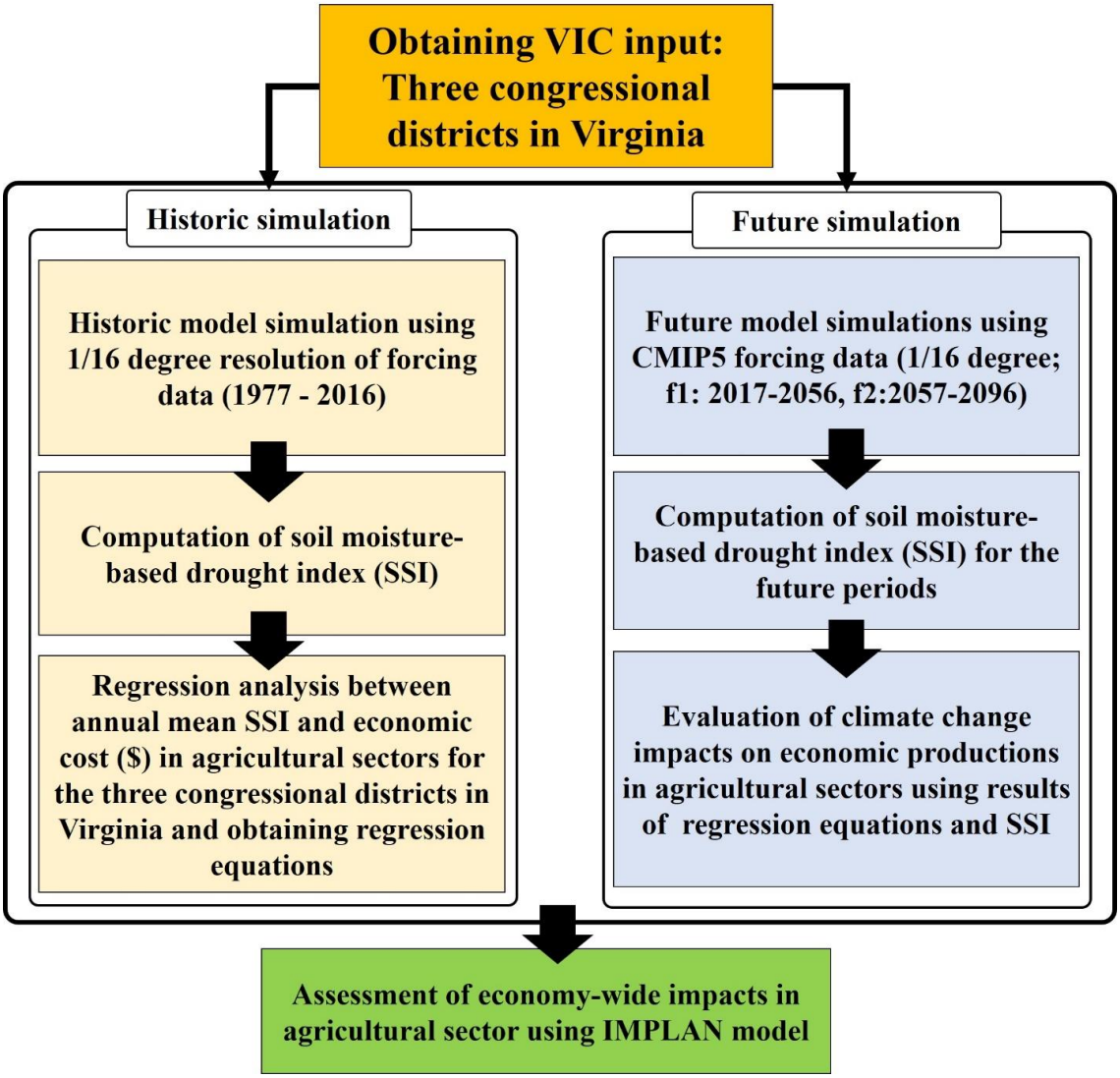

Figure 1. Flow diagram of overall processes of hydrological modeling, drought projection, and evaluation of climate change effects on economic production. VIC, Variable Infiltration Capacity; CMIP5, Coupled Model Intercomparison Project 5; IMPLAN, IMpact analysis for PLANning.

4.3.1. Study area

The study area consists of three congressional districts located in Northern VA: VA06, VA08, and VA11 (Figure 2). Additionally, VIC inputs, such as soil and vegetation parameters, are available at the corresponding areas at a 1/16-degree resolution (5–6 km). Figure 2 shows the location, topography, and land-use types of the study area and climate divisions associated with the three districts of VA. Surface elevations range from 0 m to 1,381 m (Figure 2(d)), and the mean annual precipitation and temperature for the last 40 years (1977–2016) are 1,072 mm and 18.1°C, respectively. Most of the area consists of forest (64%), while the remainder is covered by pasture/hay (20%), developed areas (13%), and cultivated crops (3%) (Figure 2(d)). Table 1 shows the different land-use characteristics of the three congressional districts. In the VA06 district, most of the area is covered by forest (69.9%), while the remainder consists of pasture/hay (19.9%), developed areas (7.8%), and cultivated crops (1.2%). The VA08 district is primarily covered by developed areas (67.3%), with a smaller area covered by forest (14.6%). The land-use composition of VA11 is similar to that of VA08, but its developed area percentage is smaller than that of VA08 (~56%) and its forest area percentage is more than twice that of VA08 (32.0%). The selected districts reflect the diverse effects of drought on agricultural production with different economic scale, land-use, and hydrologic characteristics. In addition, the selected districts overlap with several VA climate divisions (Divisions 3, 4, and 5) (Figure 2(b)).

Table 1. Land use characteristic for the three congressional districts

Land use	VA06 (%)	VA08 (%)	VA11 (%)
Barren Land	0.1	0.1	0.4
Cultivated Crop	1.2	0.6	0.8
Developed Area	7.8	67.3	56.0
Forest	69.9	14.6	32.0
Grassland	0.3	0.1	0.3
Pasture/hay	19.9	0.3	0.4
Shrub	0.2	0.3	0.7
Water	0.6	12.2	5.6
Wetlands	0.0	4.6	3.8

Figure 3 shows the time series plots of drought areas in these three climate divisions from the USDM (http://droughtmonitor.unl.edu/; Svoboda et al., 2002). In the periods 2002 to 2003, 2007 to 2008, 2011 to 2012, and 2017, these districts experienced moderate to extreme droughts that influenced agricultural production and the economy (DRTAC, 2003; VDEM, 2013). Future projections for these regions indicate that overall increases in agricultural droughts are expected (Kang and Sridhar, 2017). In addition, the agricultural-related gross income in the VA06 district is the highest in VA ($30,531,000) (USDA NASS, 2012), as agriculture is an important industry in the region. VA08 and VA11 are located in highly urbanized areas, and their agricultural-related gross incomes are the lowest in VA ($316,000 for VA11 and $735,000 for VA08). The selected districts are appropriate for analyzing the diverse effects of drought on agricultural production because they have different economic structures, different land-use, and hydrologic characteristics even though they are closely located.

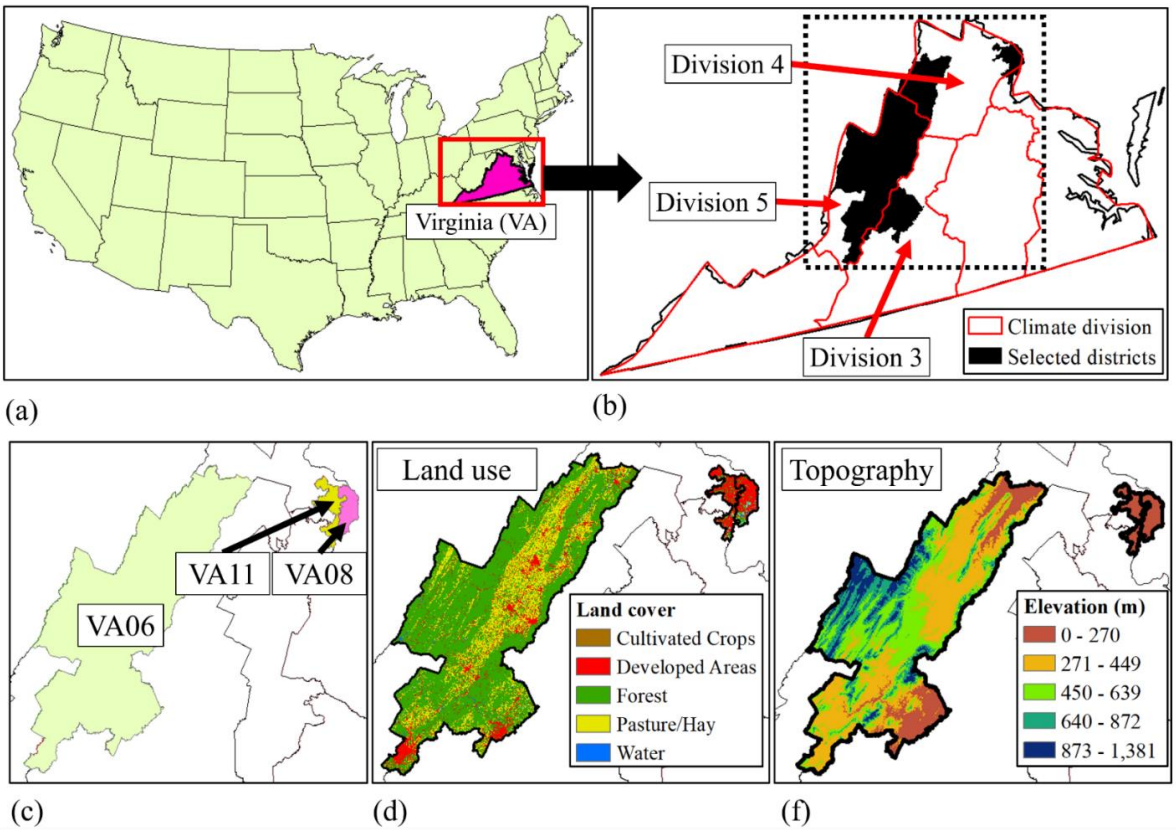

Figure 2. Location map of study region. (a) Location of VA is highlighted as pink area and red box. (b) Black areas indicate three congressional districts, and red lines represent climate divisions in VA. (c) Location map of three congressional districts (VA06, VA08, and VA11). (d) Land use map of three districts. (e) Topography of three districts. Brown to yellow colors indicate lower elevations, while green to blue colors represent higher elevations.

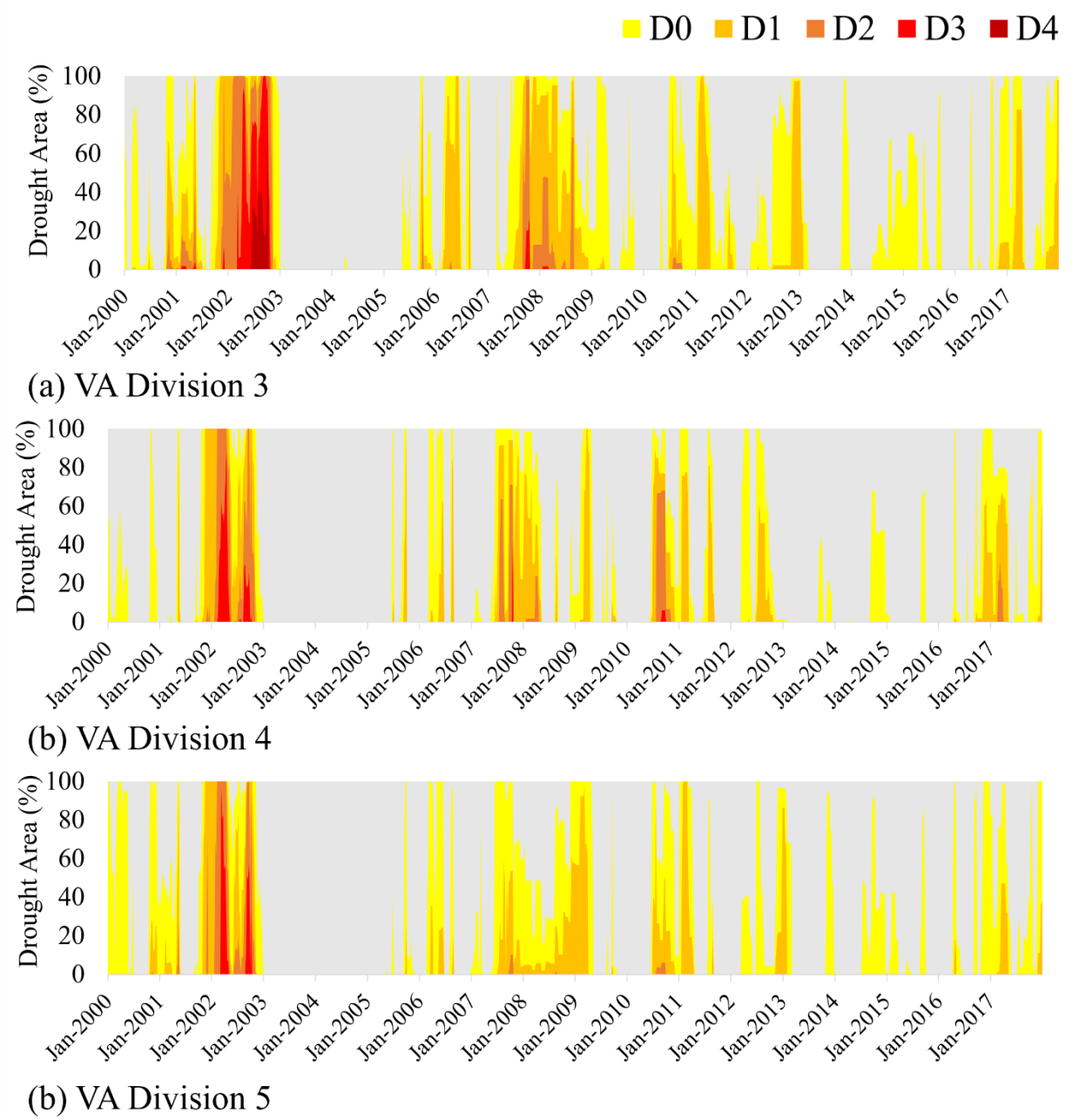

Figure 3. Drought area maps for VA climate divisions from United States Drought Monitor (USDM) from January 2000 to December 2017. Each color represents a different category of drought conditions. Yellow indicates the D0 category (Abnormal drought), orange indicates the D1 category (Moderate drought), darker orange indicates the D2 category (Severe drought), red indicates the D3 category (Extreme drought), and dark brown indicates the D4 category (Exceptional drought). (a) Drought area map for VA division 3. (b) Drought area map for VA division 4. (c) Drought area map for VA division 5.

4.3.2. VIC and IMPLAN model descriptions

Hydrologic simulations are required to obtain long-term soil moisture and soil moisture-based drought indices for both historic and future periods. The VIC model (Liang et al., 1994) is a macro-scale hydrologic model that computes water and energy budget components on a daily time step. The VIC model has been widely used to estimate the drought conditions of various river basins in the US (Shukla et al., 2011; Mao et al., 2015) as well as the impacts of climate change on drought conditions (Kang and Sridhar, 2018). Land cover in the VIC model is classified by types of bare soil or vegetation, and the soil column is divided into three layers. The hydrologic simulation is computed based on the interactions between vegetation and soil in each grid cell and weather variables, such as daily precipitation and temperature.

In this study, the VIC model is implemented at a 1/16th-degree resolution (0.0625°) with atmospheric variables (daily precipitation, maximum and minimum temperatures, and wind speed). Other model inputs, such as soil and vegetation data, are obtained from the Land Data Assimilation Systems (LDAS) (http://ldas.gsfc.nasa.gov/) at the same spatial resolution as the meteorological forcing.

IMPLAN (Minnesota IMPLAN Group, 2009) is a representative I–O and social accounting matrix model that is applied to evaluate the economy-wide impacts of drought through direct impacts on agricultural production (Howitt et al., 2014; Howitt et al., 2015; Ziolkowska, 2016). The IMPLAN model relies on datasets from the US Bureau of Economic Analysis, US Bureau of Labor, and US Census Bureau. Data on the US economy is structured based on the US Census Bureau North American Industry Classification System (NAICS) classification (Table 1). In this study, seven years of annual agricultural production for each sector are provided from the IMPLAN model for the three congressional districts in VA (2010–2016), and they are used to build a regression analysis with the annual mean SSI values. Based on the regression analysis and SSI projections, economy-wide impacts of drought on agricultural production are evaluated by the IMPLAN model. The IMPLAN model is used to generate changes of economic measurements, such as employment, labor income, value added, and industry output. Additional economic production data are obtained from the US Bureau of Economic Analysis (BEA), US Bureau of Labor Statistics (BLS), and US Census Bureau. Table 2 shows the NAICS classification used in

this study to specify direct impacts on agricultural production. An additional agricultural sector that relies solely on irrigated fields (e.g., greenhouse production) was not included.

Table 2. NAICS (North American Industry Classification System) classification for the agricultural sectors.

NAICS Classification for Virginia	Sector Description
1	Oilseed farming
2	Grain farming
3	Vegetable and melon farming
4	Fruit farming
7	Tobacco farming
10	All other crop farming
11	Beef cattle ranching and farming, including feedlots and dual-purpose ranching and farming
14	Animal production, except cattle and poultry and eggs

4.3.3. Analysis of historic and future drought projections

The VIC model is run at a daily time step for the historic period (1977–2016) with three years for the spin-up period (1974–1976), a historic period of 1977–2016, and projected future periods (f1: 2017–2056, f2:2057–2096). For the historic period, the extended and spatially refined long-term hydrologic dataset provided by Livneh et al. (2013) is used at a 1/16th-degree resolution.

For the future simulations, the CMIP5 dataset is used. However, the resolution of this dataset is coarse and must be downscaled to a high resolution for the corresponding scale of the historic simulation (1/16th-degree resolution). Thus, we use atmospheric forcing from the two General Circulation Models (GCMs), which were downscaled by the Multivariate Adaptive Constructed Analogs (MACA) method (Abatzoglou, 2013) approach to the VIC model. The MACA method uses multiple Representative Concentration Pathways (RCPs), which are low to high radiative forcing scenarios. In this study, the median (RCP4.5) and highest (RCP8.5) forcing scenarios are employed, which represent scenarios that stabilize radiative forcing at 4.5 W/m2 and 8.5 W/m^2, respectively, in the year 2100 (Riahi et al., 2011; Thomson et al., 2011). RCP4.5 is a

pathway to the stabilization of radiative forcing, and RCP8.5 is an increasing radiative forcing pathway by 2100 (van Vuuren et al., 2011). Both RCP4.5 and RCP8.5 reflect diverse hydroclimatic conditions, and they have been used in numerous studies to evaluate the impacts of climate change on droughts (Kang and Sridhar, 2017, Kang and Sridhar, 2018, Jin et al., 2018).

For the VIC model simulation, three CMIP5 models are selected, BCC-CSM1.1, CanESM2, and CCSM4, to illustrate future (f1: 2017–2056, f2:2057–2096) hydrologic states. These models have been used to evaluate the climate change impacts on drought conditions in many river basins around the globe (Orlowsky and Seneviratne, 2013; Wang and Chen, 2014; Chattopadhyay et al., 2017; Kang and Sridhar, 2018).

4.3.4. Soil moisture and drought index

Soil moisture is an essential variable in the monitoring of crop growth and agricultural production by the United States Department of Agriculture (USDA) (Bolten et al., 2010). However, reliable estimation of regional soil moisture with limited ground observations is difficult due to spatial heterogeneity in soil properties, land cover, topography, and precipitation variability (Bolten et al., 2010). Model-based soil moisture estimation provides a practical alternative, and it is widely used for agricultural drought estimations and evaluations (Sheffield and Wood, 2008). In this study, the VIC model is used to estimate the soil moisture as the basis for SSI calculation. For the computation of the SSI, the univariate form of the Gringorten plotting position formula (Equation 1) (Gringorten, 1963) is used.

$$P(x_i) = \frac{i-0.44}{n+0.12} \text{ ------ (1)}$$

where n is the number of observations, and i is the rank of the observed values from the smallest. The mean precipitation value is set to zero; values below zero indicate dry conditions, while values above zero indicate wet conditions. Table 3 shows the classification of SSI values, and lower values indicate higher drought severity.

Table 3. Classification of the Standardized Soil moisture Index (SSI) (McKee et al., 1993).

SSI Values	Drought category
2.0 and above	Extremely Wet
1.50 – 1.99	Very Wet
1.00 – 1.49	Moderately Wet
-0.99 – 0.99	Near normal
-1.00 - -1.49	Moderate Drought
-1.50 - -1.99	Severe Drought
-2.0 or less	Extreme Drought

4.4. Results and discussion

4.4.1. Historic and future climate

Figure 4 shows the precipitation and temperature changes for each CMIP5 model for the three congressional districts (VA06, VA08, and VA11) for the historic and future periods. Figure 4(a) presents the results for the f1 period, while Figure 4(b) presents the results for the f2 period. The X-axis indicates the change in precipitation (%), while the Y-axis shows the change in temperature (°C). In addition, the blue dots indicate the results of RCP4.5, and the red dots indicate the results of RCP8.5. Considerable variation exists in the projected results. For the f1 period, the maximum precipitation increase is 7.5% for the CCSM4-RCP4.5 model, and the maximum temperature increase is 2.39 °C for the BCC-CSM1.1-RCP8.5 model. In contrast, there is a 4.3% decrease in precipitation for the CanESM2-RCP4.5 model, and the minimum temperature increase is 1.9 °C for the BCC-CSM1.1-RCP4.5 model. For the f2 period, the maximum precipitation increase is 14.9% for the CCSM4-RCP8.5 model, and the maximum temperature increase is 5.2°C for the CCSM4-RCP4.5 model. In contrast, there is a 0.01% increase in precipitation for the BCC-CSM1.1-RCP4.5 model, and the minimum temperature increase is 2.8 °C for the CCSM4-RCP4.5 model. Since each model has different precipitation and temperature characteristics in the future periods, an analysis of the diverse influences of climate change on droughts and agricultural production conditions is conducted.

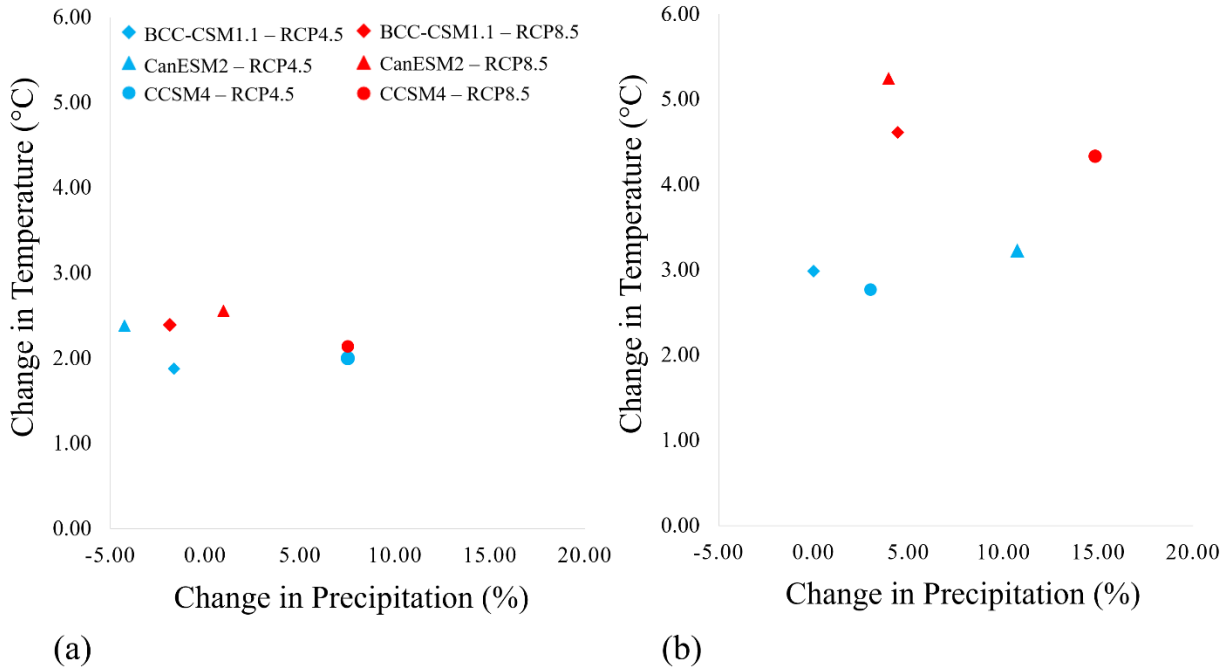

Figure 4. Scatter plots of changes in precipitation and temperature for CMIP5 climate models. The X-axis represents the change in precipitation (%), and the Y-axis represents the change in temperature (°C). Different markers represent the results of each climate model. Blue markers indicate the results of RCP4.5, and red markers indicate the results of RCP8.5. (a) Results of f1 period (2017–2056). (b) Results of f2 period (2057–2096).

Figure 5 represents the time series of annual precipitation and temperature averaged over the three congressional districts. Overall, there are increasing trends in precipitation and temperature for both ensemble means of RCP4.5 and RCP8.5. For the historic period, the annual mean precipitation is 1,064 mm and the annual mean temperature is 18.1 °C. Compared to the historic period, the results of the RCP4.5 models indicate that the ensemble means of precipitation increase by 1.2% and 5.3% and temperature increases by 2.5 °C and 3.5 °C for the f1 and f2 periods, respectively. Additionally, the results of the RCP8.5 models show that precipitation increases by 2.5% and 8.5% and temperature increases by 2.4 °C and 4.7 °C, respectively, for the f1 and f2 periods.

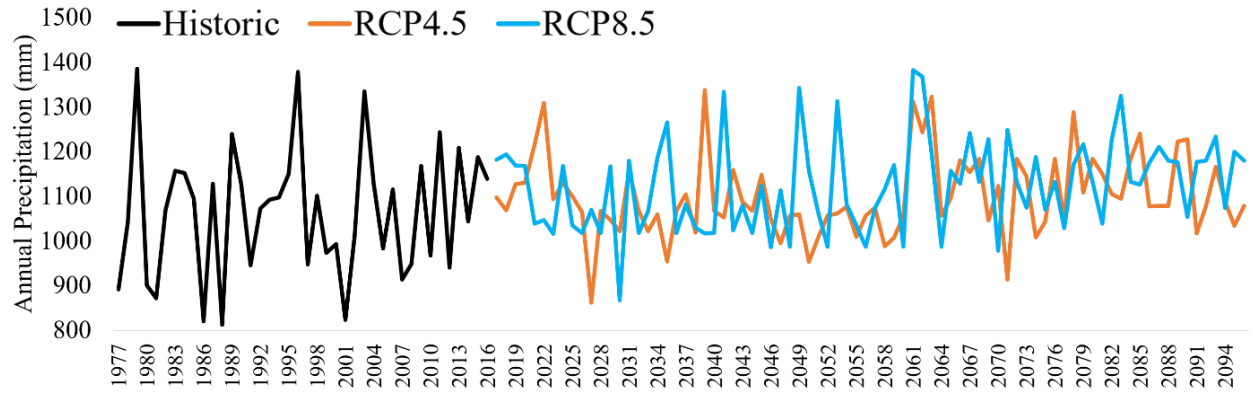

(a)

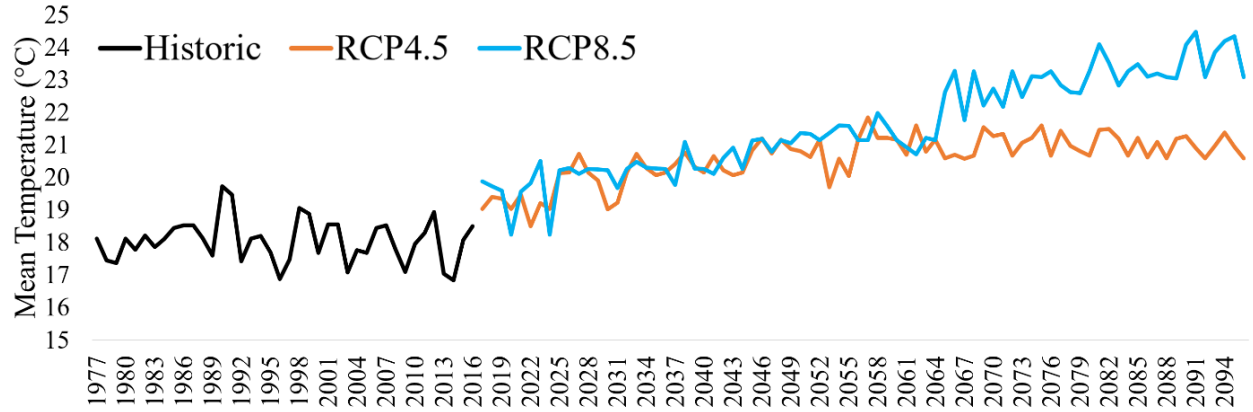

(b)

Figure 5. Time series for mean values of precipitation and temperature during historic and future periods. The black line represents the mean values of the historic period, and the orange and blue lines represent the mean values of the RCP4.5 and RCP8.5 scenarios, respectively. (a) Time series of precipitation. (b) Time series of temperature.

4.4.2. Time series of SSI and drought occurrences for districts

Figure 6 indicates the weekly time series of SSI for the two RCP models (4.5 and 8.5). As shown in Table 3, lower values of SSI indicate drought conditions, while higher values represent wet conditions. The mean SSI value for the historic period is 0.106, while those of the future periods are -0.092 and -0.040 for RCP4.5 and -0.077 and -0.098 for RCP8.5, respectively. In general, future drought severity, estimated by SSI, increases for the study area. However, considerable variations in projections are found across the districts. Table 4 shows the mean SSI values for each congressional district, and Figure 7 represents the time series of each district and

RCP. In Figure 7, an increase in drought severity is highlighted with red text, while a decrease in drought severity is highlighted with blue text. For the results of VA06, the mean values for future periods of RCP4.5 are -0.104 (f1) and -0.058 (f2), and those of RCP8.5 are -0.092 (f1) and -0.114 (f2), which indicate an increase in drought severity in the future. Additionally, some results of VA11 represent an increase in drought severity, such as the f1 period of RCP4.5 and f2 period of RCP8.5. However, the results of VA08 and some other results for VA11 indicate a decrease in drought severity.

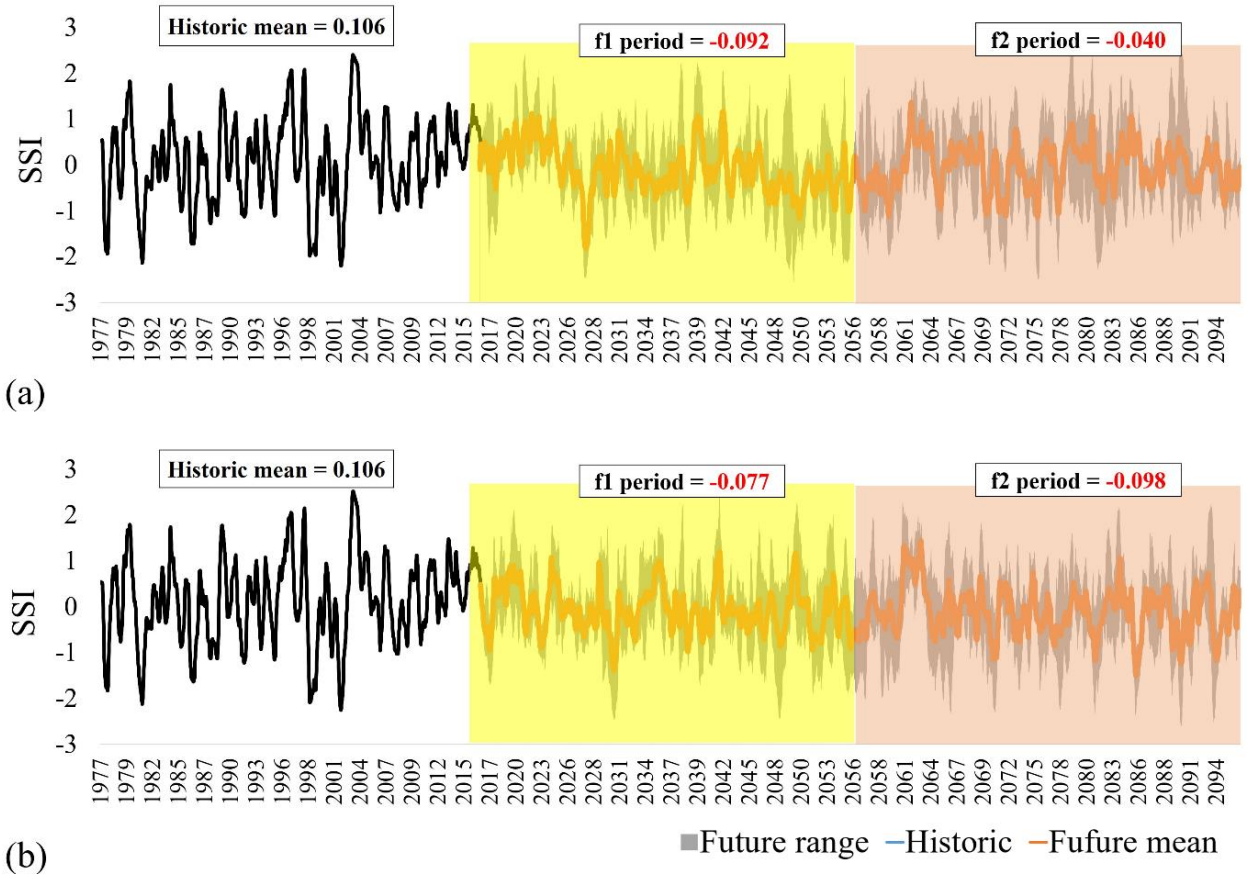

Figure 6. Weekly time series of SSI for mean values of three congressional districts in VA. The black lines indicate the mean values for the historic period, and the orange lines are the mean values for the future periods from the three climate models. The gray areas indicate the range of climate models for the future periods. The transparent yellow and orange rectangles highlight the future periods. (a) SSI for RCP4.5. (b) SSI for RCP8.5.

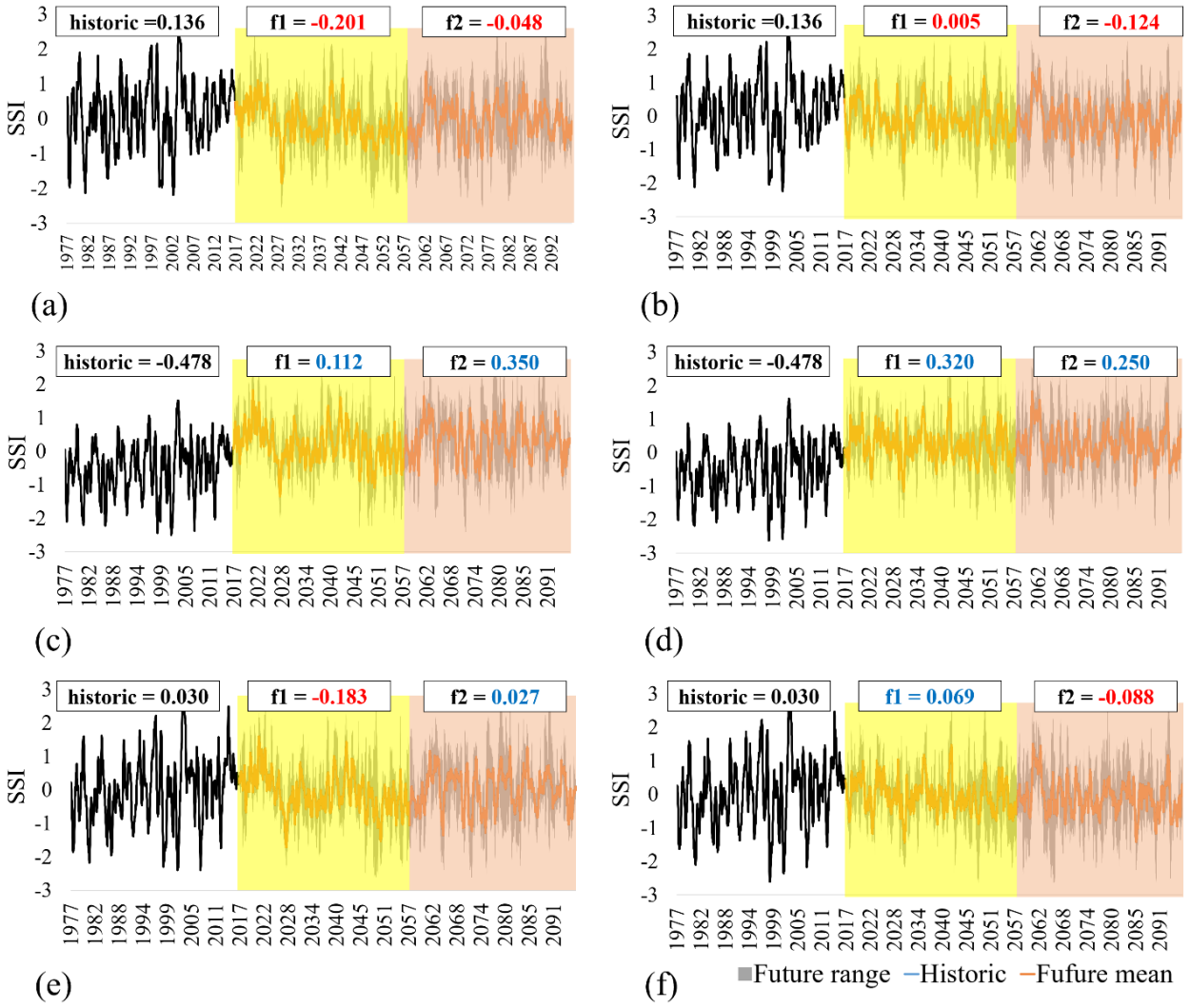

Figure 7. Weekly time series of SSI for each congressional district. The black lines indicate the mean values for the historic period, and the orange lines are the mean values for the future periods from the three climate models. The gray areas indicate the range of climate models for the future periods. The transparent yellow and orange rectangles highlight the future periods. For all figures, red text indicates an increase in drought severity, while blue text indicates a decrease in drought severity in the future. (a) Results of VA06 for RCP4.5. (b) Results of VA06 for RCP8.5. (c) Results of VA08 for RCP4.5. (d) Results of VA08 for RCP8.5. (e) Results of VA11 for RCP4.5. (f) Results of VA11 for RCP8.5.

Table 4. Mean values of the SSI for the historic and future periods of each climate model. Red text means an increase in drought severity, while blue text represents a decrease in drought severity in the future.

District	RCPs	Climate models	historic	f1 (mean)	f2 (mean)	f1	f2
All districts	RCP4.5	BCC-CSM1.1	0.106	-0.092	-0.040	-0.070	-0.167
		CanESM2				-0.372	0.230
		CCSM4				0.167	-0.184
	RCP8.5	BCC-CSM1.1		-0.077	-0.098	-0.125	-0.154
		CanESM2				-0.016	-0.276
		CCSM4				-0.091	0.134
VA06	RCP4.5	BCC-CSM1.1	0.136	-0.104	-0.058	-0.080	-0.188
		CanESM2				-0.385	0.221
		CCSM4				0.155	-0.208
	RCP8.5	BCC-CSM1.1		-0.092	-0.114	-0.139	-0.178
		CanESM2				-0.029	-0.285
		CCSM4				-0.109	0.121
VA08	RCP4.5	BCC-CSM1.1	-0.478	0.193	0.330	0.200	0.247
		CanESM2				-0.061	0.488
		CCSM4				0.440	0.256
	RCP8.5	BCC-CSM1.1		0.239	0.269	0.197	0.313
		CanESM2				0.264	0.036
		CCSM4				0.255	0.459
VA11	RCP4.5	BCC-CSM1.1	0.030	-0.080	0.039	-0.085	-0.075
		CanESM2				-0.358	0.194
		CCSM4				0.201	-0.062
	RCP8.5	BCC-CSM1.1		-0.034	-0.080	-0.106	-0.039
		CanESM2				0.007	-0.347
		CCSM4				-0.002	0.145

Figure 8 shows the seasonal comparisons of the mean soil moisture values (total column moisture). Solid black lines represent the weekly mean values of the historic period (1977–2016), and gray areas indicate the range of future periods and RCPs. Figure 8(a) and Figure 8(b) represent the results of the VA06 district (f1 and f2 periods, respectively), and there is an overall decrease in soil moisture during the period of early April to late February, which includes the crop-growing season (April to September). The VA06 district primarily consists of forest (67%), and an increase in temperature in this region would lead to an evapotranspiration increase that would decrease the amount of soil moisture.

There is a general increase in evapotranspiration for both the f1 and f2 periods, and they are shown in Figure 9(a) and Figure 9(b), respectively. By contrast, Figure 8(c) and Figure 8(d) show the results of the VA08 district where there is an overall increase in soil moisture. The VA08 district is mainly composed of developed areas (73.3%) and includes some forest regions (16.9%). Thus, the temperature increase in the VA08 district does not affect the evapotranspiration increase as much as it does in the VA06 district (Figure 9(c) and Figure 9(d)), and the precipitation increase in the future leads to an increase in soil moisture. As shown in Table 4, the biggest differences between the historic and future periods are 0.492 for the f1 period and CanESM2-RCP4.5 model and 0.421 for the f2 period and CanESM2-RCP8.5 model in the VA06 district. As shown in Figure 4, the CanESM2-RCP4.5 model is the driest in the f1 period (blue triangle), and the CanESM2-RCP8.5 model is the hottest in the f2 period (red triangle). Thus, these results imply that a decrease in precipitation and increase in temperature are the primary drivers of the increase in agricultural droughts in the future periods.

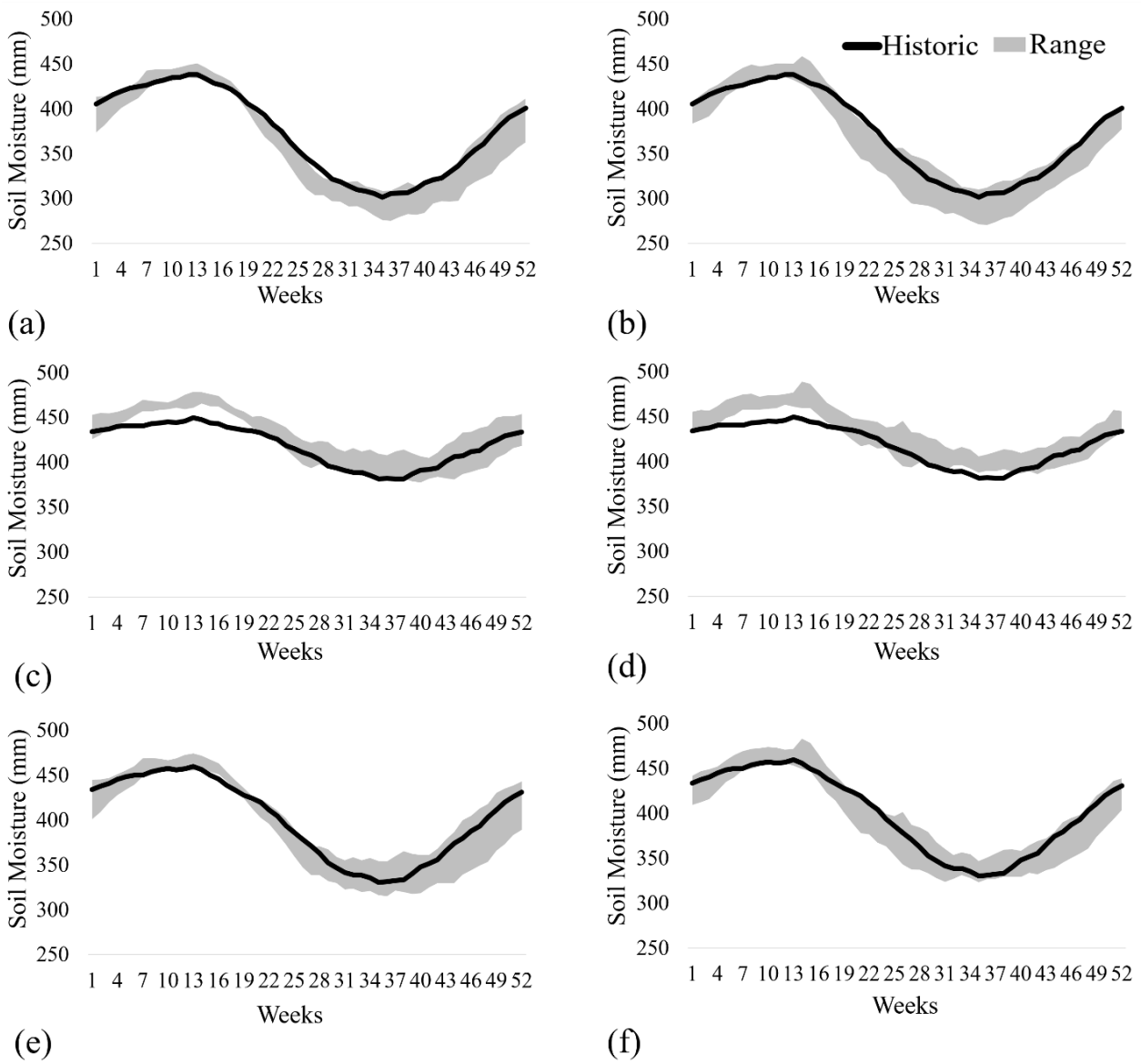

Figure 8. Seasonal comparisons of mean soil moisture values for each congressional district. The X-axis represents the weeks of the year, and the Y-axis represents the weekly mean soil moisture values (total column, mm). (a) Results of VA06 for RCP4.5. (b) Results of VA06 for RCP8.5. (c) Results of VA08 for RCP4.5. (d) Results of VA08 for RCP8.5. (e) Results of VA11 for RCP4.5. (f) Results of VA11 for RCP8.5.

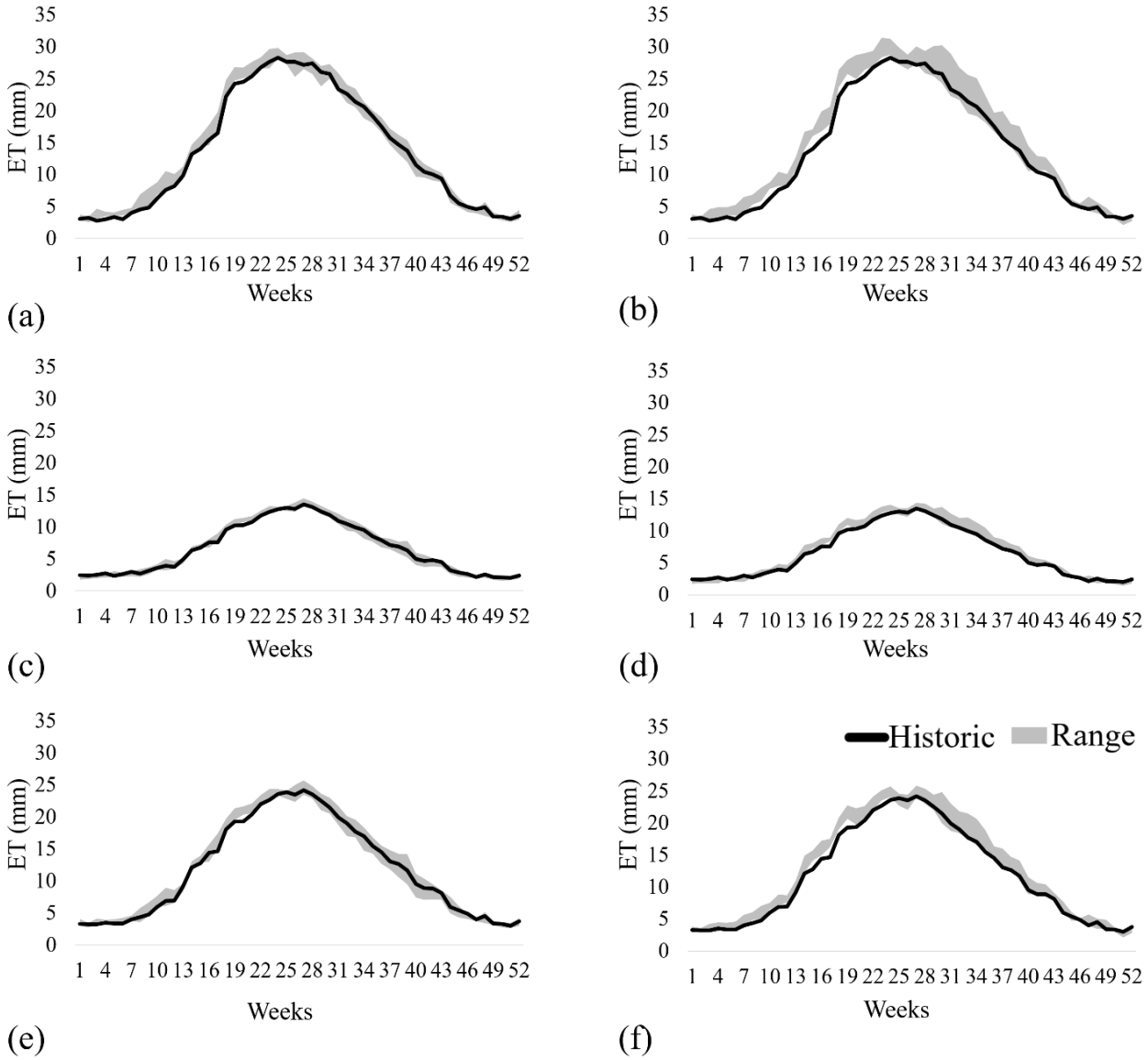

Figure 9. Seasonal comparisons of the mean values of evapotranspiration (ET) for each congressional district. The X-axis represents the weeks of the year, and the Y-axis represents the weekly mean values of ET (mm). (a) Results of VA06 for RCP4.5. (b) Results of VA06 for RCP8.5. (c) Results of VA08 for RCP4.5. (d) Results of VA08 for RCP8.5. (e) Results of VA11 for RCP4.5. (f) Results of VA11 for RCP8.5.

Figure 10 presents the spatial maps of the drought occurrence ratios based on the SSI results for the study areas. The maps of the drought occurrence odds ratios are computed based on the division of numbers of historic and future drought occurrences for each grid (future/historic). A value corresponding to or greater than one is shown in orange or red and demonstrates an increase in drought occurrence in the future period, while values less than one are shown in yellowish green and dark green and demonstrate a decrease in drought occurrences in the future. Additionally, the mean values of drought occurrence ratios are marked in each figure. From the results of the VA06 and VA11 districts, there are general increases in drought occurrences for the BCC-CSM1.1 and CanESM2 models, while there is a decrease in the CCSM4 model. Again, in contrast, there are overall decreases in drought occurrences for the VA08 district.

Similar to the time series, the results of drought occurrences are strongly influenced by precipitation and temperature change projections. For example, the CCSM4 model shows the highest increase in precipitation except for the RCP4.5 and f2 period (blue circle in Figure 4(b)), and it results in the decrease of drought occurrences. In contrast, there are increases in drought occurrences from the other two models because the magnitude of the precipitation increase is lower than that of the CCSM4 model. Additionally, the highest drought occurrence ratio of 2.95, from the CanESM2-RCP8.5 model in the f2 period, is due to a high temperature increase but a relatively low precipitation increase. The VA08 district shows different results: there is an overall decrease in drought occurrences.

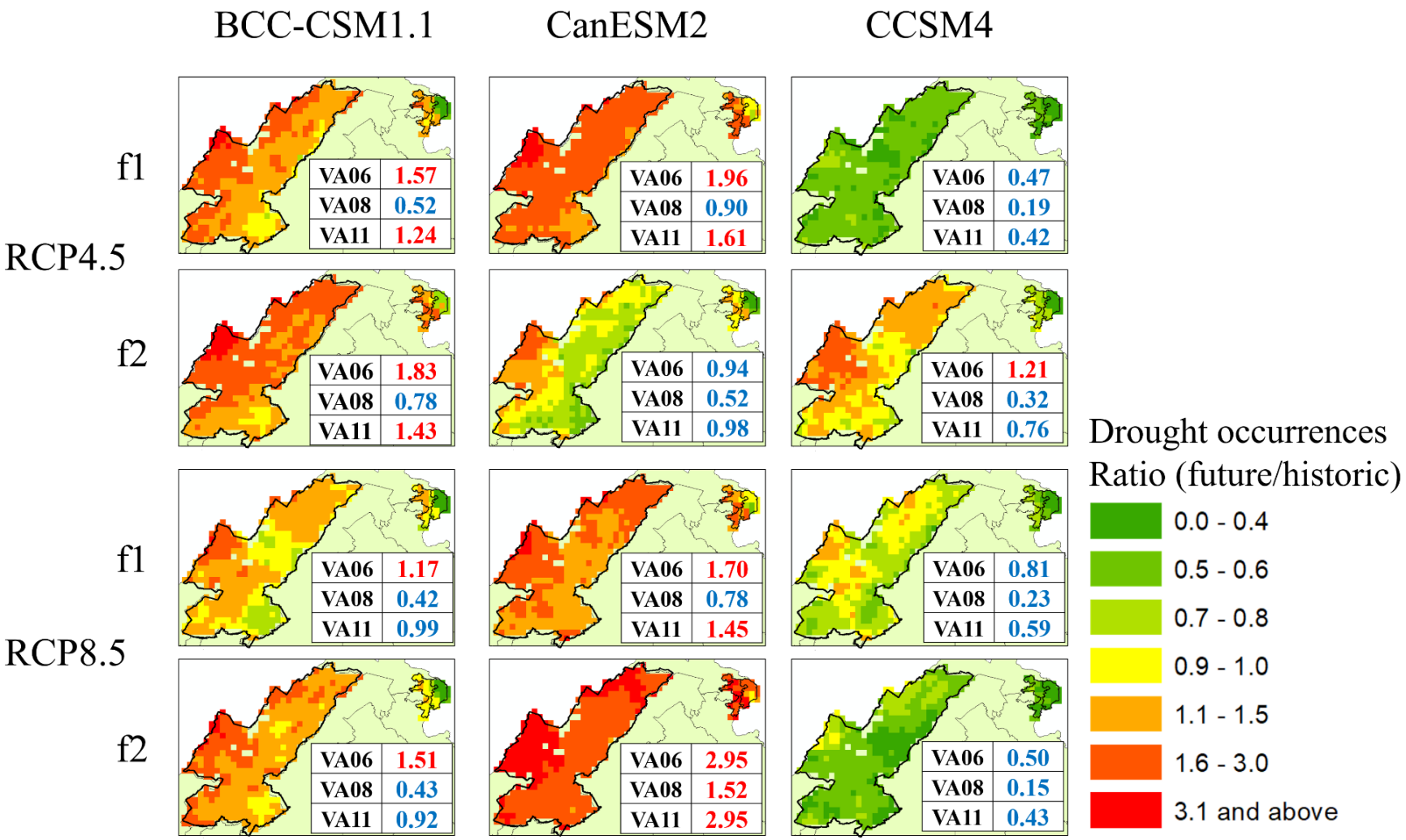

Figure 10. Spatial maps of drought occurrences based on results of SSI between historic and future periods. A value equal to or > 1 indicates an increase in drought occurrences in the future and is symbolized as orange to red, while a value < 1 is represented as yellow to green and indicates a decrease in drought occurrences in the future. Inside the figure, red text represents an increase in drought occurrence, while blue text represents a decrease in drought occurrence in the future.

4.4.3. Regression analysis of output and annual mean SSI values

In this study, simple linear regression analyses are carried out to identify the relationships between the annual mean SSI values and value of primarily rain-fed agricultural output for the three congressional districts in VA. Figure 11 shows the results of the analysis, where the X-axis represents the annual means of SSI and the Y-axis represents the annual agricultural production for seven years (2010–2016). More specifically, the Y-axis of Figure 11 represents the sum of the annual agricultural products described in Table 2 from rain-fed, not irrigated, production. Additionally, lower values of the X-axis reflect higher drought severity in a year, while higher values represent relatively low drought severity.

To identify outliers, the studentized residuals method is used to remove outliers from the observations. The studentized method is commonly used for excluding outliers of linear regression analysis. The results of all districts show that there is a strong linear relationship between the annual mean SSI values and the sum of agricultural production. Additionally, since the area of the VA06 district is larger than those of other districts, the magnitude of agricultural production for the VA06 district is higher (40 and 32 times that of VA08 and VA11, respectively).

For the result of the VA06 district, the R^2 and adjusted R^2 are 0.83 and 0.78, respectively, the regression equation is $Output(\$) = (1.36 \times 10^8 \times SSI) + 2.59 \times 10^8$, and the p-value of the estimated slope coefficient is 0.012, which is statistically significant at the p = 0.05 level. The highest mean SSI value and the sum of agricultural production are 1.00 and $379,000,000, respectively, in 2016, when the highest precipitation occurs in the VA06 district (1,139 mm). The lowest SSI and the sum of agricultural production are 0.15 and $263,000,000, respectively, in 2010, when the second-lowest level of precipitation occurs (963 mm).

For the VA08 district, the R^2 and adjusted R^2 are 0.94 and 0.92, respectively, the regression equation is $Output(\$) = (1.54 \times 10^5 \times SSI) + 2.34 \times 10^5$, and the p-value of the estimated slope coefficient is 0.0014, which is significant at the p = 0.05 level. The highest mean SSI value and the sum of agricultural production are 0.39 and $470,000, respectively, in 2014, when the highest precipitation occurs in the VA08 district (1,246 mm). However, the lowest SSI mean and the sum of agricultural production are -0.41 and $220,000, respectively, in 2011, when the lowest precipitation occurs (981 mm). Finally, for the VA11 district, the R^2 and adjusted R^2 are 0.88 and 0.85, respectively, the regression equation is $Output(\$) = (3.28 \times 10^5 \times SSI) + 8.66 \times 10^5$,

and the p-value of the estimated slope coefficient is 0.0053. The highest mean SSI value and the sum of agricultural production are 1.37 and $1,370,000, respectively, in 2016, when the highest precipitation occurs in the VA11 district (1,304 mm). However, the lowest SSI and the sum of agricultural production are -0.08 and $840,000, respectively, in 2010, when the lowest precipitation occurs (1,031 mm). Since all regression analysis results are significant, it is reasonable to apply the results to assess the impact of future projected drought on agricultural production.

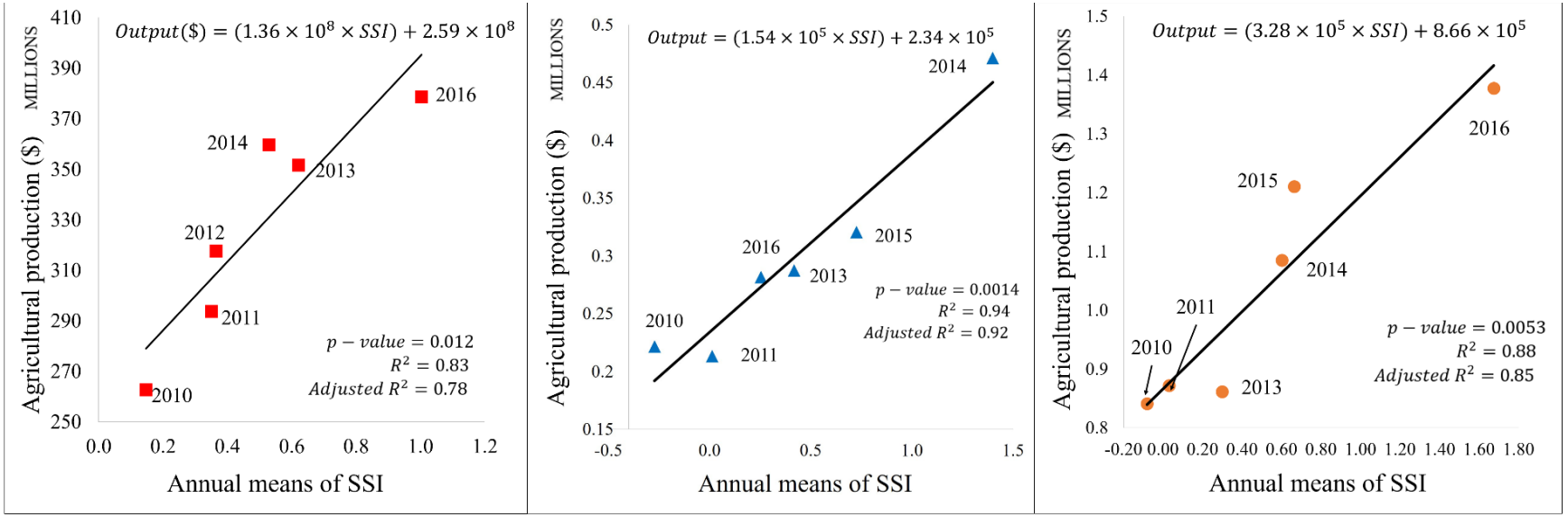

Figure 11. Scatter plots showing correlations between annual means of SSI and sum of agricultural production ($) for seven years (2010–2017). The X-axis represents the annual mean SSI values, and the Y-axis is the sum of agricultural production ($). (a) Results of VA06 district. (b) Results of VA08 district. (c) Results of VA11 district.

4.4.4. Implications of climate change impacts on agricultural productions

Table 5 shows the results of the mean values of agricultural production for both historic (1977–2016) and future periods, and they are based on the results of the time series (Table 4). In Table 4, increases in agricultural production are highlighted with blue, while decreases are highlighted with red. For the VA06 district, overall decreases in agricultural production are found under future climate change projections. The mean value of agricultural production for the historic period is $277,000,000/year. This value decreases in future periods by 11.6% and 11.2% and decreases for the f1 period under mean predictions from the RCP4.5 and RCP8.5 models, respectively. Similarly, decreases of 9.4% and 15.9% are found for the f2 period under mean predictions of the RCP4.5 and RCP8.5 models, respectively. However, significant variability remains in future production predictions. The highest production prediction for the future period is a 4.3% increase from the CanESM2-RCP8.5 model for the f2 period, while the lowest production prediction is a 25.3% decrease from the CanESM2-RCP4.5 model for the f1 period.

For the VA11 district, the mean value of agricultural production for the historic period is $876,000/year. This value decreases in future periods by 4.1% and 2.4% for the f1 period and 0.5% and 4.1% for the f2 model under the RCP4.5 and RCP8.5 models, respectively. The highest production prediction for the future period is a 6.4% increase from the CCSM4-RCP4.5 model for the f1 period, while the lowest production prediction is a 14.5% decrease from the CanESM2-RCP4.5 model for the f1 period.

Finally, there is a general predicted increase in agricultural production due to the increase in soil moisture and SSI in the future periods for the VA08 district. The mean value of agricultural production for the historic period is $160,000/year, and overall increases in agricultural production are found under future climate change projections. This value increases in future periods by 65.0% and 69.4% for the f1 period under mean predictions from the RCP4.5 and RCP8.5 models, respectively. The highest production prediction for the future period is a 93.1% increase from the CanESM2-RCP4.5 model, while the lowest production prediction is a 40.6% increase from the CanESM2-RCP4.5 model for the f1 period.

The results of the three districts show that higher precipitation increases result in an increase in agricultural production in the future periods (e.g., CanESM2-RCP8.5 and f2 period,

CCSM4-RCP4.5 and f1 period), while decreases in precipitation (e.g., CanESM2-RCP4.5 and f1 period) lead to a decrease in agricultural production.

Table 5. Mean values of sum of agricultural production for historic and future periods for each climate model (unit: million $/year). Red text represents a decrease in agricultural production, while blue text represents an increase in agricultural production.

District	RCPs	Climate models	Historic (Million $)	f1 (mean) (Unit: %)	f2 (mean) (Unit: %)	f1 (Unit: %)	f2 (Unit: %)
VA06	RCP4.5	BCC-CSM1.1	277	-11.6	-9.4	-10.5	-15.9
		CanESM2				-25.3	4.3
		CCSM4				1.1	-16.6
	RCP8.5	BCC-CSM1.1		-11.2	-15.9	-13.4	-15.2
		CanESM2				-7.9	-20.6
		CCSM4				-11.9	-0.7
VA08	RCP4.5	BCC-CSM1.1	0.160	65.0	78.1	65.6	70.0
		CanESM2				40.6	93.1
		CCSM4				88.8	70.6
	RCP8.5	BCC-CSM1.1		69.4	71.9	65.0	76.3
		CanESM2				71.9	50.0
		CCSM4				70.6	90.6
VA11	RCP4.5	BCC-CSM1.1	0.876	-4.1	0.5	-4.3	-4.0
		CanESM2				-14.5	6.2
		CCSM4				6.4	-3.4
	RCP8.5	BCC-CSM1.1		-2.4	-4.1	-5.1	-2.6
		CanESM2				-0.9	-14.2
		CCSM4				-1.3	4.2

4.4.5. Assessment of economy-wide impacts using IMPLAN

We now estimate the economy-wide gains or losses associated with future climate change. Table 6 shows the results of economy-wide impacts using the IMPLAN model for the mean values of climate models. Each row contains direct effects, indirect effects, and induced effects, and each column represents total effects on employment (number of jobs), labor income ($), and output ($). The direct effects are economic losses or gains in the agricultural sector, the indirect effects are economic losses or gains in associated sectors supplying the agricultural sector, induced effects are changes in economic activity arising from changing human behavior (e.g., decreased consumption and increased unemployment), and total effects are the sum of the direct, indirect, and induced effects. Climate change impacts on droughts are estimated to decrease the number of jobs in the VA06 district by 12.9% to 16.7% (total effect) compared to 2016 through direct and indirect effects. In addition, the industry output (total agricultural production) decreases by 16.8% to 21.7% compared to 2016. The number of jobs for the VA11 district decreases by 0.4% to 4.3% (total effect), and the industry output decreases by 0.5% to 5.1% compared to 2016. In the case of the VA11 district, soil moisture conditions in the future periods are slightly lower than or almost the same as those of the historic period, and thus, the estimated economic impacts are much smaller than those of VA06.

By contrast, the number of jobs in the VA08 district increases by 60.7% to 72.7%, and the industry output increases by 71.4% to 85.5% compared to 2016. In the case of the VA08 district, the increase in temperature does not influence the increase in evapotranspiration and decrease in soil moisture directly because the VA08 district primarily consists of developed areas (67.3%) with a smaller area covered by forest (14.6). Therefore, the precipitation increase results in an increase in soil moisture and decrease in droughts, which finally leads to agricultural production increases in the future. In addition, Table 7 shows the proportions of the selected agriculture sector to the total industry: 0.3170%, 0.0003%, and 0.0010% for the total industry in the VA06, VA08, and VA11 districts, respectively. Over the three districts, the selected agricultural production in the VA06 district contributes the most to the total industry, while that in the VA08 district contributes the least. Since the agricultural industry in VA08 is small, the sensitivity of agricultural production to climate change is higher than that in the VA06 district. The highest agricultural production ($470,000 in 2014) in the VA08 district is more than twice the lowest production

($210,000 in 2011) during the historic period. However, the differences between the lowest and highest productions are not as significant in the VA06 and VA11 districts. Thus, it can be said that small-scale agriculture is more sensitive to drought in response to climate change.

Finally, Table 4.8 shows the impact of changes in agricultural output on the overall future economy. The proportions of the agricultural sectors in each district are different (Table 4.7), and their effects show different results. There is an overall decrease in economic output of 0.05–0.07% in the VA06 district, a 0.0002–0.0003% increase in the VA08 district, and a 0.0001% decrease (virtually no change) in the VA11 district. Since only eight sectors are selected from the 536 economic sectors in VA, the results might be regarded as indicating minimal impacts. However, the suggested methods could be applied to other types of agricultural areas, and an impact analysis would be essential to estimate the societal costs of climate change.

Table 6. Mean values of economy-wide impacts on future agricultural sector.

historic	RCPs	Periods	Impact Type	Employment (%)	Labor Income (%)	Output (%)
VA06	RCP4.5	f1	Direct Effect	-11.6	-11.4	-11.5
			Indirect Effect	-3.1	-5.8	-5.5
			Induced Effect	-1.2	-3.9	-3.7
			Total Effect	**-15.9**	**-21.2**	**-20.7**
		f2	Direct Effect	-9.4	-9.3	-9.3
			Indirect Effect	-2.5	-4.7	-4.5
			Induced Effect	-1.0	-3.2	-3.0
			Total Effect	**-12.9**	**-17.2**	**-16.8**
	RCP8.5	f1	Direct Effect	-11.1	-10.9	-11.0
			Indirect Effect	-3.0	-5.6	-5.3
			Induced Effect	-1.2	-3.8	-3.6
			Total Effect	**-15.2**	**-20.3**	**-19.8**
		f2	Direct Effect	-12.2	-12.0	-12.1
			Indirect Effect	-3.3	-6.1	-5.8
			Induced Effect	-1.3	-4.1	-3.9
			Total Effect	**-16.7**	**-22.3**	**-21.7**
VA08	RCP4.5	f1	Direct Effect	59.4	64.2	54.6
			Indirect Effect	0.4	9.2	7.1
			Induced Effect	0.9	13.0	9.7
			Total Effect	**60.7**	**86.3**	**71.4**
		f2	Direct Effect	71.2	76.9	65.5
			Indirect Effect	0.5	11.0	8.5
			Induced Effect	1.1	15.5	11.6
			Total Effect	**72.7**	**103.5**	**85.5**
	RCP8.5	f1	Direct Effect	63.2	68.3	58.1
			Indirect Effect	0.4	9.8	7.5
			Induced Effect	0.9	13.8	10.3
			Total Effect	**64.6**	**91.9**	**75.9**
		f2	Direct Effect	66.0	71.4	60.7
			Indirect Effect	0.5	10.2	7.8
			Induced Effect	1.0	14.4	10.8
			Total Effect	**67.5**	**96.0**	**79.4**
VA11	RCP4.5	f1	Direct Effect	-4.2	-4.1	-4.1
			Indirect Effect	0.0	-2.3	-0.6
			Induced Effect	0.0	-1.2	-0.3
			Total Effect	**-4.2**	**-7.6**	**-5.1**
		f2	Direct Effect	-0.4	-0.4	-0.4
			Indirect Effect	0.0	-0.2	-0.1
			Induced Effect	0.0	-0.1	0.0
			Total Effect	**-0.4**	**-0.8**	**-0.5**
	RCP8.5	f1	Direct Effect	-2.4	-2.4	-2.4
			Indirect Effect	0.0	-1.3	-0.4
			Induced Effect	0.0	-0.7	-0.2
			Total Effect	**-2.5**	**-4.5**	**-3.0**
		f2	Direct Effect	-4.2	-4.1	-4.2
			Indirect Effect	0.0	-2.3	-0.6
			Induced Effect	0.0	-1.3	-0.3
			Total Effect	**-4.3**	**-7.7**	**-5.1**

Table 7. Total industry outputs and proportions of selected agricultural sectors in 2016.

	Total industry output ($)	Employment (%)	Income (%)	Industry output (%)
VA06	65,184,166,740	1.1957	0.3016	0.3170
VA08	104,823,502,176	0.0037	0.0002	0.0003
VA11	86,283,111,683	0.0115	0.0002	0.0010

Table 8. Impacts of agricultural sectors on total economy.

Districts	RCPs	Periods	Employment (%)	Labor Income (%)	Total Change (%)
VA06	RCP4.5	f1	-0.1900	-0.0639	-0.0655
		f2	-0.1543	-0.0519	-0.0532
	RCP8.5	f1	-0.1820	-0.0612	-0.0628
		f2	-0.1998	-0.0672	-0.0689
VA08	RCP4.5	f1	0.0025	0.0001	0.0002
		f2	0.0030	0.0002	0.0003
	RCP8.5	f1	0.0026	0.0002	0.0002
		f2	0.0027	0.0002	0.0002
VA11	RCP4.5	f1	-0.0005	0.0000	-0.0001
		f2	0.0000	0.0000	0.0000
	RCP8.5	f1	-0.0003	0.0000	0.0000
		f2	-0.0005	0.0000	-0.0001

4.5. Conclusion

The impacts of climate change on agricultural droughts and economic outputs are important determinants of the societal costs of climate change. This paper focuses on the economic losses associated with changes in drought severity. Long-term economic impacts in several congressional districts in Northern VA are estimated using the soil moisture simulation from the VIC model and SSI based on long-term climate projection models from CMIP5 models. The critical findings of this study are as follows:

1) The simulations of future soil moisture and agricultural droughts using SSI indicate that there is an overall increase in drought occurrences in the VA06 and VA11 districts, and the mean values are 1.38 and 1.15 times higher for all climate models and periods compared to the historic period. However, overall decreases in drought occurrences are found in the VA08 district (0.56 times) due to the different land-use composition leading to the different results of water budget components, such as ET.
2) The results of linear regression analyses indicate that there are strong and significant correlations (95% confidence interval, p-values < 0.05) between the annual mean SSI values and sums of agricultural production for the three congressional districts in Northern VA during 2010 to 2016. The strength of these associations suggests that the results of the analyses can be applied to future drought simulations and their impacts on the agricultural economy.
3) The results of SSI simulation and linear regression analyses are used to estimate future agricultural production: 9.4% to 15.9% decreases are found in the VA06 district (mean values of f1 and f2 periods, respectively), and 0.5% to 4.1% decreases are found in the VA11 district. However, 65.0% to 78.1% increases are found in the VA08 district, which correspond to the time series of SSI. In addition, the economy-wide impacts are evaluated by the IMPLAN model. The industry output (total agricultural production) decreases by 16.8% to 21.7% compared to 2016 in the VA06 district, and it decreases by 0.5% to 5.1% in the VA11 district. However, the industry output in the VA08 district increases by 71.4% to 85.5% compared to 2016.
4) Droughts and economic impacts can vary significantly, even in areas that are adjacent where land-use compositions are different. Thus, geographic (e.g., land-use) and economic factors should be incorporated simultaneously for the accurate estimation of the societal costs of climate change. In addition, urban and rural areas should be analyzed separately for the analysis of the impacts of climate change on agricultural production.
5) To perform a more reliable analysis, a higher spatiotemporal resolution and more prolonged period of economic production are required. Additionally, if a land-use change scenario is applied for future periods, more accurate simulations of economic outputs would be

available. Finally, changes in agricultural production could be smaller than the estimations due to farmers' adaptations in the future.

6) Since many factors influence economic production with frequent occurrences of natural disasters, it is a considerable challenge to separate their impacts from those of other elements and quantify them, and this study provides one means of doing so.

4.6. Reference

Abatzoglou, J. T. 2013. Development of gridded surface meteorological data for ecological applications and modelling. International Journal of Climatology 33 (1): 121-131.

Bauman, A., Goemans, C., Pritchett, J., & McFadden, D. T. (2013). Estimating the economic and social impacts from the drought in Southern Colorado. Journal of Contemporary Water Research & Education, 151(1), 61-69.

Bolten, J.D., Crow, W.T., Zhan, X., Jackson, T.J. and Reynolds, C.A., 2010. Evaluating the utility of remotely sensed soil moisture retrievals for operational agricultural drought monitoring. IEEE Journal of Selected Topics in Applied Earth Observations and Remote Sensing, 3(1), pp.57-66.

Cayan, D.R., Das, T., Pierce, D.W., Barnett, T.P., Tyree, M. and Gershunov, A., 2010. Future dryness in the southwest US and the hydrology of the early 21st century drought. Proceedings of the National Academy of Sciences, 107(50), pp.21271-21276.

Chattopadhyay, S., Edwards, D.R., Yu, Y. and Hamidisepehr, A., 2017. An Assessment of Climate Change Impacts on Future Water Availability and Droughts in the Kentucky River Basin. Environmental Processes, 4(3), pp.477-507.

Cheng, L., Hoerling, M., AghaKouchak, A., Livneh, B., Quan, X.W. and Eischeid, J., 2016. How has human-induced climate change affected California drought risk?. Journal of Climate, 29(1), pp.111-120.

CHJ, 2007. Plan especial de alerta y eventual sequía en la Confederación Hidrográfica del Jucar Confederación Hidrográfica del Júcar, Valencia, España. Retrieved from www.chj.es. Last access December 2016 (in Spanish).

Combs, S. The Impact of the 2011 Drought and Beyond; Texas Comptroller of Public Accounts: Austin, TX, USA, 2012.

Drought Response Technical Advisory Committee (DRTAC), 2003. Virginia Drought Assessment and Response Plan.

Guerrero, B., 2012. The impact of agricultural drought losses on the Texas economy, 2011. Briefing Paper, AgriLife Extension.

Ding, Y., Hayes, M.J., Widhalm, M., 2011. Measuring economic impacts of drought: a review and discussion. Disaster Prevent. Manage. Int. J. 20 (4), 434–446.

Howitt, R., Medellín-Azuara, J., MacEwan, D., Lund, J.R. and Sumner, D., 2014. Economic analysis of the 2014 drought for California agriculture. University of California, Davis, CA: Center for Watershed Sciences.

Howitt, R., Medellín-Azuara, J., MacEwan, D., Lund, J.R. and Sumner, D., 2015. Economic analysis of the 2015 drought for California agriculture. University of California, Davis, CA: Center for Watershed Sciences.

Jin Z, Ainsworth EA, Leakey AD, Lobell DB. Increasing drought and diminishing benefits of elevated carbon dioxide for soybean yields across the US Midwest. Global change biology. 2018 Feb;24(2):e522-33.

Kang, H. and Sridhar, V., 2017. Combined statistical and spatially distributed hydrological model for evaluating future drought indices in Virginia. Journal of Hydrology: Regional Studies, 12, pp.253-272.

Kang, H., and Sridhar, V., Assessment of Future Drought Conditions in the Chesapeake Bay Watershed. JAWRA Journal of the American Water Resources Association. 54(1), pp. 160-183. https://doi.org/10.1111/1752-1688.12600

Leng, G., Tang, Q. and Rayburg, S., 2015. Climate change impacts on meteorological, agricultural and hydrological droughts in China. Global and Planetary Change, 126, pp.23-34.

Livneh, B., E.A. Rosenberg, C. Lin, B. Nijssen, V. Mishra, K.M. Andreadis, E.P. Maurer, and D.P. Lettenmaier. 2013: A Long-Term Hydrologically Based Dataset of Land Surface Fluxes and States for the Conterminous United States: Update and Extensions. J. Climate 26.

Medellín-Azuara, J., MacEwan, D., Howitt, R.E., Sumner, D.A., Lund, J.R., Scheer, J., Gailey, R., Hart, Q., Alexander, N.D., Arnold, B. and Kwon, A., 2016. Economic analysis of the 2016 california drought on agriculture.

Minnesota IMPLAN Group. IMPLAN Professional, version 3.0. IMPLAN Group: Stillwater, MN, USA, 2009.

Nam, W.H., Hayes, M.J., Svoboda, M.D., Tadesse, T. and Wilhite, D.A., 2015. Drought hazard assessment in the context of climate change for South Korea. Agricultural Water Management, 160, pp.106-117.

Orlowsky, B. and Seneviratne, S.I., 2013. Elusive drought: uncertainty in observed trends and short-and long-term CMIP5 projections. Hydrology and Earth System Sciences, 17(5), pp.1765-1781.

Riahi, K., S. Rao, V. Krey, C. Cho, V. Chirkov, G. Fischer, G. Kindermann, N. Nakicenovic, and P. Rafaj. 2011. RCP 8.5-A scenario of comparatively high greenhouse gas emissions. Climatic Change 109 (1-2): 33-57.

Riebsame, W.E., Changnon, S.A., Karl, T.R., 1990. Drought and Natural Resource Management in the United States: Impacts and Implications of the 1987–1989 Drought, Westview Press, p. 174.

Schlaepfer, D.R., Bradford, J.B., Lauenroth, W.K., Munson, S.M., Tietjen, B., Hall, S.A., Wilson, S.D., Duniway, M.C., Jia, G., Pyke, D.A. and Lkhagva, A., 2017. Climate change reduces extent of temperate drylands and intensifies drought in deep soils. Nature communications, 8, p.14196.

Sheffield, J. and Wood, E.F., 2008. Global trends and variability in soil moisture and drought characteristics, 1950–2000, from observation-driven simulations of the terrestrial hydrologic cycle. Journal of Climate, 21(3), pp.432-458.

Svoboda, M., LeComte, D., Hayes, M., Heim, R., Gleason, K., Angel, J., Rippey, B., Tinker, R., Palecki, M., Stooksbury, D. and Miskus, D., 2002. The drought monitor. Bulletin of the American Meteorological Society, 83(8), pp.1181-1190.

Thomson, A.M., K.V. Calvin, S.J. Smith, G.P. Kyle, A. Volke, P. Patel, S. Delgado-Arias, B. Bond-Lamberty, M.A. Wise, L.E. Clarke, et al. 2011. Rcp4. 5: a pathway for stabilization of radiative forcing by 2100. Climatic Change 109 (1-2): 77-94.

USDA NASS, 2012 Census of Agriculture, Ag Census Web Maps. Available at: www.agcensus.usda.gov/Publications/2012/Online_Resources/Ag_Census_Web_Maps/Overview/.

VDEM (Virginia Department of Emergency), 2013. Commonwealth of Virginia Hazard Mitigation Plan. Chapter 3: Hazard Identification and Risk Assessment.

Wang, L. and Chen, W., 2014. A CMIP5 multimodel projection of future temperature, precipitation, and climatological drought in China. International Journal of Climatology, 34(6), pp.2059-2078.

Wuebbles, D.J., Kunkel, K., Wehner, M. and Zobel, Z., 2014. Severe weather in United States under a changing climate. Eos, Transactions American Geophysical Union, 95(18), pp.149-150.

Ziolkowska, J.R., 2016. Socio-economic implications of drought in the agricultural sector and the state economy. Economies, 4(3), p.19.

Chapter 5. Identification of physical mechanisms and overall processes of drought with a coupled model

5.1. Abstract

The Chesapeake Bay is the largest and the most productive estuary in the US and contributes a 5% share of the total US supply. The objective of this study is to evaluate the response of soil moisture and groundwater dynamics under drought conditions using a coupled land surface and groundwater model in the Chesapeake Bay Watershed. A coupled framework using Variable Infiltration Capacity (VIC) and MODFLOW (MF), referred to as the VICMF model, was applied to evaluate the drought conditions and compare the results of the VIC model-only simulations. For drought assessment, several combinations of variables, including precipitation, soil moisture, and water table elevation (WTE), were used in the Multivariate Standardized Drought Index (MSDI) framework. Three drought indices were derived (MSDI_PSV, MSDI_PSM, MSDI_PWM), and the accuracy of the results was verified using a performance measure (Drought Agreement (%); DA) and a statistical test. The MSDI_PWM showed better results for some drought periods, such as 2002 and 2012, because the MSDI_PWM captured drought conditions during the drought recovery period. This study emphasizes the need for an integrated surface and groundwater conditions for drought evaluation and in turn offers an improved decision-making tool to establish drought mitigation plans and risk management in the Northern Atlantic Coastal Plain (NACP) region.

5.2. Introduction

A comprehensive understanding of the hydrologic cycle and watershed processes in the terrestrial environment is essential for water budget estimation and sustainable water management under changing weather and climate extremes. Specifically, interactions between surface water and groundwater in the watersheds where the exchanges are dominant can have significant impacts on water resources, watershed management, and nutrient loadings (Bailey et al., 2016). However, the exchanges between these systems have been analyzed individually, and many models have considered improving the exchanges in a vertical direction (Niu et al., 2007; Liang et al., 2003). To give more accurate evaluations of these interactions, a fully coupled model is necessary to provide a better understanding of both surface and aquifer conditions across multiple spatial and temporal scales.

Numerous techniques and different approaches are available to investigate the patterns of groundwater and surface water interactions at various spatiotemporal scales (Panday and Huyakorn, 2004; Bailey et al., 2016; Sridhar et al., 2017). These techniques and advanced tools provide opportunities to explain the effects of these interactions on water availability, hydrologic processes, and drought conditions including the rates of evapotranspiration, surface runoff, soil moisture, and groundwater level. Sridhar et al. (2017) developed a new coupled framework using Variable Infiltration Capacity (VIC) (Liang et al., 1994) and MODFLOW models, referred to as VICMF hereafter, to investigate the influence of groundwater dynamics on water balance components and assess how changing hydrology alters recharge and thus groundwater levels. The VIC model can provide downward flux generated from the precipitation events and estimates surface atmospheric fluxes using atmospheric forcing, soil, and vegetation data over the land surface. Under certain conditions where the contribution of groundwater is adding moisture in the vadose zone, the subsurface water movement can be significant as there is upward flux from below; this can be useful for estimating the soil moisture. In addition, the VIC model includes multiple soil layers with variable infiltration rates, and a routing module that uses the linear-transfer-function model is available to simulate the streamflow in the river network system. However, the VIC model does not estimate hydrologic dynamics related to groundwater or groundwater–surface water interactions because it is applied as an uncoupled land hydrology model in the general

circulation model framework. Thus, the coupled VICMF model was developed for a more accurate understanding of the physical processes in surface–groundwater interactions.

Hydrologic models have applied water and energy balance approaches, and they are beneficial for addressing spatial distributions of water resources and drought conditions. However, hydrologic models do not capture a drought condition integrating both surface and groundwater dynamics (Oki and Kanae, 2006). The integrated framework somewhat complements these shortcomings of drought evaluations. In addition, drought indices are used for evaluating drought severity, frequency, and impact (Niemeyer, 2008), as well as for improved drought prediction (Kang and Sridhar, 2018; Sehgal and Sridhar, 2018). Numerous drought indices have been applied to assess drought conditions, and the Multivariate Standardized Drought Index (MSDI), which is calculated using multiple hydrometeorological variables, is used to identify retrospective droughts in the US (Hao and AghaKouchak, 2013; Hao and AghaKouchak, 2014). Since the MSDI can consider multiple hydrometeorological variables, MSDI applications enable us to analyze various aspects of droughts integrating surface and groundwater dynamics. In this study, the MSDI was applied to represent multivariate perspectives on drought conditions with various combinations of results (e.g., soil moisture, precipitation, water table elevation (WTE)).

The objectives of this study are 1) to identify the physical relationship between surface and groundwater variables, such as soil moisture and WTE, during drought events using the coupled VICMF model and 2) to evaluate the drought conditions using various drought indices in the Chesapeake Bay Watershed, including the Northern Atlantic Coastal Plain (NACP) aquifer system.

5.3. Methods

5.3.1. Study Area

The NACP aquifer system in the Chesapeake Bay Watershed occupies an area of approximately 28,200 km^2 between latitude 36°40' and 39°45' N and longitude 77°30' and 79°15' W (Figure 1). The climate is temperate and humid with annual precipitation of 1020 mm, and large metropolitan areas are included along with coastal areas such as Washington D.C. and Richmond. In addition, the NACP aquifer provides a widely used groundwater supply due to its thickness and

large areal extents (Masterson et al., 2016). Groundwater in the area is recharged mainly by precipitation and percolation to the water table.

The US Geological Survey (USGS) developed a groundwater flow model (MF) for the NACP aquifer system (Masterson et al., 2016), and it provides a detailed evaluation of the groundwater availability of the NACP area. In this study, only some parts of the NACP area (Chesapeake Bay region) will be collected and used for the coupled model. The inputs for this simulation analysis include information on hydraulic conductivities, recharges, drainages, and wells.

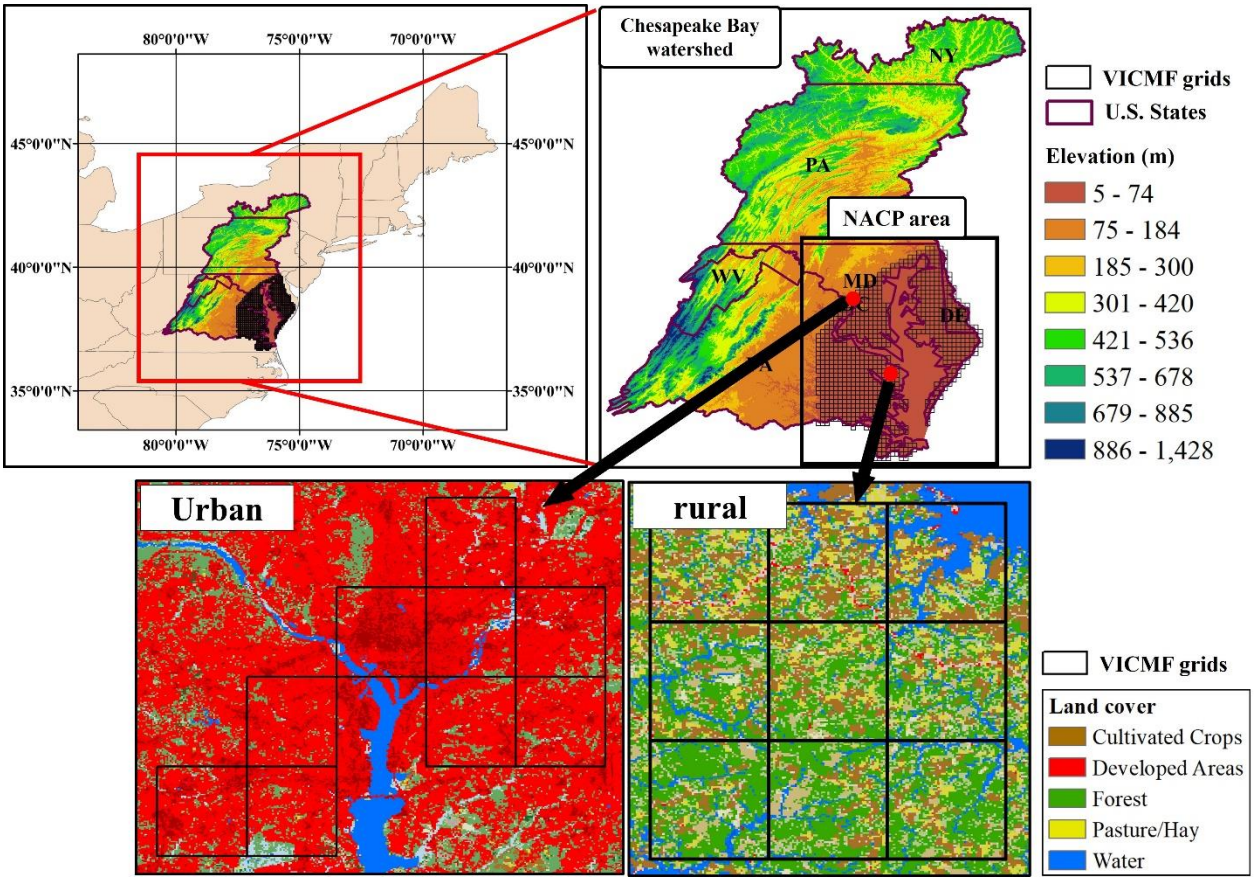

Figure 1. Location map of the study region. The upper-left figure highlights the location of the North Eastern US and the Chesapeake Bay Watershed with a red box. The upper-right figure represents the Chesapeake Bay Watershed and the NACP aquifer system (black box). The red circles represent the locations of urban and rural areas. The figures in the bottom show the land-use maps from the National Land Cover Database (NLCD) (https://www.mrlc.gov).

5.3.2. VIC and MODFLOW model

The VIC model is a physically based macroscale hydrologic model that includes a water and energy balance framework (Liang et al., 1994). The model estimates several hydrologic and atmospheric variables and applies a conceptual system to demonstrate water and surface energy budgets. Furthermore, the VIC model includes multiple soil layers with variable infiltration rates, and a routing module that uses the linear-transfer-function model is available to simulate the streamflow in the river network system. These essential characteristics of the VIC model provide an opportunity to couple the land surface scheme with a groundwater model for accurate descriptions of the entire hydrologic budgets. However, the model is applied as a land surface hydrologic model that does not estimate hydrologic dynamics with groundwater or groundwater–surface water interactions. The coupled surface and groundwater model provide a more precise understanding of the physical mechanisms of droughts.

The Modular Three-Dimensional Finite-Difference Ground-Water Flow model (MODFLOW) is a physically based, three-dimensional, and distributed finite-difference groundwater model that considers aquifer groundwater levels and routes groundwater flow in the system (Harbaugh, 2005). With the MODFLOW model, estimations of groundwater recharge, pumping, vadose zone percolation, evapotranspiration, discharge to subsurface drains, and river–aquifer interactions are available. However, the MODFLOW does not estimate surface-water budget components, such as soil moisture, surface runoff, and evapotranspiration (Bailey et al., 2016). The VICMF coupled model was developed for a more accurate understanding of physical processes with surface–groundwater interactions, and the coupled model was successfully applied to the Eastern Snake Plain Aquifer (ESPA) region of Snake River Basin (SRB) (Sridhar et al., 2017).

5.3.3. VIC-MODFLOW (VICMF) coupled model

The coupled VICMF model (Sridhar et al., 2017) is integrated with surface and groundwater inputs in the NACP Aquifer System region, where the Chesapeake Bay is located (Figure 1). The VICMF model is based on the interdependent equations that estimate the flow of water in a surface and groundwater hydrologic system (Figure 2). The groundwater area includes

the MODFLOW applications in the NACP region, and it estimates upward flux to surface zones (soil layer). The surface area consists of vegetation and soil layers (VIC model), which combines the upward flux from the groundwater area. In addition, the VIC model simulates infiltration that is recharged to groundwater zones. Finally, the MODFLOW model combines the recharge to simulate groundwater dynamic for the following day (Figure 2). The whole process of the coupled model generates WTE, soil moisture, and energy fluxes. The horizontal discretization of the groundwater model is designed to be consistent with the surface discretization, and the discharges of the groundwater model improve the estimation of soil moisture by the surface model. Parameters such as the recharge, conductance, groundwater pumping, and river statement help to simulate the coupled model with meteorological forcing.

The VIC model was applied at a 1/16th-degree resolution (0.0625°, 5 km) with atmospheric forcing data (daily precipitation, maximum and minimum temperatures, and wind speed), and there were 50 rows and 38 columns. The grid cells for the groundwater model consist of 250 rows and 190 columns, and each cell is uniformly spaced at 1 km, which is five times finer than the resolution of a VIC grid cell. Thus, the 25 grid cells (5×5) of the groundwater model were aggregated for dynamic exchanges of the coupled model (Figure 2). In addition, the NACP grid cells were realigned to match the VIC model grid cells since the grid cells in the NACP model are aligned and not geographically directed north to south (50.727° from horizontal).

Other VIC inputs, such as soil and vegetation data, were obtained from the LDAS (http://ldas.gsfc.nasa.gov/) at the same spatial resolution as the meteorological data. Moreover, this study utilized the MODFLOW parameters from the NACP groundwater model (Masterson et al., 2016), including the hydraulic conductivity. The drain package was applied to each MODLFOW grid cell to interact with VIC grid cell. The coupled model computed daily estimates of the WTE, soil moisture, and river stage for the period from 1987 to 2016.

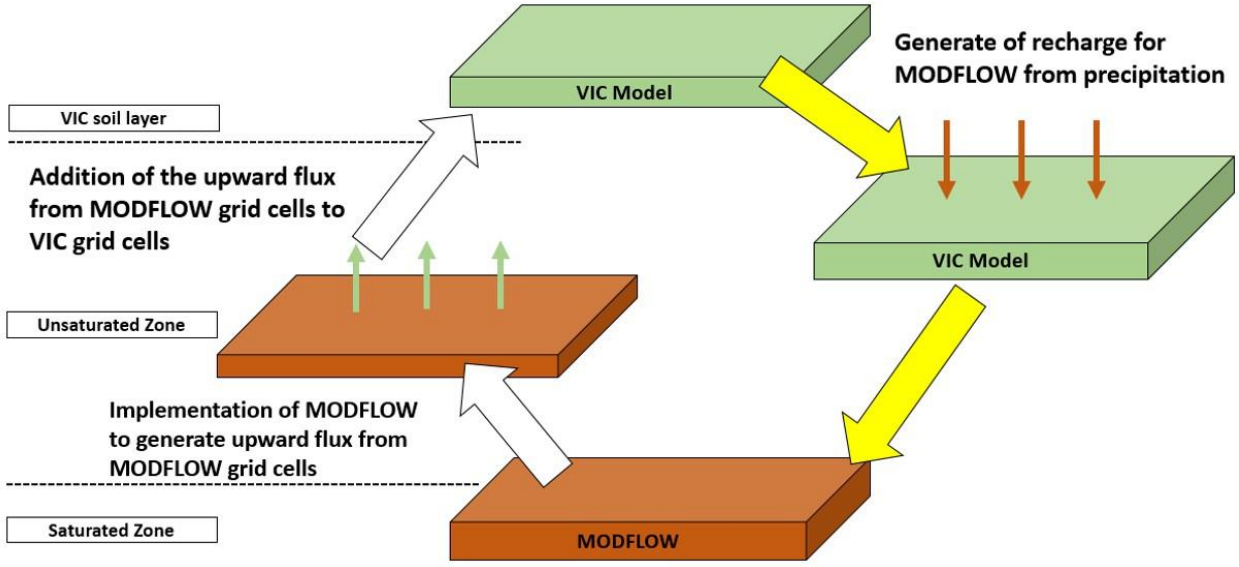

Figure 2. Overall diagram of the coupled model. MODFLOW generates the upward flux (left). The VIC model generates the infiltration, which will recharge the unsaturated and saturated areas. MODFLOW applies the recharge to estimate the upward flux for the following day (Sridhar et al., 2017).

5.3.4. Drought indices and overall descriptions of analysis

In this study, the VIC and VICMF models were used to compute the input variables required for computing the MSDI and to evaluate the drought conditions in the NACP region. The calculation of multivariate drought indices was based on the joint probability and distribution models (Hao and AghaKouchak, 2013; AghaKouchak, 2015), and the MSDI was calculated using the joint probability of long-term hydrometeorological variables (Hao and AghaKouchak, 2013; AghaKouchak, 2015). The joint distribution of two variables is described as

$$P(X \leq x, Y \leq y) = p \qquad (1)$$

where p is the joint probability of the variables used. The MSDI was then computed as follows (Hao and AghaKouchak, 2013):

$$\mathrm{MSDI} = \emptyset^{-1}(p) \qquad (2)$$

where $\emptyset$ is the standard normal distribution function.

In this study, the MSDI approach was mainly used for the estimation of drought indices, but combinations of hydrometeorological variables differed between the two models. For example, precipitation and soil moisture were used to compute MSDI for the VIC model, while multiple combinations were available with the VICMF model, such as precipitation, soil moisture, and WTE. For the VIC model, MSDI with precipitation (P) and soil moisture (S) was computed, and it was MSDI_PSV. For the VICMF model, a drought index was computed in addition to the MSDI_PSM, and it was the MSDI with P and WTE (MSDI_PWM). Each drought index was computed from the simulated results of the VIC and VICMF models, and they were subsequently used to evaluate drought events in the NACP regions during the period of 2000 to 2016.

The USDM is the most widely used drought product in the US, and it provides a weekly drought map in collaboration with the National Drought Mitigation Center (NDMC), the U.S. Department of Agriculture (USDA), and the National Oceanic and Atmospheric Administration (NOAA) (Svoboda et al., 2002). In this study, weekly drought maps from the USDM were used to verify the drought areas of each drought index from the models in the NACP region.

Figure 3 shows the time series plots of drought areas in the NACP regions from the USDM (http://droughtmonitor.unl.edu/; Svoboda et al., 2002), and there were four representative drought events in the periods of 2002, 2008, 2011, and 2012. Each drought event is highlighted with black and dashed boxes, and they are named E1 to E4, respectively.

A statistical test was performed to check the significant differences in the performances of the drought indices (e.g., MSDI_PSV, MSDI_PSM, and MSDI_PWM). A one-way analysis of variance (ANOVA) method was applied to reject the null as the mean value of DA from the same drought indices ($\alpha = 0.05$). For the multiple comparisons of two drought indices, Tukey's Honest Significant Difference (HDS) test was also carried out. If zero was included within the 95% confidence interval and the p-value was higher than 0.05, there was no significant difference between the drought indices.

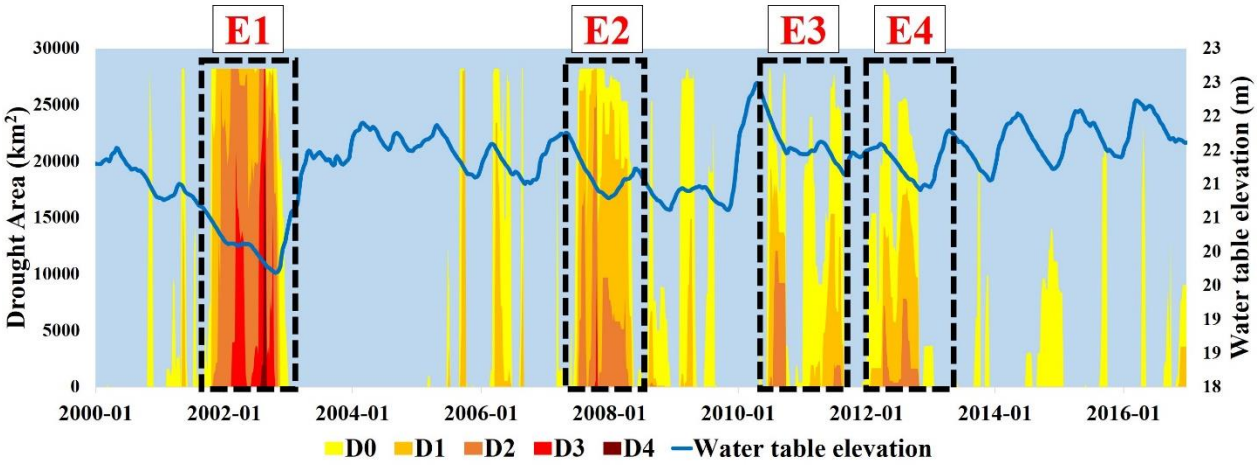

Figure 3. Drought area maps for the NACP region from the United States Drought Monitor (USDM) from January 2000 to December 2016. Each color represents a different drought condition category. Yellow indicates the D0 category (Abnormal drought), orange indicates the D1 category (Moderate drought), darker orange indicates the D2 category (Severe drought), red indicates the D3 category (Extreme drought), and dark brown indicates the D4 category (Exceptional drought). Black and dashed boxes represent the drought events (E1 to E4). Blue The blue line indicates the WTE in the NACP region.

5.4. Results and discussion

5.4.1. Soil moisture estimation of the VIC and VICMF models

In this study, soil moisture from the VIC and VICMF models was compared to analyze the impacts of groundwater dynamics. Figure 4(a) shows the seasonal comparison of total soil moisture during the study period, and the red and blue lines represent the results of the VIC and VICMF models. Overall, the mean value of soil moisture from the VIC model was higher than that of the VICMF (209.4 mm and 206.7 mm, respectively). The red line in Figure 4(b) shows the difference in weekly soil moisture between the two models, and a positive number means that soil moisture from the VIC model was greater than that of the VICMF. The soil moisture from the VICMF was slightly higher from January to April (1–16 weeks), and the VIC was higher for the rest of the period (May to December). The blue line represents the total upward flux produced by the VICMF model, and the difference in soil moisture was higher when the upward flux was relatively low (31–45 weeks). Additionally, there was a significant linear correlation between the soil moisture difference and upward flux (Figure 4(c)). In other words, the upward flux calculated

by the groundwater model was closely related to the soil moisture estimation (VICMF), which would affect the drought assessment.

Soil moisture is one of the most appropriate variables to monitor and assess the impact of water shortage on vegetated land due to its effects on atmospheric dynamics (Cammalleri et al., 2016). In addition, augmenting soil moisture via irrigation to increase plant-available water for root extraction when there is a precipitation deficit is required for crop growth and agricultural production (Bolten et al., 2010; Sánchez et al., 2016). Therefore, an estimation of reliable soil moisture using surface–groundwater dynamics is essential for the computation of drought indices.

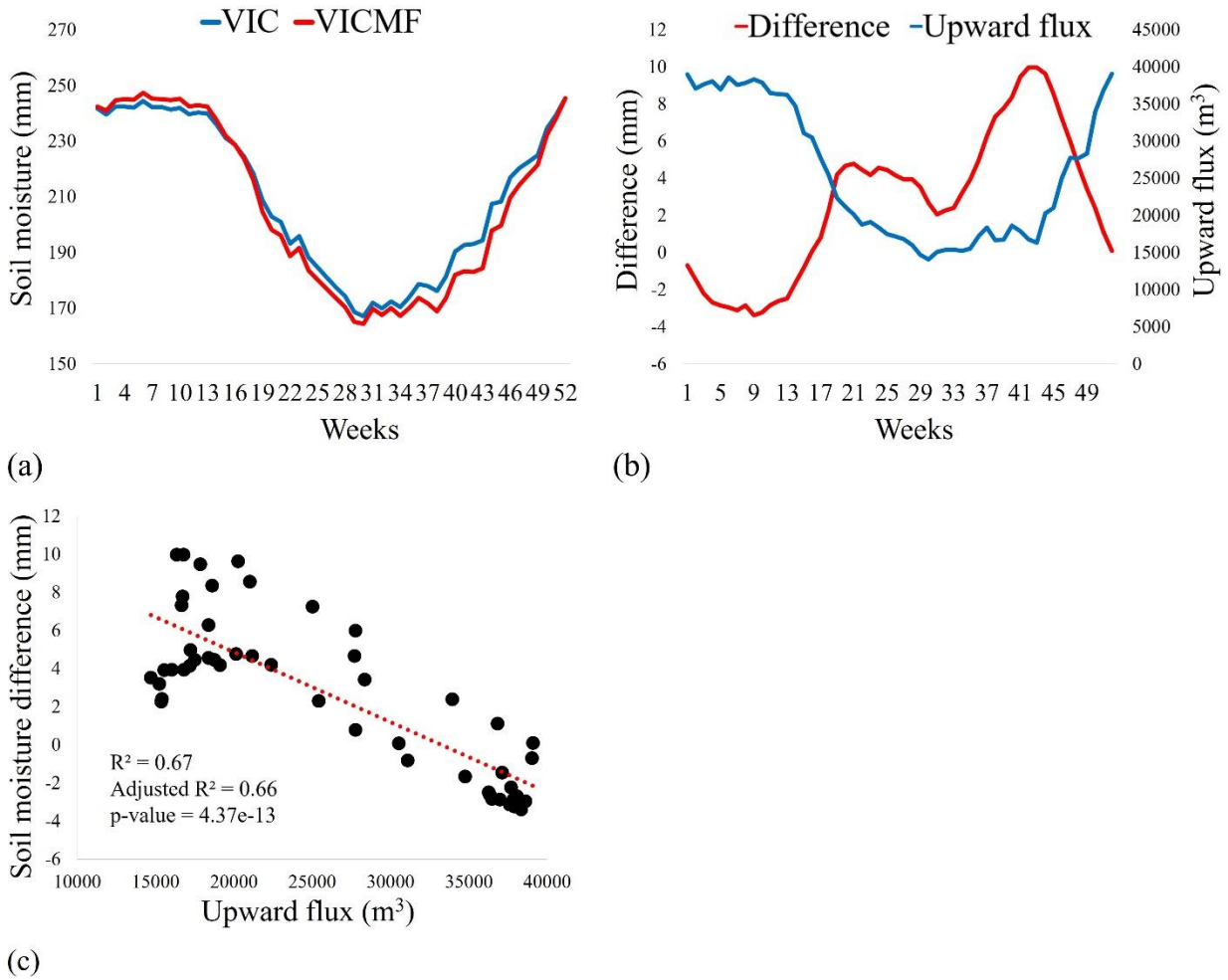

Figure 4. The results of soil moisture comparison from the VIC and VICMF models. (a) Seasonal soil moisture comparison of the VIC and VICMF models. Blue line represents the VIC, and Red line indicates the VICMF. (b) Soil moisture difference between the VIC and VICMF models and upward flux. Blue line represents the difference, and Red line indicates the upward flux. (c) Linear regression of the soil moisture difference and upward flux

5.4.2. Drought area agreement and WTE

The drought maps of the drought indices from the VIC and VICMF models were compared with the USDM drought maps to assess the accuracy of the drought indices. Figure 5 provides the DA derived from the drought indices for each drought event, which were MSDI_PSV from the VIC model and MSDI_PSM and MSDI_PWM from the VICMF model. DA was calculated as the rate of intersected areas where drought areas were correctly captured per total area of the USDM. The drought indices were computed at the same temporal scale with corresponding dates with USDM (weekly). Four representative drought events lasted more than six months (Figure 3). The longest and most serious droughts occurred in 2002, which caused the greatest decrease in WTE computed from the VICMF model.

Overall, the performances of the MSDI_PWM were higher than those of other indices for all drought events, and it was affected by the different combinations of drought indices. The DA values of MSDI_PS from the VIC (MSDI_PSV), MSDI_PS, and MSDI_PW from the VICMF model (MSDI_PSM and MSDI_PWM) were 97.5%, 97.7%, and 99.9% for the first event (E1) and 97.5%, 97.6%, and 98.1%, for E2, respectively. The DA values were 68.3%, 70.6%, and 75.7% for E3 and 91.3%, 91.7%, and 96.4% for the E4 (Figure 5). For all the drought events, the mean values of MSDI_PW were the highest. In addition, Figures 6 - Figure 9 represent the spatial comparisons of the representative drought conditions for each period, and the MSDI_PWM showed higher DA values.

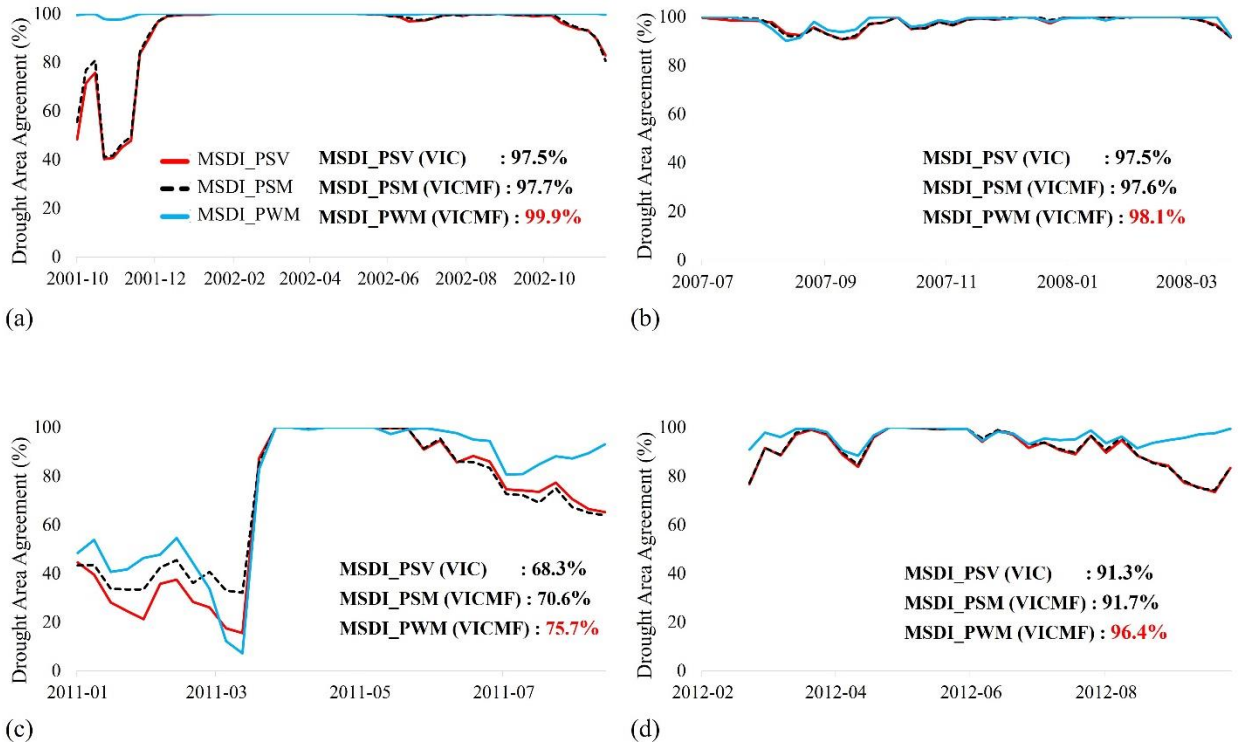

Figure 5. The Drought Area Agreement (DA) values for each drought event. The red line shows the DA values for the MSDI_PSV, the black and dashed line represents the results for MSDI_PSM, and the blue line indicates the results for MSDI_PWM. (a) E1 period (October 2001–October 2002). (b) E2 period (July 2007–November 2008). (c) E3 period (January 2011–August 2011). (d) E4 period (February 2012–September 2012).

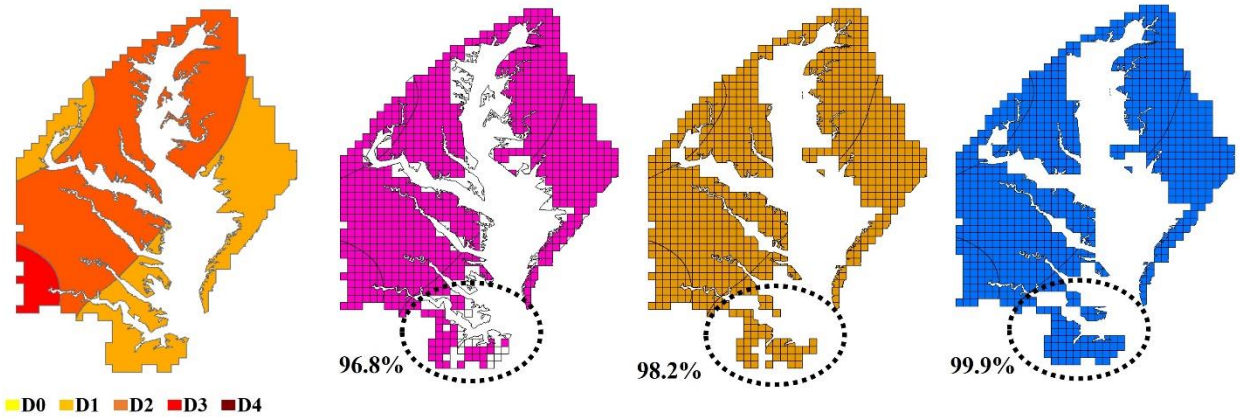

(a) USDM (b)VIC - MSDI_PSV (c) VICMF- MSDI_PSM (d) VICMF- MSDI_PWM

Figure 6. The comparison of drought areas from the (a) USDM, (b) MSDI_PSM, (c) MSDI_PSV, and (d) MSDI_PWM on June-18-2002.

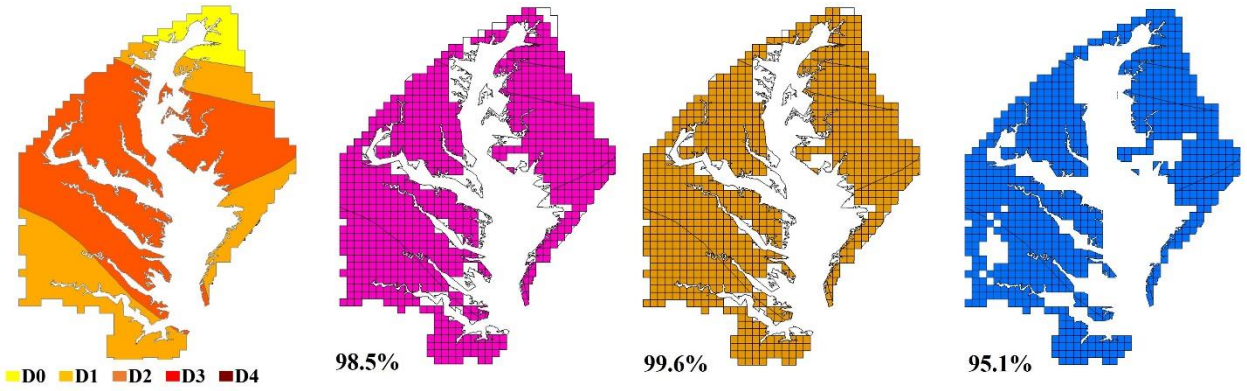

(a) (b) (c) (d)

Figure 7. The comparison of drought areas from the (a) USDM, (b) MSDI_PSM, (c) MSDI_PSV, and (d) MSDI_PWM on July-31-2007.

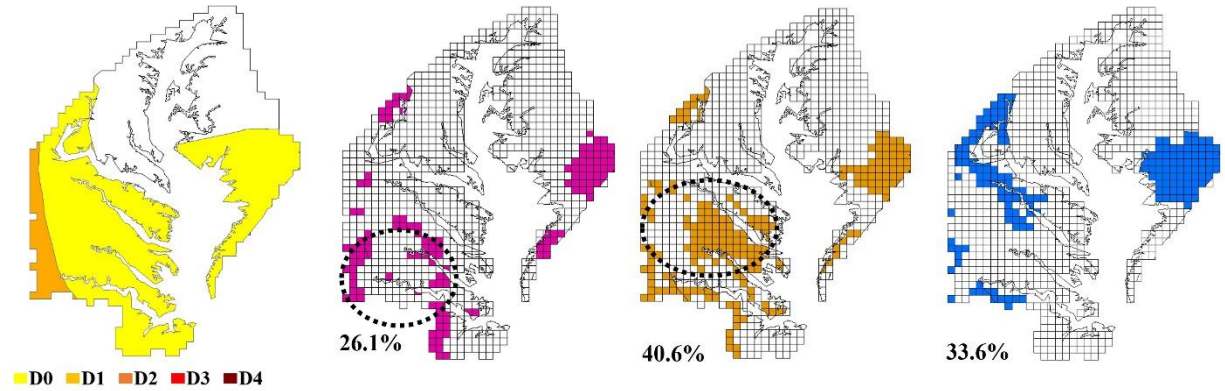

(a) (b) (c) (d)

Figure 8. The comparison of drought areas from the (a) USDM, (b) MSDI_PSM, (c) MSDI_PSV, and (d) MSDI_PWM on March-08-2011.

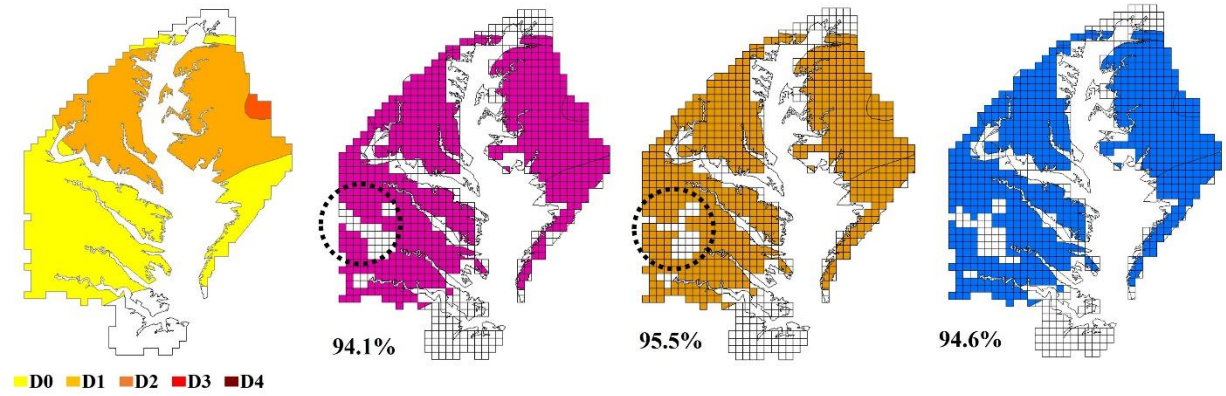

(a) (b) (c) (d)

Figure 9. The comparison of drought areas from the (a) USDM, (b) MSDI_PSM, (c) MSDI_PSV, and (d) MSDI_PWM on July-03-2012.

Figure 10 represents the comparisons of the USDM drought areas, MSDI_PSM, and MSDI_PWM. The E1 period was the most severe drought in the last twenty years in the NACP region, and MSDI_PSM and MSDI_PWM accurately captured the drought conditions. However, the performances of MSDI_PSM and MSDI_PWM differed during the drought termination period. As shown in Figure 10(b)), the green line represents the severe drought of MSDI (<-1.5), and the black and blue lines indicate the MSDI_PSM and MSDI_PWM, respectively. After October 2002, there was a drought recovery, but the slope of MSDI_PSM was much steeper than that of MSDI_PWM. Thus, some of the drought areas after October 2002 were not adequately captured by MSDI_PSM. The DA values of MSDI_PSM were rapidly decreased at the end of the E1 period (Figure 5(a)). In addition, Figure 10(c) represents the drought areas, MSDI_PSM, and MSDI_PWM for the E4 period. Similar to the results of the E1 period, the slope of MSDI_PSM was slightly steeper than that of MSDI_PWM during the drought termination period, which also affected the decrease in the DA values at the end of the E4 period (Figure 5(d)). Droughts have an enormous impact on hydrologic variables, such as runoff, soil moisture, and groundwater, but their responses vary. The drought response of groundwater is slower than soil moisture regarding both drought onset and recovery (Van Loon, 2015), which shows that the drought assessment capability of MSDI_PWM was better during the drought recovery period. For the other drought events, such as the E3 period, similar results were shown (Figure 5(c)).

Groundwater is generally viewed as a buffer resource, and the groundwater use increased during drought periods (Uddameri et al., 2017). In addition, a groundwater drought is defined by the periods of decreased groundwater recharge and groundwater levels (Van Lanen and Peters, 2000; Mishra and Singh, 2010). Thus, an analysis of WTE during drought conditions is essential since it shows groundwater availability during droughts for various regions.

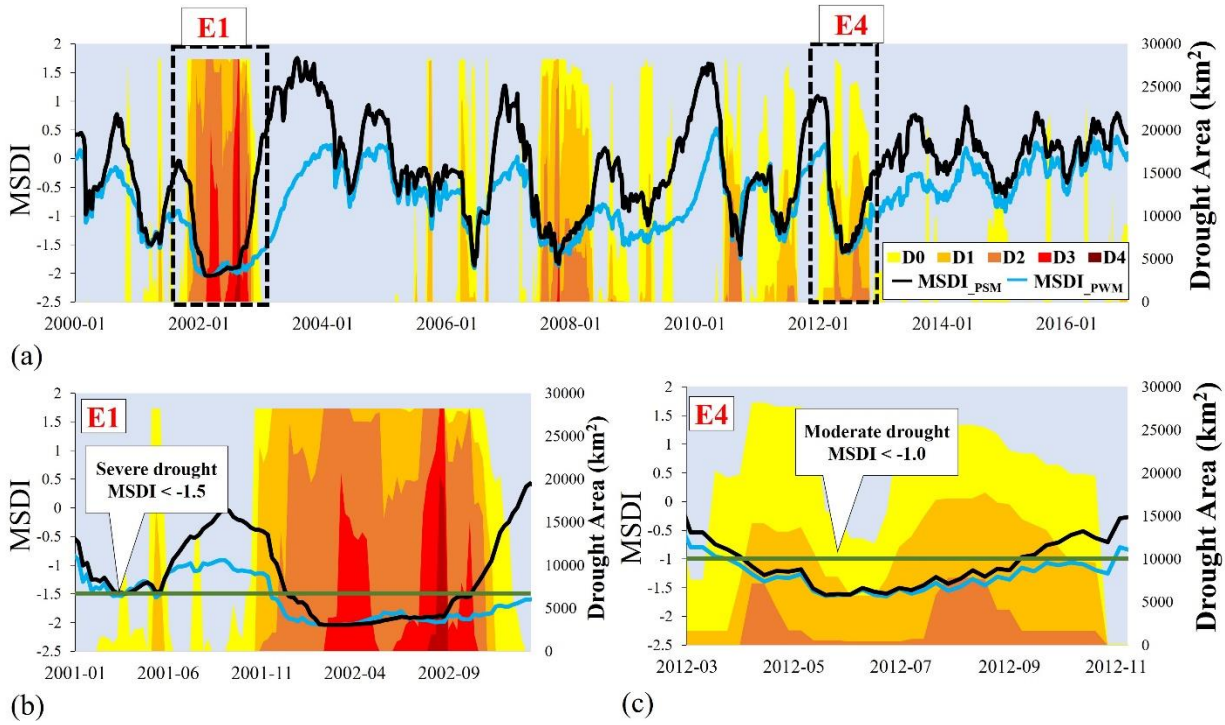

Figure 10. Drought area maps for the NACP region from the USDM, and time series of MSDI_PSM and MSDI_PWM. The black line represents the MSDI_PSM, and the blue line indicates the MSDI_PWM. (a) Drought maps and drought indices from 2000 to 2016. (b) E1 period. (c) E4 period.

Figure 11(a) and (b) were developed using long-term WTE with the VICMF model, and wet, normal, and drought conditions were divided based on the results of MSDI_PWM that showed the highest DA. Figure 11(a) shows the urban area results (Washington DC), and Figure 11(b) represents the rural area results (downstream areas of the Potomac River and the Rappahannock River). The locations and land use for the urban and rural areas are shown in Figure 1. For both urban and rural areas, WTE decreases tended to be greater during droughts (SPI < -0.5), which was more than during normal (-0.5 < SPI < 0.5) and wet conditions (SPI > 0.5). The mean values of the urban area were 32.8 m, 33.2 m, and 33.3 m for the drought, normal, and wet conditions, respectively. For the rural area, the mean values were 10.3 m, 10.5 m, and 10.6 m, respectively. Furthermore, a statistical test was performed to check the significant differences in each condition. A one-way method was used to compare three conditions (drought, normal, and wet) ($\alpha = 0.05$). For the multiple comparisons of conditions, Tukey's HDS test was also carried out. If zero was included within the 95% confidence interval and the p-value was higher than 0.05, there was no significant difference between the conditions.

For the urban area, there was a significant difference between the conditions, which were determined by one-way ANOVA (p-value < 2e-16), and the Tukey's HSD test indicated that there were significant differences among the three conditions (Figure 11(c)). For the rural area, the differences were significant for the three conditions (p-value = 5.3e-14), and the Tukey's HSD test showed that there were significant differences between drought and normal (p-value < 2e-16) and drought and wet conditions (p-value < 2e-16) (Figure 11(d)). However, there was no significant difference between normal and wet conditions. Overall, the results imply that the WTE was significantly influenced by the drought conditions in both urban and rural areas, but the magnitude of differences between drought and normal conditions for the urban area was higher (0.4 m) than for the rural area (0.2 m).

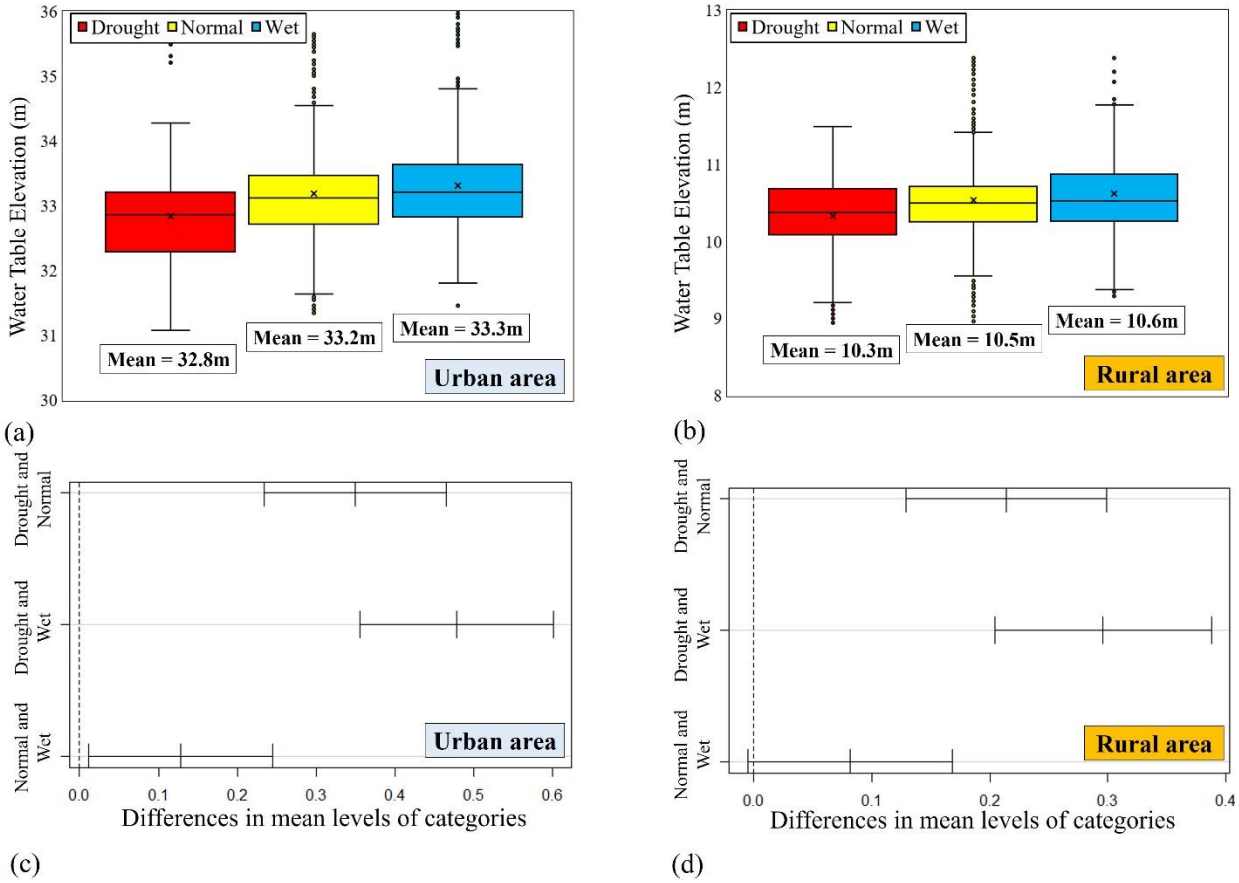

Figure 11. The results of WTE for the urban and rural areas. (a) and (b) are the box and whisker charts for the drought, normal, and wet conditions. The red box represents the drought, the yellow box represents the normal condition, and the blue box indicates the wet condition. The upper and lower whiskers represent maximum and minimum values, the first quartile represents 25%, the median represents 50%, and the third quartile represents 75% of the values. (c) and (d) are the results of Tukey's HSD test, and they show differences in the mean levels of WTE values based on a 95% confidence interval. The Y-axis represents the groups of categories for the comparisons. Each line in the figures indicates the 95% confidence interval for the comparisons.

5.4.3. Statistical test for the DA and WTE

To evaluate the performances of the drought indices from the VIC and VICMF models, a statistical test was carried out for the drought events and DA values. The ANOVA method was also employed to compare three drought indices (MSDI_PSV from the VIC, MSDI_PSM and MSDI_PWM from the VICMF) with the null hypothesis as the mean value of DA from the same drought indices ($\alpha = 0.05$). Additionally, a Tukey's HDS test was conducted for multiple comparisons of drought indices.

Table 1 shows the ANOVA results for each drought event; the p-values of E1 and E4 were less than 0.05 (rejecting the null hypothesis), which can imply that there was a significant difference in the mean values of DA for E1 and E4. However, the p-values of E2 and E3 were 0.648 and 0.551, which did not reject the null hypothesis, and there was no significant difference between the DA values. Table 1 and Figure 12 show the results of Tukey's HSD test, which confirm where the differences occurred between groups. For the E1 period, there was a significant difference between groups as determined by one-way ANOVA (p-value = 0.0036), and the Tukey's HSD test also revealed that there were significant differences between MSDI_PSV and MSDI_PWM (p-value = 0.007) and MSDI_PSM and MSDI_PWM (p-value = 0.014). For the E4 period, the Tukey's HSD test also revealed that there were significant differences between MSDI_PSV and MSDI_PWM (p-value = 0.004) and MSDI_PSM and MSDI_PWM (p-value = 0.08). The results of the E1 and E4 periods statistically prove that the performances of MSDI_PWM (MSDI with precipitation and WTE) showed better DA compared to the USDM. However, no significant differences were found for E2 and E3, but the mean values of DA from the MSDI_PWM were slightly better. In addition, even if not statistically significant, the result of MSDI_PSM from VICMF was slightly higher than that of MSDI_PSM from the MSDI_PSV, and it can be inferred that the effect of surface–groundwater dynamics can be important for drought assessment.

Table 1. ANOVA results for each drought event

	Degree of freedom	Sum of Squares	Mean Square	F	p-value
E1	2	1849	924.6	5.824	0.004
E2	2	6.7	3.4	0.435	0.648
E3	2	963	481.6	0.600	0.551
E4	2	572	286.1	6.765	0.002

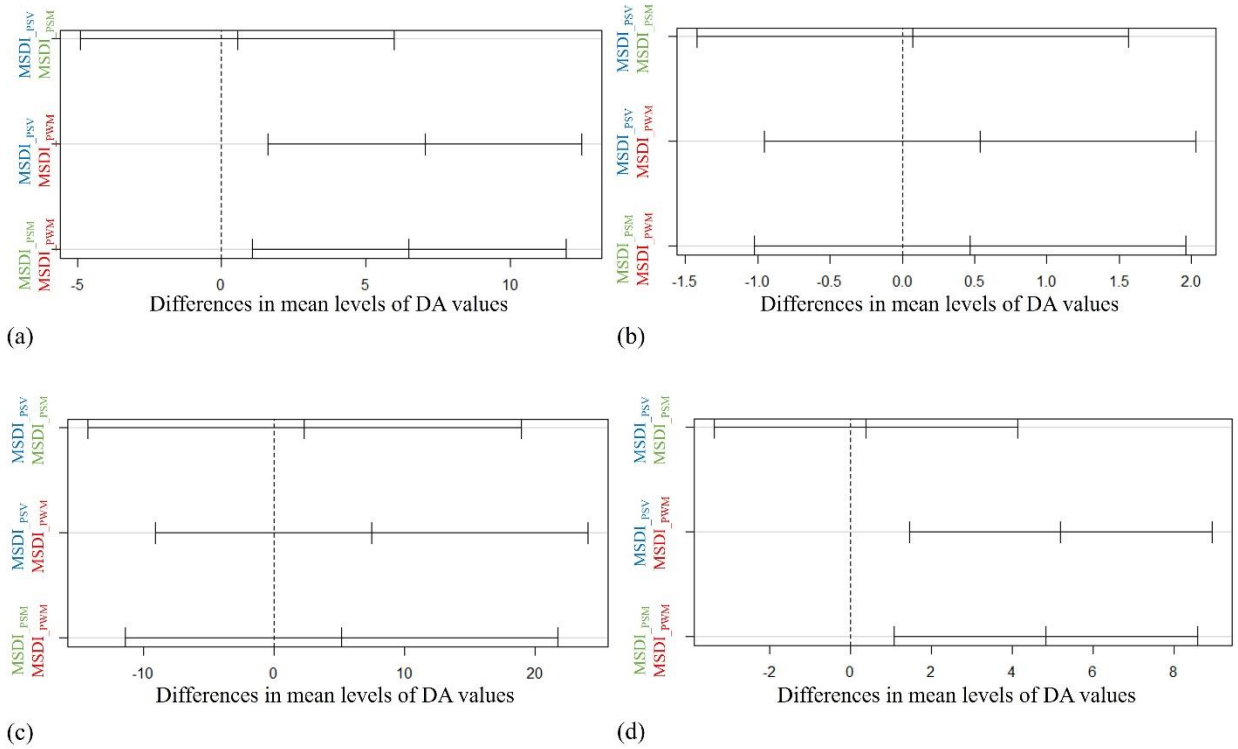

Figure 12. The results of Tukey's HSD test show differences in drought indices based on a 95% confidence interval. The Y-axis represents the groups of the drought indices for the comparisons. Each line in the figures indicates the 95% confidence interval for the comparisons. (a) E1 period. (b) E2 period. (c) E3 period. (d) E4 period.

5.5. Conclusion

The coupled framework including surface and groundwater conditions is useful for considering surface and groundwater dynamics while assessing the impact of changing hydrology on drought predictions. The coupled VICMF model was applied to the NACP region in the Chesapeake Bay, one of the largest and the most productive estuary at present. Additionally, surface hydrologic simulations using the VIC model were performed, and the results of the VIC and VICMF models were used to compute the drought indices and assess the drought conditions. The critical findings of this study are as follows:

1) The mean soil moisture values from the VIC model were higher than those of VICMF, and the soil moisture differences were greater when the upward fluxes were relatively low. The soil moisture data from the two models implies that the upward flux was linearly related to the soil moisture estimation and therefore drought assessments.

2) The performance of the MSDI_PWM was better than that of the other indices for all drought events. For all events (E1 to E4), the DA values of MSDI_PWM were 99.9%, 98.1%, 75.7%, and 96.4%, respectively, which were reliable results for the drought assessment. Since the drought evaluation capability of MSDI_PWM was better during the drought recovery period, the DA values from MSDI_PWM were better.

3) The significance of the DA values was verified by the statistical test (one-way ANOVA), and the E1 and E4 results showed that there were significant differences in the mean values of DA. In addition, the results of Tukey's HSD test revealed that there were significant differences between MSDI_PWM and the other drought indices for the E1 and E4 periods.

4) In both urban and rural areas, there were WTE decreases during drought periods, which were more than during normal and wet conditions. However, the difference between drought and normal conditions for the urban area was higher (0.4 m) than that for the rural area (0.2 m).

5) For drought assessment, an integrated modeling framework that considers climate–hydrologic–human interactions, including the groundwater condition (Uddameri et al., 2017), is recommended. Thus, the coupled approach investigated in this study may be useful to better characterize and simulate drought assessment that considers the surface–

groundwater dynamic, which in turn can serve as an effective tool for decision-making, drought mitigation, and risk management.

5.6. Reference

Bailey, R.T., Wible, T.C., Arabi, M., Records, R.M. and Ditty, J., 2016. Assessing regional-scale spatio-temporal patterns of groundwater–surface water interactions using a coupled SWAT-MODFLOW model. Hydrological Processes, 30(23), pp.4420-4433.

Cammalleri, C., Micale, F. and Vogt, J., 2016. A novel soil moisture-based drought severity index (DSI) combining water deficit magnitude and frequency. Hydrological Processes, 30(2), pp.289-301.

Hao, Z. and AghaKouchak, A., 2013. Multivariate standardized drought index: a parametric multi-index model. Advances in Water Resources, 57, pp.12-18.

Hao, Z. and AghaKouchak, A., 2014. A nonparametric multivariate multi-index drought monitoring framework. Journal of Hydrometeorology, 15(1), pp.89-101.

Harbaugh, A.W. 2005. MODFLOW-2005, the US Geological Survey modular ground-water model: The ground-water flow process. US Department of the Interior, US Geological Survey Reston, VA, USA.

Kang, H. and Sridhar, V., 2018. Assessment of Future Drought Conditions in the Chesapeake Bay Watershed. JAWRA Journal of the American Water Resources Association, 54(1), pp.160-183.

Liang, X., Lettenmaier, D.P., Wood, E.F. and Burges, S.J., 1994. A simple hydrologically based model of land surface water and energy fluxes for general circulation models. Journal of Geophysical Research: Atmospheres, 99(D7), pp.14415-14428

Liang, X., Xie, Z. and Huang, M., 2003. A new parameterization for surface and groundwater interactions and its impact on water budgets with the variable infiltration capacity (VIC) land surface model. Journal of Geophysical Research: Atmospheres, 108(D16).

Masterson, J.P., Pope, J.P., Fienen, M.N., Monti, Jack Jr., Nardi, M.R., and Finkelstein, J.S., 2016, Documentation of a groundwater flow model developed to assess groundwater availability in the Northern Atlantic Coastal Plain aquifer system from Long Island, New York, to

North Carolina (ver. 1.1, December 2016): U.S. Geological Survey Scientific Investigations Report 2016–5076, 70 p., http://dx.doi.org/10.3133/sir20165076.

Mishra, A.K. and Singh, V.P., 2010. A review of drought concepts. Journal of hydrology, 391(1-2), pp.202-216.

Niemeyer, S., 2008. New Drought Indices. Water Management, 80, pp. 267-274, http://om.ciheam.org/article.php?IDPDF=800451.

Niu, G.Y., Yang, Z.L., Dickinson, R.E., Gulden, L.E. and Su, H., 2007. Development of a simple groundwater model for use in climate models and evaluation with Gravity Recovery and Climate Experiment data. Journal of Geophysical Research: Atmospheres, 112(D7).

Oki, T. and Kanae, S., 2006. Global hydrological cycles and world water resources. science, 313(5790), pp.1068-1072.

Panday, S. and Huyakorn, P.S., 2004. A fully coupled physically-based spatially-distributed model for evaluating surface/subsurface flow. Advances in water Resources, 27(4), pp.361-382.

Van Loon, A.F., 2015. Hydrological drought explained. Wiley Interdisciplinary Reviews: Water, 2(4), pp.359-392.

Sánchez, N., González-Zamora, Á., Piles, M. and Martínez-Fernández, J., 2016. A new Soil Moisture Agricultural Drought Index (SMADI) integrating MODIS and SMOS products: A case of study over the Iberian Peninsula. Remote Sensing, 8(4), p.287.

Sehgal, V., Sridhar, V. and Tyagi, A., 2017. Stratified drought analysis using a stochastic ensemble of simulated and in-situ soil moisture observations. Journal of hydrology, 545, pp.226-250.

Sridhar, V., Billah, M.M. and Hildreth, J.W., 2017. Coupled Surface and Groundwater Hydrological Modeling in a Changing Climate. Groundwater.

Van Lanen, H.A.J. and Peters, E., 2000. Definition, effects and assessment of groundwater droughts. In Drought and drought mitigation in Europe (pp. 49-61). Springer, Dordrecht.

Chapter 6. Summary and conclusion

A robust drought evaluation approach is crucial for water resource management and for developing drought mitigation strategies, and a drought assessment framework based on the various hydrologic modeling methodologies is crucial due to increases in extreme climate variability. In this study, we proposed several drought evaluation methods using diverse hydrologic-modeling approaches: 1) a short-term drought forecasting approach with simulated hydrometeorological variables and meteorological forecasting for the entire CONUS; 2) an evaluation of drought projection in the Chesapeake Bay Watershed and five river basins in Virginia (VA) using the high-resolution datasets of future climate ensembles; 3) an assessment of economy-wide impacts of agricultural drought for several congressional districts in VA; and 4) a drought evaluation using a coupled framework, including surface and groundwater conditions. The critical findings for each chapter are as follows:

Chapter 2: The Soil and Water Assessment Tool (SWAT) and Variable Infiltration Capacity (VIC) models were used to estimate hydrologic variables and drought indices for the CONUS, and the Coupled Forecast System model version 2 (CFSv2) provided the near-real-time meteorological forecasting dataset. For the retrospective period (January 2012 to July 2017), the results of the drought simulations implied that both the SWAT and VIC models were useful for capturing overall drought conditions for the CONUS. For the forecasting period (August 2017 to April 2018), the drought forecasting by the Multivariate Standardized Drought Index (MSDI) for eight weeks of lead time was reliable (68% and 63% for the SWAT and VIC models, respectively), but the drought forecasting with longer lead times yielded inadequate results due to the increasing meteorological uncertainty. In addition, the United States Drought Monitor (USDM) was generally conservative in estimating an extreme (D3) or exceptional drought condition (D4); even long-term observation of soil moisture percentiles indicated exceptional droughts (less than 2%). The suggested drought forecasting can provide weekly drought maps that are better than existing methods (e.g., CPC drought outlook) and contributes to drought risk management, crop planning, and supporting drought mitigation strategies.

Chapter 3: This chapter evaluated future drought occurrences in the CB Watershed and fiver river basins in VA using two hydrologic models (SWAT and VIC), climate model ensembles, and several drought indices that provided diverse perspectives on drought. Both the SWAT and

VIC models were well calibrated with the streamflow observations, and the drought estimations were verified by the estimated Modified Palmer Drought Severity Index (MPDSI). The results of the agricultural drought index (SSI) implied an increase in agricultural droughts throughout the study areas, and drought increases were related to increases in evapotranspiration and surface and groundwater discharge. However, the results of other drought indices (MSDI and MPDSI) represented decreases in drought occurrences because they were strongly influenced by increases in precipitation in the future, which indicated that the combined impacts of precipitation and temperature should be considered simultaneously. The various applications of hydrologic models, climate model ensembles, and drought indices facilitate a reliable understanding of future drought predictions.

Chapter 4: The impacts of climate change on agricultural droughts and their economy-wide shocks were evaluated by the soil moisture simulation from the VIC model and SSI, climate models, and an economic model (IMPLAN) for three congressional districts in VA. There were strong and significant correlations between the sums of agricultural production and the mean values of SSI, and the results of the regression analysis were used for the future drought impacts on the economy. The results of future drought projections indicated that there was an overall increase in droughts in the VA06 and VA11 districts, but a decrease in the VA08 district due to the different land-use arrangements that resulted in the different water budget simulations (e.g., ET). For the economy-wide analysis by the IMPLAN model, the total agricultural production decreased by 16.8% to 21.7% in the VA06 district, and there were 0.5% to 5.1% decreases in the VA11 district, while there were 71.4% to 85.5% increases in the VA08 district. More reliable evaluations would be available with a land-use change scenario, but the changes in agricultural production can be smaller than the estimations because of farmers' adaptations in the future.

Chapter 5: A coupled approach (VICMF) with surface–groundwater dynamics was applied to the Northern Atlantic Coastal Plain (NACP) aquifer system in the Chesapeake Bay. In addition, surface hydrologic simulations with the VIC model were carried out in the same area, and the simulation results from the two models were used for the drought assessment. The estimates of soil moisture from the VICMF model were less than those from the VIC model due to the upward flux adding soil moisture to the vadose layers of the VICMF model. For the drought assessment, the drought evaluation capability of the MSDI_PWM was better than that of the other indices during the drought recovery period. Furthermore, the results of Tukey's HSD test showed

significant differences between MSDI_PWM and the other drought indices. The coupled framework proposed in this chapter may be useful for drought assessment in the regions where the exchanges between the surface water and groundwater systems are closely linked.

It is expected that there will be increased dynamics in hydro-climatological variables worldwide, frequent droughts will occur, and increasing water demands will compound their impacts. Drought assessment approaches using various applications of multiple hydrologic models, drought indices, and climate projections provide comprehensive insight into drought evaluations. The suggested methods present comparisons of various drought assessment techniques, and they can consider various aspects of droughts and contribute to a broader context of the enhancement of the entire hydrometeorological science and climate extremes.

Some additional investigations are still required to supplement the dissertation and future research. Even the drought assessments were mainly based on the soil moisture simulations and other hydrometeorological variables, and they were just indirectly calibrated with streamflow observations. For a more robust drought assessment, soil moisture and other variables should be directly calibrated with observations. Additionally, a higher spatial resolution and a more extended period of agricultural production data are necessary for a broader evaluation of drought impacts on the economy, and the evaluation techniques provided in this dissertation can be extended to the other economic regions of different hydrometeorological conditions. Finally, an analysis of the relationship between drought and additional hydro-geologic variables (e.g., hydraulic conductivity) would contribute to a better understanding of droughts in coupled surface and groundwater systems.